Yu Yun He
俞云鹤

Battery modelling and usage guidelines in Solar Home Systems

TU Delft

Cover picture URL: http://applision.com/introduction/28553/

Battery modelling and usage guidelines in Solar Home Systems

By

Yu Yun He

俞云鹤

in partial fulfilment of the requirements for the degree of

Master of Science

in Faculty of Electrical Engineering, Mathematics and Computer Science

at the Delft University of Technology,

to be defended publicly on Tuesday August 29, 2017 at 14:00 PM.

Supervisor:	Prof.dr.ir. P. Bauer	
Thesis committee:	Prof.dr.ir. P. Bauer	DCE&S group TU Delft
	Dr. Zian. Qin	DCE&S group TU Delft
	Dr. ir. M. Wagemaker	FAME group TU Delft

This thesis is confidential and cannot be made public until August 31, 2018.

TU Delft

Acknowledgement

First of all, I would like to express my gratitude to my parents, and my ex-boyfriend, even though we already broke up for months. Without their unconditional support from both economic (parents) and mental (ex-BF) point of view, I could not finish my study in the Netherlands.

Secondly, I would like to thank the employees in DCE&S group. I would like to thank my previous supervisor, Dr. Ir. J. Popovic, She offered me with this nice topic and led me into this research field. I would like to thank my current supervisor, Prof. Dr. Ir. P.Bauer for his guidance of my thesis.

I would like to thank all the support staff in the lab of our group, Bart, Joris, etc. They helped me ordered all the required experimental material for at least five times. I will have nothing to play the tests with without their support.

Thirdly, I would like to thank people from the external organisations, who helped me a lot with my research.

I would like to thank the employees in FAME group, the Reactor Institute Delft. Dr. ir. M. Wagemaker approved the tests operation and offered me with two extra times of extension to access their lab. With this precious opportunity, I could have finished my experiments.

I would like to thank Frans in the FAME group, he helped me with getting all through the experiments in the lab. All the failures, problems and errors I met with the tests could not be solved without his support.

I would like to thank Thomas, Leon, Jon and Luna I met from E-stone company too. They also offered me some places for operating the trial tests.

I would like to give my special appreciation to two Ph.D. students in DCE&S group, my daily supervisor Nishant and a former daily supervisor of another project, Victor. Not only for their professional instructions on my thesis, but also for their free coffee cards.

At the last stage of my thesis project, I got lots of help from friends. I should especially thank Ivan, Prateek and Thekla, they gave me many valuable suggestions on the writing of my thesis. And other colleagues working in the same student office, Michalis, Natalie and Wenrui, etc.. We kept supporting and encouraging and making fun of each other, which turned the life a bit brighter.

Finally, I would like to thank all my friends whose name are not on the list, in Delft. You made my life here unique and unforgettable.

Yu Yun he

俞云鹤

Delft, August 2017

Abstract

Nowadays, there are still some regions in developing countries lacking electrification. A solution to electrify the households in these areas with off-grid Solar Home Systems (SHS) has been proposed for some time. However, battery storage in SHS is always the limitation in both cost and lifetime point of view. Thus, a battery with stable behaviour, longer lifetime and less maintenance as well as a lower price is highly desired in SHSs. With the narrow choices on economical commercial battery technologies, there is another approach to improve the battery behaviour in SHSs.

This thesis is aiming at exploring a solution from usage perspective to maintain the battery behaviour in long-term, in SHSs. In order to achieve the goal, a tool and a method were proposed to provide a practical solution for battery performance preservation in SHSs.

In this study, two battery technologies which are commonly applied in SHSs were explored: the $LiFePO_4$ battery and the Valve Regulated Lead-acid battery

Firstly, an accurate battery dynamic model based on the electrical equivalent circuit was constructed for both battery technologies separately. Series of experiments were performed to obtain the relevant parameters. This model was built for low current applications, which is lower than 1 C, typically suitable for SHS applications. This model was on battery cell level and with a great accuracy with a < 2% error

Secondly, a performance based battery lifetime prediction model was built, and the battery capacity was selected as the index of the ageing process. The modelling was achieved by applying a new concept, which is the rate of normalised capacity fading, with respect to capacity throughput. Another series of experiments were operated for the exploration of the relationship between stress factors and the rate of battery ageing. The experimental data is the foundation of the battery lifetime model.

Thirdly, a usage guideline for each battery technology was proposed by analysing the lifetime test data. Then one practical usage guideline application method was simulated. The application of the usage guideline has a noticeable improvement in the battery behaviour in long term scale.

In conclusion, the modelling of the battery including both dynamic behaviour as well as lifetime prediction provides a tool for future exploration. With this tool, the design and sizing of the battery storage system, as well as the management of appropriate battery usage in SHS would be easier. The method proposed for battery capacity preservation is the usage guideline. The usage guidelines offered wide choices on user side implementations regarding battery capacity preservation.

Table of content

List of figures

List of tables

List of abbreviations and symbols

List of Abbreviations

AGM	Absorptive Glass Mat
Ah	Ampere Hour
ANN	Artificial Neural Network
CC-CC	Constant Current-Constant Current
CC-CV	Constant Current-Constant Voltage
CF	Charge Factor
CPE	Constant-Phase Element
Cte-	Close To Equilibrium
DOD	Depth Of Discharge
e.m.f/EMF	Electromotive Force
EEC(M)	Equivalent Electrical Circuit (Model)
EIS	Electrochemical Impedance Spectroscopy
EOC/D(V)	End Of Charge/Discharge(Voltage)
EOL	End Of Life
EV	Electric Vehicles
EXP	Experiment
$LAM_{PE/NE}$	Loss Of Active Material On Positive And Negative Electrodes
LFP	$LiFePO_4$ Battery
LIB	Lithium Ion Battery
LLI	Loss Of Lithium Inventory
OCV/VOC	Open Circuit Voltage
PV	Photovoltaic
SEI	Solid Electrolyte Interface
RC	Resistor-Capacitor
SHS	Solar Home System
SIM	Simulation
SOC	State Of Charge
SOH	State Of Health
VRLA	Valve Regulated Lead-Acid Battery

List of Symbols

C	Battery capacity
C_{dsb0}	Maximum dischargeable capacity of a fresh battery
cf_r	Relative coulombic efficiencies
C_{IA}	Maximum discharged battery capacity influenced by current
dF	Differential capacity fading
dQ_{th}	Differential capacity throughput
F	Amount of faded capacity (in unit of Ah)
I_{cell}	Battery cell current
I_{cr}	Current in C rate form
I_m	Main branch current
n_{eq}	Number of equivalent cycles
nF	Normalised differential capacity fading
Q	Amount of electrical charge
Q_{th}	Capacity throughput
Rl/Cl	RC pair representing the voltage relaxation in long time window
r_{nF}	Rate of normalised capacity fading according to capacity throughput
Ro	Ohmic resistance
Rp	Parasitic branch resistance
Rs/Cs	RC pair representing the voltage relaxation in short time window
SOC_{dev}	SOC deviation
SOC_{avg}	Averaged operational SOC
subscript c or ch in dynamic battery model	Charge stage
subscript d or dis in dynamic battery model	Discharge stage
T	Temperature
V_{cell}	Battery cell voltage
η_c	Coulombic efficiency
η_e	Energy efficiency

1 Introduction

1.1 Thesis motivation

This project is motivated by the increasing demand of Solar Home Systems (SHS) in rural areas of developing countries. A SHS is a Solar Photovoltaic(PV) –Based power system for individual household domestic applications [1]. The main focus of this thesis is on the battery storage part of the SHS. The purpose of this study is to investigate how batteries of different technologies perform in SHS and what are the usage limitations introduced when optimising the system for longer battery lifetime in SHS.

Some regions in developing countries like South Africa, India and Cambodia, are far away from having a robust power grid. Thus, one important option to obtain low-cost electricity for households in remote areas with no grid connection could be the use of off-grid Solar Home Systems (SHS). Since the electrical power demand of these households is usually low in comparison to households in big cities or developed countries, small-scale PV system could completely meet their energy requirements. Batteries in these SHSs are used to overcome the time mismatch between PV generation and load consumption. Nonetheless, even when a technical solution is available, some other considerations need to be taken for such households. Most of these households have deficient income, and the local governments in these regions have limited funds. This means there would be a cost constraint. Additionally, some of these rural areas may be far away and thus difficult to access for people (e.g. technicians and energy professionals) to ensure a regular maintenance of the SHS. Therefore, batteries employed in these SHSs should be of low-cost and reliable, i.e. able to work with reduced or even no maintenance.

The manufactured batteries of the same technology have a range of warranted lifetime under relatively heavy stresses. That means there is a large potential to extend its lifetime apart from the warranted lifetime if the battery is used with caution. Using the battery with caution is including: control the ageing rate and constrain it in an acceptable range from an application aspect, and this can be achieved by controlling the usage profile of the battery.

As a conclusion, the focus of this study is the exploration and acquisition of a usage guideline for different battery technologies (in cell level). The expected achievement of this study is to offer a practical tool and a method, with which the battery lifetime can be extended from an application point of view.

1.2 Objectives and research questions

In order to make the final goal of this study clear and attainable, main objective and the sub-objectives are addressed in this section.

1.2.1 Main objective

The main objective of this study is: To develop **a tool** and **a method** that includes the usage guideline of different battery technologies in low power off-grid SHSs.

The whole study is in cell level, and the battery technologies are $LiFePO_4$ (LFP), and Valve regulated Lead-acid (VRLA).

1.2.2 Sub-objectives

In order to achieve the main objective, several sub-objectives should be accomplished. These sub-objectives are blocks to build the main objective.

1. Construct the dynamic battery cell models for two technologies, LFP and VRLA
2. Build a State of Health (SOH) model which can predict the lifetime of the battery cell
3. Identify the suitable usage guideline for each battery technology and apply the usage guideline on the SHS
4. Evaluate the achievements of two battery technologies and make some comparisons on the results

Sub-objective 1 and 2 are the steps of building **the tool**, and sub-objective 3 is to obtain the **method** for the application.

The summary of these objectives is shown in Figure 1-1.

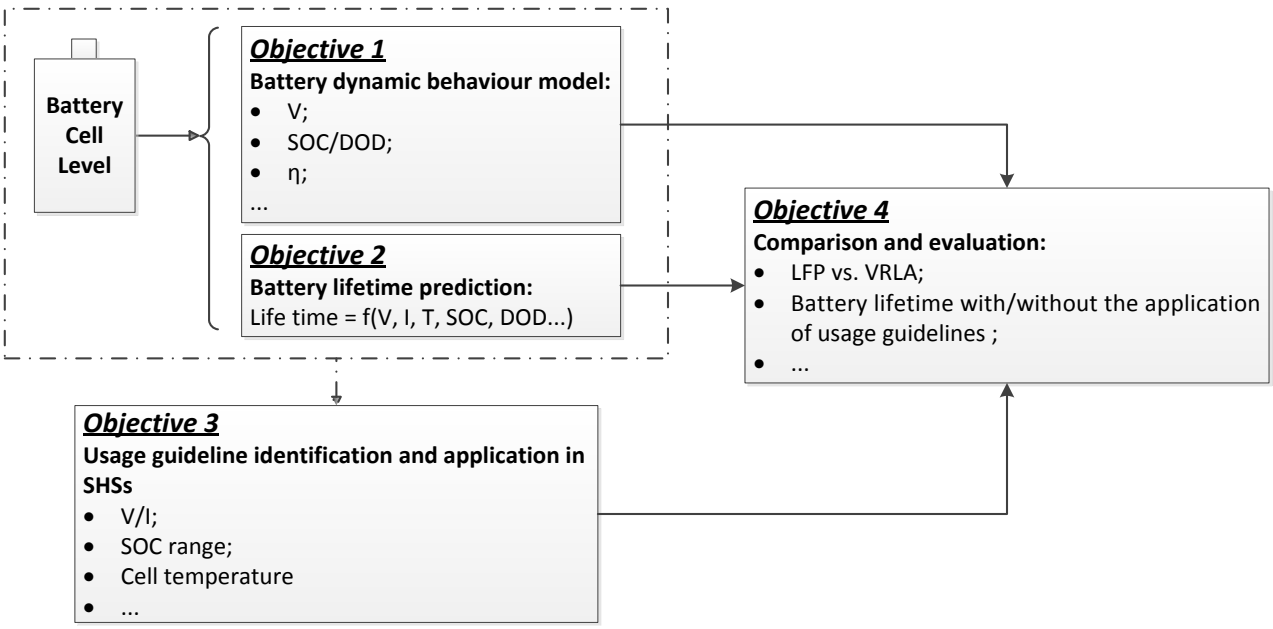

Figure 1-1 Objectives of the thesis

1.3 Research questions

Each objective introduced in Section 1.2 is corresponding to one main research question:

- **Q1# How should the battery cell dynamic behaviour be modelled?---For Objective 1**

This question is about how to construct a battery dynamic model with which the external characteristics of the battery can be reflected in the model. In what way the required data can be obtained, and how to use the data to build the model.

- **Q2# How to predict the battery cell's lifetime? ---For Objective 2**

To answer this question is to look for the possible stress factors which influence the battery lifetime significantly in the first step. Secondly is to pick an index parameter to represent the progress of the battery lifetime. Thirdly is to find a method to extract the necessary data and integrate the data into the lifetime prediction model.

- **Q3# How should the usage guidelines be obtained and how to apply them in SHSs? ---For Objective 3**

This question focuses on seeking an instruction of the battery operation in SHS, to improve the battery performance in long term scale. Moreover, how to convert the instructions into practical applications in SHSs.

- **Q4# How to compare the results and evaluate the achievements? ---For Objective 4**

This question is meant to explore what specifications can be used to make the comparison between the results of both technologies. In what way could the achievements be evaluated.

1.4 Methodology

The flowchart of the objectives and its methodology is shown in Figure 1-2. The dominant methodologies for each subject are introduced in this section.

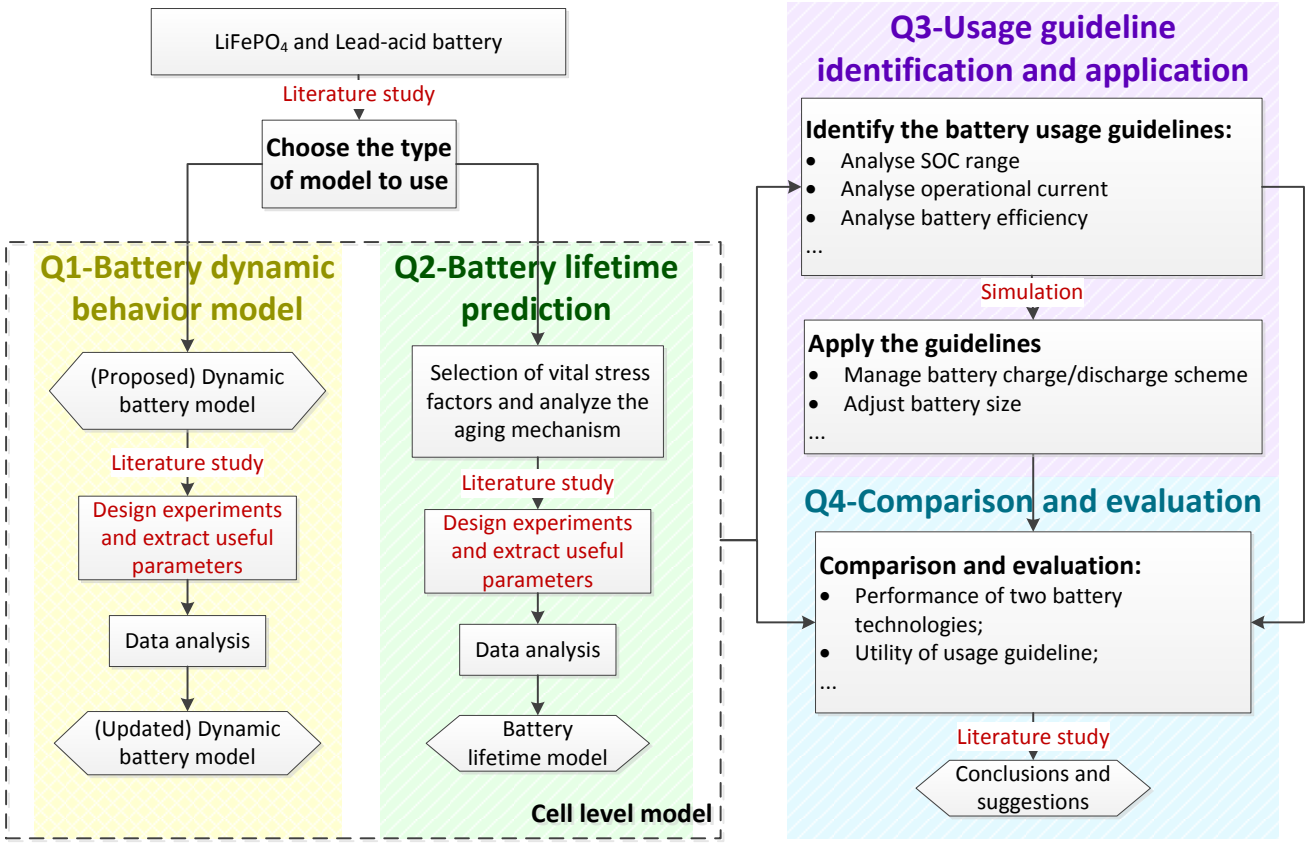

Figure 1-2 Flowchart of objectives and methodology

Objective 1:

Dynamic modelling of battery in storage and electrical behaviour is achieved by literature reviewing, designing and operating the proper experiments. This objective is introduced in Chapter 3.

Objective 2:

Battery lifetime modelling is empirically based with literature review providing background knowledge. This objective is explained in Chapter 4.

Objective 3:

Data analysis, modelling and simulation are the main tools. The essential data is acquired from experiments. This objective is interpreted in Chapter 5.

Objective 4:

This objective is not independent, it is a task throughout the whole project. Each achievement of the other objectives should be analysed and evaluated. Data analysis and simulation are the major methods. This objective is distributed in the whole thesis.

1.5 Thesis outline

The whole thesis is constructed as below:

For better understanding, some basic literature review and background knowledge introduction of the thesis are in Chapter 2. Some approaches and modelling methods that have been used in the study is also introduced briefly.

In chapter 3 and 4, the empirical based cell level model is introduced.

The construction of battery dynamic behaviour model is placed in Chapter 3 and the battery lifetime model is interpreted in Chapter 4.

In Chapter 5, first of all, a battery usage guideline is summarised from the experimental results. Then it is the simulation of a practical application case, with and without the implementation of the usage guidelines addressed in the first part of this chapter.

Chapter 6 is the final conclusion and the suggestions of the whole thesis.

2 Background knowledge

2.1 Parameter definitions

In order to model the real performance of a battery, some characteristics must be included in this battery model and the key parameters should be defined clearly.

a) Capacity

It represents the energy that is possible to store in the battery and it is decided by the chemical reactions occurring inside the battery. The capacity is not constant since the chemical reactions can be influenced by many factors: the operational temperature, end of discharge voltage (EODV), the discharge current and the battery state of health. [2]

There are several definitions of cell capacity. From a theoretical view, the *theoretical battery capacity* is defined as the total electric charge involved in the electrochemical reaction and represented in the form of coulombs or ampere-hours.[2] From an application perspective, the *rated or a nominal capacity* is defined as the total energy available when a fresh battery is discharged at a certain discharge current (specified as a C-rate) from full state to the cut-off voltage under standard conditions.[3] These specific values of C-rate and EODV are defined by the manufacturer.

For engineering purposes, neither of these two definitions is suitable. Since the electric charge involved in the chemical reaction is difficult to be measured and the C-rate can hardly be kept constant during discharge in real life applications. Moreover, the maximum dischargeable capacity of a fresh battery could probably larger than the claimed rated capacity. However, after a period of usage, the maximum dischargeable capacity of the cell will keep decreasing and the constant nominal/rated capacity may no longer meaningful.

Even though discharge current influences the capacity, the loss of capacity due to discharging with a high C-rate can be compensated by adding more lower rate discharge stages.[4] Hence, if correct discharge strategy employed, the maximum dischargeable capacity (or "the real" capacity) can be calculated by integral discharging current by the discharging time, as shown in (2.1) [5].

$$Capacity(Ah) = \int_0^t i \times dt \tag{2.1}$$

Hence, in this thesis the ***maximum dischargeable battery capacity*** is referred as "battery capacity" if not specified. Its definition: **the maximum amount of electric charge that can be extracted from the full state battery until the EODV according to discharge C-rate; or until the EODV is reached while a sufficiently small discharge current which is defined by the manufacturer is drawn under standard temperature 25 ℃.**

b) State of charge (SOC)

This parameter can show the fraction of the energy that left in the battery. As introduced in a), the exterior capacity varies depending on the usage conditions, the exterior SOC changes as a result. The actual SOC which is of interest for this thesis depends on the ***maximum dischargeable battery capacity*** which is defined in a).

Hence, the SOC in this thesis refers to the ***real SOC*** unless specified and it is defined as: **the percentage of the maximum possible electric charge that is present inside a rechargeable battery.**[6] It is calculated by the ratio between the difference of the battery capacity and the net electric charge discharged from a battery since the last full state of charge and the battery capacity. The expression of SOC is in Eq.(2.2) [3]

$$SOC = \frac{Q_t - Q_e}{Q_t} \qquad (2.2)$$
$$Q_e(\mathrm{t}) = \int_0^t I_m(\tau) d\tau$$

Where Q_t is the temperature dependent battery capacity and Q_e is the net electric charge discharged from a battery since the last full state of charge. I_m is the mian branch current.

c) Depth of discharge (DOD)

The DOD is another parameter used to represent the capacity left in a battery which is related to the SOC and it is defined in this thesis as: **the ratio between net discharged charge from a battery since the last full state of and the battery capacity.** The DOD is zero when the battery is full and one when the battery is empty. The expression of DOD is in (2.3) [3]:

$$DOD = 1 - SOC = \frac{Q_e}{Q_t} \qquad (2.3)$$

d) Electromotive force (e.m.f)

The electrochemical force/chemical potential of a specific type of battery cell has a constant value under standard conditions because of its thermodynamic properties. This value will vary in a certain range, given by the chemical characteristics of the cell composition and the kinetic progress when it is working. With the "chemical characteristics" refers to the material and composition of its electrodes and electrolyte.

The ***electromotive force*** of a cell is defined as: **the algebraic sum of the potential difference of two half cells, which is the chemical potential of redox reactions happening on the two electrodes.** [7]

e) Open circuit voltage (OCV, or VOC) and cte-OCV

The open circuit voltage (OCV) is **the potential difference across its terminals when there is no current flow in or out of a reversible cell**.[8] If the battery rests enough time (depending on the battery technology) with no current flow, then the OCV can be called Close-to-Equilibrium open circuit voltage (cte-OCV)[9], [10] can be regarded as the estimated e.m.f value, as defined in c).[6]

In this thesis, the cte-OCV is defined as: **the potential difference across its terminal when there is no current flow in/out of a reversible cell, after enough time, to be regarded as the representative of e.m.f value.**

If not specified, OCV or VOC in this thesis is used as cte-VOC.

f) Current rate (C-rate)

The current rate, which is also called C-rate, is defined here as: **the magnitude of charge/discharge current equal in Amperes to the <u>nominal capacity</u> of the battery in Ampere hours.**[6] The C-rate represents the speed of charge/discharge and it can be calculated by using equation (2.4). [5]

$$1\,C - rate = \frac{\text{nominal capacity}}{1\text{ hour}}(A) \qquad (2.4)$$

A different C-rate current can be obtained by multiplying the 1 C-rate or dividing it by 1/τ hour(s), as shown in (2.5).[5][8]

$$\tau C-rate = \tau \times 1C-rate = \tau \times \frac{\text{nominal capacity}}{1\text{ hour}}$$
$$\tau C-rate = \text{nominal capacity} \div \left(\frac{1}{\tau}\text{hours}\right) \quad \textbf{(2.5)}$$

g) Efficiency

When charging or discharging a reversible battery, neither can all energy applied to a battery be effectively stored nor can all the available electric charge inside a battery be retrieved successfully. The efficiency is used to represent the ability of a battery to store/retrieve electric charge or energy. The efficiency of a battery is not always constant even in one cycle, and it depends on the SOC, cell temperature and current.[11] To clarify, the overall cycle efficiency in this thesis means the efficiency of a whole cycle, which is an empty battery first be charged to full state then fully discharged to empty.

There are two commonly used overall cycle efficiencies: one is the **capacity/coulomb/ampere-hour efficiency** and the other is the **energy efficiency**. They are defined in equations (2.6) and (2.7) respectively.[8]

$$\eta_c = \frac{\int_0^t i_{dis}\,dt}{\int_0^t i_{ch}\,dt} \quad \textbf{(2.6)}$$

$$\eta_e = \frac{\int_0^t v_{dis} \times i_{dis}\,dt}{\int_0^t v_{ch} \times i_{ch}\,dt} \quad \textbf{(2.7)}$$

Where the $v_{ch/dis}$, $i_{ch/dis}$ represent the battery voltage and current during charge/discharge respectively.

The reciprocal of the coulombic efficiency is called charge factor (CF).

h) Capacity throughput

Capacity throughput is defined as: **An integral of the electric charge that has been pushed into and taken out from the battery during a specific time duration.** The equation to express it is in (2.8).

$$Q_{th} = \int_{t1}^{t2} i(t)\,d\tau \quad \textbf{(2.8)}$$

i) Equivalent cycle

The equivalent cycle is defined as: **The amount of capacity throughput that one battery has performed, divided by the capacity throughput required for one full-cycle charge and discharge according to its rated capacity. Which is divided by two times of the rated battery capacity.** It can be presented in equation (2.9):

$$n_{eq} = \frac{Q_{th}}{2 \times C_{rate}} \quad \textbf{(2.9)}$$

2.2 Battery in SHSs

Off-grid SHS is proving to be an important element to deal with energy poverty issues around the world[12], [13]. The most critical component of a SHS is the battery. The battery is not only the most expensive part but also the one with the shortest life time in a SHS. While a PV system's lifetime is considered to be around 25 years, a typical battery in a SHS has an approximate lifetime of 5-8 years[14], [15].

Battery parameters such as Depth of Discharge (DOD), State of Charge (SOC), temperature, as well as the load e.g. C-rate, peak power are intricately interrelated with each other and with the battery lifetime. Because of this, the sizing of a SHS's battery is not a trivial task. It demands a significant understanding of the factors that affect the battery's lifetime. For example, the average operational DOD and current impact the battery lifetime significantly. These two factors are in turn linked to the battery sizing [16] as a function of the supply and demand profile. Thus, to predict the battery's lifetime from external characteristics, which can be measured or calculated, a dynamic model of a battery is required.

2.3 Battery technologies of interest

2.3.1 Choose battery technologies

The batteries explored in this thesis are to be implied in off-grid SHSs, which are located in regions far away from cities in developing countries. For this reason, candidate battery technologies are required to have a good performance, longer lifetime and with lower cost.

There is a variety of battery technologies in the market and the most commonly available technologies are Lead-acid, NiCd, NiMH and lithium-ion (LIB). As can be seen from Figure 2-1, Li-ion battery has the best performance in both specific power and energy density.

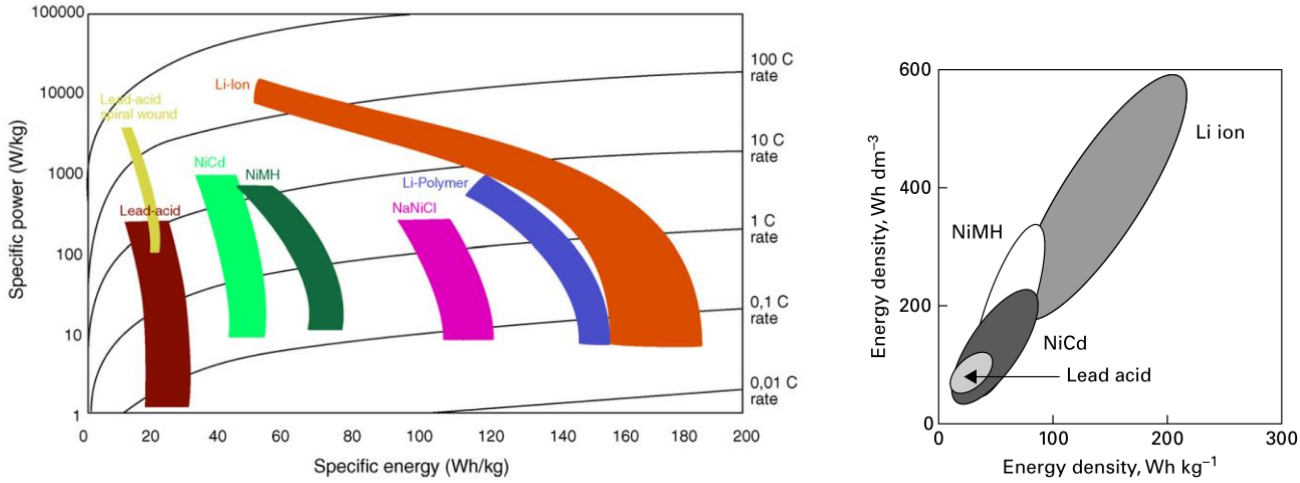

(a) **(b)**

Figure 2-1 (a) Ragone chart (Fig.1 in[17]); (b) Comparison of energy density by volume and weight for most commonly commercial rechargeable battery technologies (Fig 10-16 of [5])

$LiFePO_4$ battery (LFP) is a type of lithium ion battery that uses $LiFePO_4$ as the cathode. LFP has lots of advantages compare with other types of Li-ion batteries:[18][19]

- The raw material is inexpensive to get and is less toxic than other commonly seen materials in batteries, e.g. Co, Ni, Mg;
- It has a good theoretical capacity (~170mAh/g) and a longer lifetime;
- It has a great chemical and thermal stability, which makes it a safer product than the other LIBs;
- It is not only environmentally friendly, but also relatively easy to produce and recycle

- The voltage of its cathode (~3.3V Li/$LiFePO_4$) is helping to reduce the side reactions that caused by the electrolyte decomposition while increasing the energy.
- The price of raw material Phospho-olivine and the manufacturing cost of LFP is relatively low in comparison with the other kinds of LIBs.([20])

Table 2-1 Comparison among commonly available batteries[21], [22]

Battery tech	Energy efficiency [%]	Cycle life	Cost [Capital cost in Euro/kWh]
Lead-acid (flooded type)	72–78	1000–2000 cycles at 70% DOD	50–150
Lead-acid (valve regulated)	72–78	200–300 cycles at 80% DOD	50–150
Nickel Cadmium (NiCd)	72–78	3000 cycles at 100% DOD	200–600
Lithium ion	≈100	3000+ cycle at 80% DOD	700–1000

In Table 2-1, a basic comparison of three characteristics among four common available battery technologies is summarized. It can be observed that the Lead-acid is the cheapest technology in the market. The valve regulated type of Lead-acid battery (VRLA) is sealed, so it has less risk of liquid leaking in comparison with flooded type. Moreover, this type of lead-acid battery is completely maintenance free. It will be introduced in detail in the next section.

Taking all the requirements into consideration, two representative technologies, Lead-acid (valve regulated type, cheapest one) and $LiFePO_4$ (best performance with good stability) have been chosen to be compared in this thesis.

2.3.2 Chemical basics

2.3.2.1 $LiFePO_4$ battery

The basic mechanism of Li-ion battery operation is reversible lithium insertion/extraction. [23] The extracted Lithium ions move from anode to cathode and insert into the cathode when discharging and the situation is in reverse when charging. Figure 2-2 illustrates the operational mechanism of Li/$FePO_4$ battery when discharging and Figure 2-3 shows the structure of (Li)$FePO_4$.

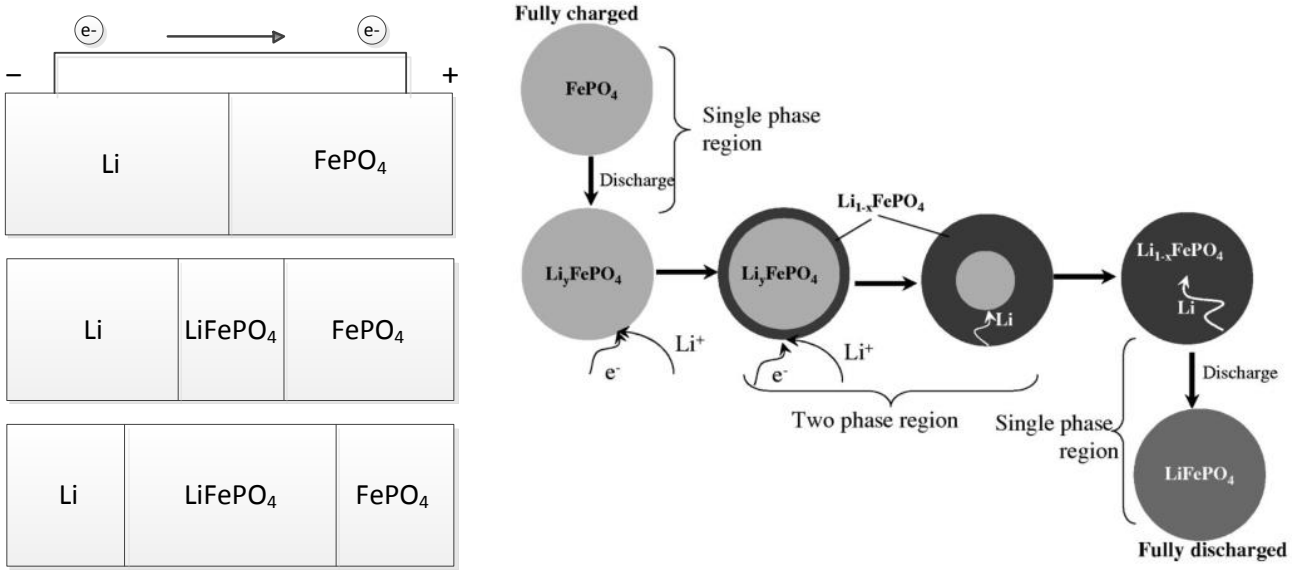

(a) Schematic representation of Li/$FePO_4$ cell construction in different discharge stage

(b) The illustration of one model which hypothesizes the juxtaposition of Li^+ at the cathode and the movement of the phase boundary[18]

Figure 2-2 Mechanism of Li/$FePO_4$ battery when discharging

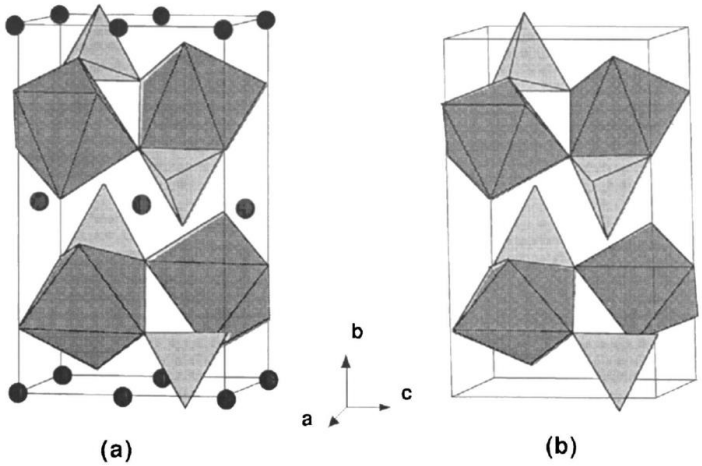

Figure 2-3 Crystal structure of (a) $LiFePO_4$ and (b) $FePO_4$ (Fig.6 of [23])

The reactions of Li^+ extracted from $LiFePO_4$ to charge the anode and Li^+ inserted into $FePO_4$ during discharge are expressed in (2.10) and (2.11) respectively. [23]

$$LiFePO_4 - xLi^+ - xe^- \rightarrow xFePO_4 + (1-x)LiFePO_4 \quad \textbf{(2.10)}$$

$$FePO_4 + xLi^+ + xe^- \rightarrow xLiFePO_4 + (1-x)FePO_4 \quad \textbf{(2.11)}$$

The overall reaction is written as:[18]

$$FePO_4 + Li^+ + e^- \underset{\text{Charge}}{\overset{\text{Discharge}}{\rightleftharpoons}} LiFePO_4 \quad \textbf{(2.12)}$$

Two typical LFP battery charge/discharge voltage curves for different C-rates and with different lifetime conditions are shown in Figure 2-4. It can be observed that the nominal voltage of LFP during discharge is around 3.3V.

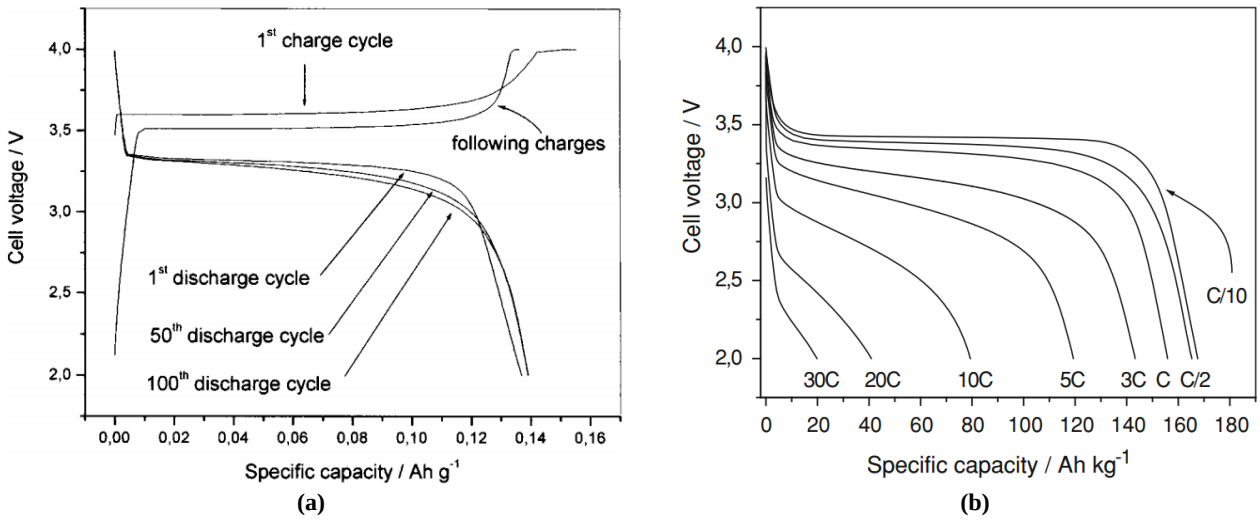

Figure 2-4 (a) Charge and discharge voltage profile at different cycle numbers with 1C (Fig. 3 in [24]); (b) Discharge voltage profile with different C-rate (Fig. 8.8 a in [25]) ;

2.3.2.2 Lead-acid battery

The lead-acid battery has a long history and is almost the cheapest storage battery for any applications. A Lead-acid battery is basically composed of PbO_2 anode and Pb cathode immersed into the sulphuric acid solution H_2SO_4. Under normal conditions, the reactions occurs on Anode are:[26]

$$\begin{aligned} PbO_2(s) + 4H^+ + 2e^- &\underset{\text{Charge}}{\overset{\text{Discharge}}{\rightleftharpoons}} Pb^{2+} + 2H_2O \\ Pb^{2+}(aq) + SO_4^{2-}(aq) &\underset{\text{Charge}}{\overset{\text{Discharge}}{\rightleftharpoons}} PbSO_4(s) \end{aligned} \tag{2.13}$$

The reactions take place on Cathode side are: [26]

$$\begin{aligned} Pb(s) &\underset{\text{Charge}}{\overset{\text{Discharge}}{\rightleftharpoons}} Pb^{2+}(aq) + 2e^- \\ Pb^{2+}(aq) + SO_4^{2-} &\underset{\text{Charge}}{\overset{\text{Discharge}}{\rightleftharpoons}} PbSO_4(s) \end{aligned} \tag{2.14}$$

The overall reaction of the lead-acid battery is expressed as: [26]

$$Pb(s) + PbO_2(s) + 2H_2SO_4(aq) \underset{\text{Charge}}{\overset{\text{Discharge}}{\rightleftharpoons}} 2PbSO_4(s) + 2H_2O(l) \tag{2.15}$$

As can be seen in the chemical formula (2.13) to (2.15), unlike the ion transport mechanism in the Li-ion battery, the mechanism of the Lead-acid battery is a dissolution-precipitation, and these reactions are known as double-sulphate reactions.[2]

General, the Lead-acid battery has a nominal voltage of 2 V during discharge, and its cut off discharge voltage is around 1.7 V. When charging or discharging the battery, the concentration of the H_2SO_4 solution (or Specific gravity) varies with the battery SOC level. A schematic of the voltage change and the corresponding variation of the Ah level, specific gravity level are shown in Figure 2-5.

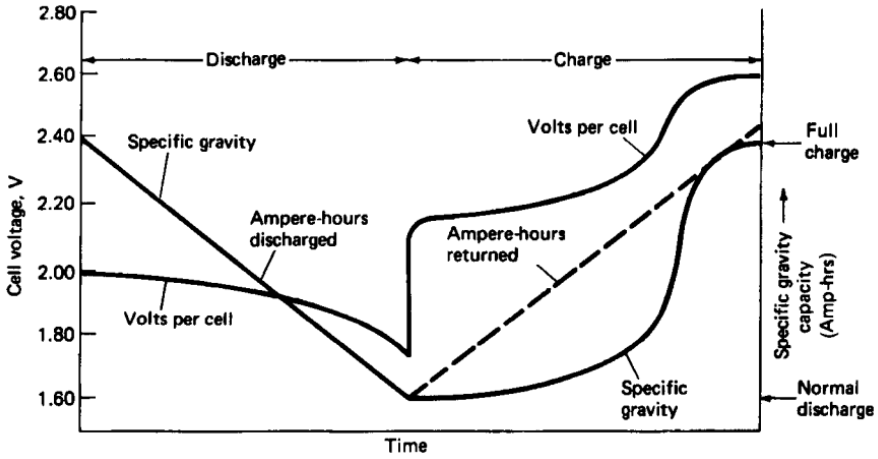

Figure 2-5 Variation of Voltage, Ah level, Specific gravity level when charge/discharge in constant rate [2]

The lead-acid battery is thermodynamically unstable in open circuit condition and when overcharged. In these cases a self-discharge process will happen on each electrode and leads to gassing as well as water decomposition.[27] It is reported that the gassing reaction may happen when the battery voltage reaches 2.35-2.4 V approximately, which is when the SOC is around 75-80%. From then, the water decomposes while the battery is charging and the charge acceptance is gradually and continuously reduced until the battery is fully charged. [26] The gassing voltage also changes with temperature. The overcharge (when remarkable gassing happens) voltage is 2.39V at 25 ℃, this value changes inversely with the temperature variation.[2]

The gassing reactions which occur on the Anode and the Cathode are written in (2.16) and (2.17) respectively. [27]

$$PbO_2 + H_2SO_4 \rightarrow PbSO_4 + H_2O + \frac{1}{2}O_2 \quad \textbf{(2.16)}$$

$$Pb + H_2SO_4 \rightarrow PbSO_4 + H_2 \quad \textbf{(2.17)}$$

Due to the gassing and water decomposition, regular maintenance is necessary for conventional lead-acid battery (flooded lead-acid battery). The maintenance is mainly to refill the water. Water should be refilled after recharge and to reach the high acid level line. The refilled water should be either distilled, deionised or demineralised water.[27]

In order to overcome this problem, the Valve Regulated Lead-Acid (VRLA) Battery, also called Sealed Lead-Acid battery or maintenance free Lead-acid battery, was invented. The basic idea of this new-generation lead-acid battery is either absorb a little electrolyte in the separator or immobilise the electrolyte in the gel.[2] The former type of VRLA is called absorptive glass mat (AGM) and the latter type of VRLA is called Gel VRLA.

This designation is meant to force the formation of "oxygen-recombination cycle" at the Cathode. The oxygen generated at the Anode goes through fissures (in Gel VRLA), or through channels (in the AGM VRLA) to the Cathode and is recombined to water. The reaction is written as:[28]

$$Pb + \frac{1}{2}O_2 + H_2SO_4 \rightarrow PbSO_4 + H_2O + Heat \quad \textbf{(2.18)}$$

Simultaneously, the Hydrogen is still generated, but is limited to a very low rate since the oxygen cycle shifts the potential of the cathode to a much lower level. The accumulated Hydrogen can be released by a valve to make sure that the cell will not suffer from high pressure, that is where the name "valve regulated" came from.[28] As long as the overcharge current remains low (≤0.01C), the hydrogen production rate can be balanced by the corrosion rate of the Anode. If the recharge rate is too high after the cell is fully charged, the

oxygen recombination rate is slower than the oxygen generation rate, then the cell may start venting and result in more irreversible water losses.[29]

Nevertheless, there is still water loss happens from Hydrogen generation during the lifetime of the cell and the consumed water cannot be refilled like a flooded Lead-acid battery because the VRLA is expected permanently sealed.[28] There is no demand of regular gas release and water refill, causing the VRLA "maintenance free".

2.3.3 Battery specifications

For single battery cell, there are three main shapes of LFP and two main shapes of VRLA.

The LFP single cell can usually be found in three different shapes: the cylindrical cell, often with a solid case; the prismatic cell, often with a semi-hard plastic case and the pouch type single cell, often with a soft, flat case. Which means the cylindrical cell is more rigid than the other two types. Cylindrical cells contain spirally-wound electrodes, which is favourable in fabrication and the solid cylindrical container can provide even distribution of pressure on electrodes symmetrically.[30]

Two main shapes of VRLA single cell are: cylindrical and prismatic. The cylindrical container can sustain higher internal pressure and relatively higher temperature without deformation than the prismatic design. [2]

Furthermore, even cylindrical cells cannot stack as dense as prismatic cells when scale-up, the cylindrical cells will not be hindered by the dimensions like prismatic cells.[31] Therefore, the cylindrical shape cells are chosen in this thesis.

Two battery cells chosen for the experiments in this thesis are A123systems® APR26650M1B and Cyclon® AGM D single cell. The battery specifications are listed in Table 2-2

Table 2-2 Specifications of the battery that picked for experiments[32][33]

Specifications	A123systems® APR26650M1B	Cyclon® AGM D single cell
Cell Dimensions (mm)	Ø 26 × 65	Ø 34.2 × 61.5
Cell Capacity (nominal, Ah)	2.5	2.5
Voltage (nominal, V)	3.3	2
Operating Temperature	-30 ℃ to 55 ℃	-40 ℃ to 80 ℃
Life Cycles	Discharge@10C, 100% DOD: >1000	Discharge@ 0.1C, 100% DOD: ≈300
		

2.4 Battery modelling introduction

As introduced in Chapter 1, one of the objectives of this study is to model the chosen battery. The behaviour of the battery can be divided into two parts according to the time scale: long term behaviour and short term behaviour. The short term behaviour is more related to the dynamic response of the load under certain environmental conditions, for example, the voltage response, the state of charge and the battery temperature variation. These behaviours can be observed within one cycle. Modelling the short term behaviour of a battery is helpful in obtaining useful parameters which may apply in the battery lifetime modelling. It can also be used in the development of the battery control/manage system.[34] In this thesis, the short term behaviour of the battery model is called **battery dynamic model**.

The long term behaviour of a battery is a result of the accumulated short term behaviours. It is mostly reflected on the battery capacity and power fading. Modelling the battery long term behaviour is another objective of this

study. During the lifetime of a battery, its performance will continuously get worse in comparison to a new battery. When the battery reaches its end of life, it is considered as cannot be used anymore, which means obsolescence. A proper long term battery model can play a vital role in battery usage determination and battery replacement prediction.[35] In this thesis, the long term battery behaviour model is called **battery lifetime model**, or **state of health (SOH) model**.

2.4.1 Battery dynamic model

2.4.1.1 Introductions

Many efforts have been putting into the establishment of battery models. Depending on the accuracy, complexity, compatibility and universality, there are several technical methods to approach an expected battery model. Generally, there are three levels of battery model according to the degree of physical insight: white box (i.e. electrochemical/physical model), grey box (e.g. equivalent electrical circuit model) and black box (e.g. artificial neural network).[34] In order to reach different requirements, there are four criteria [36] that can be used to evaluate whether a battery model is suitable or not:

- Accuracy. To what extent does the model represent the behaviour of a real battery? Do all of the battery external variables match to the experimental results (e.g. voltage, current, SOC)? Can this model display the dynamic performance of a battery? Is the long term behaviour of the battery included in the model?
- Configuration effort. Is the in-depth chemical theory required while building the battery model? Is the number of variables acceptable and how many parameters are able to be represented by this model?
- Computational complexity. Will the simulation take a long time?
- Analytical insight. How can the reflection of battery kinetic and the understanding of its chemical mechanism be obtained from this model? Are these explorations in battery modelling sufficient and efficient?

There are many methods to model the behaviour of a battery. Summarised from literature review, it is found that common modelling methods can be classified into five categories.

- Electrochemical/physical model
- Experimental model
- Analytical model
- Abstract model
- Bio-inspired black box model.

The electrochemical model looks deep inside of a battery and describes the chemical reactions happen in the battery. It is the most accurate, but the most complex model among all these five categories. More than 50 parameters need to be set during modelling, which requires a high level of background knowledge and understanding of electrochemistry from the designer or user. Due to its high accuracy, electrochemical models are now mostly used to evaluate other models instead of simulation for the application.[37]

The experimental model describes particular features of the battery by using simple equations that obtained from experiments. Since the relation between battery behaviours and the unknown variables are measured from experiments, it is easy to configure but only suitable for specific cases. This model also has the lowest accuracy and less requirement of thorough understanding of electrochemical theories.[34][36]

Analytical models are always intuitive, and it describes the battery behaviour by expressing some typical processes. For example, Rakhmatov and Vrudhula's model describes the diffusion process of active material in the battery and Kinetic Battery Model using chemical kinetic progress as its theoretical basis.[37][38] Analytical models require a fairly deep understanding of the battery and have a good precision.

Abstract model provides an equivalent representation of battery behaviour. These models have less analytical explorations of battery but have good compatibility with other components in the system.[36] One

representative example is equivalent electrical circuit model, which is easily built and commonly used by electrical engineers.[39] Discrete-time model and stochastic model are also in the group of abstract model.

The Bio-inspired black box method uses intelligent models, e.g. Artificial Neural Network (ANN) and Support Vector Machine (SVM) to present the battery behaviour. The performance of black-box models is largely depending on the earlier stage training procedure as well as the data that is used. In-depth understanding of electrochemical knowledge is also not mandatory when using this type of models. However, for the accuracy purposes, large amount of parameters is often required. [40]

As a summary, the comparison of these five battery categories is listed in Table 2-3.

Table 2-3 Comparison of five battery model categories [34][36]

Model type	Accuracy	Computational Complexity	Configuration Effort	Analytical Insight	Applications
Electrochemical	Very high	Very high	Very high	Low	Battery design
Empirical	Low	Very Low	Low	Medium	Only for constant operating conditions
Analytical	High	Medium	Low to Medium	High	Task scheduling, analysis of discharge methods for multi-battery systems
Abstract	Medium	Medium	Medium to High	High	Real-time Control, SOC estimation
Black-box	Medium	Medium	Medium to High	Low	Off-line analysis

2.4.1.2 Equivalent electrical circuit model

The equivalent electrical circuit model (EECM) has a good compromise of computational time, precision, complexity and exploration depth. The EECM models the battery with only electrical components so it has a good compatibility with other electrical models and it is easy to implement on battery management systems. Moreover, the construction of EECM does not have a much comprehensive co-relation with (does not require too much understanding?) the electrochemical processes inside the battery, hence battery modelling by EECMs do not have any limitation on distinct battery types. That means EECMs can be used to simulate batteries of different technologies.[41]

The commonly seen EECMs can be divided into two main groups: the Impedance based model and the Thevenin model. Usually, a Thevenin model has one or more pairs of resistor-capacitor that connected in series, and an Impedance model often includes frequency-dependent non-ideal electrical elements. [42]

For different types of cells, there are several common functional elements:[37], [38]

- A capacitor representing the capacity of the cell in unit of Ah;
- A discharge-rate normaliser to determine the lost capacity at high discharge rates
- Some electrical components to indicate the internal resistance of the cell;
- An OCV (open circuit voltage) vs SOC lookup table
- An external circuit as the load

All the important battery characteristics and the electrochemical kinetics, which are expected in a battery model, can be presented in an EECM in different forms. Apart from the construction, the parameter extraction method is disparate between two model types. The parameters for a Thevenin model can be extracted by pulse charge/discharge experiments and step response analysis, which is measured from battery's external behaviour. The parameters in Impedance model are obtained from the experimental results of Electrochemical Impedance Spectroscopy (EIS), which is an insight into battery's internal chemical characteristics.[42][43] Apparently, the impedance-based model has higher accuracy but the Thevenin model is less time consuming, but both of them can be combined and complement each other. It will be introduced in detail in Chapter 3.

2.4.2 Battery lifetime model

Long term battery modelling has several similar ways of expression, for example battery life time prediction model; battery ageing/capacity degradation model and battery state of health model.

All of them have the purpose of showing how much irreversible damage has occurred or how long the battery can last before obsolescence on a long term scale. The quantification of the end of life (EOL) point is different for various battery technologies. The EOL for a sealed nickel-cadmium cell is considered to be when it can no longer provide 80% of its rated capacity.[7] The li-ion battery end of life is defined as: when the usable capacity in the cell is less than 70-80% of the rated capacity or the peak power capability is less than 70-80% of the rated power.[44][45][46] The end-of-life point of a lead-acid battery is defined as 80% rated capacity.[29]

The battery ageing properties can be modified from both time and usage scale. If only took time has passed since the fresh battery into consideration, the ageing is called calendar ageing. The cycle ageing is named from the depletion because of purely usage since a fresh battery. In another word, the calendar ageing is the battery getting demolished when the battery under storage conditions and cycle ageing is battery getting faded by operating. In this study, the battery performance is explored for off-grid SHSs applications, which has an intensive cyclic requirement on the battery. Additionally, the focus of this study is how the long-term battery performance influenced based on its usage. Therefore, the battery ageing during only cycling is explored.

Generally, there are two approaches to estimate the long term behaviour of the battery: the weighted throughput model and the performance based model. The weighed throughput model can estimate the left lifetime of a battery by comparing its capacity-throughput (in unit of Ah), power-throughput (in unit Wh) or equivalent cycle numbers to the suggested throughput value at the end of life (EOL) point. The word “weighed” means stress factors of different usage conditions are weighed-counted in comparison to the reference throughput value. The performance based model keep monitoring or simulating the battery, and noting down the changes of the battery’s performance continuously. If its performance drops below a pre-set threshold, this battery is considered reached the EOL point. The performance of the battery often refers to its representative parameters, e.g. capacity, high-rate discharge power and charge-acceptance. [35][47][48] Even though the weighted throughput is simple and is possible to provide the estimated battery lifetime immediately, the performance based model is more accurate. Moreover, predicting the battery lifetime according to its performance is intuitive. Hence, the performance based battery lifetime prediction method was chosen in this study. The detailed introduction is in Chapter 4.

The application of performance based model requires a battery dynamic model which can simulate the battery performance. The following models can meet the demand:[35][47]

- Electrochemical models
- Equivalent circuit models
- Analytical models
- Artificial neural networks (ANN)

All of these models have been introduced in Section 2.4.1.1.

3 Battery dynamic behaviour modelling

3.1 Introduction

This chapter introduces the approach used to model the equivalent electrical and dynamic battery behaviour. The modelling approach is built from kinetic and electrochemical systems theory. Behind all these work is the support of the kinetic and electrochemical theory of electrochemical systems.

The first section presents an introduction to the substantial mechanisms of such systems.

3.1.1 Kinetics of battery reactions

The battery charge and discharge actions are chemical reactions. The thermodynamic characteristics of materials determine whether a chemical reaction can occur spontaneously while the kinetic properties determine the rate of the reaction. To simulate the dynamic behaviour of a battery, the kinetics of chemical reactions need to be considered in the model.

The fundamental principle of batteries is the redox reaction. Two electrodes are oxidised or reduced in the electrolyte. Equation (3.1)[8] shows the basic reactions occurring in both electrodes, and Figure 3-1 illustrates the basic reactions are happening in an electrochemical cell when discharging.

$$O_x + ne \rightleftharpoons \text{Red} \tag{3.1}$$

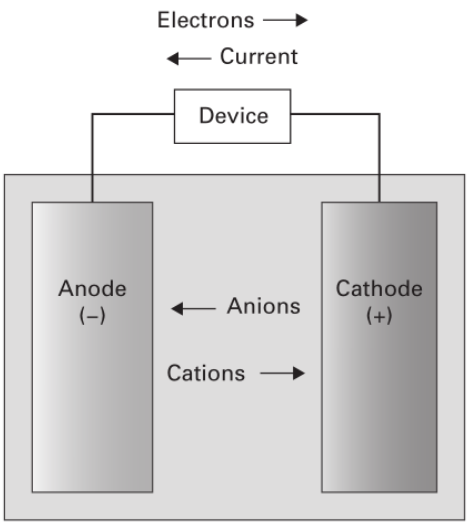

Figure 3-1 Basic component and reaction of an electrochemical cell while discharging spontaneously (Fig. 5-1 in [5])

In ideal conditions, when the battery is in an open circuit state, the reactions that occur in both electrodes are in an equilibrium state. The standard cell voltage is equal to the potential gap between the two electrodes, as mentioned in Section 2.1. However, the situation will be different when the cell is connected to a load. When

there is a current flow out of/into the battery, the cell voltage will deviate from the equilibrium state. The external load polarise two electrodes and leads to an overpotential (overvoltage) inside the battery. With the potential difference, there is anions/cations flow between the two electrodes, with which the battery is charged/discharged. Basically, two main characteristics need to be presented in a dynamic model: the charge storage ability and the electrical response behaviour to the load. The charge storage ability is related to battery capacity, and the electrical response refers to the voltage behaviour of the battery. The product of these two features (capacity and voltage) is the energy storage ability of the battery. For the charge storage ability, the most important characteristics are: battery capacity and the coulombic efficiency, which has introduced in chapter 2. This efficiency is related to side reactions inside the battery. The voltage response behaviour is dependent on the battery's internal constructions and its chemical characteristics.

There are two main principles cause the overpotential[8]:

a) "Ohmic" or "i^2R" loss in the bulk of the electrolytes phases.

b) "Electrode" losses which include "activation voltage" and "concentration overvoltage". The activation voltage is related to the charge transfer process on the electrode-electrolyte interface. The "concentration overvoltage" may be caused by depletion and accumulation of electro-active materials near the electrode surfaces.

Hence, the overpotential can be expressed by equation (3.2):[5]

$$E_{polarization} = E_{ohmic} + E_{activation} + E_{conventration} \tag{3.2}$$

This equation can also be rewritten as equation (3.3):[2]

$$E = E_0 - \left[(\eta_{ct})_a + (\eta_c)_a\right] - \left[(\eta_{ct})_c + (\eta_c)_c\right] - i \times R_i = i \times R \tag{3.3}$$

Where:

E_0: Electromotive force or open-circuit voltage (OCV) of the cell;

$(\eta_{ct})_a$; $(\eta_{ct})_c$: Activation polarisation or charge-transfer overvoltage at the anode and the cathode;

$(\eta_c)_a$; $(\eta_c)_c$: Concentration polarisation at the anode and the cathode;

i: Operating current of the cell on load;

R_i: Internal resistance of the cell;

In **Figure 3-2**, the contributions of polarisation are drawn versus the different current level and the different capacity level.

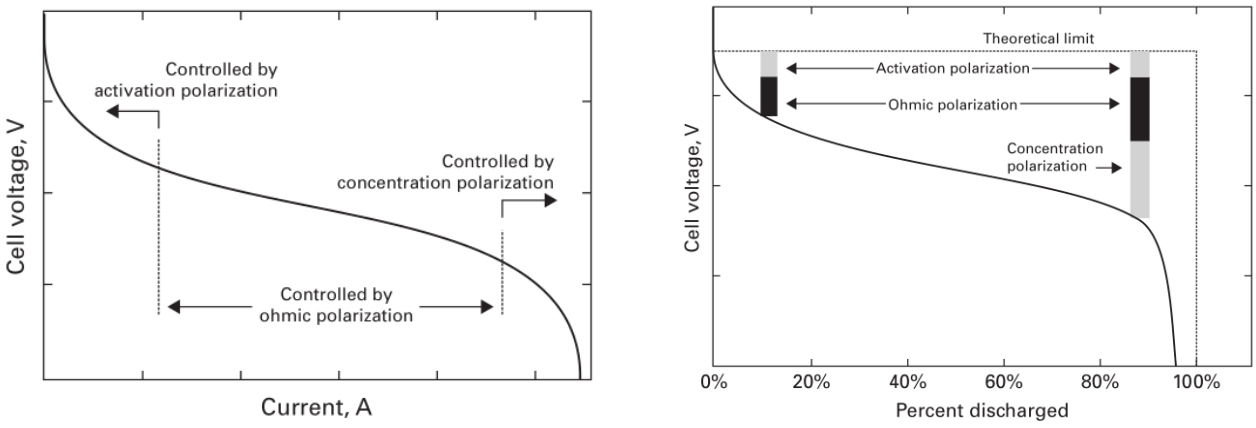

Figure 3-2 Polarization versus (a) Operating current; (b) Capacity that has been discharged. [5]

This kinetic property of a battery is important in the modelling process. In order to understand the mechanism behind it, the solid-solid and solid-liquid interfaces inside a battery need to be considered. The physic properties,

especially electrical characteristics change dramatically at the interfaces, leading to a unique electrical conductivity distribution in the system. When a potential difference is applied on this system, e.g. an external voltage source, each of the interfaces in the system will be polarised exclusively. [49] This contributes to the polarisation inside the battery, which is observed as a voltage drop.

The Electrochemical Impedance spectroscopy (EIS) method is one approach to investigate the bulk or interfacial region inside electrochemical systems based on this concept. The EIS technique is basically applied small amplitude sinusoidal perturbation (current or voltage) with a certain frequency range on the target electrochemical system, and then measuring the complex impedance of this system. The observed impedances are the electrical responses from the bulk and interfacial region materials inside the electrochemical system. These measured impedances can be plotted in a complex plane, which is called Nyquist plot and used to portray the target electrochemical system.[49][50]

The interpretation of the complex impedance plot can be an analytical, mathematical method, or the well-known equivalent electrical circuit (EEC), which has been selected to model the battery in this thesis, as explained in section 2.4.1. Moreover, the EIS method is used to detect the intrinsic electrical properties of the battery and an EEC can produce a model which can physically explain the processes occurring in the system, to some extent.[51]

Even though the electrical components in the EECM of a battery are correlated with some chemical processes and the selected initial proposed construction of an EECM is based on the EIS experiments, the implementation of an EECM is quite different to a pure EIS method:[52]

1, EIS measurements use an AC current with a broad range of frequency, while an EECM treats electrical components as independent of the frequency.

2, The EIS result may show different characteristics of the positive and the negative electrode as well as those of their interface with the electrolyte of the battery separately. On the contrary, an EECM treats the features, such as polarisation, transfer and diffusion phenomenon from both electrodes as the entire characteristic of the whole battery.

3, When the EEC components are determined, the parameter extraction of these components could be simply curve fitting.

Nevertheless, the EIS exploration can instruct how to choose electrical components in modelling the battery with equivalent electrical circuit model.

3.1.2 Construction of the proposed EEMC

In order to build an accurate model of the battery, the first step is to clarify how an equivalent circuit can represent the model. A good battery model should capable of predicting both the battery storage capability information and the voltage response to the load. An electrical circuit model can describe both of these characteristics.[39]

3.1.2.1 Storage circuit

A circuit representing the battery charge storage is required to simulate: the battery capacity (which is the charge storage ability), and the amount of charge is left in the battery (which is SOC).

It should be noticed that the amount of electric charge that flows in and outside of the battery is subject to losses. As explained in Chapter 2, neither all the current applied on a battery can be effectively stored nor all the charged available inside a battery can be retrieved successfully. Hence, only the **mian branch current** is count in the storage circuit, which is the electric charge flow that can be authentically stored in the battery and able to be extracted out completely.

There are three parameters should be modelled in the storage circuit: the accessible battery capacity, the SOC and the open circuit voltage.

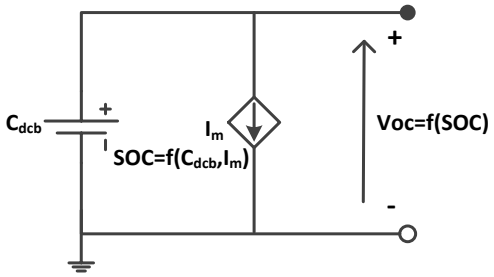

Figure 3-3 Illustration of charge storage circuit represented by EEC (modified from [42])

3.1.2.2 Voltage response circuit

A voltage response circuit model focuses on the internal structure of the battery, with which it is possible to imitate the electrical response of the battery under different loads.

Despite the technology, all of the batteries share common components, e.g. electrode-electrolyte interface, bulk electrolyte and separator. This allows the creation of a common EEC kinetic model which can be evaluated for different technologies.[49] In an electrochemical system consisting of electrodes, bulk media and the electrode-electrolyte interfaces, there are several typical chemical processes which can be detected and modelled by corresponding electrical components. These are summarised in Table 3-1.[51]

Table 3-1 Electrochemical processed and the interpreted electrical components

Electrochemical processes	Places where processes happen	Example of electrical components
Electric charging of the electrochemical double layer	Between the interface of electrode and its surrounding electrolyte	Capacitor
Sorption (adsorption and desorption) of charged species	At the interface, primarily in the compact portion of the double layer at the electrode surface	Sorption impedance
Faradaic charge transfer	Near the electrode surface in the double layer	Charge transfer resistor
Impedance related to mass transportation	Diffusion mainly happens between electrode surface and electrolyte because of concentration gradient, forming a diffusion layer	Detected as complex diffusion impedance
	Migration and convection mainly in bulk electrolyte: forming;	Resistor
Conduction and relaxation phenomenon	The bulk media and other components in this system	A conduction resistor or inductor

EIS experimental results can provide a reference when constructing the EECM. For one Nyquist plot of a battery, there is more than one way to translate the measured EIS results into an electrical circuit, but there are basically three elements that exist in the circuit without any doubts according to many authors.[53]–[61] They are: an ohmic or bulk resistor serves as media conduction resistance, an RC pair where R is the charge transfer or polarisation resistance and C represents the double layer. How to choose and assemble the rest of the electrical components are dependent in each case. Conclusively, a common EECM which works for both battery technologies can be encapsulated as follows.

For both battery technologies, the **conductivity** of the electrolyte is modelled by a resistor since the resistance from the electrolyte is proportional to the current. This resistor is an **ohmic resistor**. At the interface between the electrode and the electrolyte, there is a double layer exists, which acts exactly like a capacitor and it reflects the effective area for charge transfer reactions.[62] Therefore, a small **capacitor** is used to simulate the charge/discharge of the **double layer** (C). However, the current will continuously conduct through the double layer after the layer has been charged/discharged. That means the single capacitor will cause an open circuit

when it is fully charged, which is unconformity with the real battery behaviour. Hence, a resistor is modelled in parallel with the capacitor to represent the charge transfer process. [58][63][26] The **resistor** is meant to model the barrier of the interface. When the electrode is at its standard potential, the barrier is called **charge-transfer resistance** (R_t) and when the electrode is at a non-standard potential, the barrier is called **polarisation resistance**, R_p.[63] Apart from that, another component is required to simulate the diffusion of ions in the electrode-electrolyte interface and in the bulk of the electrolyte. A **pseudo-capacitor** or **frequency-dependent Warburg impedance** can be used to model the electrolyte **diffusion phenomenon** [58][61][26].

However, all of these elements are on the electrode level, which means a complete battery model may need two series of the components mentioned above. Some authors used two pairs of RC circuits to represent the reactions that happen at two electrodes separately [55], [62], [64]. For the electrical engineering application, it is too complex to model each electrode separately. Some authors also simplify the model for both electrodes at the same time by using one set of EEC since both electrodes contribute to the reactions mentioned above [52], [65]. A schematic diagram of half-cell, which is a specific electrode-electrolyte interface, and a figure of one complete battery cell is shown in Figure 3-4.

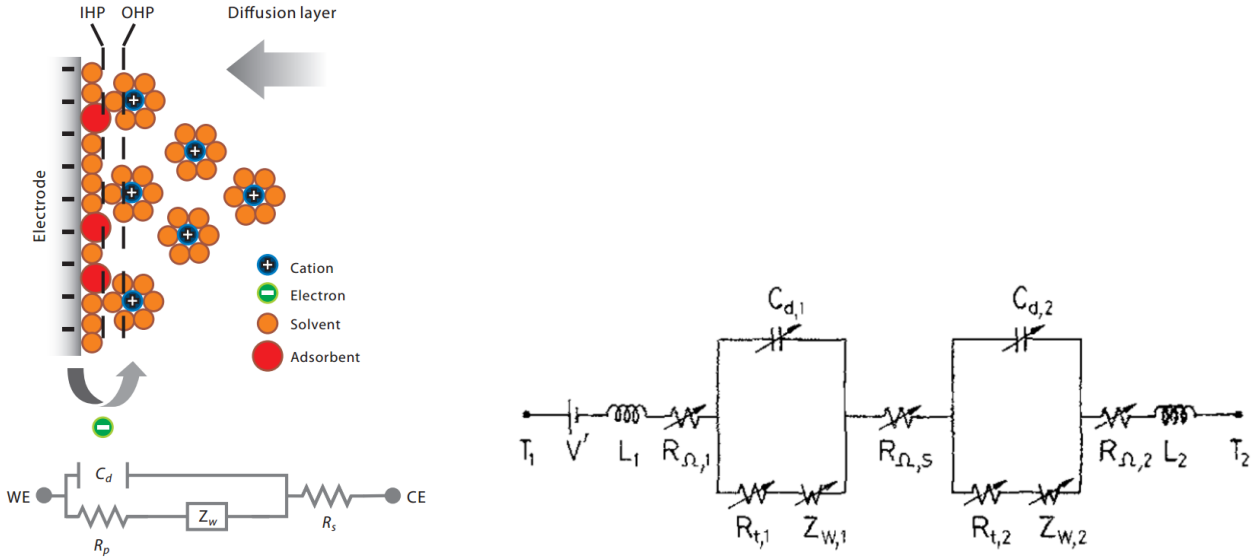

(a)

(b) all the elements with suffix 1 means one electrode and 2 represents the other electrode; suffix s means the solution and the separator

Figure 3-4 (a) The chemical component, reaction and their corresponding electrical component in half-cell.(Fig.1-a in [63]); (b) A sample EECM of one complete battery cell consisting two electrodes(Fig.1 in [62])

Although two battery technologies share similar basic EECM format, there are some different components between them. For comparison, sample electrode-electrolyte interface EIS detection Nyquist plots of both technologies and their corresponding EEC are presented in Figure 3-5 and Figure 3-6.

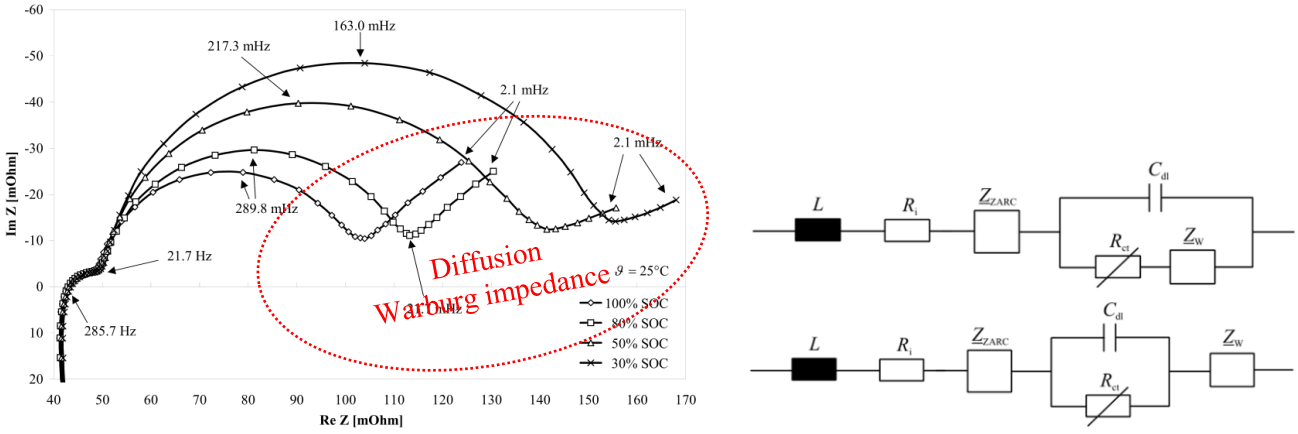

(a) (b)

Figure 3-5 (a) Sample impedance spectra of a Li-ion battery at different SOC (Fig. 5.4 in[66]); (b) Two simplified EECM of Li-ion (Fig 5.8 & 5.9 in [66])

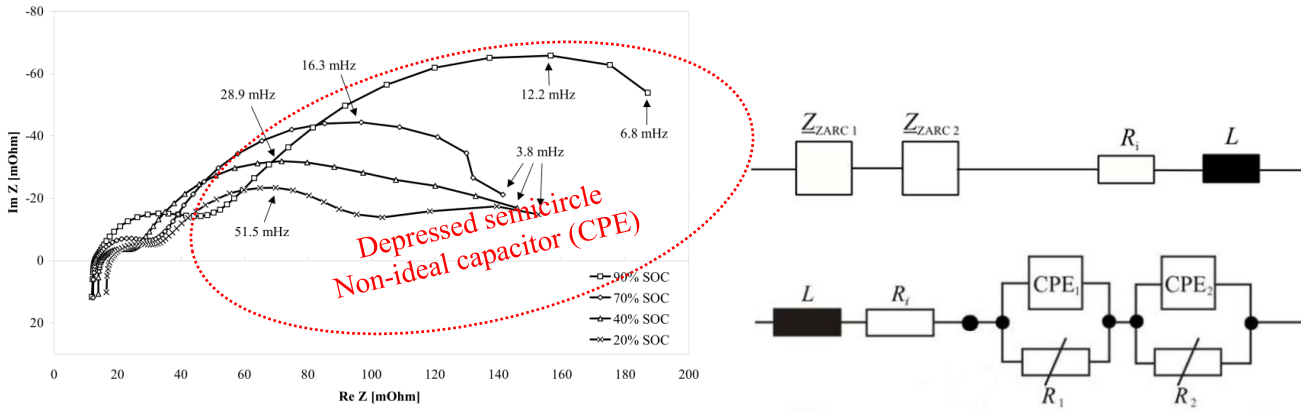

(a) (b)

Figure 3-6 (a)Sample impedance spectra of a VRLA battery at different SOC; (b) Two simplified EECM of VRLA (Fig 6.10 in [66] and Fig. 8 in [54])

The diffusion phenomenon which is detected as a 45° 'tail' in the red dash-line circle in Figure 3-5(a), can be hardly observed in a lead-acid battery in comparison to LFP battery. That is because the chemical process during the charge/discharge of a Li-ion battery is dominated by Li ion diffusion between two electrodes. On the contrary, the diffusion of ions in lead-acid batteries is mainly occurring between the electrolyte bulk and the electrodes. Hence, in some simplified models, the diffusion influence was neglected in the electrode of the lead-acid battery, which means the Warburg impedance can be eliminated from the electrode-electrolyte interface. [62][66]

For the Nyquist plots of both battery technologies, the curve contains an arc shape in the middle-frequency range. However, the arc curve of a lead-acid battery is not as ideal as that of an LFP's. This depressed semi-circle that is marked in a red dash-line circle in Figure 3-6(a) is often modelled by the non-ideal electrical component — ZARC element, which is a resistor in parallel with a constant-phase element (CPE). In an ideal case, the CPE transforms into a normal capacitor. [53][67]

However, some modelling tools cannot simulate non-ideal electrical elements intuitively (e.g. ZARC elements and Warburg impedances). In this case, these non-ideal elements can be simplified and replaced by common electrical elements or their combinations. [59] The approximation of ZARC element could be a series of RC circuits, and the estimation of Warburg element can be a ladder network of RCs.[66] The Warburg element can be further simplified into a serial connection of RC circuits. [66][68]

Hence, a further simplified EECM to represent the internal impedance and the voltage response of a battery is series of RC pairs, which is equivalent to the construction of Thevenin model. One diagram of the electrical response circuit is shown in Figure 3-7 and the number of RC pairs in called the order of RC circuit, e.g. two RC pairs is called 2nd order RC circuit.

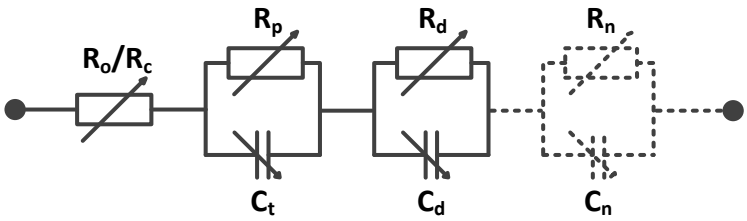

Figure 3-7 Illustration of electrical response circuit

3.1.2.3 Parasitic circuit

The electrical components interpreted in the previous subsections describe the behaviour of the battery based on its main reactions. However, additional elements need to be used to model a parasitic branch considering side reactions (losses) inside the battery. During operation, not all the energy input of a battery becomes involved in its main (charging/discharging) reactions. The rest losses may be consumed in side-reactions like gassing. Moreover, when the battery is at idle, there are still side reactions happening such as self-discharge on both electrodes.

As introduced in the Chapter 0, this study focuses on applying a battery in an off-grid SHS, which requires a heavy daily usage, meaning that there is almost no idle time for the battery. Moreover, both Li-ion and VRLA batteries have relatively low self-discharge rate, around 4-10% capacity per month for VRLA and 2-5% per month for Li-ion (Table 3.1 in [11] & Table 7.2 in [5]). Moreover, it is considered that for VRLA, the self-discharge will become a problem only when the cell was stored without regular freshening charge.[69] Hence, in this thesis, the battery self-discharge in idle is neglected, and the parasitic branch modelling focus only on the losses present under operation.

For modelling the gassing reaction of VRLA battery, a conductor in series with a power source is often chosen. The parasitic is usually constructed as a resistor if the targeted side reaction is self-discharge.[39][66][70][71] The illustration of the parasitic branch circuit is in Figure 3-8.

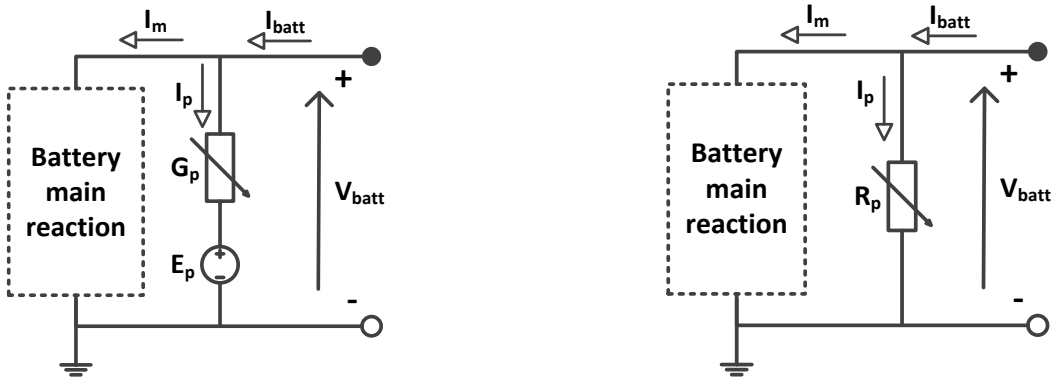

(a) **(b)**

Figure 3-8 Illustration of parasitic branch (modified from[39][66][70][71])
(a) parasitic branch meant for modelling gassing loss
(b) parasitic branch meant for modelling self-discharge loss

3.1.2.4 Overall battery EEC construction

As a summary, for both battery technologies, some part of the model is slightly different but they share the basic common construction of EEC which is shown in Figure 3-9.

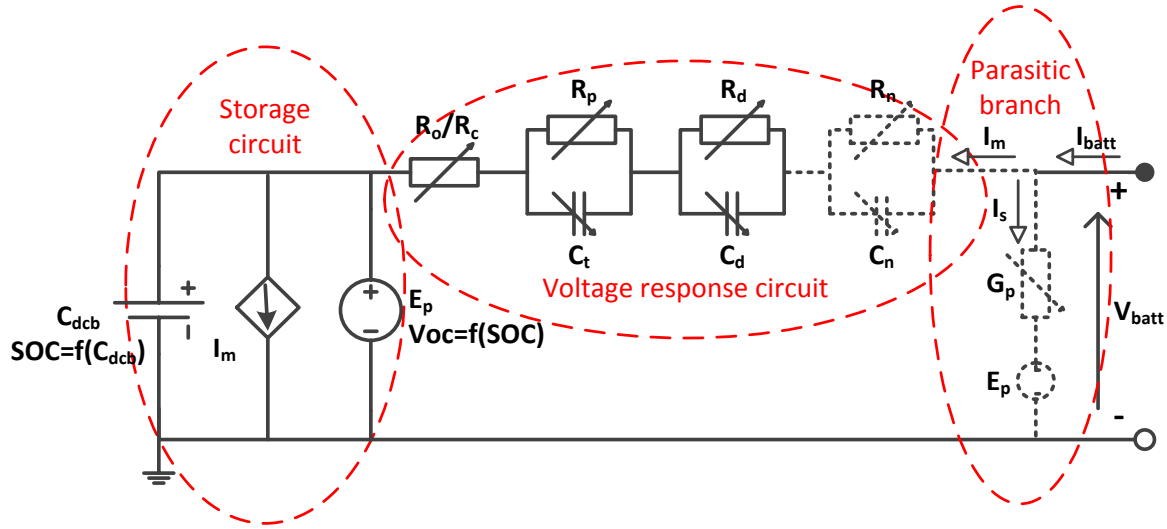

Figure 3-9 Illustration of the overall EECM construction

C_{dsb} represents the maximum dischargeable battery capacity, *Ep* is the electrical motive force, which replaced by the close to equilibrium open circuit voltage.

3.2 Proposed battery model

3.2.1 Lead-acid battery model

The dynamic behaviour of the battery is firmly influenced by the conditions under which the battery is operating. In order to model the behaviour of a lead-acid battery, how the performance (i.e. the actual capacity, voltage and efficiency) of the battery is affected by the operational or environmental conditions should be summarised. This subsection describes the battery model used in this study, together with the factors considered to affect the behaviour of the battery.

3.2.1.1 Storage circuit

a) Capacity

One of the most important characteristics of a battery is its capacity. As defined in Chapter 2, the actual capacity is used in this model.

Within a temperature range, 10 to 30 ℃ in this case, the battery capacity can be estimated from the capacity under reference temperature. This behaviour is described by Eq.(3.4)

$$C(T) = C_f \cdot \left[1 + \delta\left(T - T_f\right)\right] \tag{3.4}$$

Where C_f is the battery capacity under reference temperature, i.e. 20℃ in this case and δ is the capacity changing coefficient depending on the temperature variation. Normally it is considered as 0.5-1% capacity change per degree Celsius

Depending on the required precision for modelling, the equation used to express the relationship between capacity and temperature could be much more complex. In [72], the capacity of a battery varies with C-rate and the temperature is expressed as Eq. (3.5).

$$C = \frac{C_T}{1 + aI^b}(1 + \alpha\Delta T + \beta\Delta T^2) \tag{3.5}$$

Where C_T is the maximum capacity that the battery contains under a certain temperature T, and it can be measured by discharging the battery with low-current level. ΔT refers to the difference between the temperature under which the battery is working and the standard temperature. The parameters a and b are empirical parameters and α, β are temperature correction factors. I is the load current.

In [73], the capacity of a battery is modelled as:

$$C(I,\theta)_{\theta=constant} = \frac{K_C C_{0*}}{1+(K_C-1)(I/I^*)^{\delta}} \times (1+\frac{\theta}{-\theta_f})^{\varepsilon} \quad \textbf{(3.6)}$$

Where K_c, δ and ε are empirical coefficients, I^* is a specified current, e.g. nominal current and $C_{0*}=C_0(I^*)$. θ_f is the electrolyte freezing temperature

in [74] a simplified equation (3.7) based on [73] is given, where the temperature coefficient is changed into a temperature dependent capacity look up table, as in equation (3.7):

$$\begin{aligned} C(I,\theta) &= \frac{K_C C_{0*}}{1+(K_C-1)(I/I^*)^{\delta}} \times K_t \\ K_t &= LUT(\theta) \end{aligned} \quad \textbf{(3.7)}$$

b) SOC

There are two main types of SOC indication methods: the direct measurement method and the book-keeping method. The direct measurement method is based on the relation between measured battery variables and the SOC. The variables used are: battery voltage, battery impedance and the voltage relaxation time after a current interruption. However, most of these relations are temperature dependent. The book-keeping method is basically current measurement and integration during charge/discharge, i.e. coulomb counting. [27] In battery modelling, coulomb counting is the direct way of SOC indication and the battery behaviour, or external variables are the output of the model. Hence, the coulomb counting method is used in this model to determine the SOC.

The SOC can be expressed by equation (3.8) [3]:

$$\begin{aligned} SOC &= 1-\frac{Q_t - Q_e}{Q_t} \\ Q_e(t) &= \int_0^t I_m(\tau)d\tau \\ I_m &= I_{batt} - I_{side-reaction} \end{aligned} \quad \textbf{(3.8)}$$

Where Q_t is the temperature dependent true capacity and Q_e is the energy that can actually be extracted from the battery starting from its full state. I_m is the mian branch current, which is the result of load current applied to the battery subtract the current consumed in side-reactions.

c) Cte-VOC

The state of charge of a battery can be estimated by the open circuit voltage, if the slight influence of temperature and the state of health is neglected. For a lead-acid battery, the SOC and VOC were found has a linear relationship in [75]. As a simple extension, S.Pang et al. [76] developed an equation which describes the relation between Voc and SOC:

$$V_{OC}(t) = a \cdot SOC(t) + b \quad \textbf{(3.9)}$$

In equation (3.9), both *a* and *b* are coefficients obtained empirically.

More than that, since the open circuit voltage is slightly influenced by the temperature. The VOC expression can be extended into equation (3.10) [77] by considering the influence of temperature.

$$EMF = SOC \cdot A_{SOC,T} + EMF_{min} \quad \textbf{(3.10)}$$

Where *EMF* is the electrochemical motive force, which can be represented by cte-VOC and EMF_{min} is the EMF value when the *SOC* is zero. $A_{SOC,T}$ is the slope that can represent how the *EMF* changes with *SOC* and the temperature.

If consider the temperature influence, according to [71][73], the VOC can be expressed as in equation (3.11) [71].

$$VOC = E_p - K_e(273+\theta)\ln(SOC) \tag{3.11}$$

E_p: open-circuit electrochemical potential representing the equilibrium EMF of the battery under no-load conditions;

K_e: battery-voltage change per unit temperature, V/K.

3.2.1.2 Voltage response circuit

a) Ohmic resistance

The ohmic resistance or bulk resistance represents the conductivity, or its reciprocal the resistivity, of the electrolyte and the electrical pathways, which means it largely relies on the electrolyte concentration (or the specific gravity of the electrolyte in another way). It has been found that the electrolyte specific gravity is an ideal indicator of SOC[78]. Hence it can be deduced that the ohmic resistance is a function of SOC. A conclusion that has been consistently found by many authors [55], [57], [62], [79] that the ohmic resistance will increase with the decrease of SOC.

Equation (3.12) proposed in [73] describing the relation between the ohmic resistance and the SOC:

$$R_0 = R_{00}\left[1 + A_0\left(1 - SOC\right)\right] \tag{3.12}$$

Moreover, the ohmic resistance changes with temperature [55], [57], [66], [80]. In [71] an equation (3.13) to estimate the ohmic resistance which considers the influences of both temperature and SOC is developed:

$$R_p = R_{p0}\left(1 - \beta\theta\right) - R_{cp}\ln\left(SOC\right) \tag{3.13}$$

Where R_{p0} and R_{cp} are internal resistance coefficients and β is the temperature change coefficient in the unit of deg^{-1}.

Furthermore, it has been found that the ohmic resistance is a function of the current. S.Tian[81] explored how the ohmic resistance varies with current and developed Eq. (3.14):

$$R_0(I) = \alpha_{R0} \cdot I^{-\beta_{R0}} \tag{3.14}$$

Where both α_{R0} and β_{R0} are empirical coefficients.

b) RC elements

In [64] a model was developed with two pairs of RC circuits to represent both electrodes separately. It was found that both charge transfer resistances vary with SOC and a ‘U’ shaped curve was drawn from experimental results. It was also found that both double layer capacitances are in functions of SOC and a reverse ‘U’ shaped behaviour was found in relation to the SOC. However, the RC elements are found monotonic decrease while SOC increases from 0 to 100% according to [80]. More than that, the values of RC elements change with temperature in a monotonic trend as well [80].

In [55] two pairs of RC circuits are used to represent two electrodes as well, and it is also reported that all these RC elements are functions of both SOC and temperature. It was also found that RC elements may vary with the DC current.[57]

Since the charge transfer resistance and double layer capacitance are combined into RC pair, the value of capacitance can be calculated from the resistance. Depending on the time constant.

The battery was modelled in [65] as one pair RC circuit model the RC element was expressed as the function of SOC, as shown in equation (3.15).

$$R_t = k\left\{\frac{1}{\left[SOC\cdot(1-SOC)\right]^{1/2}}\right\}$$
$$C_s = h\cdot\left\{\frac{\left[SOC\cdot(1-SOC)^{1/2}\right]}{\omega^{3/2}}\right\}^{1/2} \quad (3.15)$$

The model contains two pairs of RC elements also proposed in some papers, e.g. [66]. The equation of the first resistance is:

$$R_1(I_{R1}) = a + b\cdot\tanh\left(c\cdot(I_{R1}+d)\right) \quad (3.16)$$

Moreover, the second resistance is estimated in (3.17):

$$R_2 = \frac{d\eta}{dI}$$
$$I = I_0\cdot\left(e^{\frac{n\cdot\alpha\cdot\eta}{U_T}} - e^{\frac{-n\cdot(1-\alpha)\cdot\eta}{U_T}}\right) \quad (3.17)$$

Where η is the battery over potential, n and α are coefficients, and U_T is the temperature dependent voltage

The corresponding capacitors can be calculated easily from resistors as shown in (3.18)

$$C_1 = e\cdot R_1^{(\xi_1-1)}$$
$$C_2 = f\cdot R_2^{(\xi_2-1)} \quad (3.18)$$

To summarise, the value of the RC elements are the function of SOC, current and temperature.

3.2.1.3 Parasitic reaction branch

This subsection describes the method used by previous studies to model the parasitic branch of the battery.

In [71], a self-discharge conductance Gs was used to represent the side reactions as shown in equation (3.19).

$$G_s = G_{s0}\exp\left[A_{s0}V_{batt} + A_{s\theta}(\theta-\theta_f)\right] \quad (3.19)$$

Where V_{batt} is the battery voltage, θ is the battery temperature, and θ_f is the reference temperature. G_{s0}, A_{s0} and $A_{s\theta}$ are experimental parameters.

In [66], instead of modelling the side branch circuit, the author modelled the current loss directly, and the equation is:

$$I_{gas} = I_{0\_gass}\cdot e^{k_1\cdot(U-U_{0\_gas})} - e^{k_2\cdot(\vartheta-\vartheta_0)} \quad (3.20)$$

Where I_{gas} is the gassing current, $U_{0\text{-}gass}$ is the decomposition voltage of the water which is equal to 1.22 V. θ_0 is the reference temperature set to 27 ℃, and the rest of the parameters were obtained from experiments.
Another approach is also modelling the parasitic branch as a conductance in [73], and is described by equation (3.21).

$$G_p = G_{p0}\cdot\exp\left(\frac{V_{PN}}{v_{P0}+A_p\cdot\frac{1-\theta}{\theta_f}}\right) \quad (3.21)$$

Where V_{pn} is the voltage of the side reaction, θ is the battery temperature, θ_f is the electrolyte freezing temperature. All the other parameters G_{p0}, v_{p0} and A_p are constant for a particular battery
Another approach was used in [82], where the side reactions were modelled by a coulombic efficiency as shown in the equation (3.22).

$$\eta_c = 1 - \exp\left(\frac{a}{\frac{I}{Q_{\text{cref}}} \times \frac{1}{C_{ref}} + b} \times (SOC - 1) \right) \tag{3.22}$$

Where η is the efficiency, Q_{cref} is the capacity measured under a sufficient small C-rate C_{ref}, e.g. 1/120 C. a and b are experimental parameters.

3.2.2 LFP battery model

3.2.2.1 Storage circuit

a) Capacity

In short term operation, the available battery capacity can be influenced by operating current and the battery's temperature, which may cause errors in battery SOC prediction.

Experiments in [83] show that both charge and discharge specific capacity of LFP battery increased when the temperature rises. This phenomenon may relate to an enhanced lithium diffusion rate, less polarisation and faster kinetics under elevated temperature. Higher current density results in a reduction of accessible cell capacity. This is because the critical lithium transport rate per unit area limits the restoration of the capacity by the current. The capacity does not fade physically but induced by the lag between reaction rate and diffusion rate.[84][23]

Hence, the discharged battery capacity can be expressed in the modified Peukert equation[85]:

$$C_{dis,I,T} = \frac{\partial C_{dis}}{\partial I_{dis}} C_{dis,I_{dis}} + \frac{\partial C_{dis}}{\partial T} C_{dis,T} + C^{cte} \tag{3.23}$$

Where C_{dis} is the discharged capacity, I_{dis} is the discharge current, T is the operating temperature, and C^{cte} is a constant.

b) SOC

For a LFP battery, the SOC is expressed in the same way as a VRLA battery, which done by the coulombic counting method, as described by equation (3.8).

c) Cte-VOC

In dynamic operating conditions, the cte-OCV is considered as a function of the SOC and the battery's temperature. While a higher current may lower the accessible capacity, it has no impact on the OCV.[23] A Lower temperature (<<25℃) may slightly reduce the OCV of the cell, but the fluctuation of OCV at a higher temperature (>25℃) was hardly observed. [86] These slight variations of OCV under different temperatures were also detected in [87].

A polynomial equation can represent the OCV as a function of the SOC [86], as it is shown in equation (3.24).

$$V_{OC} = a_1 \times SOC^6 + a_2 \times SOC^5 + \ldots + a_6 \times SOC + a_7 \tag{3.24}$$

Because of the shape of the VOC-SOC curve, the OCV can also be expressed by a double exponential equation [88]:

$$V_{OC} = V_0 + a \times (1 - \exp(-b \times SOC)) + c \times \left(1 - \exp\left(-\frac{d}{1 - SOC}\right)\right) + e \times SOC \quad \textbf{(3.25)}$$

Additionally, other previous studies used an experiment-based OCV-SOC-temperature look up table to represent OCV.[87]

The OCV can also be expressed as a function of both SOC and temperature [89]:

$$V_{OC} = a_1 - \exp \times \left(a_2 \times (SOC - a_3)\right) + a_4 \times SOC + a_5 \times (SOC - a_6)^2 + b_1 \times T_{cell} + b_2 \times T_{cell}^2 \quad \textbf{(3.26)}$$

3.2.2.2 Voltage response circuit

Experimental results from previous studies [90][91][92] indicate that the internal impedance is strongly influenced by the temperature, the SOC, and the current. Further more, the internal impedance show a relatively inverse behaviour in charge/discharge processes.[90][91]

Since the ohmic resistance is mainly a representative of the conductivity of the electrolyte, it is significantly influenced by the temperature. The relation shows that its value increases when the temperature decreases. [90][92]

Experiments also show that ohmic resistance does not change significantly with the SOC, but charge transfer resistor is a function of the SOC. [90][92] However, some EIS tests show that the SOC has some impact on ohmic resistance values. [93]

The charge transfer resistance also shows an explicit exponential dependent on the temperature, which may because of the kinetic of the intercalation reaction. [93] The charge transfer resistance can be expressed by a polynomial function or expressed according to Arrhenius equation: [90]

$$R_{ct}(T) = \frac{1}{A \times \exp\left(\frac{-E_a}{RT}\right)} \quad \textbf{(3.27)}$$

Where T is the operating temperature, E_a is the activation energy, and R is the gas constant.

Additionally, the double layer capacitance is also a function of SOC but independent of the temperature. The Overall battery resistor changes with the operating current. [90] It has been observed that the charge transfer resistor is a function of the current and can be expressed in Eq.(3.28) [91]:

$$R(I_R) = R_1 \times \left(\frac{\ln\left(k_1 \times I_R + \sqrt{(k_1 \times I_R)^2 + 1}\right)}{k_1 \times I_R}\right) \quad \textbf{(3.28)}$$

$$R(I_R = 0) = \lim_{I_R \to 0}\left[R(I_R)\right] = R_1$$

The diffusion resistance is also found as a function of the SOC [92]. In [39], it has been considered that all the impedances are the function of SOC. While in [94], all the battery's internal resistances, with the exception of the ohmic resistance, are expressed as a function of the SOC.

$$R = a + b \times (SOC)^c + d \times \exp\left[e \times (1 - SOC)\right] \quad \textbf{(3.29)}$$

3.3 Experimental design

From the literature review in the previous section, it can be concluded that for both battery technologies even though there is some disagreement, each of the internal impedances of both battery technologies is, to some extent, influenced by the SOC, the temperature and the current, as shown in Figure 3-10. Hence, to obtain a proper dynamic battery model, a battery should be tested with all three variables.

This thesis mainly focuses on the usage of the battery. Hence the variety of operating temperature is not included in this thesis. All experiments in the laboratory are performed with the temperature control inside the room set to 22-24 ℃. Therefore all experiments can be considered as under constant room temperature conditions.

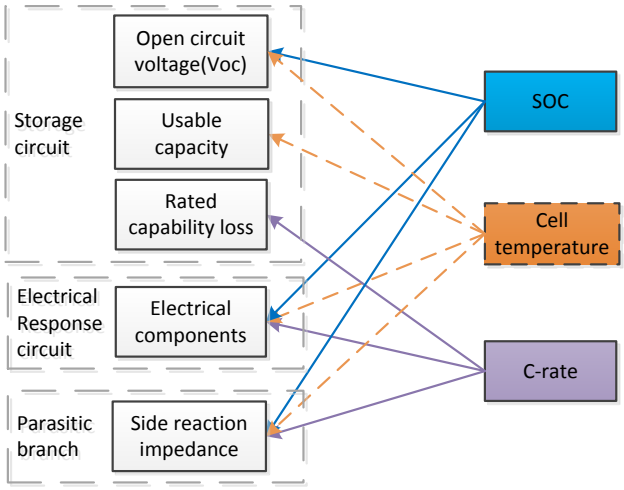

Figure 3-10 Components, important parameters in the battery model and the influenced variables

The recommended charge-discharge methods for both technologies are listed in Table 3-2. The selection of the charge-discharge method in this study is based on this table.

Table 3-2 Recommended charge/discharge method for both battery technologies [32], [95][96][97]

Battery brand	**A123systems® APR26650M1B**	**Cyclon® AGM D single cell**
Recommended charge method	Continuous charge: CCCV with 1C Fast charge: CC with 4C	1, CC: constant current charge until a dramatic voltage rise observed then reduce the charge current 2, CV: minimum 0.4C inrush current with 2.45-2.5V constant voltage 3, CCCV: Constant current charge till voltage reach 2.45-2.5V then constant charge till current drop under 0.002C 4, 2.25-2.35V for float charge
Recommended discharge method	Maximum 20C continuous discharge; Maximum 48C pulse discharge (10 seconds)	CC discharge less than 2.2C Maximum 26C discharge to 1.5V
End of charge condition	CC: Voltage>=3.6V CCCV: 3.6V with current <=0.01C	CC: Voltage>=3.6V CCCV: 2.45-2.5V with current drop <= 0.002C
End of discharge condition	CC: Voltage<=2V CCCV: 2.5V with current <=0.01C	Depending on discharge rate set end of discharge voltage:

C-rate	0.05	0.1	0.2	0.4	1	2	>5
EODV	1.75	1.7	1.67	1.65	1.6	1.55	1.5

The resolution of the tester is essential for the measurement. The technical specifications of the battery tester is listed in Table 3-3.

Table 3-3 Technical specifications of the battery tester [98]

Specifications	
Number of Test Channels:	96 channels
Voltage Ranges:	available up to 180 V maximum
Voltage Accuracy:	0.02% of full scale voltage
Voltage Resolution:	16 bit
Current Ranges:	Single Current Range 1 mA to 2000 A; Four Current Ranges: 150 μA, 5 mA, 150 mA, 5 A
Current Accuracy:	0.02% of full-scale current on 5 Amp Multi-range channels
Current Resolution:	16 bit
Time Resolution:	10 mS standard, with 5 mS and 1 mS as an option
Data Recording Rate:	200 data points per second per system standard
Data Recording Interval:	ΔTime (minimum 10 mS standard, 5 mS and 1 mS as an option), ΔV, ΔI, ΔAh, ΔWh, ΔT, ΔP
Operating Modes:	Constant Current, Constant Voltage, Constant Power, Constant Resistance, Voltage Scan (Cyclic Voltametry)

3.3.1 Storage circuit: cte-OCV-SOC test

The purpose of this set of experiments is to obtain the relation of the cte-OCV and the SOC since the cte-OCV can indicate the SOC. As explained before (Section 2.1), in a particular state, if the battery rests enough time then the open circuit voltage can be considered as close-to-equilibrium OCV(cte-OCV).

In this case, the cte-OCV should be measured at different SOCs, and the battery is fully discharged before the measurement. The battery is a monotonic charge to full then discharged in steps of 5% SOC. Coulombic counting approaches the SOC demarcation. After each step, the battery rest for a constant time to get the close-to-equilibrium (cte-) state, and then the voltage was noted as the cte-OCV value.

Nonetheless, previous studies provide many suggestions on the experimental resting time to reach the cte-OCV state.

- For lithium ion batteries, some authors suggest the acceptable shortest rest time is 1 hour for cte-OCV measurements.[99][100]
  A series of experiments on different rest time for cte-OCV measurement was taken in [101] and the shortest rest time was one hour, and the longest one was 96 hours. After the comparison, a resting time between 6-26 hours was recommended.
  Experiments in [102] showed that if the voltage change after 3 to 8 hours rest was less than one mV, then it indicates the error can be neglected, and the voltage value can be considered as the cte-OCV.

  Hence, in order to achieve measurement accuracy as well as save experimental time, a 3 hours resting time in cte-OCV measurement for LFP battery is taken.

- For VRLA battery, it is suggested that if the voltage changes less than 0.25mV/cell/h, the battery voltage can be regarded as cte-VOC. In order to reach this stage, the battery has to rest at least 3 hours.[28] Although, longer necessary resting times have also been reported.[103]
  A series of OCV measurement tests have been performed in [104], [105], and it is found that voltage of

a battery under no load will not stabilize before 4 hours rest. However, they developed a method which can be used to estimate the real OCV by using the voltage measured with much shorter resting time (at least 30 minutes). With the estimated OCV value, the OCV-SOC function could be achieved with a short testing duration.
In [103] a series of experiments also performed and it was concluded that if the voltage under no load is measured one hour or longer after the operation, it is not necessary to estimate the real OCV. Since the calculated SOC error between the measured value and the estimated OCV is insignificant and the result is acceptable.

Hence, a rest period of 4 hours is employed as a trade-off.

For both battery technologies, the test C-rates were set at 0.2 C. The value is relatively low, and for both battery technologies, the whole tests can be finished within five working days.

After all, the charge/discharge voltage hysteresis is modelled by the internal resistance. The summary of the OCV-SOC tests for both battery technologies is listed in Table 3-4, and the concept curves of the measurement is in Figure 3-11.

Table 3-4 Summary of OCV-SOC tests

Battery tech-	State	Method	Voltage limitation [V]	Cut off condition	Step size	Rest time between steps	Rest time for battery stabilization
LFP	Charge	CCCV	3.6	I<=0.01C	5% SOC	3 hours	3 hour
	Discharge	CCCV	2.5	I<=0.01C		3 hours	3 hour
VRLA	Charge	CCCV	2.5	I<=0.002C		4 hours	4 hour
	Discharge	CC	1.67	V<=1.67V		4 hours	4 hour

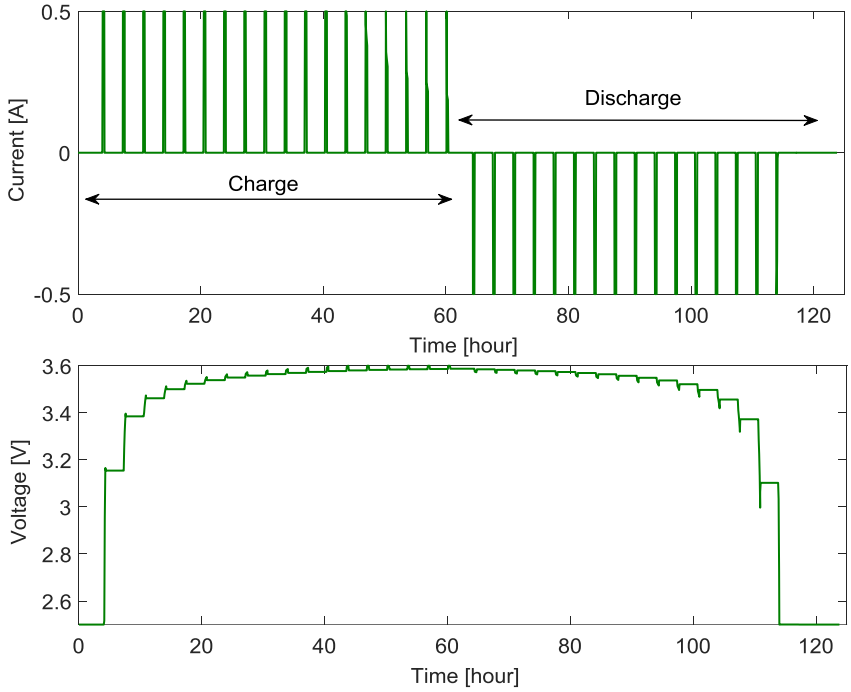

Figure 3-11 Concept of OCV-SOC measurement result curve, LFP is taken as the example.

3.3.2 Electrical response circuit: Internal impedance extraction

This series of tests have the objective of facilitating the resistance calculation. The parameter extraction method is voltage relaxation (also called step response). This approach requires less time and lower cost than the conventional technology, e.g. the Electrochemical Impedance Spectroscopy technology.[101] This method was also applied and introduced in detail in [106][101].

As introduced in Section 3.1.1, there is a voltage polarisation deviates from the equilibrium state whenever there is a load applied on both sides of the battery. Vice versa, the polarisation recovery back towards the equilibrium state whenever the load is disconnected. Hence, a voltage relaxation phenomenon is observable in a non-load interval (also called rest interval) when the battery is operating.

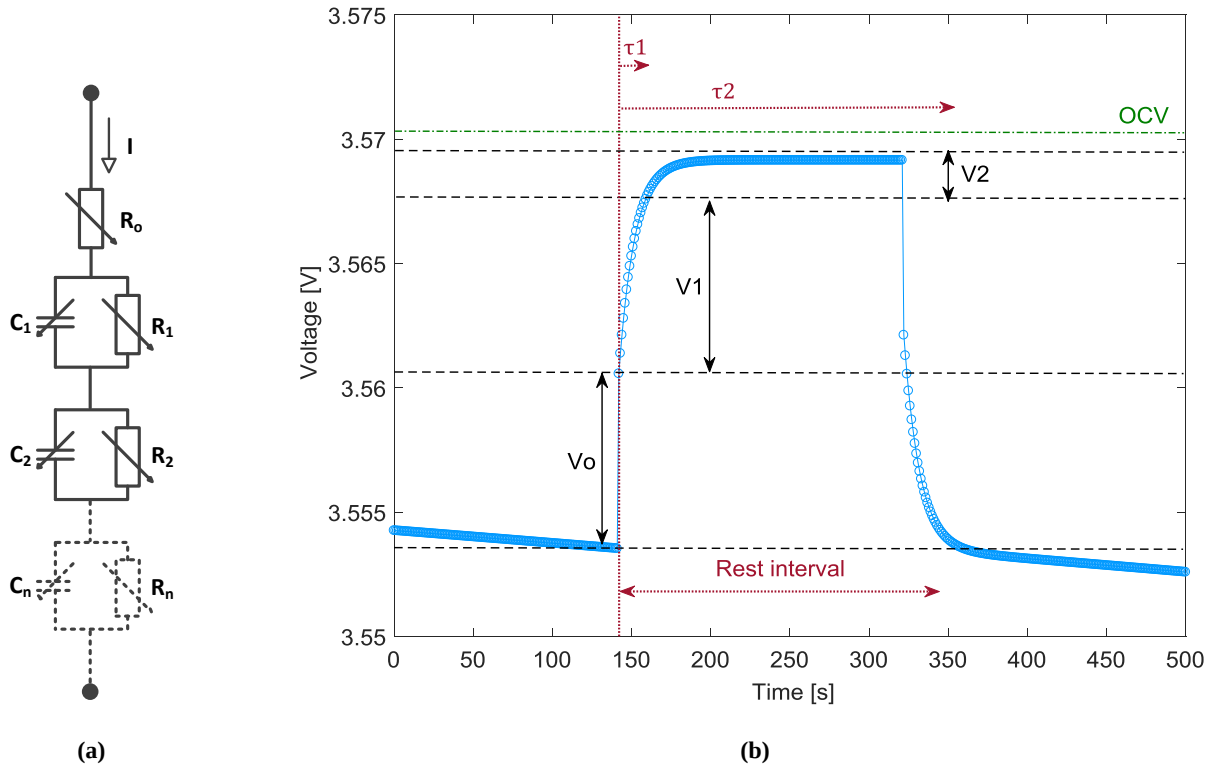

(a) **(b)**

Figure 3-12 One example of voltage relaxation during rest interval in discharge.
(a) the corresponding electrical elements (b) the voltage relaxation curve

Taking the non-load rest interval during a discharge stage as an example, as shown in Figure 3-12 (b). The voltage response can be divided into two parts: one is an instantaneous voltage jump right after the load paused, and the other part is a gradual increase of the voltage towards the cte-OCV in the rest of time. Those two voltage responses are correlated with two electrical parts: one is an ohmic resistance, and the other is resistor/capacitor pairs, as introduced in the construction of EECM model.

Generally, there is an expected time window for each of the voltage response. Assume an EECM contains two RC-pairs. A boost of voltage tension right after the load disconnected, which within a five seconds time-window as suggested[101], is considered induced by the ohmic resistance. The time window for the rest gradual voltage increase caused by the RC pairs is called time constant. It can reflect the speed of voltage changing, that is the voltage changes faster if the time constant is smaller. [90] The increase in voltage right after the immediate voltage increase in a short time, which is expected around 10 seconds[106] is the short term voltage response, which relates to the first RC-pair. The following increase in voltage is then treated as the long term voltage response, which correlated with the second RC-pair as shown in Figure 3-12 (a). It is possible to increase the number of RC-pairs and divide the voltage relaxation into more parts, with which the accuracy of the model is improved. Eventually, the relaxation voltage will reach cte-OCV if the rest interval is long enough, as explained in Chapter 2.

Curve fitting method was applied on each of the voltage relaxation results. The recognition of each part of the voltage and the corresponding time constant was done by "nonlinear least squares curve fit" in Matlab[101][106]. The recognised voltage and time constant values were then fitted into the RC circuit complete response equations [107] to obtain the values of electrical elements in the model. The equations are listed below from Eq. (3.30) to Eq. (3.33)

$$V_{interval} = V_1 * \left(1 - e^{\frac{-t}{\tau_1}}\right) + V_2 * \left(1 - e^{\frac{-t}{\tau_2}}\right) + V_O \quad (3.30)$$

$$V_{OC} = V_{ini} + V_O + V_1|_{(t\to\infty)} + V_2|_{(t\to\infty)} \quad (3.31)$$

$$R_O = \frac{V_O}{I} \quad (3.32)$$

$$R_{1(2)} = \frac{V_{1(2)}}{I}; C_{1(2)} = \frac{\tau_{1(2)}}{R_{1(2)}} \quad (3.33)$$

The electrical elements in the model are tested under different SOC and current, and the test procedure is similar to the test in[39][108][109].

First, the battery is fully discharged before the measurement. During the test, the battery is monotonically charged to full then discharge with steps of 0.15Ah instead of 5% SOC. Between each operation step, the battery was disconnected from the load and rest for some time in order to record the voltage relaxation phenomenon. The voltage relaxation curves that resulted from each step are then analysed by using the step response method. The test procedure is performed under different C-rates as well, and then the value of each electrical component under different SOC and C-rates were obtained.

For the length of relaxation time, the typical choice is to rest 1 min between steps, but some authors also tried much less time, e.g. 20 s [109] and 40 s [110]. It is reported that a longer rest interval may increase the accuracy[101]. Hence a three mins rest interval was chosen in this experiment.

In between the charge and discharge tests, the battery needs to rest to reach the equilibrium state before the next test. Battery state will get closer to equilibrium if it is allowed to rest for a longer time, but it may take several days for the battery back to a complete equilibrium state.[101] Usually, the recommended resting time is one hour for both LFP and VRLA battery technologies in experiments.[108][111][112] In this case, the one hour rest time in between the charge and the discharge for parameter extraction tests is taken.

The summary of this series of tests is listed in Table 3-5 and the concept I-V curve of the test is in Figure 3-13.

Table 3-5 Summary of parameter extraction tests

Battery tech-	State	Method	Voltage limitation [V]	Cut off condition	Step size	Voltage relaxation duration	Rest time for battery stabilization
LFP	Charge	CCCV	3.6	I<=0.01C	0.15 Ah	3 mins	1 hour
	Discharge	CCCV	2.5	I<=0.01C		3 mins	1 hour
VRLA	Charge	CCCV	2.5	I<=0.002C		3 mins	1 hour
	Discharge	CC	Depending on C-rate	V<= cut off V		3 mins	1 hour

C-rate to test and the EODV for VRLA	0.05	0.1	0.15	0.2	0.25	0.3	0.4	0.5
	1.75	1.7	1.68	1.67	1.665	1.66	1.65	1.64

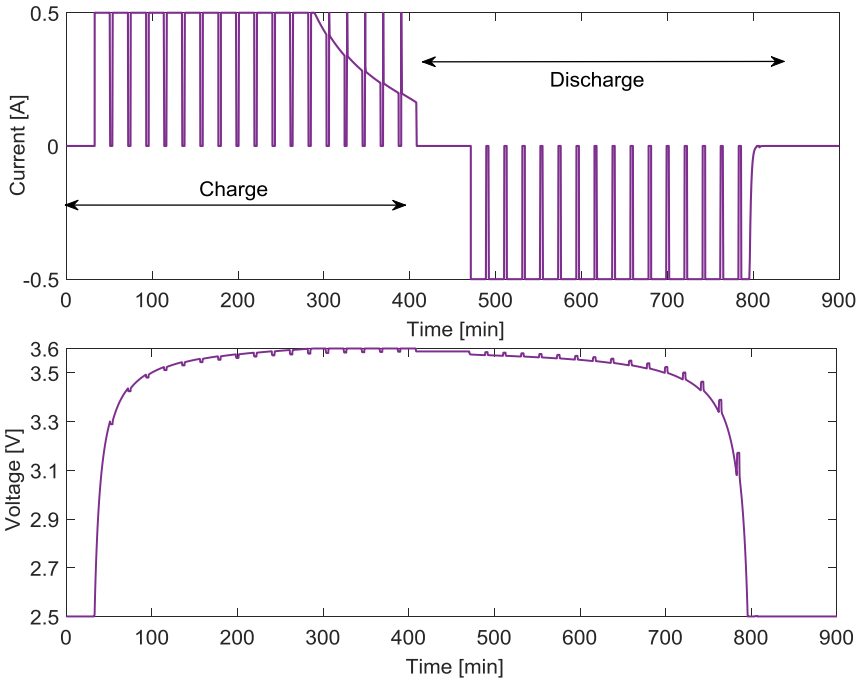

Figure 3-13 Concept current and voltage curve of the measurement with 0.2C-rate

3.3.3 Parasitic reaction circuit: Coulombic efficiency measurement

When charging a lead-acid battery, there are significant charge losses exist, which significantly influence the battery dynamic behaviour especially when the battery at a high SOC. The coulombic efficiency is a function of both SOC and C-rate, and the general trend is: [2], [29], [113]

- When SOC<85% the coulombic efficiency is no less than 90-95%;
- The coulombic efficiency is dropped to 75% when SOC>90%;
- When SOC>95%, the efficiency could drop to less than 50%.
- The coulombic efficiency is lower when battery is charged with higher current

This charge loss is mainly due to gassing and oxygen recombination, but the transient gassing phenomenon can be quite complex and unpredictable especially for VRLA batteries.[114] For accurate gassing phenomenon study and modelling, physical/chemical methods are usually applied,[115], [116], but chemical/physical based study is quite complex and beyond the scope of this thesis. Therefore, a simplified measurement was applied to estimate the coulombic efficiency in this thesis and the test procedure is similar with [82].

The coulombic efficiency was roughly measured and calculated from the integral-recharge-efficiency, and the test procedure is:

1. Fully charge and discharge the battery to measure the initial battery capacity
2. Discharge the battery to a specific SOC value x% and note down the discharged capacity Qd
3. Fully recharge the battery and record the recharged capacity Q_c
4. Calculate the recharge efficiency Q_d/Q_c and assume it is the averaged integral recharge efficiency at middle SOC point between x% and 100%, which is (x+(100-x)/2)%
5. Back to step 2 and repeat the following steps until enough data points are obtained.
6. Test the whole procedure under different C-rate

Then the averaged integral recharge efficiency was fitted into this equation Eq. (3.34) to get the roughly estimated coulombic efficiency as a function of SOC and C-rates.

$$\eta_c = 1 - \exp\left(\frac{b}{\frac{I_{ref}}{I_{test}} + c} \times (SOC - 1)\right) \tag{3.34}$$

The experimental setting and procedure is detailed are summarised in Table 3-6 and Figure 3-14

Table 3-6 Experimental setting for coulombic efficiency measurement for VRLA battery

SOC value x%	**Tests in high SOC range >90%:** **90% to 99%, 1% per step**	**Tests in low SOC range <90%:** **10% to 90%, 10% per step**
C-rate	0.1C,0.2C,0.3C,0.4C	

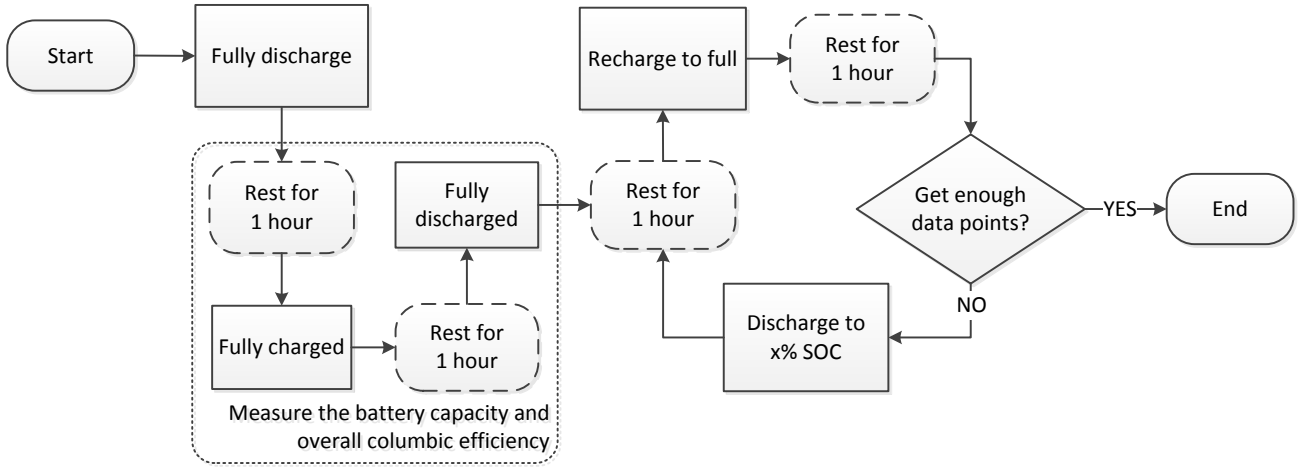

Figure 3-14 Illustration of coulombic efficiency test procedure for VRLA batteries

3.4 Experimental results

3.4.1 Storage circuit

3.4.1.1 Battery capacity

As introduced in Section 2.1, battery operates with higher C-rate may have a rated capacity loss compared to those cycled at lower C-rate. However, the battery capacity defined in this thesis is maximum dischargeable battery capacity, which means it highly depends on the charge-discharge method. For charging the battery of both technologies, no matter what the C-rate is in the constant current stage, there is always a constant voltage stage followed to make sure the battery is fully charged.

However, when discharged, only LFP has a recommended CCCV method. LFP battery capacity measured under different current and the result is shown in Figure 3-15(a). It can be seen that the battery capacity does not have any losses related to C-rate. However, for VRLA battery, there is no recommended CCCV discharge method can be found in literature and only CC method was available. The measured result in Figure 3-15 (b), shows the battery capacity has a strong current dependent feature.

In this case, the VRLA maximum discharged battery capacity with a CC discharge strategy can be regarded as a function of operational current.

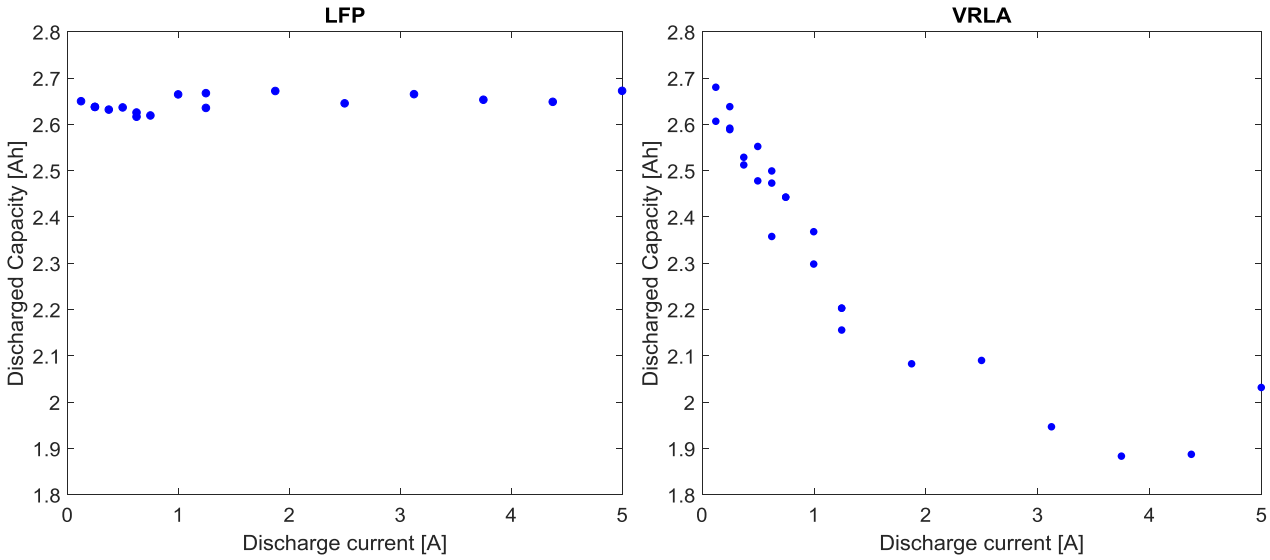

Figure 3-15 Battery cell capacity measured with different current

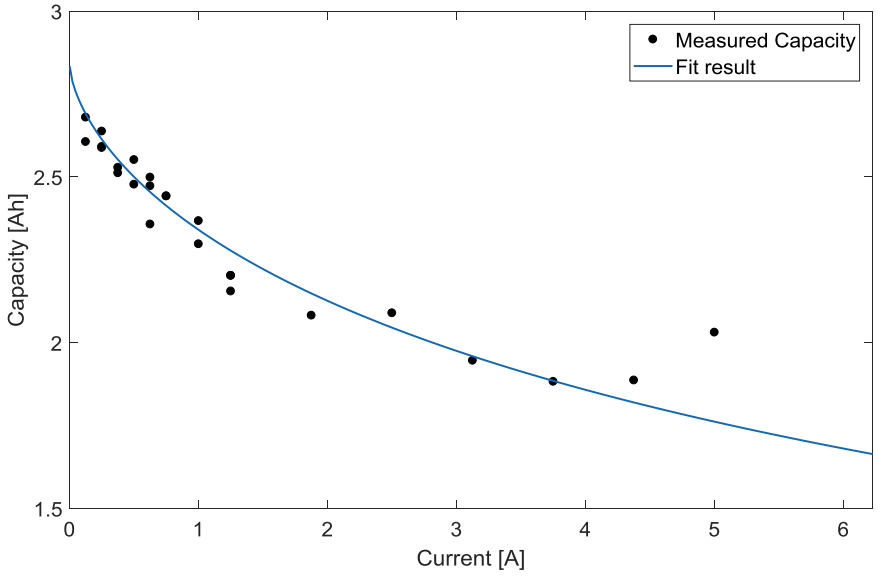

Figure 3-16 Measured VRLA battery capacity under different operational current and the fitted result

The measured capacity is fitted into the equation which was modified from Eq. (3.7)[74]. The measured data and fitted result is in Figure 3-16 and the equation is in (3.35)

$$C_{IA}(I)=\frac{1.134\times Q_{ref}}{1+(1.134-1)\times\left(\frac{I}{I_{ref}}\right)^{0.6582}} \tag{3.35}$$

Where Q_{ref} is the capacity measured under reference current I_{ref}, in this thesis, the I_{ref} is chosen as 0.5A, which is 0.2C and Q_{ref} is 2.5Ah.

3.4.1.2 Cte-VOC-SOC

a) LFP

As can be seen in Figure 3-17(a), the cte-VOC is a function of SOC. It increases dramatically when SOC close to 100% and decreases fast when SOC drops nearly 0%. The measured cte-VOC during charge/discharge has a hysteresis phenomenon, but it will be contained in the internal resistance modelling instead of in VOC.

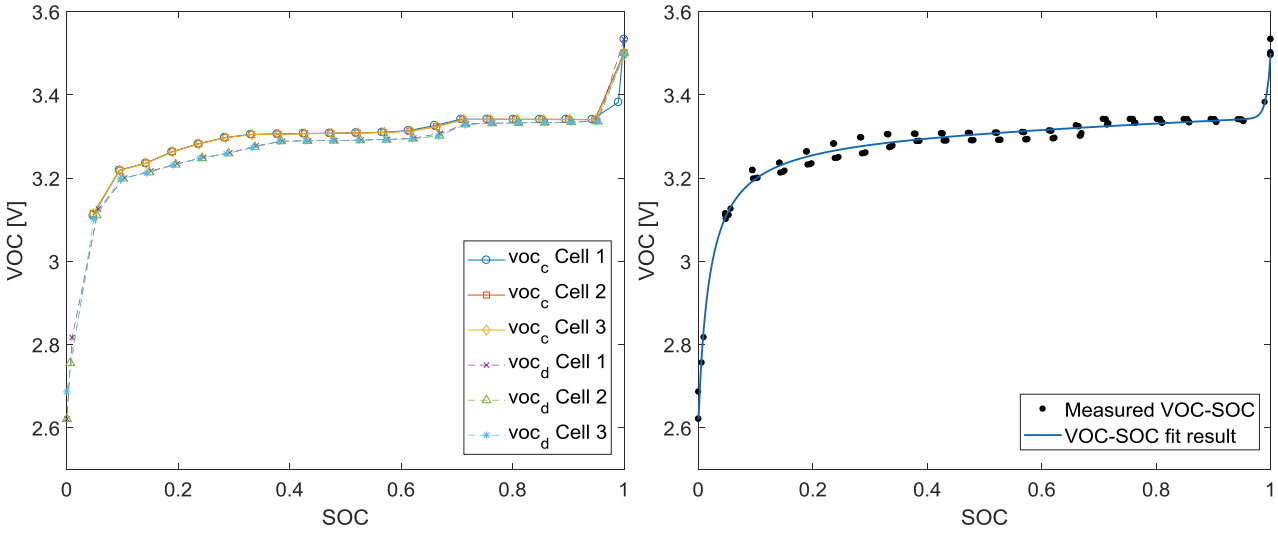

(a) **(b)**

Figure 3-17 Measured open circuit voltage versus SOC of LFP battery (a) the hysteresis of VOC when charge and discharge the battery separately; (b) the measured data points and the fitted curve

According to paper[88], the cte-VOC can be perfectly fitted into a double exponential curve. The fitting result is drawn in Figure 3-17(b) and the fitted equation is in Eq.(3.36).

$$cte - V_{OC} = 3.307 \times e^{\frac{-0.004117}{SOC+0.01772}} + e^{138.7\times(SOC-1.013)} + 0.05098 \times SOC \quad \textbf{(3.36)}$$

b) VRLA

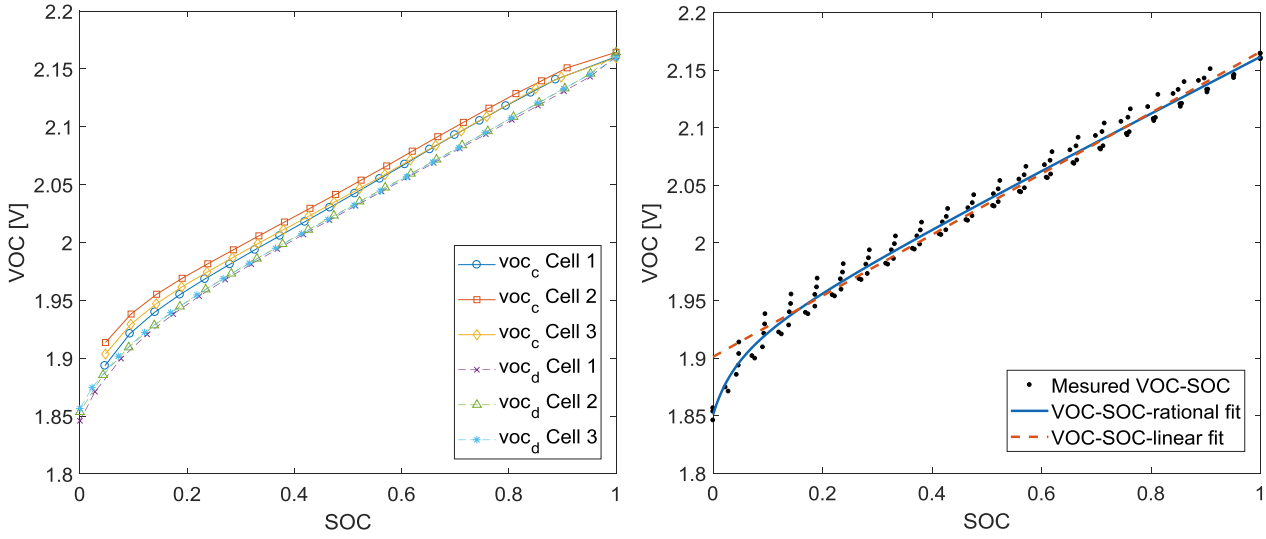

(a) **(b)**

Figure 3-18 Measured open circuit voltage versus SOC of VRLA battery
(a) VOC measured during charge and discharge separately;
(b) the measured data points and the fitted curve

In many papers as introduced in the proposed battery model and the manufacturer data sheet, it is suggested that the cte-VOC of VRLA versus SOC shows a linear relation. However, it is found that a rational fitting is better than linear fit especially when the battery is at low SOC, as plotted in Figure 3-18. Hence the empirical based rational equation (3.37) is then proposed and employed instead of the linear equation as in Eq.(3.9).

$$cte - V_{OC} = \frac{0.2428 \times SOC^2 + 1.935 \times SOC + 0.09876}{SOC + 0.05336} \tag{3.37}$$

3.4.2 Voltage response circuit - LFP battery

Many papers suggest model the LFP battery with second order RC circuit[39], [110], [117]. During curve fitting it was found that second order circuit has a decent accuracy as well as suitable complexity, so the LFP battery is modelled with second order RC circuit. This two pairs of RC are meant to fit the voltage relaxation curve in two time-windows. Since normally this two time-windows have at least an order of magnitude difference[109], these two RC pairs are then named with RC short and RC long for convenience. The ohmic resistance to model the electrolyte conductance is then named with ohmic resistance.

3.4.2.1 Experimental results

The whole data extraction method is similar to the method in [106]. Firstly, pick a C-rate with which the electrical elements were analysed and expressed as the function of SOC. Then using the result achieved with this C-rate as a reference, exploring how operational C-rate changes the internal impedance. The reference C-rate picked is 0.2C, which is the same as the one applied in VOC-SOC tests. Since charge and discharge are two reversed processes, they were modelled separately for convenience.

In the following four figures (Figure 3-19 to Figure 3-22) are the measured and fitted results of those electrical elements. In those figures, Ro means ohmic resistance, Rs/Cs are the values of RC pair representing the voltage relaxation in the short time-window, and Rl/Cl are used to represent the voltage relaxation in the long time-window. In all equations, suffix c means charge stage and d means discharge stage. The meanings of those electrical elements symbols are the same in the following content.

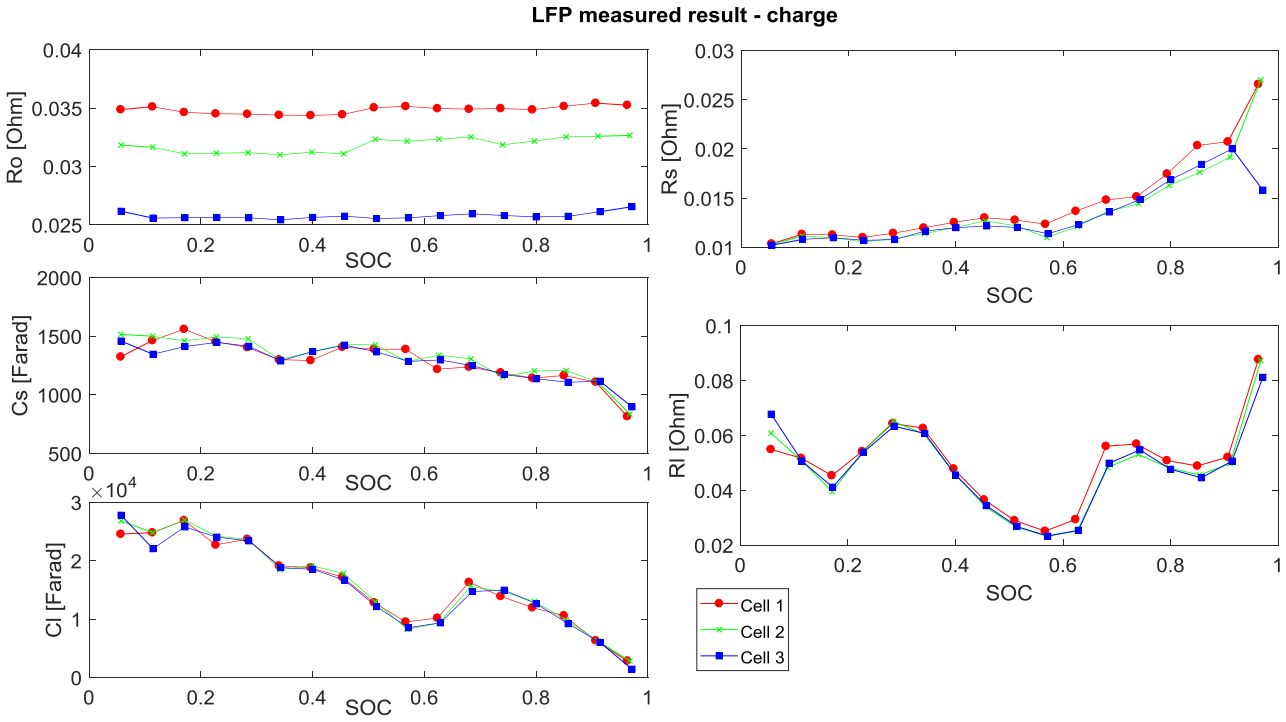

Figure 3-19 Values of electrical elements versus SOC of LFP batteries measured and fitted during charge, with 0.2C-rate

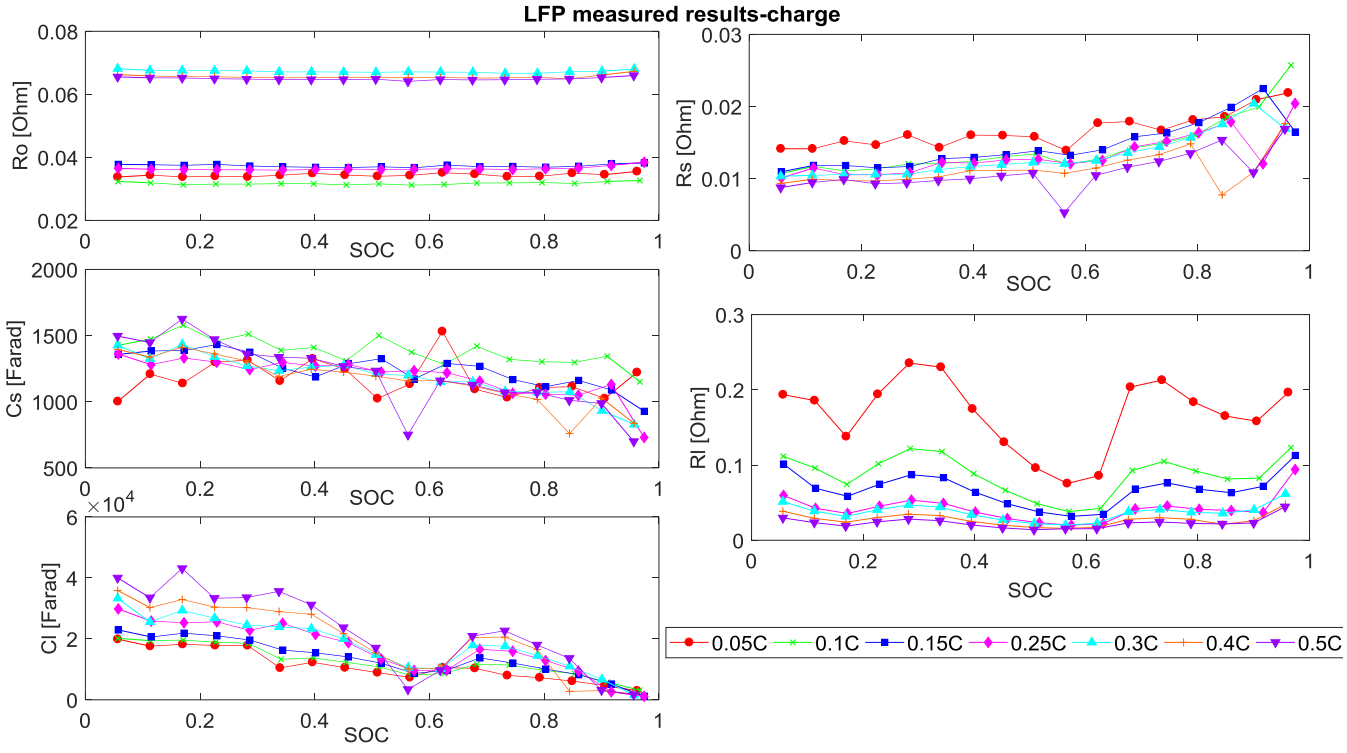

Figure 3-20 Values of electrical elements versus SOC and different C-rate of LFP batteries measured and fitted during charge

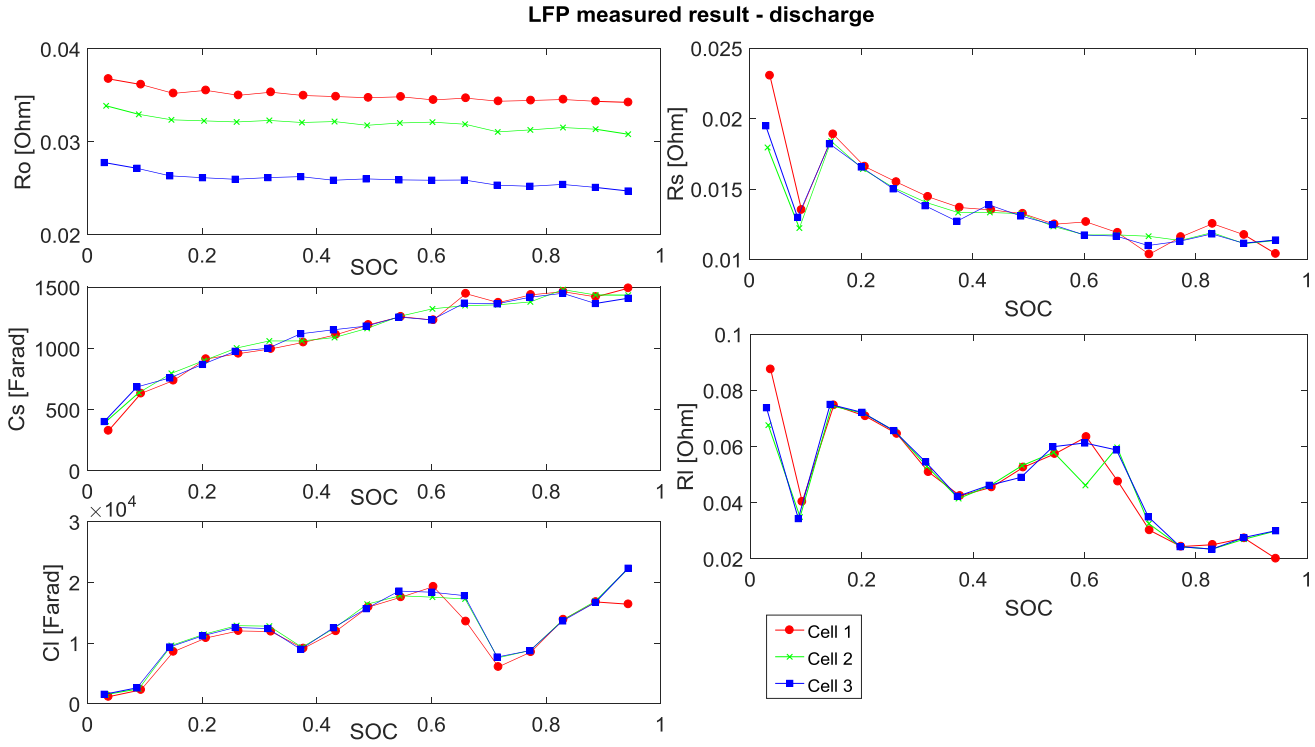

Figure 3-21 Values of electrical elements versus SOC of LFP batteries measured and fitted during discharge, with 0.2C-rate

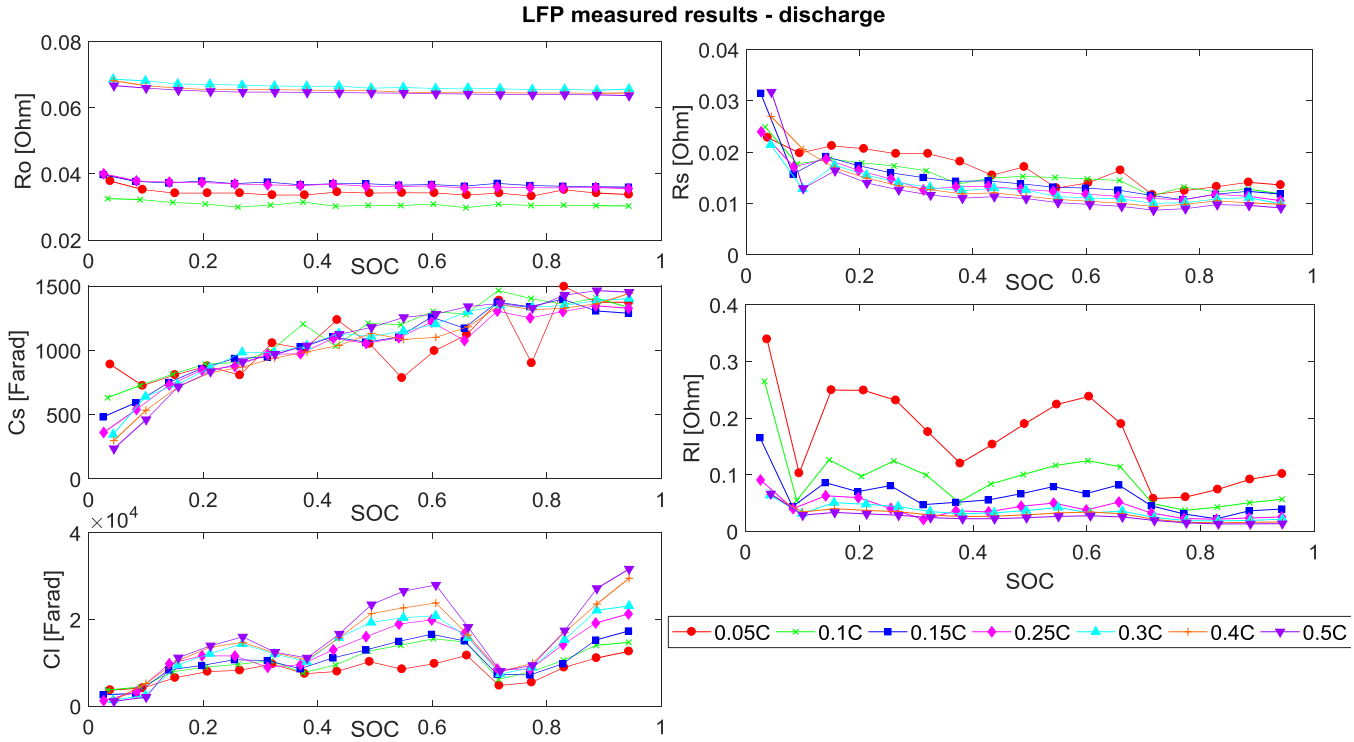

Figure 3-22 Values of electrical elements versus SOC and different C-rate of LFP batteries measured and fitted during discharge

From those measured and fitted results, some conclusions can be drawn as:

- Except for Ro, all the other electrical elements show a strong dependency on SOC
- All the electrical elements do show an inverse behaviour versus SOC in charge and discharge
- Operational current influences Rs, Rl and Cl in both charge and discharge processes

Therefore, all the elements would be expressed as the function of SOC for a better accuracy, even though Ro does not varies too much with different SOC values. Elements Rs, Rl and Cl would be modelled as the function of both SOC and C-rate.

3.4.2.2 Data analysis

First of all, all the elements are fitted into functions of SOC.

Charge:

$$Ro_{c\_LP}(SOC) = 0.0334 \cdot SOC^4 - 0.06141 \cdot SOC^3 + 0.03985 \cdot SOC^2 - 0.01104 \cdot SOC + 0.04918 \quad (3.38)$$

$$Rs_{c\_LP}(SOC) = 0.01036 \cdot exp(0.295 \cdot SOC) + 3.829e-6 \cdot exp(8.363 \cdot SOC) \quad (3.39)$$

$$Cs_{c\_LP}(SOC) = 1451 \cdot exp(-0.3283 \cdot SOC) - 9.562e-08 \cdot exp(22.43 \cdot SOC) \quad (3.40)$$

$$\begin{aligned} Rl_{c\_LP}(SOC) = {} & 0.9515 + 0.05887 \cdot cos(x \cdot w) - 0.06694 \cdot sin(x \cdot w) - 0.01243 \cdot cos(2 \cdot x \cdot w) \\ & -0.04918 \cdot sin(2 \cdot x \cdot w) - 0.02577 \cdot cos(3 \cdot x \cdot w) - 0.01927 \cdot sin(3 \cdot x \cdot w) \\ & x = SOC; w = 4.494 \end{aligned} \quad (3.41)$$

$$\begin{aligned} Cl_{c\_LP}(SOC) = {} & 1.672e4 + 7346 \cdot cos(x \cdot w) + 6107 \cdot sin(x \cdot w) + 3910 \cdot cos(2 \cdot x \cdot w) + 859.6 \cdot sin(2 \cdot x \cdot w) \\ & +1356 \cdot cos(3 \cdot x \cdot w) - 4264 \cdot sin(3 \cdot x \cdot w) \\ & x = SOC; w = 4.76 \end{aligned} \quad (3.42)$$

Discharge:

$$Ro_{d\_LP}(SOC) = 0.04153 \cdot SOC^4 - 0.09593 \cdot SOC^3 + 0.07794 \cdot SOC^2 - 0.0273 \cdot SOC + 0.05125 \quad (3.43)$$

$$Rs_{d\_LP}(SOC) = -0.0325 \cdot SOC^3 + 0.06854 \cdot SOC^2 - 0.04985 \cdot SOC + 0.02432 \quad (3.44)$$

$$Cs_{d\_LP}(SOC) = 909 \cdot exp(0.4785 \cdot SOC) - 764.6 \cdot exp(-7.692 \cdot SOC) \quad (3.45)$$

$$\begin{aligned} Rl_{d\_LP}(SOC) = {} & 219.3 \cdot SOC^8 - 1031 \cdot SOC^7 + 1986 \cdot SOC^6 - 2021 \cdot SOC^5 \\ & +1167 \cdot SOC^4 - 381 \cdot SOC^3 + 65.8 \cdot SOC^2 - 5.111 \cdot SOC + 0.1754 \end{aligned} \quad (3.46)$$

$$\begin{aligned} Cl_{d\_LP}(SOC) = {} & 1.22e4 - 2988 \cdot cos(x \cdot w) - 2455 \cdot sin(x \cdot w) - 1326 \cdot cos(2 \cdot x \cdot w) - 3567 \cdot sin(2 \cdot x \cdot w) \\ & -5139 \cdot cos(3 \cdot x \cdot w) - 1171 \cdot sin(3 \cdot x \cdot w) \\ & x = SOC; w = 5.522 \end{aligned} \quad (3.47)$$

After the achievement of the SOC dependent functions, it is then the analysis of current dependent equations. The method is, using the value measured under different C-rate divided by the value measured by reference C-rate (0.2 C), as in Figure 3-23(b), and fit those quotient values as the function of C-rate, or with SOC as well.

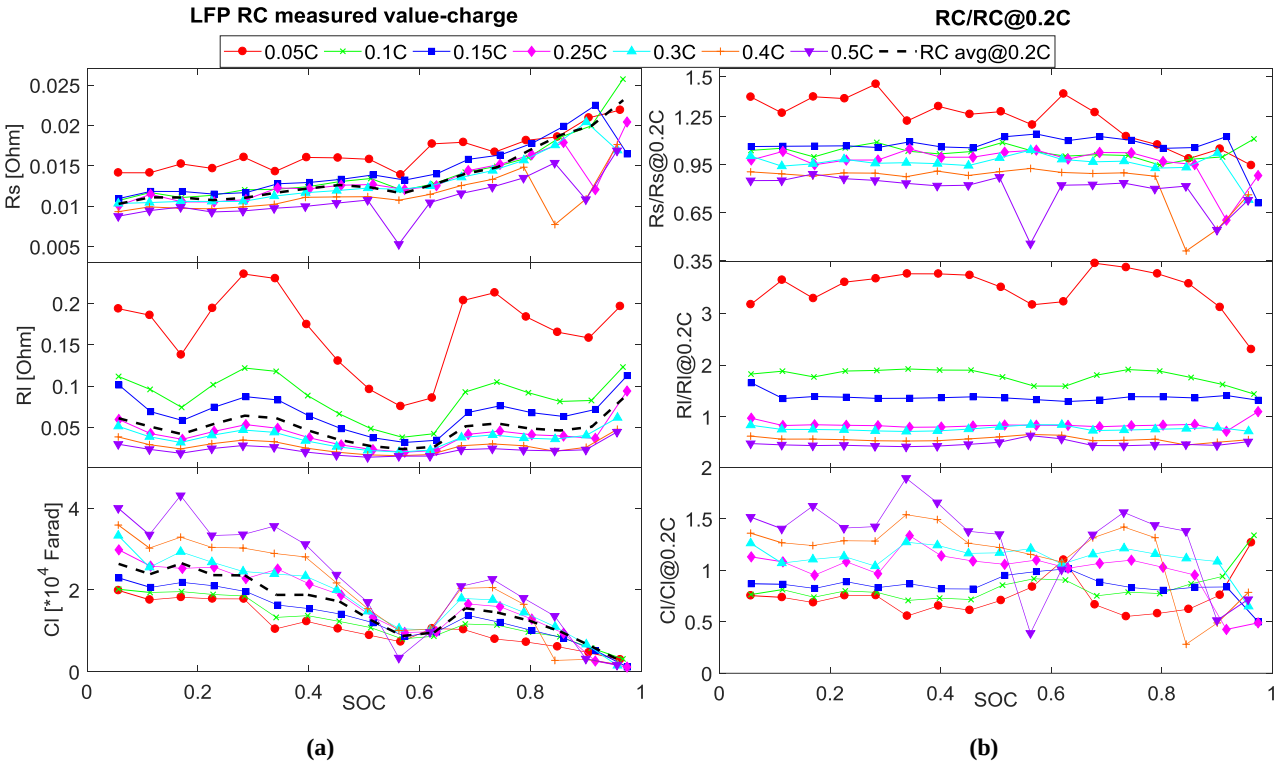

Figure 3-23 Measured electrical elements' values and the quotient values of LFP battery during charge (a) measured value to be fitted and the reference value (b) quotient values of those elements; R/C@0.2C means elements value measured with 0.2 C

In Figure 3-23 (a) are the three elements (Rs, Rl, Cl) which strongly dependent on operational current. In Figure 3-23(b) the quotient values are drawn versus SOC. In order to show the impact of current clearly, all those quotient values are plotted versus C-rate, as in Figure 3-24.

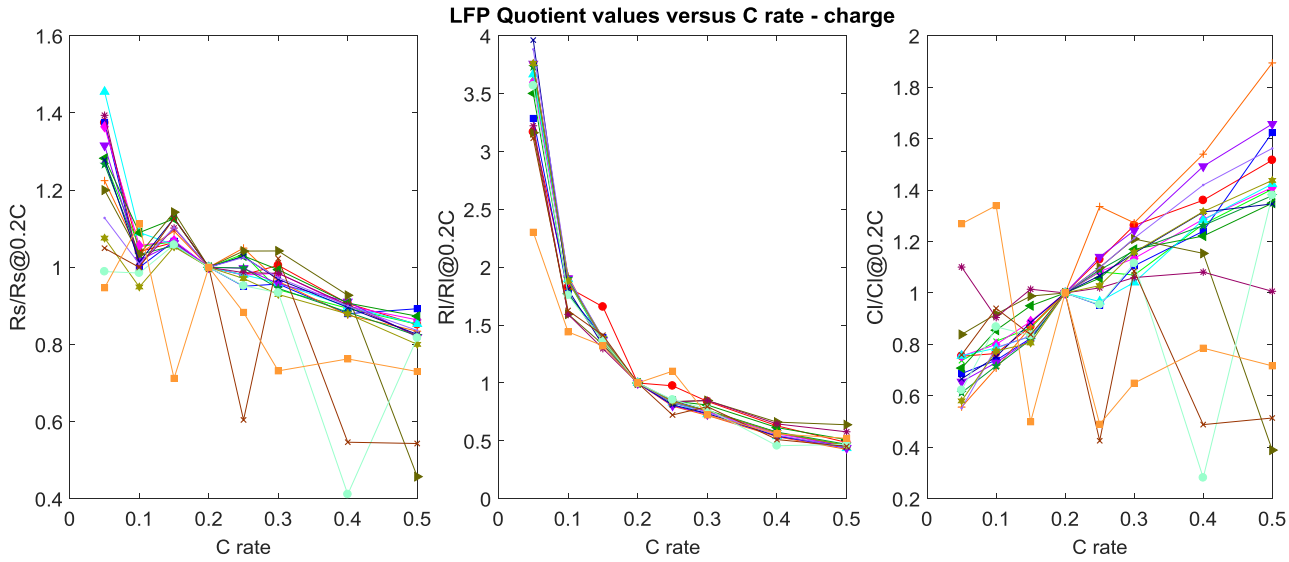

Figure 3-24 The quotient values during charge projected to different C-rate

Rs and Rl decrease when the operational current increased, but Cl shows an inverse C-rate dependency.

The same method of data processing was also applied to discharge values and the results are shown in Figure 3-25

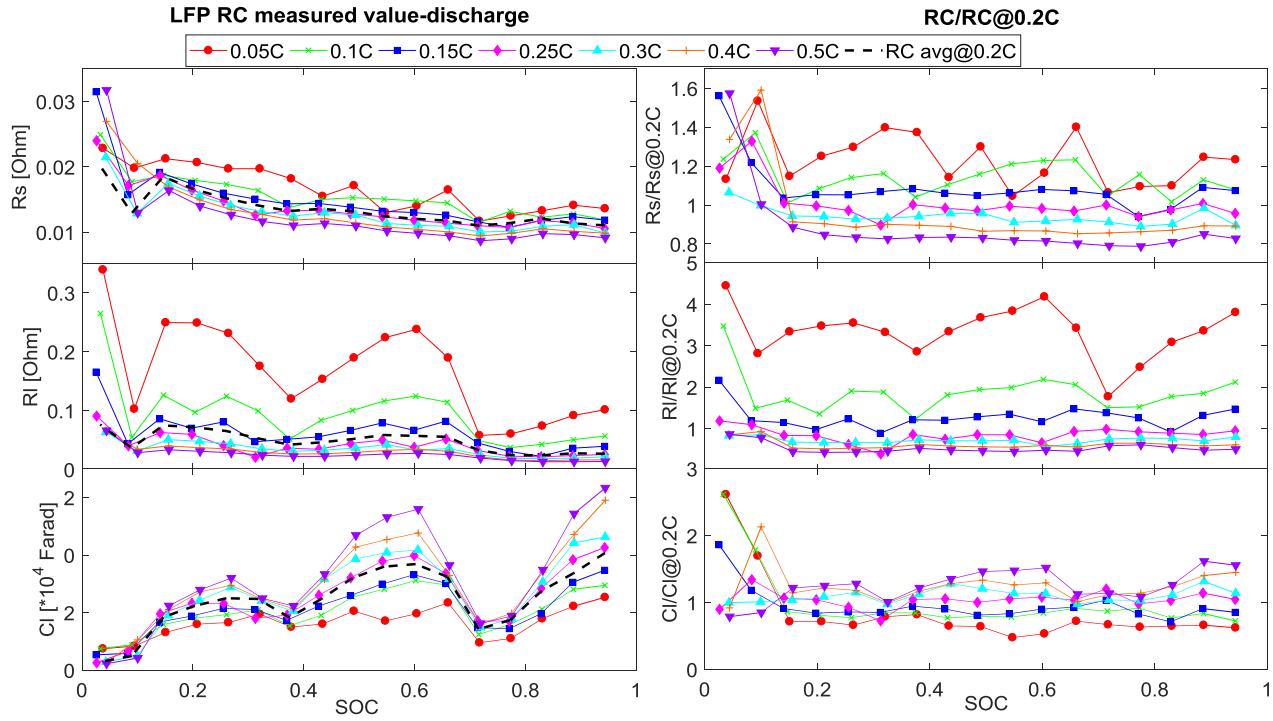

Figure 3-25 Measured electrical elements' values and the quotient values of LFP battery during discharge (a) measured value to be fitted and the reference value (b) quotient values of those elements;

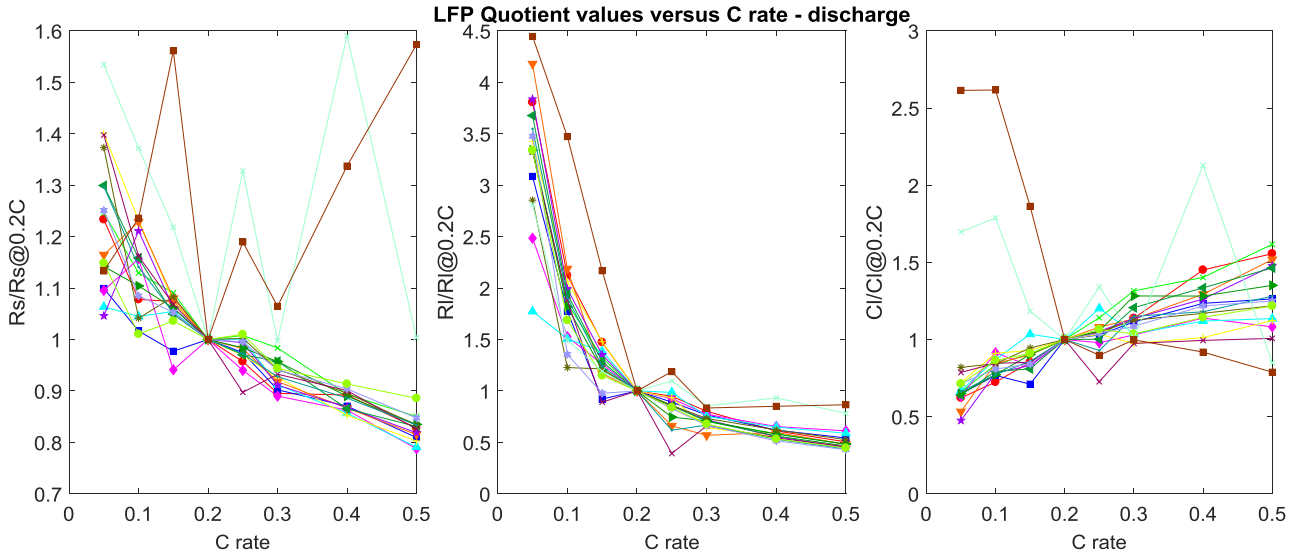

Figure 3-26 The quotient values during discharge projected to different C-rate

The elements in discharge stage show the same trend under different C-rate as during charge. Both Rs Rl decrease but Cl increase when C-rate increase.

The quotient values were then fitted into C-rate, some of them also taken the SOC into consideration to improve the accuracy. The achieved equations are listed below:

Charge

$$Rs_{c\_LP} / Rs_{c\_LP}@0.2C\left(I_{cr}, SOC\right) = \left(0.2304 \cdot I_{cr}{}^{2} - 0.775 \cdot I_{cr} + 1.1458\right) \times \left(-0.2068 \cdot SOC^{2} + 0.1532 \cdot SOC + 1.011\right) \quad \textbf{(3.48)}$$

$$Rl_{c\_LP} / Rl_{c\_LP}@0.2C\left(I_{cr}, SOC\right) = \left(7.677 \cdot exp\left(-28.9 \cdot I_{cr}\right) + 1.7054 \cdot exp\left(-2.789 \cdot I_{cr}\right)\right) \times \left(-0.1976 \cdot SOC + 1.169\right) \quad \textbf{(3.49)}$$

$$Cl_{c\_LP} / Cl_{c\_LP}@0.2C\left(I_{cr}, SOC\right) = \left(-1.272 \cdot I_{cr}{}^{2} + 2.346 \cdot I_{cr} + 0.5817\right) \times \left(-0.08145 \cdot SOC^{2} + 0.06667 \cdot SOC + 0.9769\right) \quad \textbf{(3.50)}$$

Discharge

$$Rs_{d\_LP} / Rs_{d\_LP}@0.2C\left(I_{cr}, SOC\right) = \left(1.084 \cdot exp\left(-0.534 \cdot I_{cr}\right) + 0.4643 \cdot exp\left(-14.45 \cdot I_{cr}\right)\right) \times \left(0.03161 \cdot SOC^{2} - 0.07195 \cdot SOC + 1.032\right) \quad \textbf{(3.51)}$$

$$Rl_{d\_LP} / Rl_{d\_LP}@0.2C\left(I_{cr}, SOC\right) = \left(1.307 \cdot exp\left(-1.872 \cdot I_{cr}\right) + 6.3160 \cdot exp\left(-20.67 \cdot I_{cr}\right)\right) \times \left(0.04198 \cdot SOC + 0.9656\right) \quad \textbf{(3.52)}$$

$$Cl_{d\_LP} / Cl_{d\_LP}@0.2C\left(I_{cr}\right) = \text{-}2.322 \cdot I_{cr}{}^{2} + 2.473 \cdot I_{cr} + 0.5983 \quad \textbf{(3.53)}$$

Hence, for those elements are the function of C-rate, the final equations would be:

$$RC\left(SOC, I_{cr}\right) = RC_{0.2C}\left(SOC\right) \times \left[RC / RC@0.2C\left(I_{cr}, SOC\right)\right] \quad \textbf{(3.54)}$$

In Figure 3-27 and Figure 3-28 are the comparison of measured and fitted values of those elements.

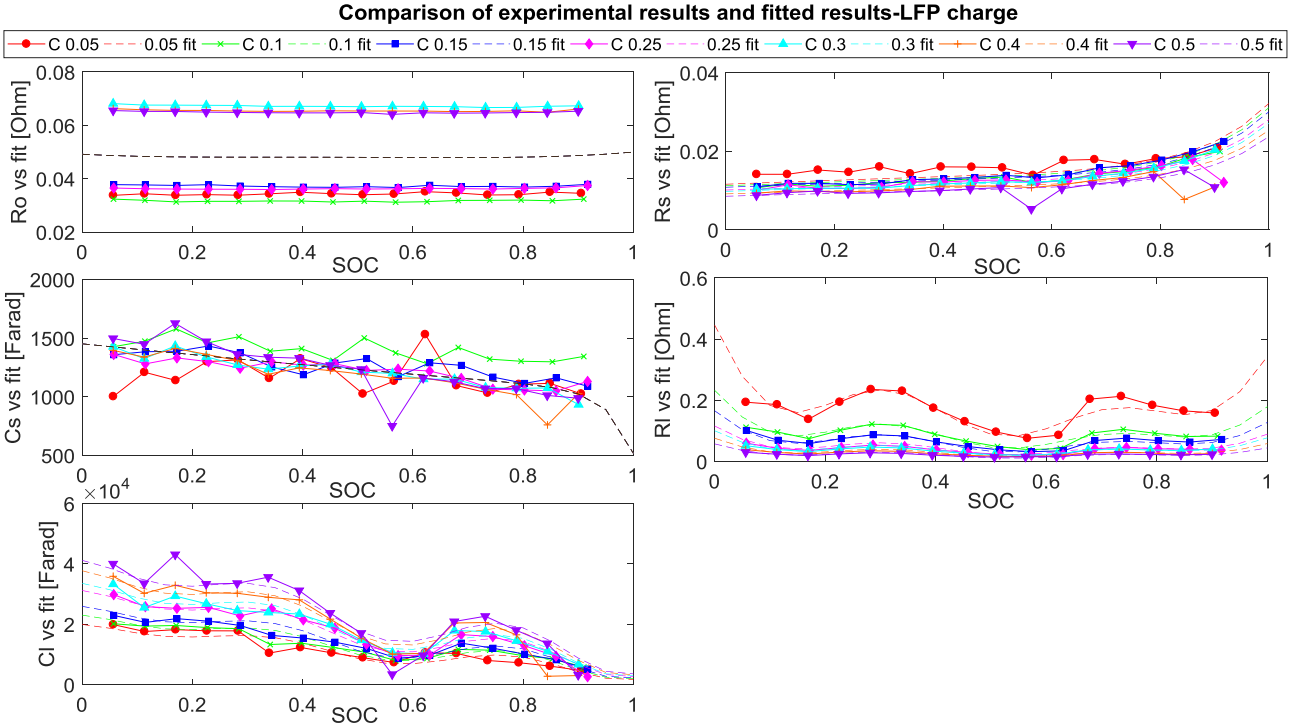

Figure 3-27 Comparison of measured and fitted data: LFP batteries during charge

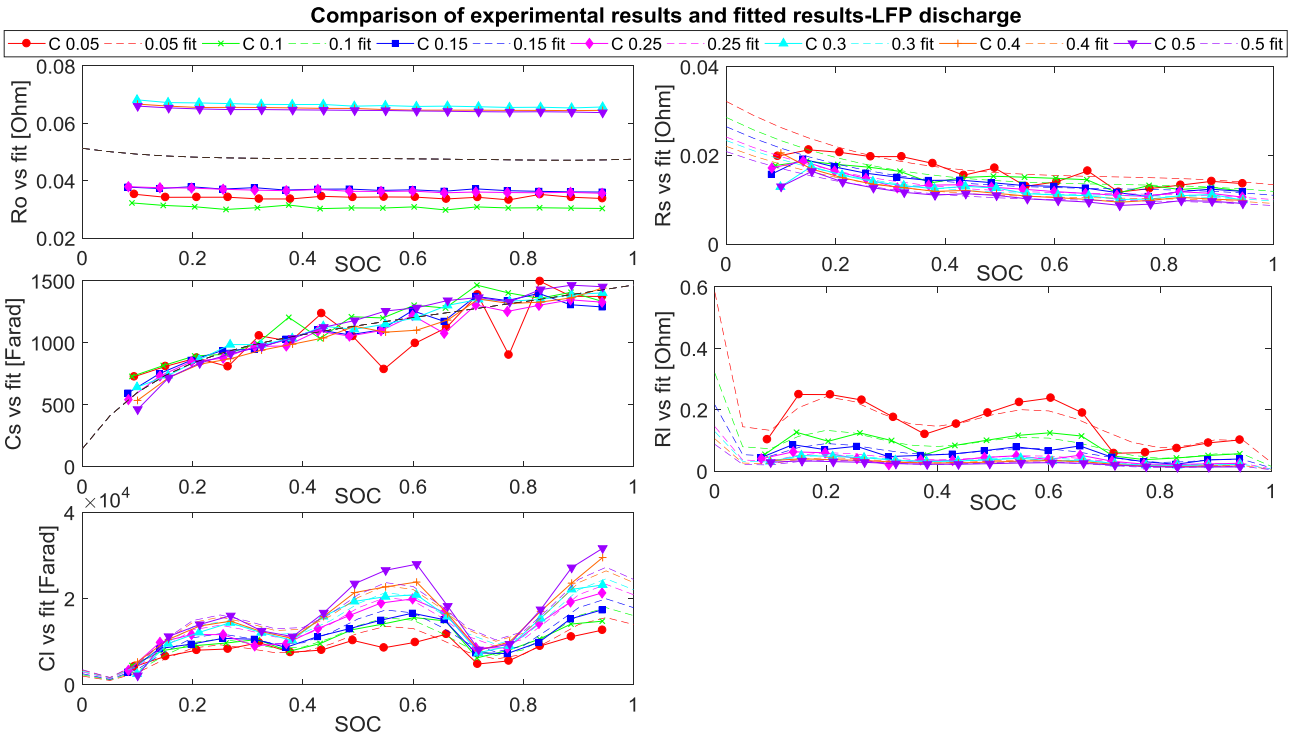

Figure 3-28 Comparison of measured and fitted data: LFP batteries during discharge

From these two figures, it can be observed that the fitting of all the electrical elements for battery model construction has a superior accuracy.

3.4.3 Voltage response circuit - VRLA battery

In proposed models, many authors suggested a one order RC circuit for lead-acid battery modelling. In order to choose an optimised EECM structure, the fitting comparison for one to three orders of RC circuits in plotted in Figure 3-29.

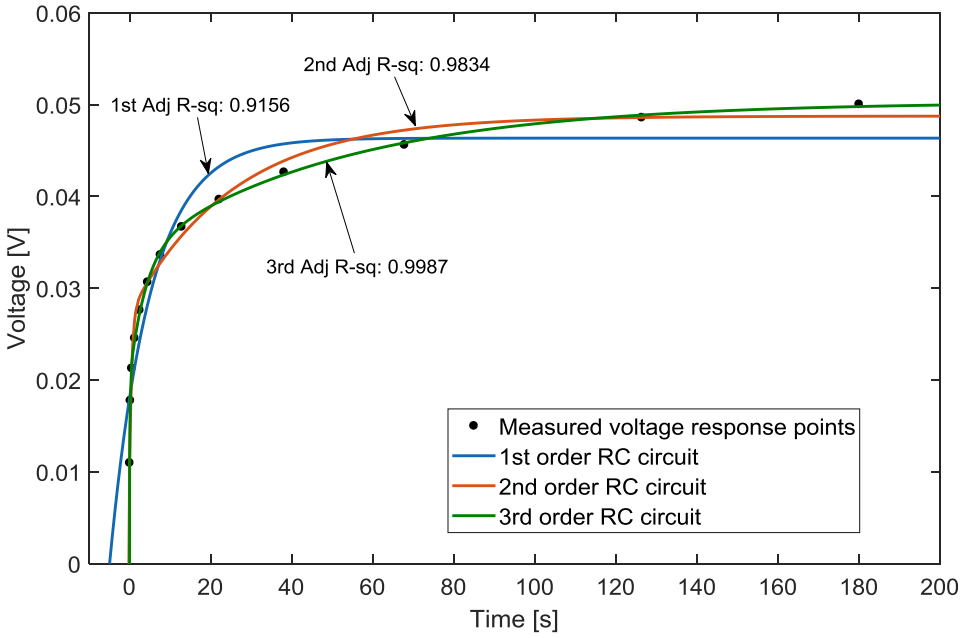

Figure 3-29 Comparison of accuracy with modelling VRLA battery into different orders of RC circuits

From the curve, one can conclude that second order of RC circuits have sufficient accuracy. In addition, model the battery with a higher order of RC circuit means more equations are required to represent added RC elements. That is to say, the second order RC circuit is not as complex as the third order one. So the second order RC circuits were also applied in VRLA dynamic modelling.

3.4.3.1 Parasitic branch

A VRLA battery has non-negligible side reaction gassing, which is the primary source of electrical charge losses. All the electrical elements should be calculated based on the current involved in the main reaction, so the first task is to model the mian branch current.

The measure coulombic efficiency results are plotted in Figure 3-30.

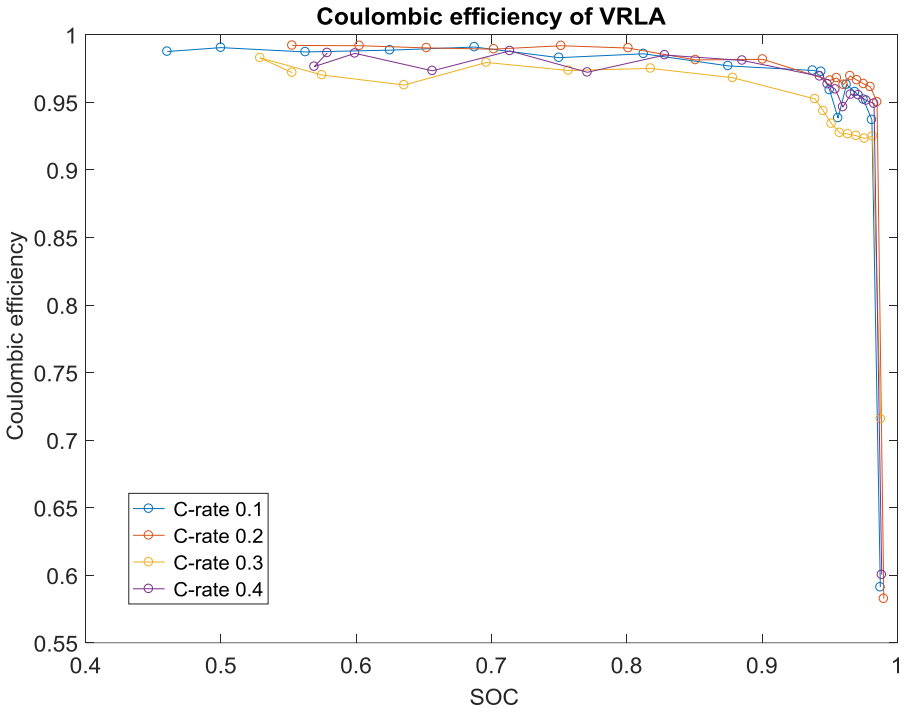

Figure 3-30 Measure coulombic efficiency of VRLA battery with SOC and with different C-rate

From the literature review in Section 3.2, the coulombic efficiency is expected to decrease when current increases. However, the efficiency measured with 0.2C is higher than that measured with 0.1C, and the result measured with 0.4C is larger than the one measured with 0.3C. It is because 0.1C and 0.3C measurements were operated on the same battery and another battery was tested with 0.2C and 0.4C. The differences between batteries may lead to this consequence. Nevertheless, the coulombic efficiency tested with higher C-rate do lower than one tested with lower C-rate on the same battery. Therefore, the coulombic efficiency was fitted into an exponential equation [82], as the function of both SOC and C-rate. The result is in Eq. (3.35)

$$\eta_c\left(I_{cr},SOC\right)=0.977\times\left(1-\exp\left(\frac{5.466}{5.569e-3\cdot\frac{I_{cr}}{0.2}+0.03745}\times\left(SOC-1\right)\right)\right) \tag{3.55}$$

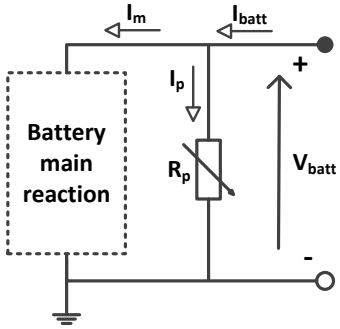

Figure 3-31 Illustration of the final selection in parasitic branch modelling of VRLA battery

The mian branch current can be modelled easily as the product of battery current and the coulombic efficiency in Eq.(3.56). Since the losses in side reactions including gassing phenomenon are modelled as the coulombic efficiency entirely, the parasitic branch is then modelled as a simple resistor but not a conductor in series with a

power source. Both of them are introduced in Section 3.2. The updated parasitic branch is in Figure 3-31, and the parasitic resistor is modelled in Eq.(3.57)

$$I_m = I_{cell} \times \eta_c ; I_p = I_{cell} - I_m \tag{3.56}$$

$$R_p = \frac{V_{cell}}{I_p} = \frac{V_{cell}}{I_{cell} \times (1 - \eta_c)} \tag{3.57}$$

Where V_{ell} and I_{cell} is the voltage and current of the cell; I_m is the current involved in the main reaction; I_p is the current on the parasitic branch; R_p is the resistor of the parasitic branch, and η_c is the coulombic efficiency.

3.4.3.2 Experimental results

Similar to the previous chapter, the measured and fitted results of all electrical elements in VRLA batteries are in Figure 3-32 to Figure 3-35.

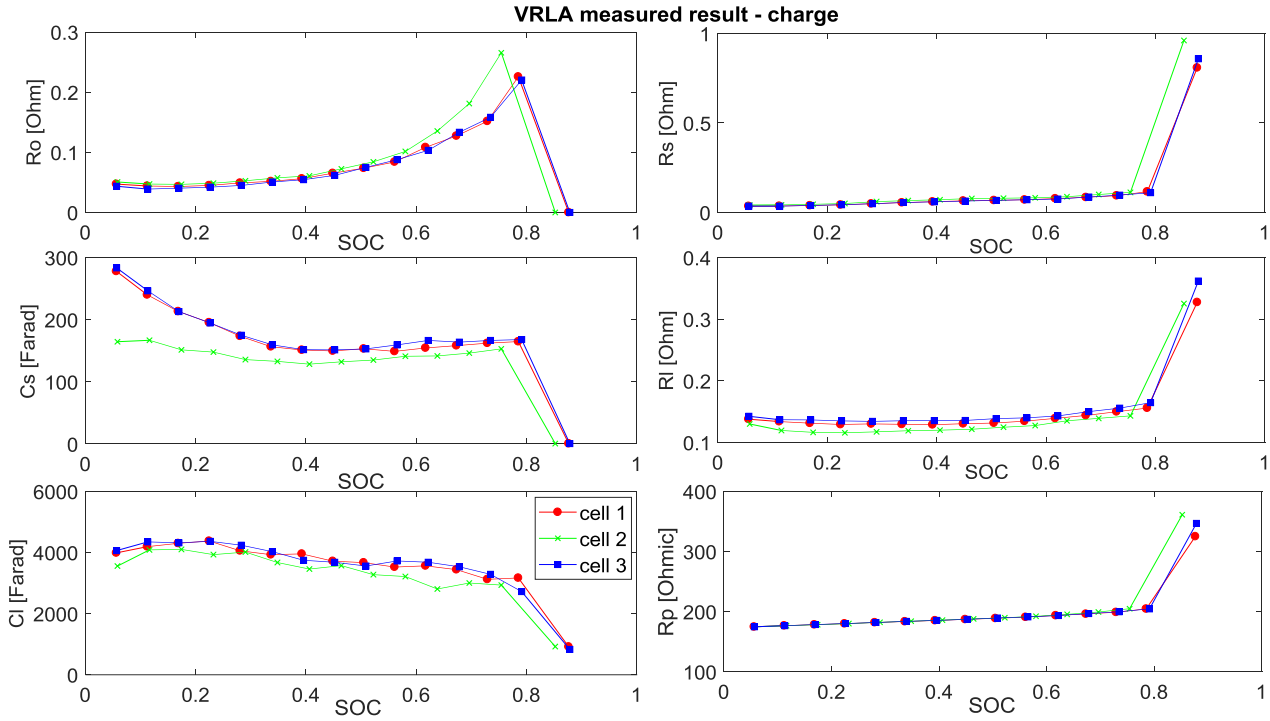

Figure 3-32 Values of electrical elements versus SOC of VRLA batteries measured and fitted during charge, with 0.2C-rate

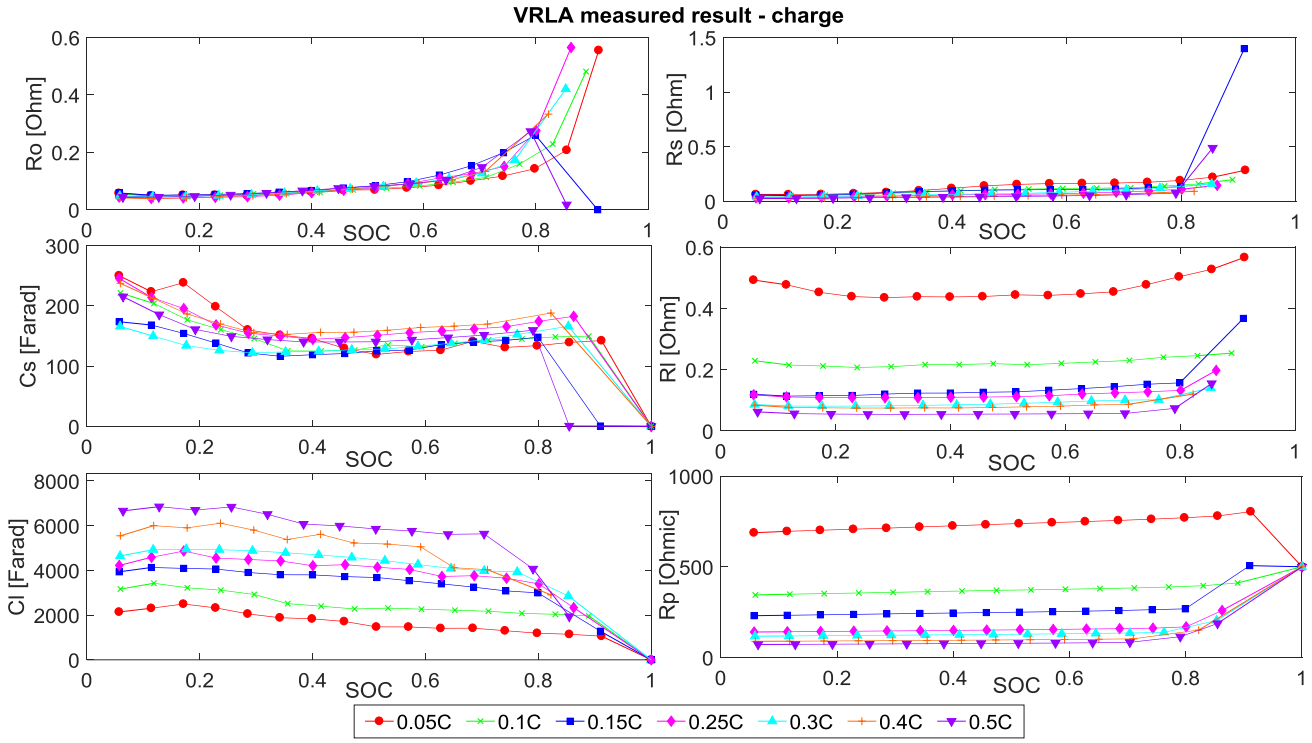

Figure 3-33 Values of electrical elements versus SOC and different C-rate of VRLA batteries measured and fitted during charge

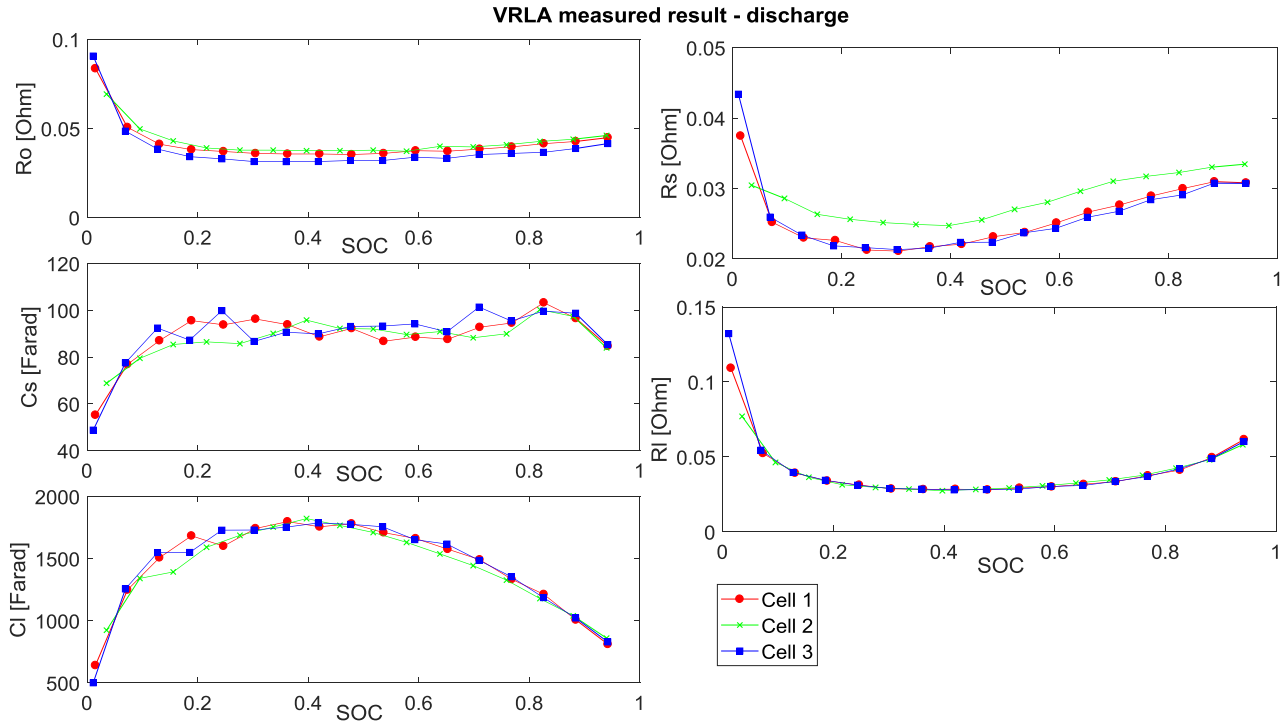

Figure 3-34 Values of electrical elements versus SOC of VRLA batteries measured and fitted during discharge, with 0.2C-rate

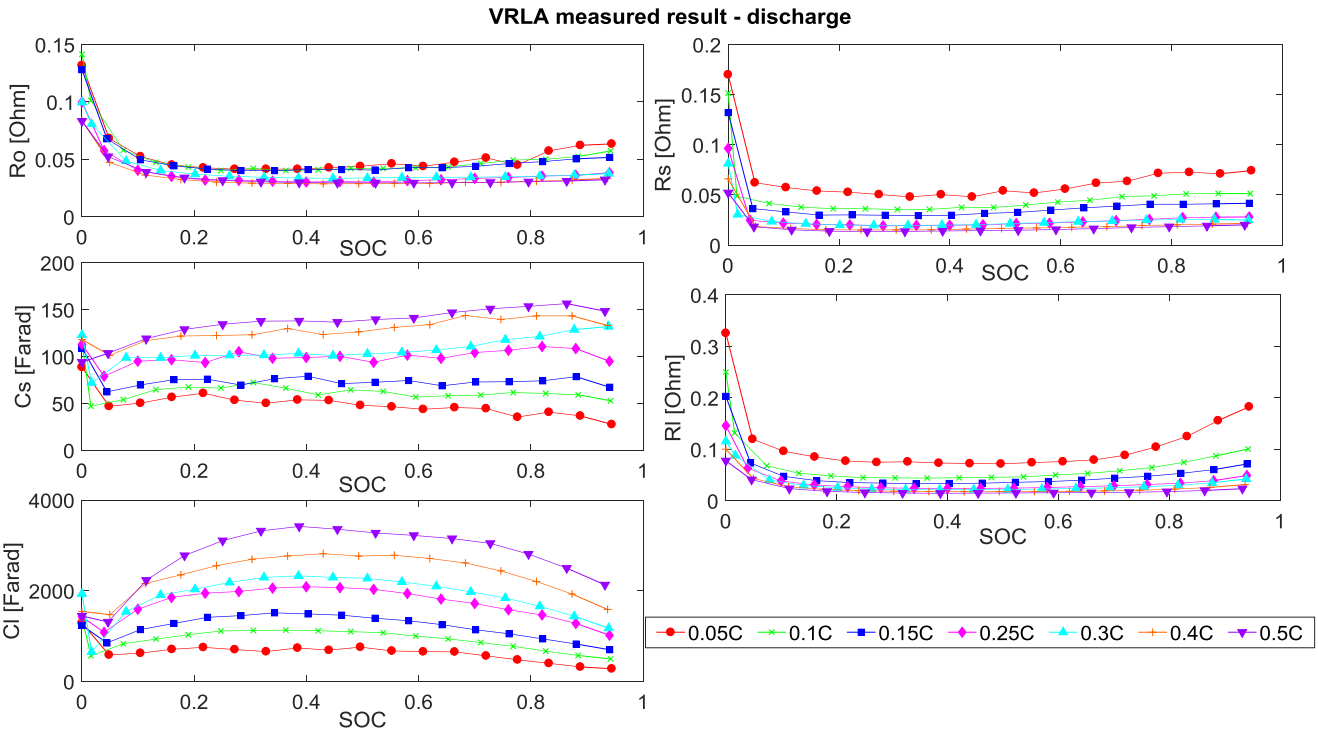

Figure 3-35 Values of electrical elements versus SOC and different C-rate of VRLA batteries measured and fitted during discharge

The plotted Rp values in Figure 3-32 and Figure 3-33 were calculated from coulombic efficiency, and it is independent of the main reaction circuit, the figure was only meant to compare the Rp value with other elements' value, so there will be no equation for Rp in the model. That is because the side reaction losses are modelled with the coulombic efficiency, which introduced Section 3.3.3.

From that measure and fitted results, some summaries can be made:

- For VRLA batteries, all the electrical elements show a strong dependency on SOC
- All the elements also show an inverse trend versus SOC in charge stage and discharge stage
- For current dependency, elements in charge and discharge have diverse behaviours. In charge process (Figure 3-33) only Rl and Cl values show a clear operational current reliance. In discharge process (Figure 3-35), all the elements are evidently influenced by the operational current. Therefore, the Rl and Cl in discharge stage and all the elements in charge stage would be modelled as the function of operational current.

3.4.3.3 Data analysis

The fitted SOC dependent electrical elements equations are listed below:

Charge:

$$Ro_{c\_VA}(SOC) = 0.03782 \cdot exp(1.301 \cdot SOC) + 4.226e-6 \cdot exp(12.64 \cdot SOC) \quad \textbf{(3.58)}$$

$$Rs_{c\_VA}(SOC) = 4.246e-13 \cdot exp(29.05 \cdot SOC) + 0.03787 \cdot exp(1.467 \cdot SOC) \quad \textbf{(3.59)}$$

$$Cs_{c\_VA}(SOC) = -2666 \cdot SOC^4 + 4113 \cdot SOC^3 - 1558 \cdot SOC^2 - 112.6 \cdot SOC + 229.3 \quad \textbf{(3.60)}$$

$$Rl_{c\_VA}(SOC) = 4.952 \cdot SOC^4 - 7.819 \cdot SOC^3 + 4.168 \cdot SOC^2 - 0.8406 \cdot SOC + 0.1783 \quad \textbf{(3.61)}$$

$$Cl_{c\_VA}(SOC) = -8768\cdot(SOC-1)^3 - 1.961e4\cdot(SOC-1)^2 - 1.512e4\cdot(SOC-1) \quad \textbf{(3.62)}$$

Discharge

$$Ro_{d\_VA}(SOC) = \frac{0.01226\cdot SOC^3 + 0.007354\cdot SOC^2 + 0.02339\cdot SOC + 0.003575}{SOC + 0.03138} \quad \textbf{(3.63)}$$

$$Rs_{d\_VA}(SOC) = \frac{0.01341\cdot SOC^3 + 5.996e-4\cdot SOC^2 + 0.02\cdot SOC + 6.888e-4}{SOC + 0.01043} \quad \textbf{(3.64)}$$

$$Cs_{d\_VA}(SOC) = -1116\cdot SOC^4 + 2320\cdot SOC^3 - 1640\cdot SOC^2 + 458.5\cdot SOC + 49.67 \quad \textbf{(3.65)}$$

$$Rl_{d\_VA}(SOC) = \frac{0.1373\cdot SOC^4 - 0.1344\cdot SOC^3 + 0.04953\cdot SOC^2 + 0.01366\cdot SOC + 0.003415}{SOC + 0.01673} \quad \textbf{(3.66)}$$

$$Cl_{d\_VA}(SOC) = -6879\cdot SOC^4 + 1.73e4\cdot SOC^3 - 1.877e4\cdot SOC^2 + 8425\cdot SOC + 492.4 \quad \textbf{(3.67)}$$

All of the equations listed above were selected with a cautious trade-off between complexity and accuracy.

After the acquisition of the SOC dependent equations of the circuit elements, it is then the current dependent equation exploration. The same fitting method as introduced in the Section 3.4.2.2 was applied to VRLA battery data analysis in operational current dependent modelling. The measured data with different operating current was divided by the value measured with reference current (0.2 C). All the quotient results are plotted versus SOC and C-rate separately in Figure 3-36 to Figure 3-38

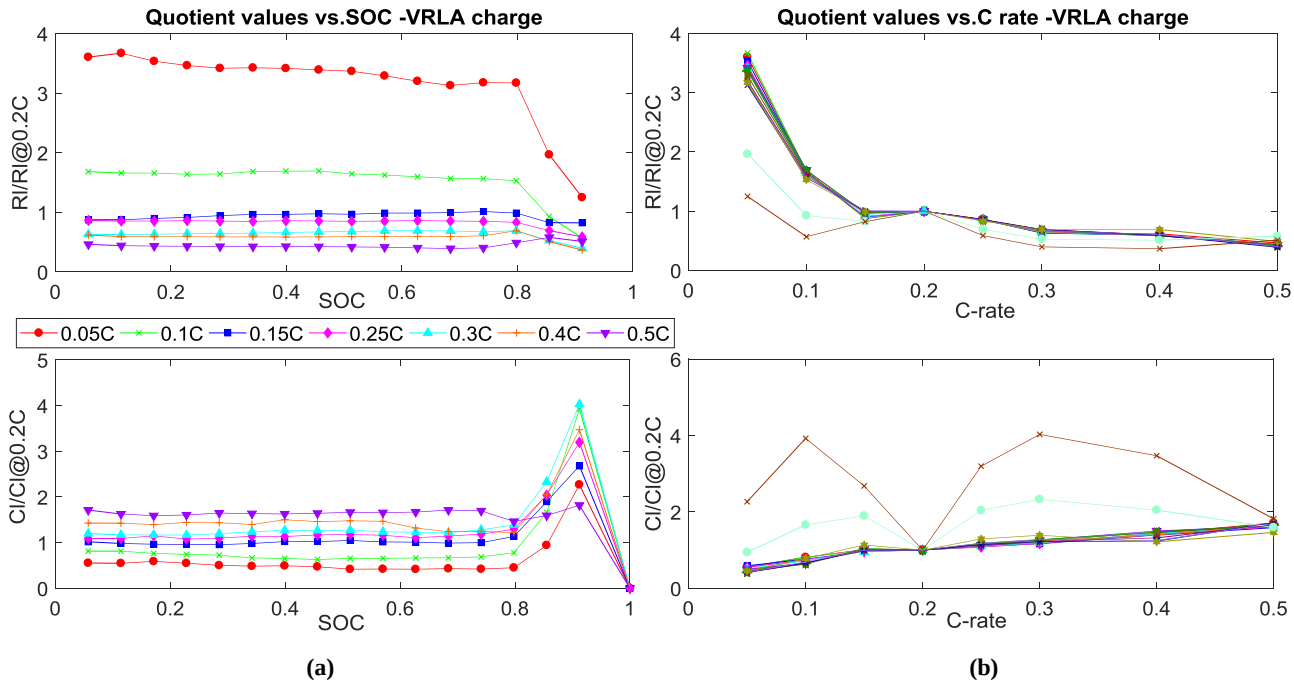

Figure 3-36 The quotient values of electrical elements of VRLA battery during charge
(a) quotient values of those elements versus SOC (b) quotient values projected to different C-rate;
R/C@0.2C means elements value measured with 0.2 C

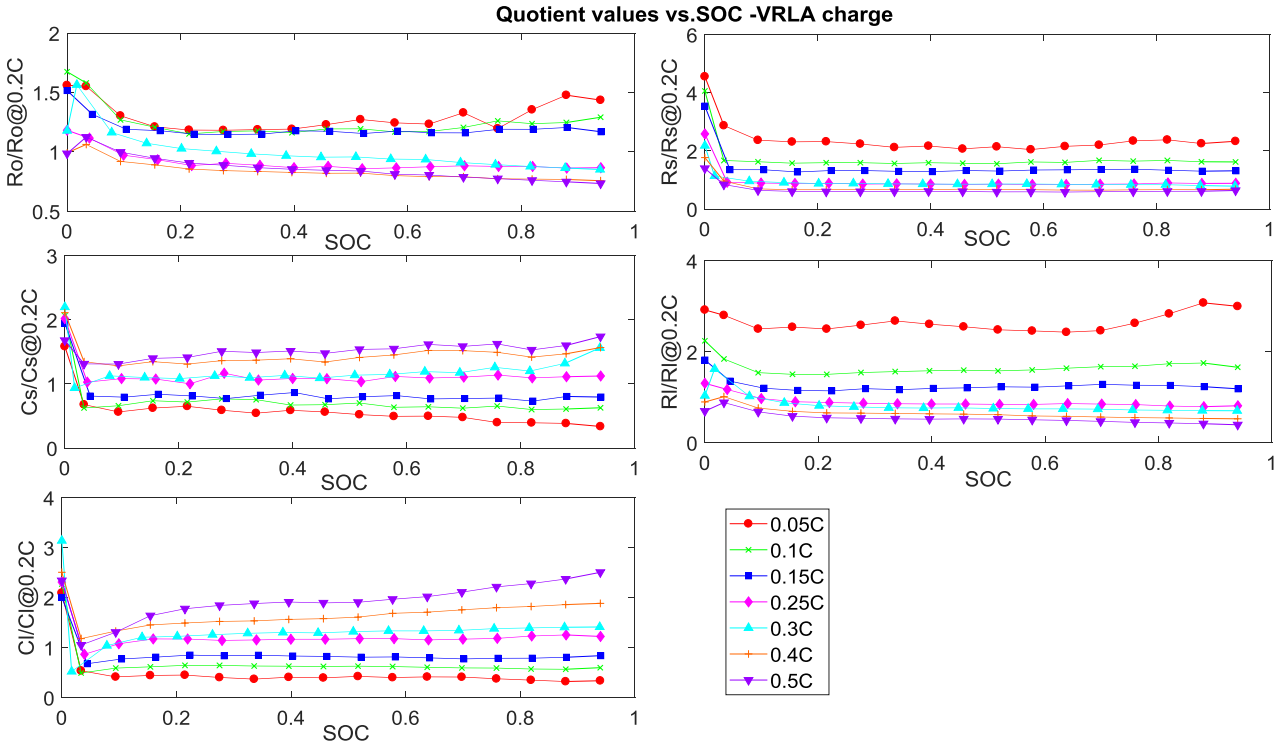

Figure 3-37 The quotient values of electrical elements of VRLA battery with SOC during discharge

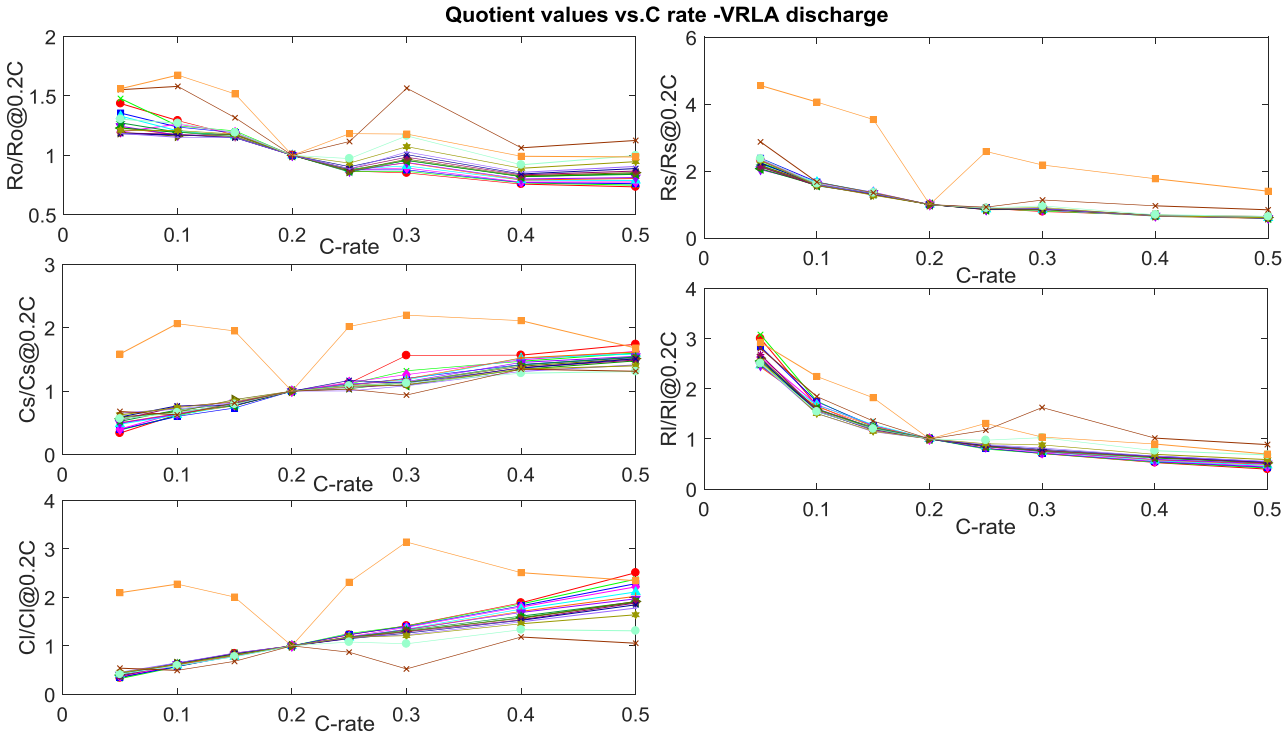

Figure 3-38 The quotient values of VRLA batteries during discharge projected to different C-rate

The fitted results of all equations are listed below:

Charge

$$Rl_{c\_VA} / Rl_{c\_VA}@0.2C\left(I_{cr}, SOC\right) = \begin{pmatrix} 9.8198e-4 \cdot exp\left(-48.992 \cdot \left(I_{cr}-0.2\right)\right) \\ +0.67172 \cdot exp\left(-5.6015 \cdot \left(I_{cr}-0.2\right)\right)+0.3273 \end{pmatrix} \times\left(-2.191 \cdot SOC^3+2.62 \cdot SOC^2-1.006 \cdot SOC+1.12\right) \quad \textbf{(3.68)}$$

$$Cl_{c\_VA} / Cl_{c\_VA}@0.2C\left(I_{cr}\right) = 11.66 \cdot \left(I_{cr}-0.2\right)^3-4.366 \cdot \left(I_{cr}-0.2\right)^2+2.43 \cdot \left(I_{cr}-0.2\right)+1 \quad \textbf{(3.69)}$$

Discharge

$$Ro_{d\_VA} / Ro_{d\_VA}@0.2C\left(I_{cr}, SOC\right) = \begin{pmatrix} -78.342 \cdot \left(I_{cr}-0.2\right)^4+25 \cdot \left(I_{cr}-0.2\right)^3 \\ +4.6032 \cdot \left(I_{cr}-0.2\right)^2-2.1016 \cdot \left(I_{cr}-0.2\right)+1 \end{pmatrix} \times\left(0.4411 \cdot exp\left(-16.19 \cdot SOC\right)+0.9853 \cdot exp\left(0.01733 \cdot SOC\right)\right) \quad \textbf{(3.70)}$$

$$Rs_{d\_VA} / Rs_{d\_VA}@0.2C\left(I_{cr}, SOC\right) = \begin{pmatrix} 6.6819e2 \cdot exp\left(-0.0011936 \cdot \left(I_{cr}-0.2\right)\right) \\ +0.15861 \cdot exp\left(-14.305 \cdot \left(I_{cr}-0.2\right)\right)-667.3473 \end{pmatrix} \times 1.003 \cdot exp\left(0.01652 \cdot SOC\right)+0.3767 \cdot exp\left(-20.89 \cdot SOC\right) \quad \textbf{(3.71)}$$

$$Cs_{d\_VA} / Cs_{d\_VA}@0.2C\left(I_{cr}, SOC\right) = \left(-3.3295 \cdot \left(I_{cr}-0.2\right)^2+2.7116 \cdot \left(I_{cr}-0.2\right)+1\right) \times\left(0.9504 \cdot exp\left(0.0464 \cdot SOC\right)+0.3536 \cdot exp\left(-609.2 \cdot SOC\right)\right) \quad \textbf{(3.72)}$$

$$Rl_{d\_LP} / Rl_{d\_LP}@0.2C\left(I_{cr}, SOC\right) = \begin{pmatrix} 0.13707 \cdot exp\left(-16.624 \cdot \left(I_{cr}-0.2\right)\right) \\ -1.021 \cdot exp\left(0.91595 \cdot \left(I_{cr}-0.2\right)\right)+1.8839 \end{pmatrix} \times 0.9371 \cdot exp\left(0.05663 \cdot SOC\right)+0.421 \cdot exp\left(-13.09 \cdot SOC\right) \quad \textbf{(3.73)}$$

$$Cl_{d\_LP} / Cl_{d\_LP}@0.2C\left(I_{cr}, SOC\right) = \left(3.8298 \cdot \left(I_{cr}-0.2\right)+1\right) \times\left(0.5753 \cdot exp\left(-674 \cdot SOC\right)+0.8458 \cdot exp\left(0.2202 \cdot SOC\right)\right) \quad \textbf{(3.74)}$$

The function used to get the final equations for these elements is the same with Eq. (3.54).

The fitted electrical elements' value for model construction are compared to the experimental results and plotted in Figure 3-39 and Figure 3-40.

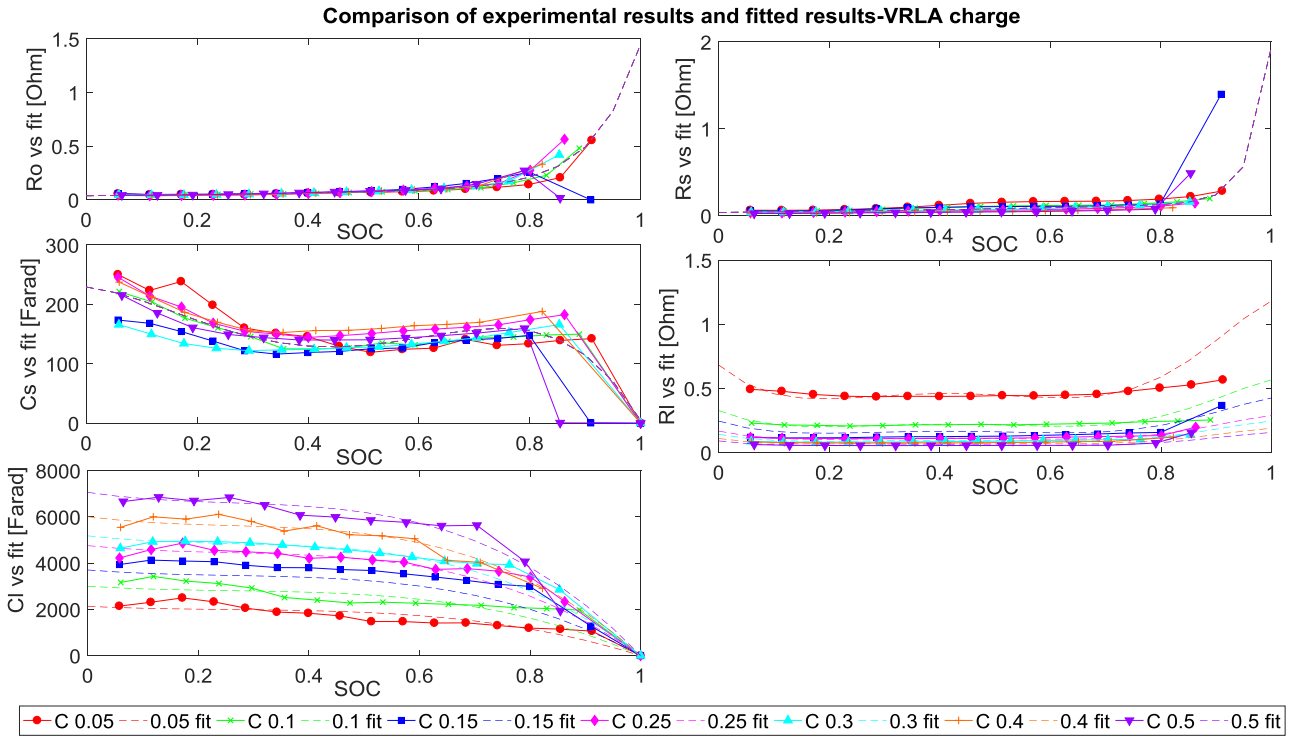

Figure 3-39 Comparison of measured and fitted data: VRLA batteries during charge

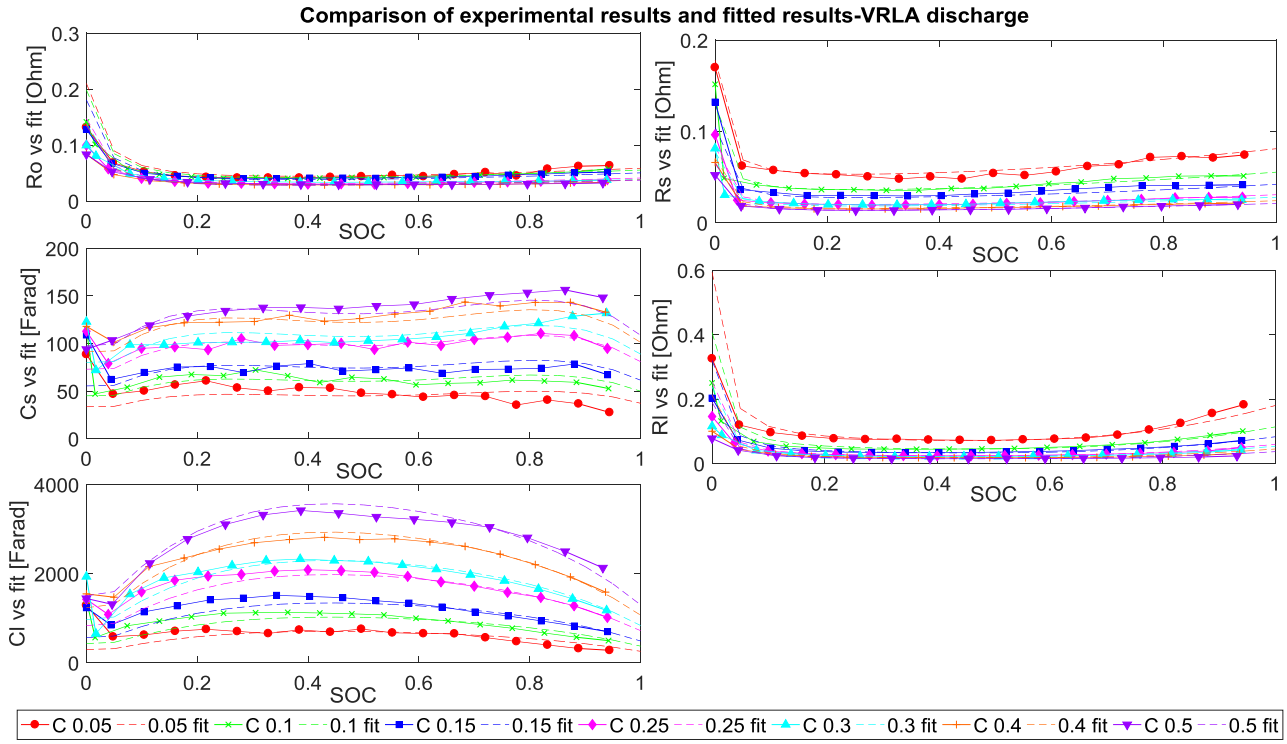

Figure 3-40 Comparison of measured and fitted data: VRLA batteries during discharge

These two figures indicate an excellent accuracy of the circuit elements modelling.

3.4.4 Modelling and simulation results

In the end, it is the simulation results compare with the experimental data. In order to quantify the model accuracy, all the modelled and measured voltage were calculated in Eq.(3.75).

The CV stages were omitted from the calculation because the real measurement pause steps in CV stages were completed by the tester and it is unable to be duplicated with the simulation.

$$error = \frac{V_{sim} - V_{\exp}}{V_{\exp}} \times 100\% \tag{3.75}$$

Where V_{sim} is the simulated voltage and V_{exp} is the voltage gained from experiments.

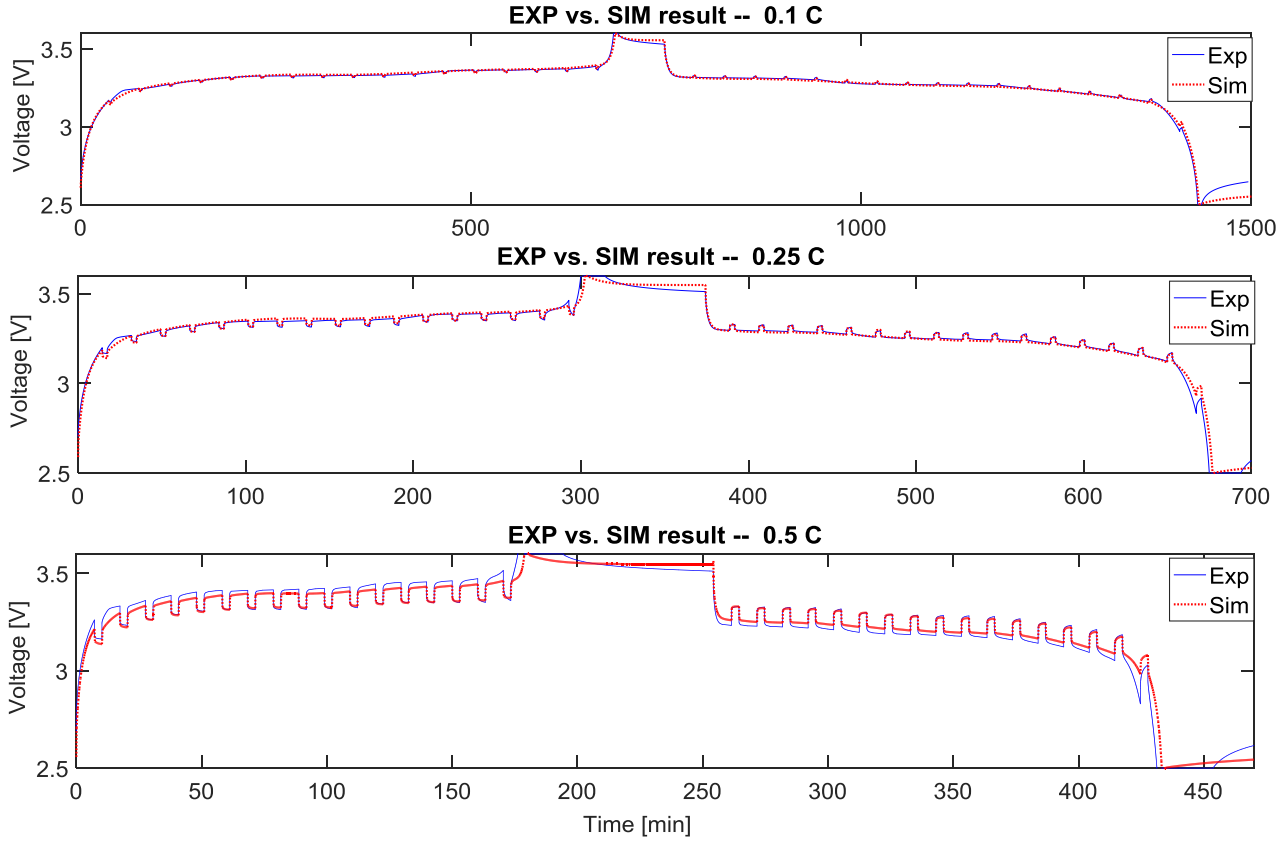

Figure 3-41 Comparison of experimental result and simulation result-LFP battery

In Figure 3-41 are some samples of the comparison with simulated results and the experimental results of LFP batteries.

For LFP batteries, the maximum averaged error among all different C-rates is 1.7636%. The discrepancy of the wedges shaped charge/discharge steps is mainly due to the differences in ohmic resistance. The error from ohmic resistance counts at least 0.5%.

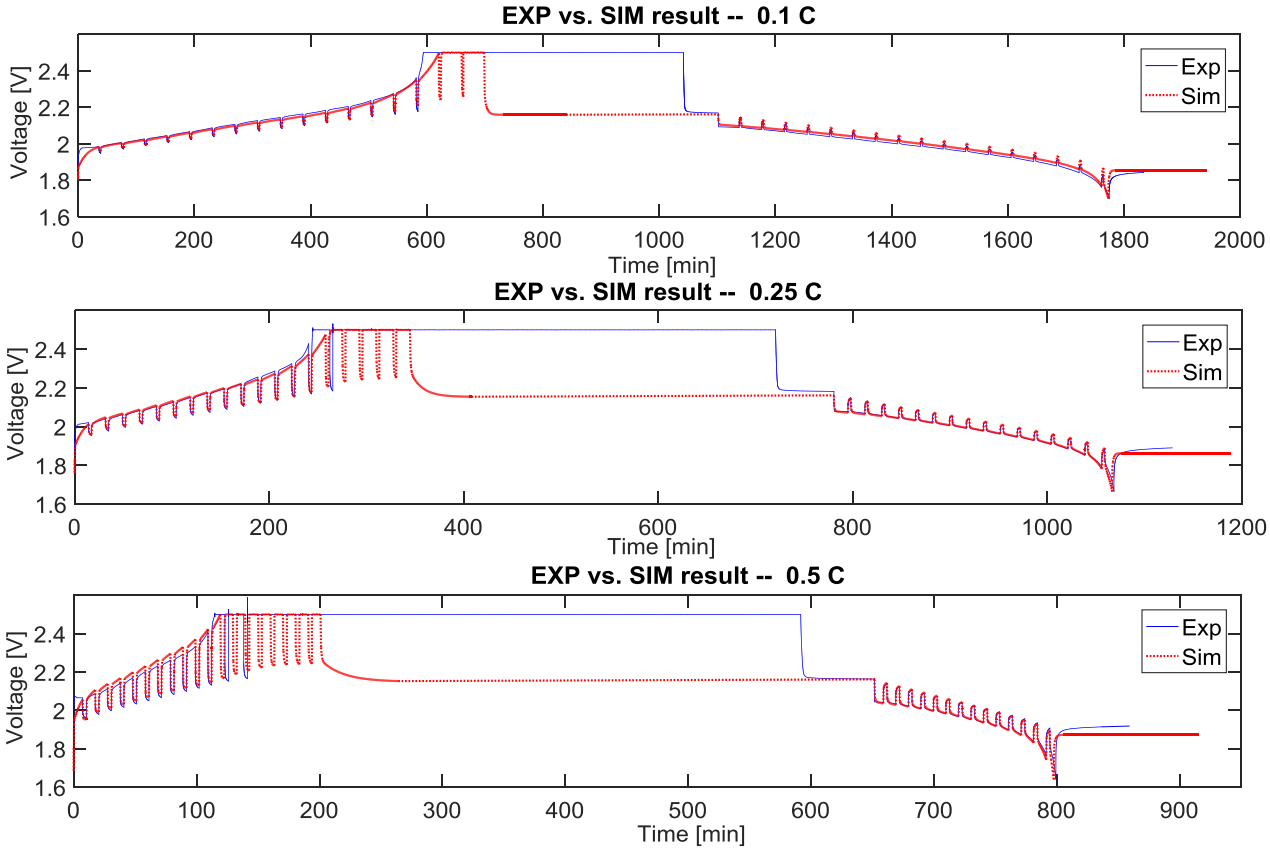

Figure 3-42 Comparison of experimental result and simulation result- VRLA battery

The comparison of sample simulated and experimental results of VRLA batteries are in Figure 3-42.

For VRLA batteries, the maximum averaged error among all different C-rates is 1.0354%.

The dynamic models of both battery technologies are therefore considered accurate.

3.5 Conclusion

In the chapter, the tests of the dynamic behaviour of both battery technologies was described.

Then, the relevant parameters were extracted then applied in the model.

The next chapter is then the long term battery behaviour exploration including SOH model design, lifetime experiments.

4 Battery lifetime modelling

4.1 Introduction

In this chapter, how the battery lifetime was modelled and how the experiments were designed and operated are introduced.

As introduced in Chapter 2, the battery ageing only because of cycling is explored and the battery performance-based lifetime modelling method is employed. Since the battery is for SHS implementations, the storage capability of the battery is considered as the most important parameter. Therefore, the battery capacity is chosen as the performance parameter with which the battery lifetime can be expressed in a state of health (SOH) equation.

The end of life (EOL) point definition in different papers for different battery technologies is introduced in Chapter 2. In this study, the EOL point is defined according to the literature review in Section 2.4.2 as: the battery capacity is less than 80% of the maximum dischargeable capacity of a fresh battery (C_{dsb0}), which is the C_{dsb0} minus the maximum tolerable irreversible capacity loss F_{EOL}.

During the whole life of one battery, its capacity decreases irreversibly in different rate according to the application manners. The part where the capacity reduction is highly dependent on the application is important to the research. By comparing the remaining battery capacity and the original capacity of a fresh battery, one can observe its ageing process. In this way, the battery lifetime can be predicted and modelled for the chosen application.

The SOH can be written in the form that from the fresh battery to the EOL point, the SOH drops from 100% to 0%. Since the sign of the EOL point is when the total amount of irreversible capacity loss reaches a certain normalised the fresh capacity. The 100% to 0% SOH from the beginning to the end of life can be expressed as: one minus the fraction of the irreversible capacity loss to the maximum tolerable irreversible capacity loss. The equation (4.1) is modified from [106]:

$$SOH = \left(1 - \frac{F}{F_{EOL}}\right) \times 100\% \qquad \textbf{(4.1)}$$
$$F = f\left(Q_{th}, SOC, I, T, ...\right);\ F_{EOL} = 20\% \times C_{dsb0}$$

Where F is the irreversible capacity loss, F_{EOL} is the maximum tolerable irreversible capacity loss, C_{dsb0} is the maximum dischargeable capacity of a fresh battery. Q_{th} is the capacity throughput, I is the operational current and T is the battery temperature. The irreversible battery capacity loss is a result of different stress factors, which will be introduced in detail in next section.

The key unknown variable in the SOH equation (4.1) is F, the amount of irreversible capacity loss. Many stress factors influence the F value and the variation of F value. In order to model the F value, things need to know are what are the stress factors for two battery technologies, and what are their interrelations.

4.2 Battery ageing mechanism

4.2.1 LFP battery ageing mechanism

4.2.1.1 General Introduction

As mentioned in chapter 2, Lithium-ion battery is a type of battery that both electrodes served as hosts for lithium ion (Li^+), and the ions insert, extract from the electrodes and move from one side to another.

The most common negative electrode (anode) material is different forms of carbon, e.g. graphite. There are varieties choices of positive electrode (cathode) materials. Both electrodes are combined with support materials, for example, binder or conductivity enhancers. Moreover, the electrodes are coated with a thin layer then connected to a current collector.[118]

The most frequently used electrolyte for Li-ion batteries is the liquid electrolyte, which composed of organic solvents and supporting lithium salts.[30] However, the stable window of electrolyte vs Li is between 0.8V to 4.5V, and the working voltage of graphite anode is around 0.05V vs Li, which is out of the electrolyte stability window [119]. Which means, the anode side electrode-electrolyte interface is unstable. A chart of the stable windows is in Figure 4-1.

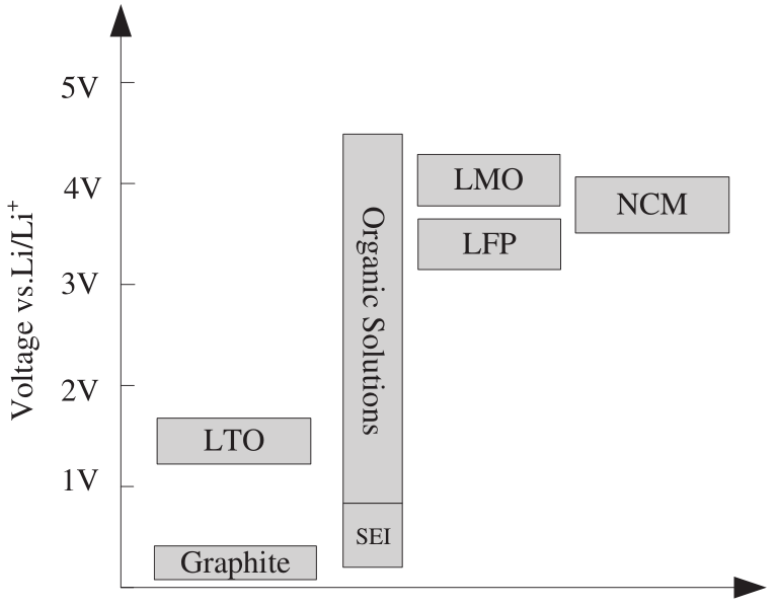

Figure 4-1 Voltage vs Li/Li^+ of different electrode materials and the stability window of common liquid organic electrolytes (Fig.2 of [120])

Due to the instability at the anode-electrolyte interface, the electrolyte solution can easily get reductive decomposition in the initial stage of charge then form a passive film on the surface of the anode. After the formation, this passive film helps in restraint further solvent decomposition by blocking electron transport. In the meanwhile, this film still allows Li-ions' getting through during cycling in the ideal case [121]. Thus, this film acts as a solid electrolyte, and it is often called Solid Electrolyte Interface (SEI) [122].

The ageing mechanism in Li-ion batteries is different when it is happening on the cathode or the anode, and the electrolyte related ageing mainly takes place at the electrolyte-electrode interface [123]. In the sense of battery degradation, the most critical part of the cell is considered as the negative electrode/electrolyte interface, which is the SEI [124]. That is because, the battery performances in long-term scale, i.e. safety, cyclability, irreversible charge loss, self-discharge and rate capability, rely heavily on the SEI quality [31][121].

In general, for all types of Li-ion batteries, the degradation possibly take place on the anode side are:[123][31][125]

1. Degradation related with formation and growth of SEI:
    - The SEI grows over time, inducing lithium ions loss and the electrolyte decomposition continuously

- After a period of cycling time, the insertion-extraction of Lithium ions will make this layer unstable. This unsteady may lead to further surface reactions and may eventually isolate the graphite particles from the current collector.
- The growth of the layer can result in the increase of charge transfer resistance and impedance on the anode. The rise of the impedance is related to power fade. Moreover, the increased impedance may limit the accessibility of lithium ions to the surface of the anode, which leads to the irreversible capacity loss.

2. Loss of recyclable Lithium ions
    - The loss of recyclable lithium ions may result in self-discharge, and it is considered as the dominant reason causing the reduction of Li-ion battery capacity
    - The initial irreversible loss of lithium ions contributes to the SEI formation, which mainly occurs in the charge state at the beginning of cycling, especially in the first cycle.
    - In the later stage of battery cycling, the loss of lithium ions is mainly caused by the side reactions with the decomposed electrolyte compounds and the water
3. Structure change of the anode (Graphite)
    - The insertion-extraction of lithium ions could cause cracks on the graphite particles and makes the graphite particles less oriented than their original state. The orientation of the graphite particles is related to the reversible capacity of the anode
    - The particle size of graphite anode has strong influence on the thermal stability of the anode
    - The stability of graphite anode also depends on the solvent chemical features. The solvent molecules migrated with Lithium ions and co-intercalated into the graphite particles with the Lithium ions. Those solvent molecules that in the graphite lattice will block the entry of Lithium ions. Further co-intercalation of solvent molecules will increase the danger of complete exfoliation and amorphization of the graphite.
4. Lithium metal plating
    - When the battery is charged at a low temperature, an inhomogeneous current distribution can lead to the parasitic reaction of metallic lithium plating and the dendrite growth on the anode
    - The dendrites can disconnect and isolate the separator from the electrolyte. In some extreme cases, these dendrites can even tunnel the separator and cause a short-circuit and thermal runaway in the battery.
    - The metallic Li can react with the electrolyte, accelerating the fading of the battery

All the above mechanisms are suitable for all types of Li-ion battery with a graphite anode.

Even though the degradation that happens in cathode is different between materials, the common features can be summarised as below: [123][31][126]

- Degradation of crystalline structure of positive materials during cycling
- Chemical decomposition/dissolution reaction in electrolyte
- Build-up of the passivation film, which limits the active surface area and clogging the electrode
- Mechanical modification of the cathode surface

Although Lithium-ion batteries with different cathode chemistries may have distinct behaviours, the common ageing mechanisms are linked to the negative electrode and the SEI layer stability. It also considered that the anode is the most critical part in lithium battery lifetime. [124]

4.2.1.2 LFP battery

For cathode chemical characters, it is widely agreed that olivine $LiFePO_4$ is more stable and less reactive in non-acid or non-protic solutions at elevated temperatures than many other types of the cathode. In standard $LiPF_6$ solutions, which unavoidably contain trace HF, the LiFePO4 cathode is stable at a moderate temperature, e.g. around 30 ℃. Therefore, the degradation of LFP batteries can be focused on the anode side. [127][128][129]

4.2.1.2.1 Battery performance when ages

- Capacity loss

It is considered that the capacity fading of LFP batteries are mainly due to the loss of active Lithium ions and batteries lose their capacity while cycling. There is a loss of active lithium in the formation of SEI layer at the beginning of LFP cycling [130][131][132][133]. As a consequence, the amount of active lithium is less than the capacity of both electrodes, leading to lithium as the restraining factor of battery capacity fading. When the battery ages, the material loss from anode or cathode is less than the active lithium losses, and the material loss does not directly relate to the capacity loss. [130]

When the battery ages, the pre-existing cracks on the electrode surface grows gradually under the stress and the SEI layer degrades as well. The active lithium forms small lithiated species and deposits them at the negative electrode. The active lithium is also consumed in fixing and repairing the destabilised SEI layer and in forming new SEI on newly exposed electrode surfaces. As a result, there are consecutive active lithium losses in each cycle.[130][131][132][134][133] Hence, the perturbation to the SEI layer accelerates the lithium loss.

It is also considered that the lack of reversibility of Fe^{2+}/Fe^{3+} redox reaction is remediable by the lithium replenishment. Thus, the reduced reversible Fe^{2+}/Fe^{3+} redox reaction is in line with the loss of active lithium [131], which is the direct cause of capacity loss. In addition, the reduction of the redox reaction may aggravate by cycling and an elevated temperature.[131]

- Impedance increase

Apart from capacity loss, battery impedance is also increased when battery ages, which may harm to the power capability. An area-specific impedance resistance increase was observed in experiments especially when discharge at high DOD [133]. EIS measurement in [132] shows that both electrodes experienced some impedance rise when ageing and a remarkable high increase rate of impedance at cathode interface is observed. The conclusion drawn in [135] is the impedance increase on the anode side is more than on the cathode side. However, paper [130] declares that the EIS and HPPC measurement showed a negligible impedance increase, which means the influence of age on LFP batteries is because of the capacity fading rather than the resistance increase.

4.2.1.2.2 Factors influence battery ageing

- Time and usage

For especially capacity fading, the calendar capacity loss is strongly influenced by time, temperature and the storage SOC. [31] Under a certain temperature, the calendar capacity loss simply follows the time kinetic principle, which related to the chemical reaction kinetics [136]. When the battery is in operation, it may suffer from both cycle ageing and calendar ageing because calendar and cycle ageing are additive. Hence, battery under cycling may get through more severe capacity fading than in storage [137][138]. It is suggested that the capacity loss increases linearly with cycle numbers [127].

- Operational C-rate:

An increasing operational current can accelerate the overall capacity loss of the battery. However, the fading behaviours of two electrodes are distinguished under different current. The post-electrochemical half-cell analysis shows that graphite electrode (anode) experiences remarkable capacity fading with low C-rate under standard conditions, while the capacity and power fading of LFP electrode (cathode) is more noticeable under higher C-rate.[132] Researches in [133] proved it with a similar result at the cathode, and this phenomenon occurs probably because of low electric conductivity and lithium diffusivity in $LiFePO_4$ electrode. Experiments in [139] show that increasing operational current may accelerate the battery degradation heavily. Moreover, the

increased current on charge and discharge may have a different impact on battery degradation. The cell lifetime is more sensitive to discharge rate than the charge rate. On the other hand, over charge is worse than over discharge for the battery cycle life. Experiments in [140] report an accelerated capacity fading caused by higher discharge C-rate (3C) at room temperature. However, an opposite conclusion was obtained in [141] that the cell lifetime is influenced more by charging rate than discharging rate. In addition, high C-rate always not independent from excessive room temperature, since high C-rate always leading to a rapid heating up of the cell.

- Temperature:

It was found from experiments that temperature firmly impacts the capacity fading of the LiFePO4 battery on both calendar ageing and cycle ageing [138][142]. Both high (>>25 ℃) and low (<<25 ℃) temperature may accelerate the battery fading rate. Both capacity and power have a more severe degradation at a lower temperature than at higher temperature[143]. Cycle losses increase with elevated temperature was also observed in experiments [144]. The substantial mechanism is a rising temperature aggravates the decay of the cathode, promotes the decomposition of the electrolyte and accelerates the lithium consumption, especially when the temperature is higher than 45 ℃ [145]. When the battery is in storage, the main capacity fading reason is still the loss of cyclable Lithium ions. The lithium loss is caused by side reactions that take place at the anode interface, and a higher storage temperature exacerbates this ageing progress [146][135][142]. Apart from that, the overall cell impedance increased under higher storage temperature as well. [146]

- SOC and its variation

It is reported that both too high or too low operational SOC level do harm to cell lifetime since the SOC level correlates with the electrode potential level [123]. Some authors considered that a higher operational SOC might lead to a worse active material loss and an impedance increasing [147]. At a specific C-rate, the larger operational DOD (depth of discharge) (>50%) may cause more capacity fading than a smaller operational DOD (<50%). However, the DOD still shows less significant influence than the time and the cell temperature in battery ageing [148]. Some authors separated the DOD into averaged SOC and ΔSOC two variables and it was found that higher averaged SOC and higher ΔSOC lead to faster battery fading [106][136][149][150]. Some researchers also declare that the DOD even does not affect the fading rate at all [151].

Although controversy still exists in how ageing impacted by operational SOC and its variations, it is clearly agreed that storage SOC does influence the battery calendar ageing rate. When a LiFePO4 battery is stored at a higher SOC, the battery ageing process is always more severe, but the influence of SOC is less than a higher temperature [135][136][142][146].

4.2.2 VRLA battery ageing mechanism

There are many reasons for the ageing process of VRLA battery, and the main ageing mechanisms are summarised and listed.

- Anode (PbO_2) corrosion
- Irreversible sulfation (formation of lead sulphate in the active mass)
- Positive active mass degradation/softening (shedding, sludge)
- Water loss/drying out. (This is a damage mechanism especially for VRLA batteries, since water in flooded Lead-acid battery can be refilled)

The inappropriate usage methods which may give rise to these ageing phenomenon are:

- Ah throughput (workload since employed)
- Operating current
- SOC state (time at low SOC; storage time before use; degree of overcharge; time between full charges)
- SOC variation (partial cycling; under-charge;)
- Battery temperature

It is considered that the corrosion of the anode is the natural process of ageing which happens while the cycles increased. The anode corrosion is also regarded as the main reason that causes ageing and the final EOL of a VRLA battery. However, apart from this natural process, many stress factors may aggravate the anode corrosion, and an irregular usage pattern may cause severe degradation of the negative plate, separator and other parts [152]. All of them are introduced in detail below:

- Positive grid corrosion and water loss

Positive-grid corrosion happens during float application or overcharge, and it is related to the magnitude of the current [153]. When is the battery is undergoing gassing, the depletion of water and the increasing H^+ ions makes the acidity around positive electrode rises. In the meantime, a dilution effect takes place at the negative electrode. These processes increase the positive-grid corrosion (anode corrosion) and the water loss.

A higher overcharge voltage may cause a worse water loss [154]. Operating at a high temperature increases the corrosion of positive grid and accelerates the water dry-out as well. Charging the battery with an excessively high voltage and high current leads to a high positive potential, which also aggravates the positive grid corrosion.

- Sulfation

Sulfation means the irreversible accumulation of lead sulphate on the electrode plate.[28]

The irregular current regime, e.g. heavy-cycling/deep-cycling and undercharging may arouse the sulfation of the positive mass [155][156]. It is also reported that a negative plate sulfation could happen due to the oxidation of negative mass, which may be on account of the bad seal property of the valve. [155]:

If the battery remains at a partial discharge or under the charged state for a long time, or if the battery is usually working under these conditions, the re-crystallisation of $PbSO_4$ will become a threat to the battery lifetime. [153]

The negative plate shows a higher tendency of sulfation than the positive plate [153]. High rate charge, irregular charge and continuous usage in under-charge state will cause the accumulation of lead sulphate at the negative electrode. Experiments in the paper [152] have revealed that 20% sulfation happens at the anode while 40% sulfation is taking place at the cathode. Sufficient charge can eliminate the sulfation happening at the anode, but 20% sulfation will still be left at the cathode. If the battery always works at undercharge condition, the sulfation of cathode would eventually restrict the capacity.

- Softening of positive active-material

Softening means the $PbSO_2$ particles lose the coherence with each other and with the grid, then becoming electrical isolates and no longer be able to participate in the discharge process [28], [153], [155].

It is considered that cycling regime is the dominant reason that initiates the softening of positive active material.[153] For example, prolonged cycling and the deep cycle may cause severe soften[153], [156]. The high discharge current can cause softening of the positive material at the anode as well. [155]

- Interdependency

Even though the ageing mechanism can be separated into different types, they are often inter-dependent.

For example, the corrosion of grid will lead to an incremental resistance to the current flow. This sequence may cause the improper charge of active mass, which will finally result in sulfation of the active mass.

Overcharge may give rise to the water loss, and the sulfation is one of the results of water loss. However, undercharge could arouse sulfation of positive mass as well. There is a small range between undercharge and overcharge, but a suitable high charge voltage may help in counteracting the sulfation. Hence, the end of charge voltage should be limited in a suitable range [153], [155].

High discharge current causes a significant capacity loss. The high operating rate can dry out the electrolyte by increasing the battery temperature. High cell temperature will decompose the lignin attached on negative plate, which limits the battery capacity [152], [155]. However, charge at a moderately higher temperature can, to some degree, counteract the active mass degradation. Nevertheless, an excessive working temperature will certainly exacerbate the grid corrosion or plate sulfation. [153]

Deep-cycling may increase the danger of the short circuit since deep-cycle will raise the degradation of active mass, which may lead to the short circuit. [153]

The VRLA batteries are unstable under open circuit or overcharge conditions. The gassing phenomenon still makes the VRLA cells suffer from irreversible self-discharge.[26]

4.3 Battery lifetime prediction method and experimental design

4.3.1 Stress factors selection

As introduced in the above session, there are mainly four stress factors that may influence the ageing process of both battery technologies. So the ageing processes can be expressed as the function of Ah throughput, with the other weighting factors as parameters of the function. [157], [158]:

- Ah throughput (workload since employed)
- Charge/discharge rate
- SOC state and SOC variation or DOD and other SOC-related stress factors (e.g. time at low SOC; storage time before use; degree of overcharge; time between full charge; partial cycling; under charge)
- Battery temperature

How these stress factors influence the battery performance, and their interactions are shown in Figure 4-2.

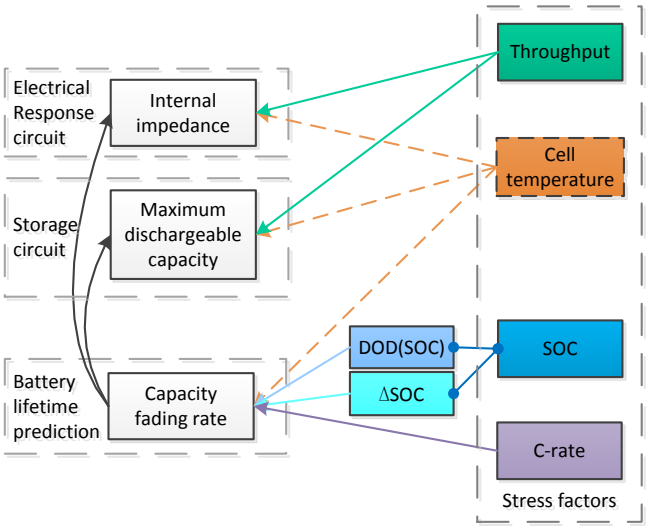

Figure 4-2 How stress factors influence battery performance

However, unlike the battery that is used in the electronic devices or the electric vehicles (EV), the batteries applied in SHS may face quite a different usage situation. The batteries use in electronic device/EV can always be charged with a standard charger, but the charging regime of battery in SHS is highly reliant on the weather conditions. Depending on different load pattern and battery sizing method, the application conditions of battery in SHS are much more complicated than those used in EVs, electronic devices.

D.U.Sauer et al. [159] did a systematic investigation of four different types of battery application in PV systems. The result in Figure 4-3 shows that SOC of the battery may have entirely different distribution for various implementations.

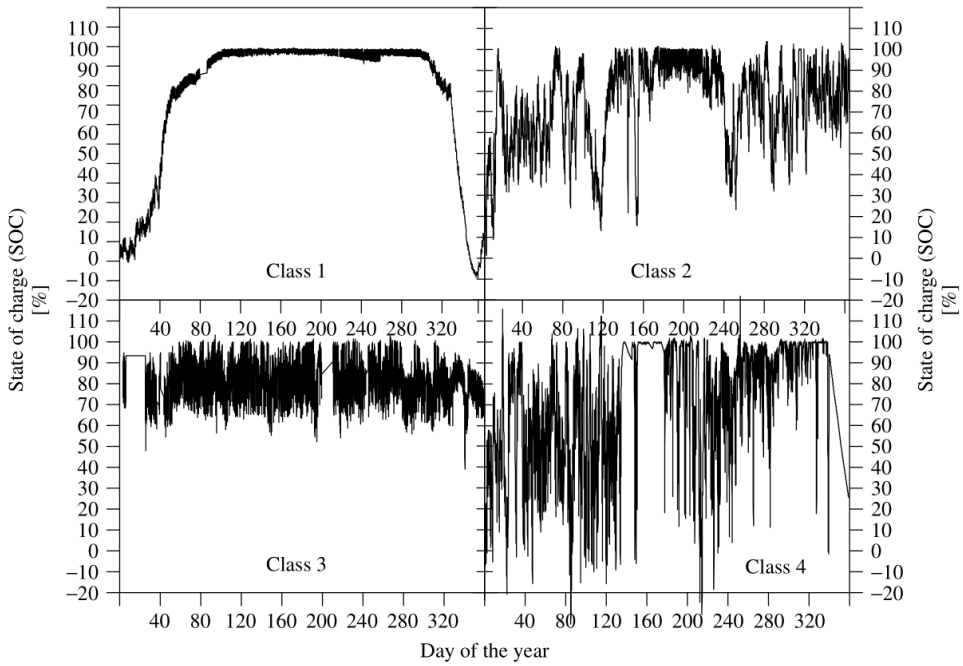

Figure 4-3 SOC of battery that employed in four various PV systems (Fig.5 in [159])

A part of the EU research project Benchmarking [160] investigated how lead-acid battery lifetime is influenced by stress factors under different applications in off-grid renewable energy systems. As introduced above, the stress factors that are resulting in the death of battery are related to the ways batteries are used in SHSs. Each generation-load pattern combination has its dominant stress factors. This project summarised six typical categories of battery application that contains distinct dominant ageing stress factors. The category is defined by "a certain range of the numerical values of stress factors which taken as a whole describe the operating conditions concisely and compactly". Batteries belonging to the same category are subjected to similar operating conditions and a similar combination of stress factors. [160] Two examples of dominant stress factors in different battery application categories are draw in radar plot in Figure 4-4

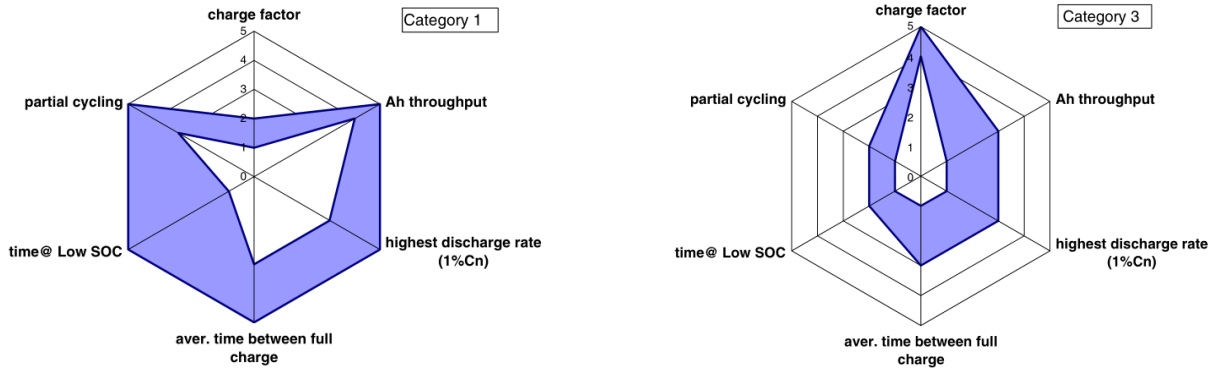

Figure 4-4 Radar plot diagrams of two categories as an example (Fig.3 in [160])

From Figure 4-3and Figure 4-4 it can be seen that ageing model with only two variables C-rate and DOD (which is SOC level) as common battery ageing model is not precise for SHSs. It is because the combination of only these two variables cannot cover all the possible critical ageing probabilities in SHSs. As a result, it is suggested that for any PV battery test procedure, it is important to duplicate the shallow cycling, deficit-charge cycling, and under charge as found in practical implementations of PV systems.[161]

In order to get a balance between the preciseness and the complexity in modelling, an idea modified form [106] and [150] is applied. The method is using the averaged SOC and the deviation of SOC during a certain time to represent the DOD level and the change of DOD.

The time interval for calculation is named micro-cycle, and it is defined as a period of charge followed by a period of discharge, or the other way around. If using the current sign as an indicator, a positive current means to charge the battery and a negative current means to discharge the battery. Then, a micro-cycle consists of three current zero-crossing points: starting with a current cross from negative to positive then back to negative, and the following crossing from negative to positive is the end of this micro-cycle. The final zero-crossing point of the previous micro-cycle is also the start point of the next micro-cycle.

The averaged SOC and SOC deviation during this micro-cycle are calculated along with capacity throughput instead of time with Eq.(4.2).

$$\begin{aligned} SOC_{\text{avg}} &= \frac{1}{Q_{th}^{n} - Q_{th}^{n-1}} \int_{Q_{th}^{n-1}}^{Q_{th}^{n}} SOC(Ah)\, dQ_{th} \\ SOC_{dev} &= \sqrt{\frac{3}{Q_{th}^{n} - Q_{th}^{n-1}} \int_{Q_{th}^{n-1}}^{Q_{th}^{n}} \left(SOC(Ah) - SOC_{avg} \right)^{2} dQ_{th}} \end{aligned} \tag{4.2}$$

Where Q_{th} means the capacity throughput and *n/n-1* represent the counting number of zero-crossings.

The capacity throughput is directly proportional to the time when the C-rate is assigned during cycling so that the capacity throughput can replace the time in cycle ageing modelling[138]. In real-life implementations, it is hard to define the number of cycles that have been processed. Hence, to give a unified scale to weigh the battery ageing process, the "capacity throughput" in the unit of Ampere hour (Ah) is employed. For convenience, SOC swing will be first used in the experimental plan. It is the pendulum of SOC around the averaged SOC, and it will be introduced in the next section.

The operational battery current rate, in general, is lower than 0.1C, and the lowest current could even be 1/150C to 1/100C in SHSs[1], [162]. Since the battery is working in such a low C-rate, the battery ageing due to high C-rate is no longer in consideration. Moreover, the high temperature is often correlated with high C-rate, but the C-rate in this study is low, the impact of temperature was then not considered in the first place either.

In conclusion, only capacity throughput, averaged SOC and SOC variation were explored in detail in this study.

4.3.2 Test procedure

The whole test procedure consists of two parts, one part is cycling the battery with different stress factors (Stress cycle) for a certain amount of capacity throughput, and the other part is the battery state measurement. The battery measurement test profile is similar to the internal impedance extraction test, which is introduced in Section 3.3.2.

Before the whole test started, the battery was fully discharged, and one battery state measurement was applied with the 0.2 C-rate. From this test, not only the maximum dischargeable capacity can be obtained but the internal impedance can also be extracted. From the battery state measurements interspersed between ageing tests, how the ageing process taking place on batteries can be detected. Each result of the battery state measurement is treated as one battery state data point during ageing.

After the first battery state measurement, it is then the stress cycle. The stress cycle is meant to give a stress continuously on each battery for a certain time to inducing fading on batteries. In order to provide the fading stress with the same interval on two battery technologies, a 50 Ah capacity throughput, which is ten equivalent cycles, is chosen. Another battery state measurement follows the stress cycle. The rest duration between charge/discharge in test cycle and stress cycle is taken as 15 minutes for LFP[163], 1 hour for VRLA[112].

As a summary, the whole test procedure is one battery state measurement followed by one stress cycle, then another battery state measurement. Keep operating the entire loop until enough battery state data points are obtained. Since this study is interested in battery ageing trend and how stress factors influence the fading rate, the amount of data point evaluation was then picked according to these two points of interests. The "enough battery state data points" is decided according to either if the fading rate is visible, or the battery capacity reaches the EOL threshold.

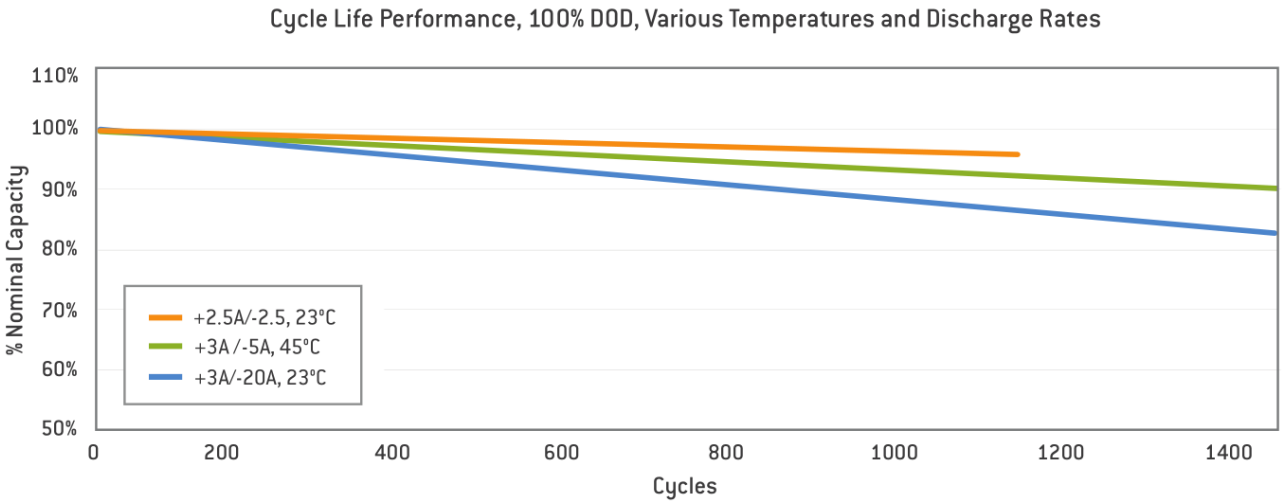

(a)

Figure 7-1: Cycle Life and DOD for CYCLON® Battery Cells

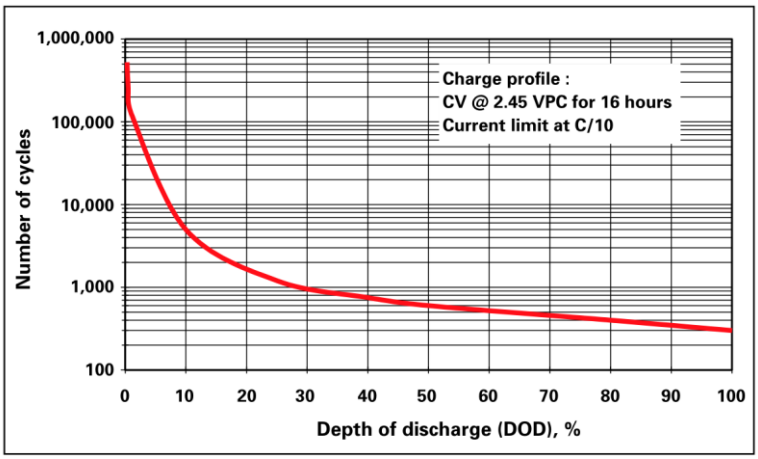

(b)

Figure 4-5 Expected Battery lifetime curves from manufacturer (a) LFP[32]; (b) VRLA[95]

The whole tests were operated in unified C-rate for two battery technologies separately. The test C-rate chosen for LFP battery is 1C and for VRLA is 0.2C. According to the manufacturer (as shown in Figure 4-5(a)), the LFP battery ageing trend cannot be observed clearly before 200 cycles even with much higher discharge current. For VRLA battery cycled with 0.1C, its lifetime could be at least 300 cycles. In this case, if the test C-rate was chosen according to the common battery operation C-rate in PV systems, which is smaller than 0.1C, the whole lifetime tests may take years to finish. In this situation, the ageing experiments need to be accelerated so the ageing behaviour can be demonstrated quicker. Accelerating ageing tests can be easily approached by continuously cycling the battery with a higher rate. [31] Nevertheless, the higher C-rate cannot be too aggressive in case of raising the battery temperature too much. For LFP battery, 1 C-rate is a recommended operation C-rate[32], and working at lower than 0.2C can ensure that the VRLA battery has proper performance, e.g. good charge efficiency [97]. Therefore these two values are chosen. Apart from that, another lifetime test with lower C-rate (0.5C) for LFP battery was added in order to compare the influence caused by the current.

In addition, charge factor and charging voltages are two crucial ageing stress factors for VRLA battery. Even though they would not be a problem since the charging strategy for VRLA battery is the optimised one (CC-CV, as introduced in chapter 3). It will still become an issue during lifetime tests if they were not intentionally controlled. Therefore, all the charging processes in stress cycles were forcibly converted into CV whenever the voltage reaches 2.5V. Besides, the offset charge factor of coulombic efficiency variation in different SOC stages

was also taken into consideration. In this case, the stress factors are ensured to be only the averaged SOC level and the SOC swing.

For both technologies, the test procedures are shown in Figure 4-6 and the voltage/SOC curves of cycle life measurement concept are in Figure 4-7. The design of different batteries test with a different combination of stress factors (averaged SOC and SOC swing) is summarised in Table 4-1.

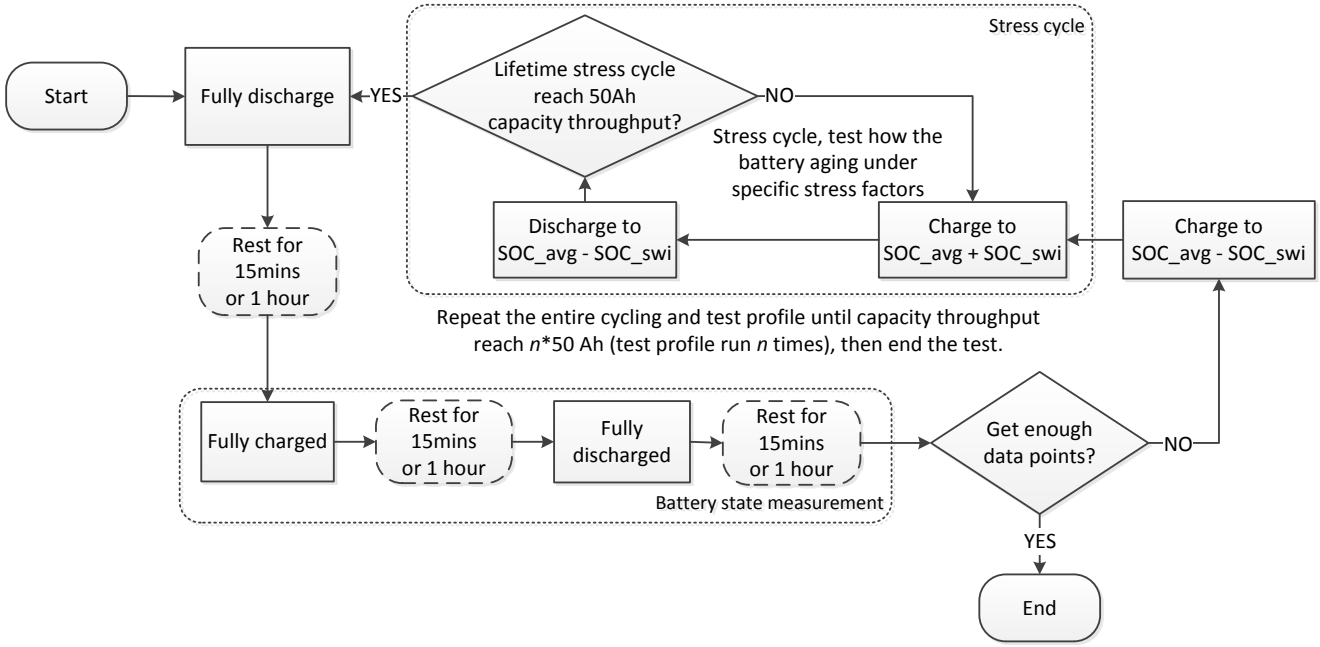

Figure 4-6 Life time test procedure

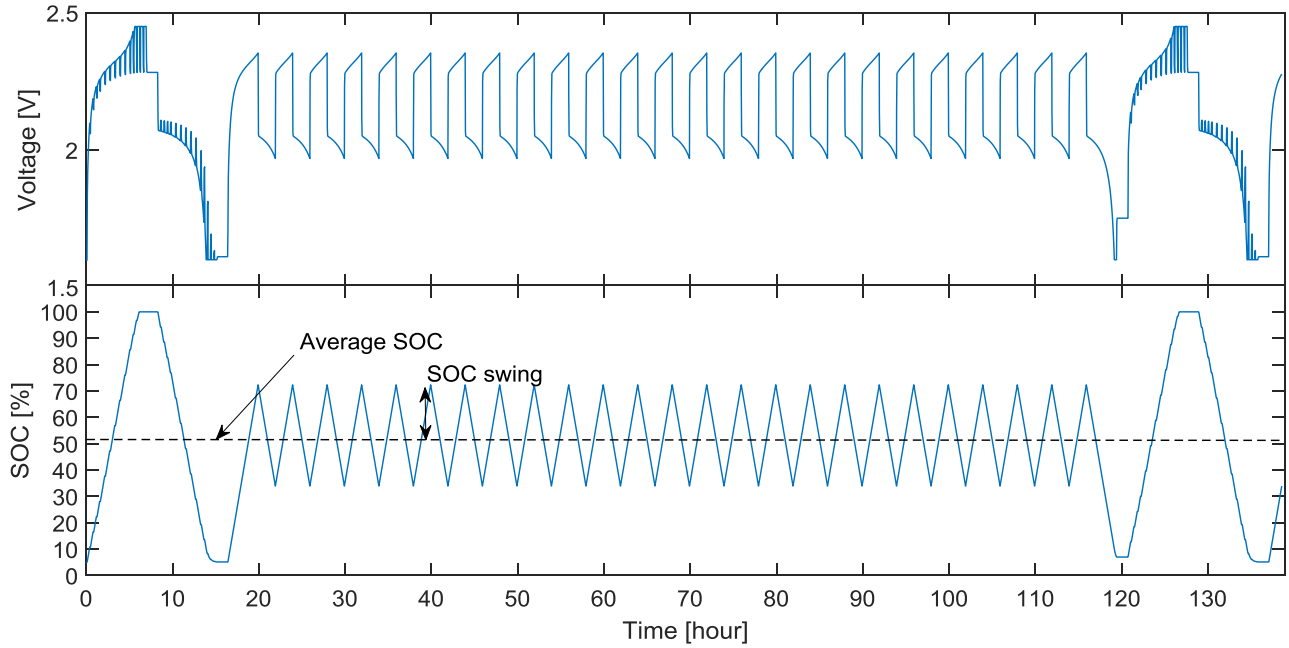

Figure 4-7 Concept curves of testing procedure for two state measurement and one stress cycle in between

Table 4-1 Summary of lifetime test design

Stress factor	Battery technology	C-rate	SOC_avg [%]	SOC_swi [%]	For VRLA: offset Charge factor in stress cycles
Averaged SOC and SOC deviation	VRLA and LFP	VRLA: 0.2C; LFP: 1C	30	20	1.01
			70	20	1.05
			50	20	1.01
			50	10	1.01
			50	5	1.01
			30	10	1.01
			30	5	1.01
			70	10	1.01
			70	5	1.04
	Only LFP	0.5C	70	20	1.03

Each of the stress factor combination was tested on separate battery cells. The selection of the compensate charge factor was refer to the literature review in Chapter 3.3.3.

4.4 LFP battery experimental results and the lifetime modelling

4.4.1 Capacity

The capacity changing of LFP batteries is drawn in Figure 4-8, and the legend "avg + *x*, swi + *y*" means the battery cycled under the stress factor combination: averaged SOC *x*, SOC swing *y*. The legend with sign "*" represents the result of the battery tested with 0.5 C-rate. The legend in this section has this unified meaning so it will not be repeated henceforth. The meaning of the stress factors are explained in Section 4.3.1

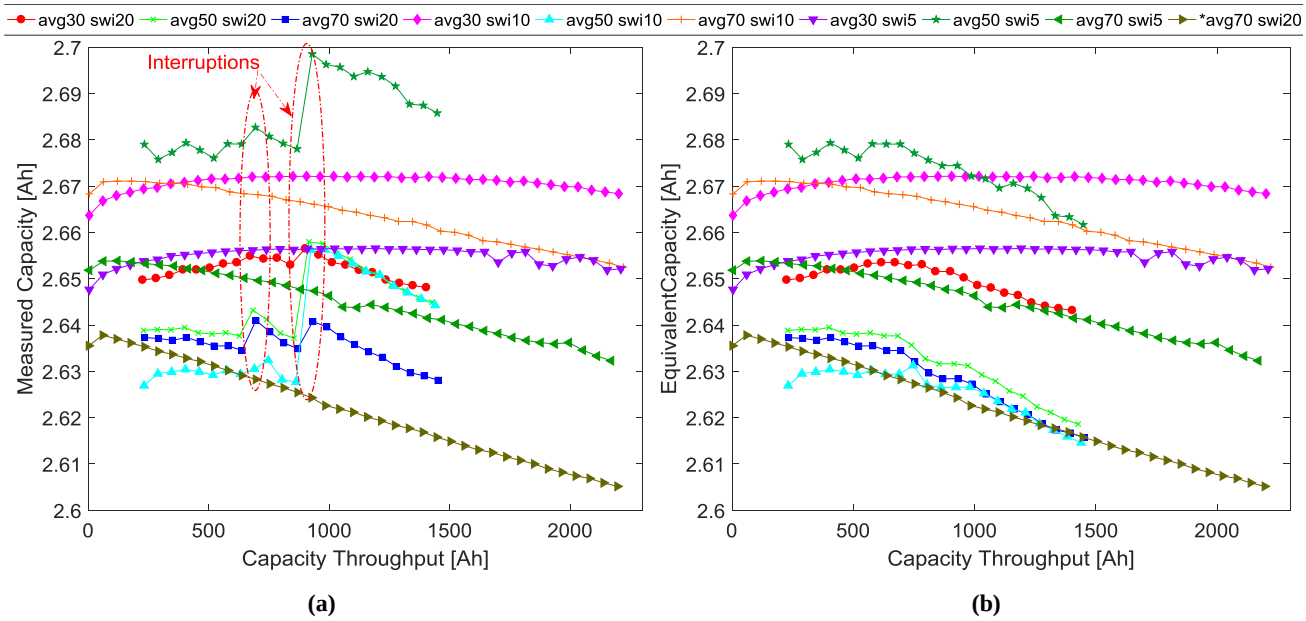

Figure 4-8 Capacity changing of LFP batteries (a) measured capacity (b) equivalent capacity

Figure 4-8(a) shows the measured battery capacity. It can be seen that the overall trend of the battery capacity under different stress factors is first increased then decreased. Batteries cycled with various stress factors show a distinguished capacity fading rate. It can be observed that batteries cycled under higher averaged SOC and higher SOC swing has an approximate higher trend of fading speed.

In this Figure 4-8(a), two undulations were recorded on those batteries: avg30-swi20, avg50-swi20, avg70-swi20, avg50-swi10, avg50-swi05. This is because of unpredicted interruptions. These five tests also missed the first 4 data points, and it was because of the programming error that the data was not recorded correctly. During the experiments, the tests were paused for some time due to the lab movement, the first pause was 11 hours and the second one was 27 days. In those two pauses, the battery capacity recovered. This phenomenon might be due to the recovery of reversible capacity fading with the break in continuous stresses, which caused by charge redistribution.[164] Similar phenomenon was also observed in [165], [166], and a sample is in Figure 4-9.

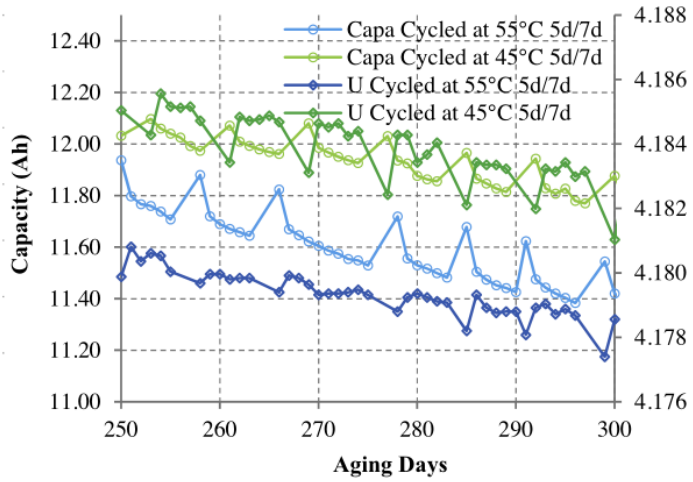

Figure 4-9 Capacity fading and voltage drop when Graphite//Cobalt manganese nickel oxide battery ageing with recovery (Fig.4 (d) in[166])

According to Figure 4-8(a), it can be seen that even though the capacity recovered a bit during the pause, the fading rate did not change after the experiments resumed. Moreover, the capacity fading rate is more attractive than the absolute value of capacity, so the recovered capacity was removed, and the curves were shifted to compare the fading rate. The edited figure is shown in Figure 4-8(b).

It should be noticed that the curve shift is only meant to show the fading trend more clearly. Those data points influenced by interruptions are deleted in the following fading rate related calculations to preserve the accuracy.

Apart from that, it also can be observed that the test curves in those two figures have an unequal amount of data points. That is because those tests were operated in two batches due to limited experimental channels, and each batch has the same number of data points. Besides, the experiments were terminated as long as the fading trend can be observed in a limited test, as introduced in Section 4.3.2.

The capacity of each fresh battery is different because of slightly uneven manufacturing, so the further relative capacity changing analysis was made. In Figure 4-10, the relative battery capacity change versus capacity throughput and versus test time is shown in (a) and (b) separately. In this comparison, the first 4 data points of the other five tests were also deleted so all of the ten tests have the same start point.

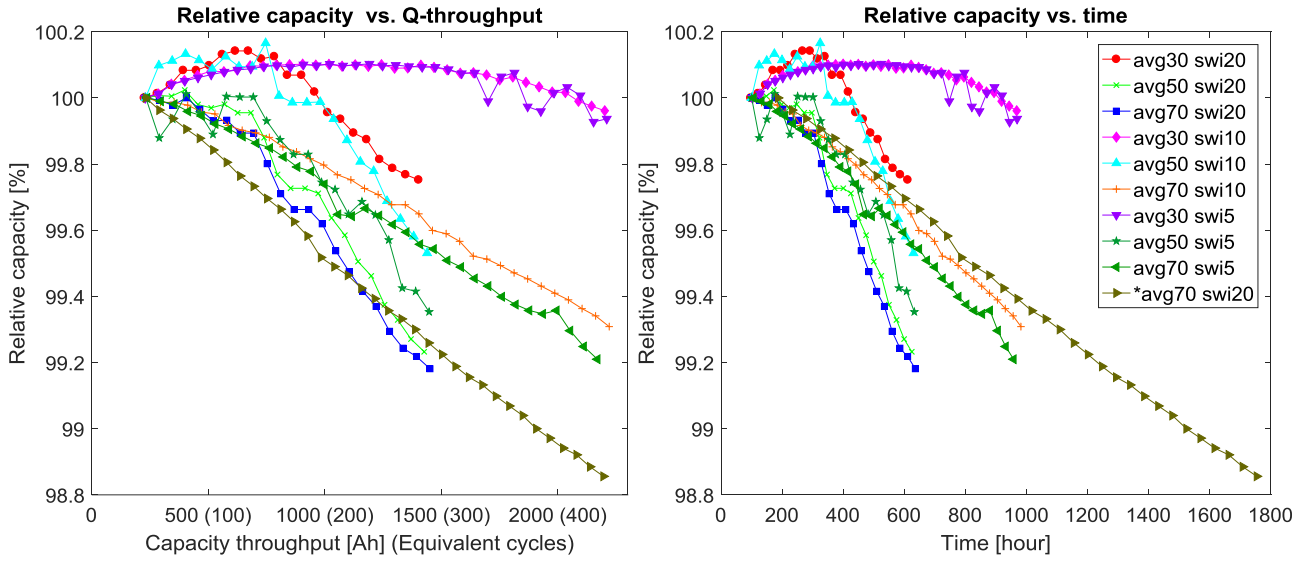

(a) **(b)**

Figure 4-10 Relative capacity changing of LFP batteries (a) versus capacity throughput (b) versus time

It was expected that the capacity fading trend of LFP battery is linear to the number of cycles because the main ageing mechanism of LFP is a linear loss of Li inventory [133][10]. However, it can be observed that not all the fading rate in the experiments shows a relatively linear trend, especially those batteries tested with average 30% SOC and 10%, 5% SOC swings (avg30-swi10 & avg30-swi5). It might be that cycling the battery under different stress factors made the dominant ageing mechanism of some batteries no longer be due to the loss of Li ions.

The capacity fading of LFP batteries could be due to the combination of more than one mechanisms, and each of them contributed to different fading rates. In [167], three representative ageing rate from three distinct ageing mechanisms are simulated from the case study: loss of active material on positive and negative electrodes (LAM_{**PE}, LAM_{**NE}) and loss of lithium inventory (LLI). The rate curve of these three mechanisms versus battery cycle numbers is shown in Figure 4-11(a). In addition, according to [168], it is possible to give an assumption of what are the dominant ageing mechanisms in one ageing process from a capacity fading curve. An example is drawn in Figure 4-11(b). The capacity fading trend of five degradation modes was simulated and compared with the test results in order to recognise the main fading mechanisms.

Therefore, the experimental results of this thesis could be explained that different stress factors induced different dominant fading mechanism, leading to the various fading trends.

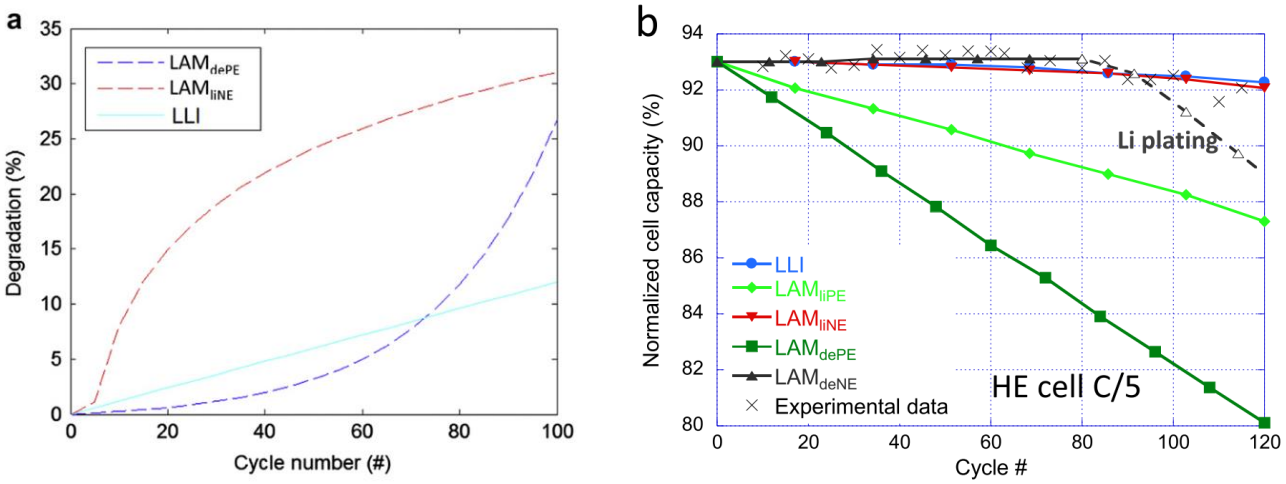

(a) (Fig. 10. (a) in [167] **)** **(b) (Fig. 9 (b) in** [168]**)**

Figure 4-11 Simulation of different fading mechanisms

Apart from that, the capacity of some batteries (e.g. avg50-swi10, avg30-swi20, avg30-swi10, avg20-swi5) increased even until 150 equivalent cycles then turned to decrease. This inconsistent phenomenon was also detected in [168][169], and it was unexplained, which needs further exploration in the future.

Since not all the LFP battery capacity declined at a constant rate, it is not comprehensive to generalise the fading trend into a constant value. In this case, the capacity fading rate is then calculated differentially to represent the battery ageing process. The calculation equation is expressed as the following form in Eq. (4.3).

$$r_{nF} = \frac{nF}{dQ_{th}} = \frac{dF / C_{dsb0}}{dQ_{th}} = \frac{\left(C_{th}^{n} - C_{th}^{n-i}\right) / C_{dsb0}}{Q_{th}^{n} - Q_{th}^{n-i}} \quad \textbf{(4.3)}$$

This equation is meant to calculate the normalised capacity fade in a certain amount of capacity throughput. For example, pick two data point *n-i* and *n* from the experimental data. The capacities measured in these two points are C_{n-i}, C_n and the capacity throughput in between these two points is Q_{th}^{n} - Q_{th}^{n-i}. The capacity loss (dF) in between these two points is C_{th}^{n} - C_{th}^{n-i}, and the normalised capacity fading in between these two points (nF) is simply calculated by dF/C_{dcb0} where C_{dcb0} is the maximum dischargeable capacity of the fresh battery. Five was chosen for LFP batteries as the interval between two points (i) to smooth the curve and reduce the error.

In the battery lifetime modelling, the concept of r_{nF} is then employed and the r_{nF} is the rate of normalised capacity fading, which is defined as: the normalised differential capacity loss per differential capacity throughput. The rate here is with respect to capacity throughput instead of time and the unit of r_{nF} is percentage per Ampere-hour [%/Ah]

Even though the operational C-rate is not explored in detail in this study, one test with lower C-rate (0.5 C) was still operated to examine how much would the C-rate may impact on the lifetime of LFP battery. The result in Figure 4-10(a) shows that battery cycled under lower C-rate does not have any remarkable advantage. However, Figure 4-10(b) reveals that battery cycles with lower C-rate do have a longer lifetime in the sense of cycle time instead of capacity throughput. A similar conclusion was drawn in [127] that the battery capacity loss increases with reduced current for given cycle numbers, but the situation was opposite in a given length of cycle time. It was also concluded in [168] that C-rate does not have much influence on battery lifetime in the scale of cycle numbers. Since the capacity throughput was chosen as the ageing coordinate in this thesis, the ageing influenced by C-rate was then not considered.

The stress factors that may influence battery lifetime that this thesis focused on are: capacity throughput, averaged operational SOC (averaged SOC in short for convenience in the following content) and operational SOC deviation (SOC deviation in short). In order to obtain the impact of those stress factors, the Rate of

normalised capacity fading r_{nF} is drawn versus these three factors respectively in Figure 4-12. All the SOC swing has been calculated and converted into SOC deviation by using the equation (4.2) in the previous chapter.

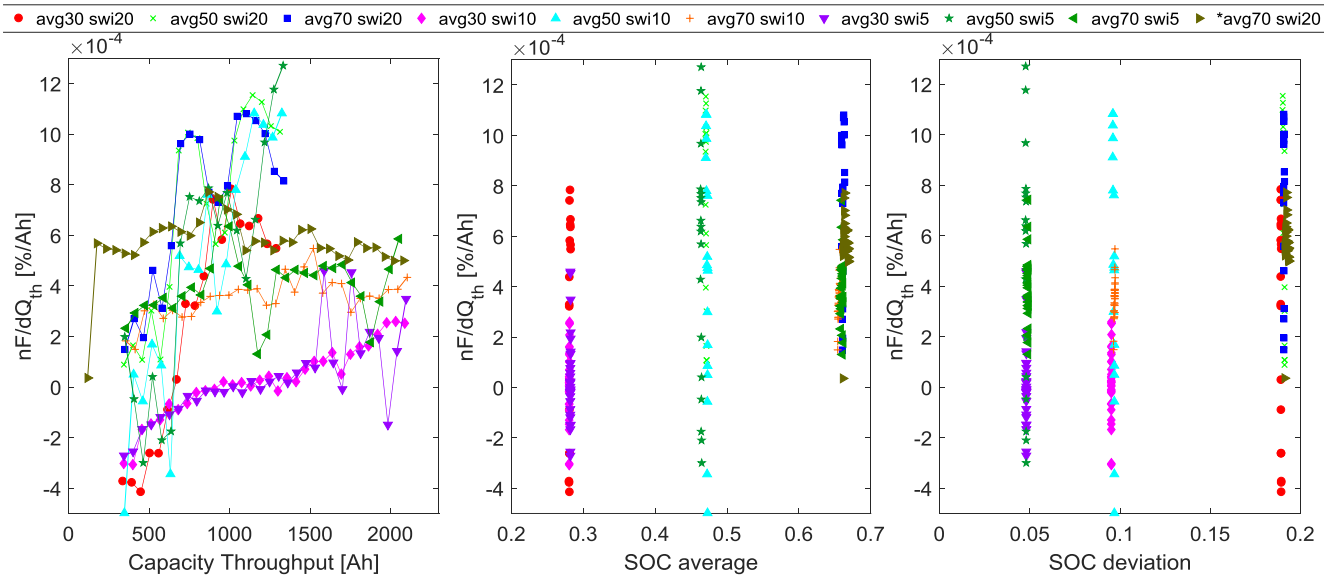

Figure 4-12 Rate of normalised capacity fading of LFP batteries versus (a) Capacity throughput (b) Average cycled SOC (c) SOC deviation

From Figure 4-12 (a) it can be observed that r_{nF} has a relative linear trend versus capacity throughput. Figure 4-12 (b) shows that mean cycling SOC does have an impact on battery fading rate that a higher averaged SOC is leading to a higher fading rate. However, how SOC deviation impacts the battery fading does not show a clear clue in Figure 4-12 (c). In order to have a better understanding of how SOC deviation influence the battery fading, the r_{nF} under different SOC deviation with same averaged SOC were drawn with the solid line and points in Figure 4-13.

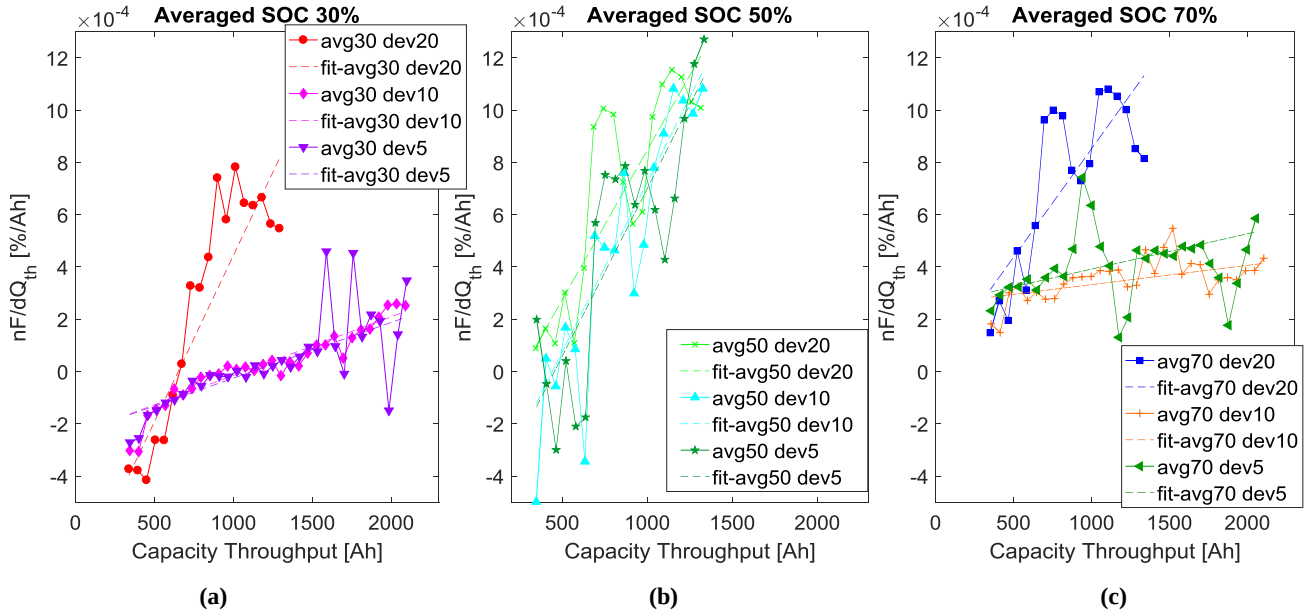

Figure 4-13 Rate of normalised capacity fading and their linear fitted results under different SOC deviation with different averaged SOC of LFP batteries

The curves in Figure 4-13 (a) and (c) show that batteries cycled at 20% SOC deviation have a higher fading trend, but all three curves in Figure 4-13 (b) have the similar fading trend. The experiments were operated in two batches and the first batch (avg30-swi20, avg50-swi20, avg70-swi20, avg50-swi10, avg50-swi05) were

interrupted due to lab movement. Before the lab moving, the room temperature was not under restricting control, and then the lab was moved into a well-equipped room with enduring temperature control. That might be the reason leading to the unstable results of the first batch and the inconsistency between two batches. Hence the SOC deviation is not modelled in this study.

Then, the r_{nF} is modelled as a linear function of capacity throughput to represent the capacity fading process, and the parameters of this linear function are modelled only as a function of averaged SOC. The linear fitting results are drawn with a dash line in Figure 4-13 and the equation of r_{nF} is written in Eq. (4.4).

$$r_{nF}\left(SOC_{avg}, Q_{th}\right) = p_1 \times Q_{th} + p_2$$
$$p_1 = f_1\left(SOC_{avg}\right); p_2 = f_2\left(SOC_{avg}\right) \quad \textbf{(4.4)}$$

Where p_1 is the linear slope and p_2 is the y intercept, both of them being functions of averaged SOC.

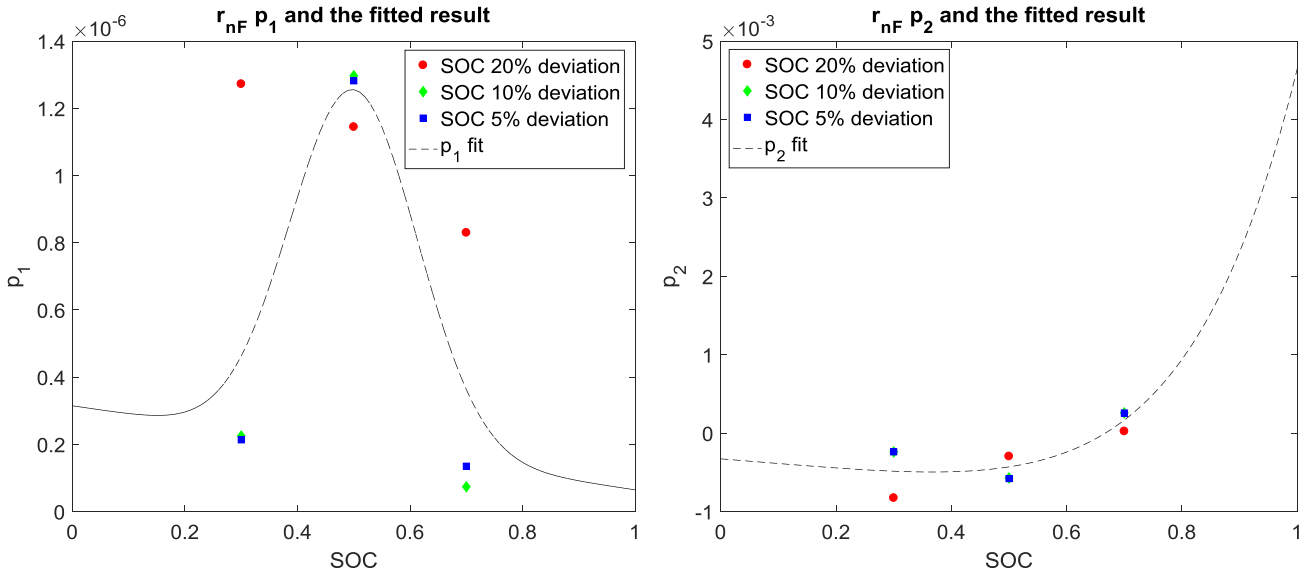

(a) **(b)**

Figure 4-14 Parameters of linear fit equation of r_{nF}, for LFP batteries
(a) Slope of the linear equation (b) y intercept

The parameters of these linear fitting results are drawn in Figure 4-14. Gaussian distribution was employed to represent the slope value, and the value of y intercept was fitted into an exponential equation. Both averaged SOC dependent parameters are written in Eq. (4.5) and Eq. (4.6).

$$p_1 = 1.066e-6 \times \exp\left(-\left(\frac{SOC_{avg\_rate} - 0.5}{0.16}\right)^2\right) - 2.502e-7 \times SOC_{avg\_rate} + 3.147e-7 \quad \textbf{(4.5)}$$

$$p_2 = -5.713e-4 \times \exp\left(2.729 \times SOC_{avg\_rate}\right) + 2.435e-4 \times \exp\left(4.008 \times SOC_{avg\_rate}\right) \quad \textbf{(4.6)}$$

One thing to be noticed is that the r_{nF} is modelled as a function of averaged SOC which according to the rated capacity. The real battery capacity does not always equal to the rated capacity, and the continuous decreasing of capacity when its ageing will lead to a restricted SOC drift when the battery is heavily faded. Therefore, the real averaged SOC should be transferred into averaged SOC according to rated capacity when applying the r_{nF} equation. The transfer function is in Eq. (4.7).

$$SOC_{avg\_rate} = SOC_{avg} \times \frac{C_{dsb}}{C_{rated}} \quad \textbf{(4.7)}$$

After obtaining all those parameters, the accumulated amount of capacity fading is then expressed in Eq. (4.8).

$$F = C_{dsb0} \times \int_0^{Q_{th}} r_{nF}\ dQ_{th} \tag{4.8}$$

Where C_{dsb0} is the maximum dischargeable capacity of the fresh battery, Q_{th} is the capacity throughput from the new cell till then. Since the averaged SOC is calculated after each micro-cycle, which is defined in Section 4.3.1, the capacity fading is also calculated in step of each micro-cycle, and dQ_{th} means the capacity throughput of each micro-cycle. The battery capacity fading is modelled by the normalised capacity loss, so the SOH is possible to be expressed directly with accumulated normalised capacity fading, as shown in Eq. (4.9)

$$SOH = \left(1 - \frac{\int_0^{Q_{th}} r_{nF}\ dQ_{th}}{20\%}\right) \times 100\% \tag{4.9}$$

Even though the capacity fading can be modelled by using the existing experimental data, more things can be done in the future. Only 400 equivalent cycles max were operated in this study, and the capacity drop is less than 1% when the experiments were terminated, which indicates the performed experiments are far from the complete cycle life.

Some other studies finished the entire lifetime tests of LFP batteries until they reached the EOL point [170][171]. These research also proved that the capacity fading trend is strongly nonlinear in the battery's whole lifetime. The fading trend was modelled with one simplified equation or with the segmental method in these studies. However, no work has been done from the electrical point of view, on summarising the entire trend of fading includes the influence of throughput, into one continuous model according to the knowledge of the author. It is worthy to prolong the test time and have further studies on the capacity throughput dependent fading rate in the future works.

4.4.2 Other critical parameters

Apart from the main performance parameter which is used to model the battery lifetime (capacity), some other key performance parameters are also deserving to be explored besides modelling.

4.4.2.1 Overall efficiencies

Firstly, the interesting parameters are the overall coulombic efficiency and the overall energy efficiency evolution during ageing. The efficiencies were calculated in each battery state measurement, with these two equations Eq. (4.10) and (4.11), which is the same as its definition in chapter 2.

$$\eta_c = \frac{\int_0^t i_{dis} dt}{\int_0^t i_{ch} dt} \tag{4.10}$$

$$\eta_e = \frac{\int_0^t v_{dis} \times i_{dis} dt}{\int_0^t v_{ch} \times i_{ch} dt} \tag{4.11}$$

Where $\eta_{c/e}$ is the overall coulombic and energy efficiency respectively and the $v_{ch/dis}$, $i_{ch/dis}$ represent the battery voltage and current during charge/discharge respectively.

In Figure 4-15, the coulombic efficiency of LFP batteries are presented, the spikes appeared around 500-1000 capacity throughput are due to some interruptions because of the lab movement. The coulombic efficiencies of all the batteries are almost constantly equal to one. Some values are larger than one because of the measurement resolution, but the error is smaller than 2‰ despite the spikes, which is considered accurate.

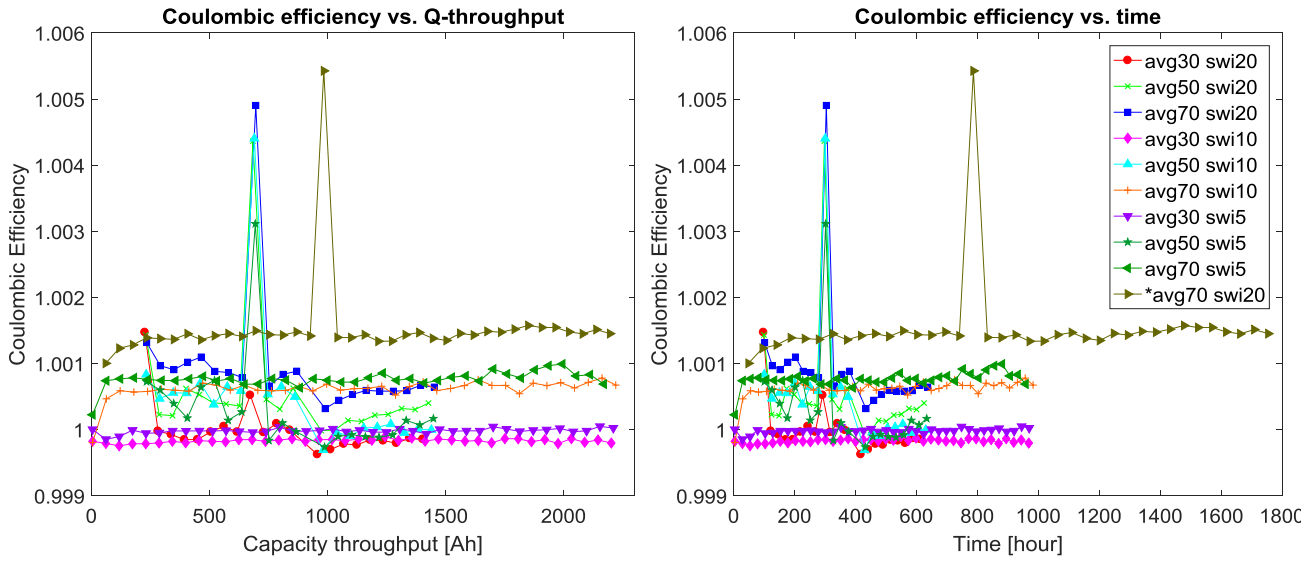

(a) **(b)**

Figure 4-15 Coulombic efficiency of LFP battery versus (a) capacity throughput (b) time

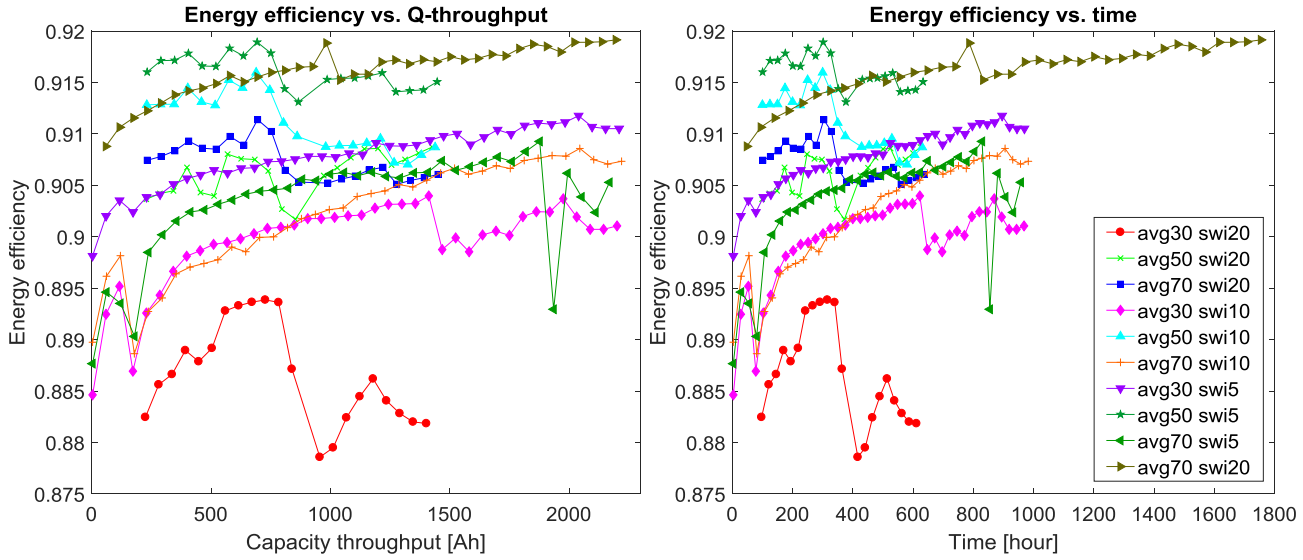

(a) **(b)**

Figure 4-16 Energy efficiency of LFP battery versus (a) capacity throughput (b) time

The measurement results in Figure 4-16 shows most of the batteries have their energy efficiency higher than 90% during the whole tests. In the progress of ageing, the energy efficiency of all the batteries except one (avg30-swi20) remained constant or even slightly increased.

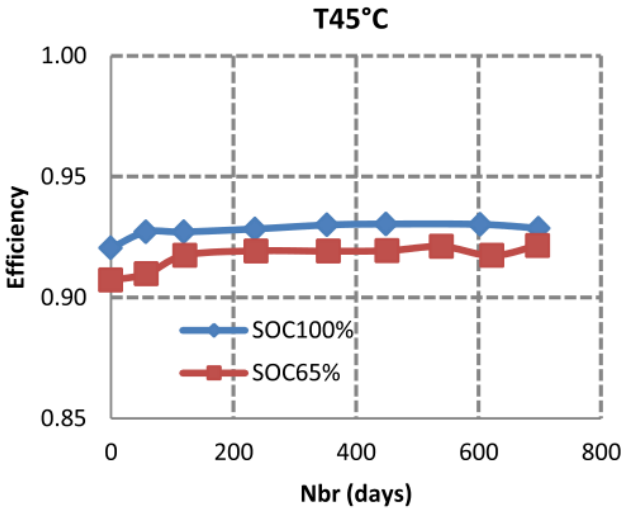

(a) Energy efficiency of LFP battery during calendar age (Fig. 9 in [172]**)**

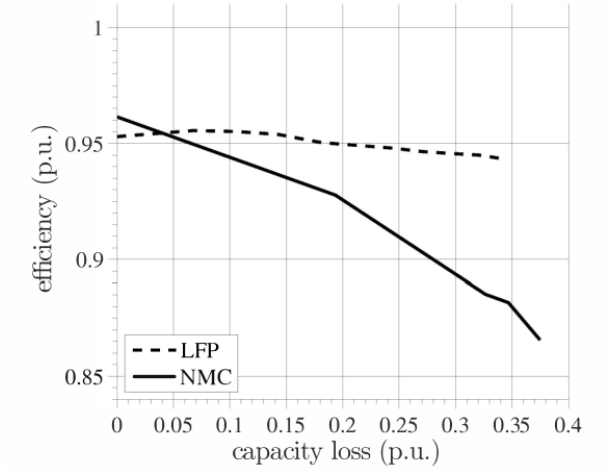

Figure 7: Mean energy efficiency vs. capacity loss.

(b) Energy efficiency of LFP battery during cycling age (dash line) (Fig.7 in [173]**)**

Figure 4-17 Energy efficiency of LFP during (a) calendar age (b) cycling age

Similar results in both calendar ageing and cycling ageing of LFP batteries are observed in [172][173], as shown in Figure 4-17. The energy efficiencies of LFP batteries are relatively constant even in severe ageing conditions, and some of the energy efficiencies show a mild increasing trend at the beginning of ageing. It might be that the ageing of LFP batteries at the end of the tests did not even reach the turning point from where the energy efficiency stop increasing, but remains constant. In addition, the energy efficiency itself is a complex parameter that related to e.m.f, internal resistance and SOC, which can have further explorations in the future.

4.4.2.2 Resistance

Other interesting parameters in battery lifetime tests are the battery internal impedances, because these impedances are vital parameters in determining the battery dynamic behaviour evolution during battery life. The accurate internal resistance analysis method, which is introduced in chapter 3, is too complex and time-consuming. All the data needed for the precise modelling of battery's dynamic behaviour evolution during ageing has been recorded in the tests. The method would be the same as introduced in Chapter 3 and the detail analysis is left for the future work. In this Section, a simplified mean-resistance calculation method was used to check the overall trend of internal resistance during ageing.

The averaged internal resistance was calculated over the capacity throughput interval during charge and discharge separately. Since the internal impedance is a function of current, the CV stage was excluded from the mean resistance calculation. The equation for average internal impedance calculation is in Eq. (4.12).

$$R_{\text{tot\_avg}} = \frac{1}{Q_{th}^{end} - Q_{th}^{start}} \int_{Q_{th}^{start}}^{Q_{th}^{end}} \frac{V_{cell}}{I_{cell}} dQ_{th} \tag{4.12}$$

Where the Qth is again means the capacity throughput and the end and start represent the start and the end of the charge/discharge.

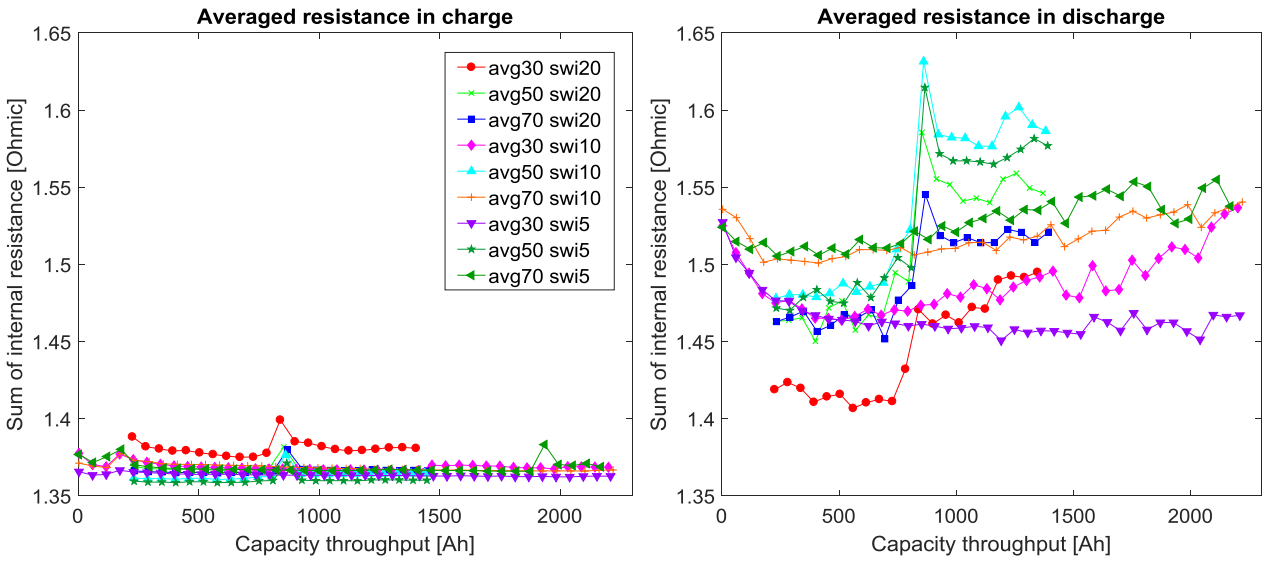

(a) **(b)**

Figure 4-18 Averaged internal resistance of LFP batteries during (a) charge (b) discharge

In Figure 4-18, the discharge impedance is higher than the charge impedance, which is in accordance with the result in [173]. Only the discharge resistance shows an increased trend during ageing and the charge resistance is nearly constant all the time. Moreover, the experimental results in [142] discovered that the global shape of EIS spectra is not affected by ageing, and the conclusion is the dynamic model built for the fresh battery is still valid for use even to simulate a severely aged battery.

4.5 VRLA battery experimental results and the lifetime modelling

4.5.1 Capacity

As introduced in the previous section, the battery was turned to CV charge whenever its voltage reached 2.5V in stress cycles. The time spent on CV charge is unpredictable because the EOC point is depending on the current drop. As a result, the capacity throughput within similar test time for each battery still differs from others even if all the batteries were tested in one batch. Hence, the capacity changing of VRLA batteries is also plotted versus both capacity throughput and operational time. The measured capacity value is drawn in Figure 4-19, and the relative capacity changing is shown in Figure 4-20.

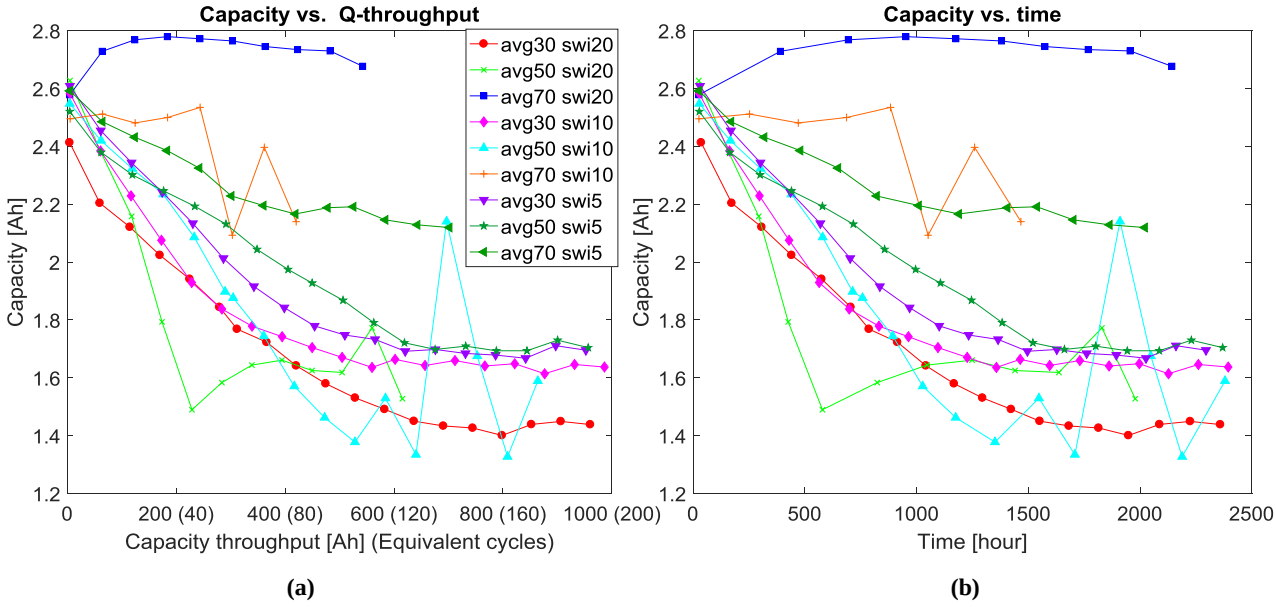

(a) **(b)**

Figure 4-19 Capacity evolution of VRLA batteries versus (a) capacity throughput (b) time

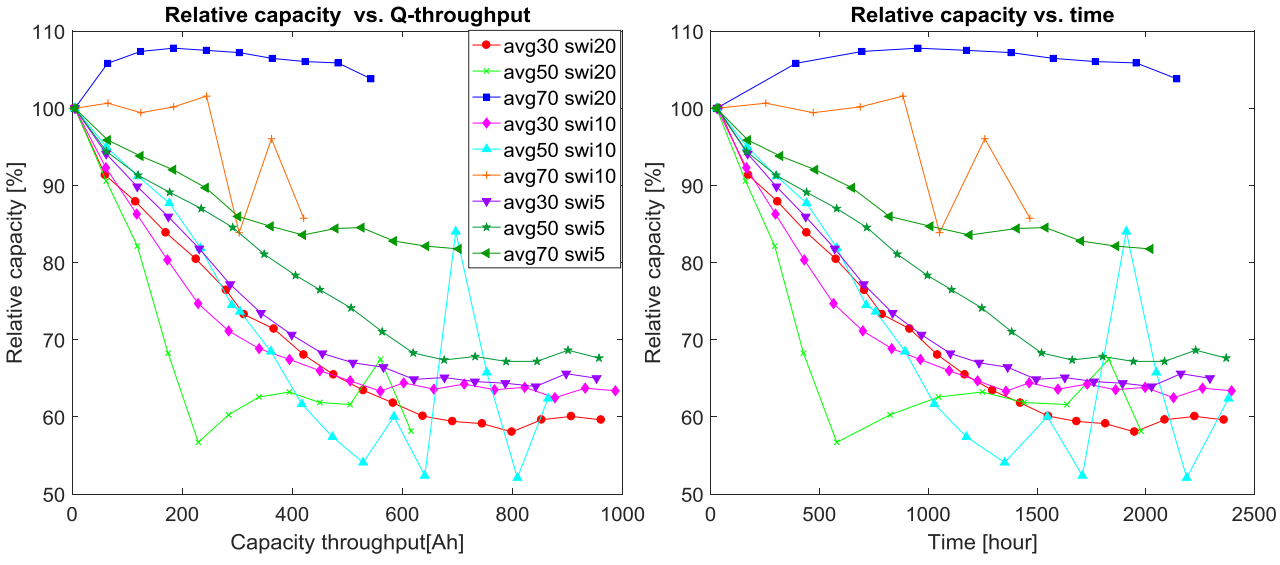

(a) **(b)**

Figure 4-20 Relative capacity evolution of VRLA batteries versus (a) capacity throughput (b) time

Some interesting conclusions can be encapsulated from these two figures.

Even though the capacity of two batteries (avg70-swi20, avg70-swi10) increased a bit at first, all of the tested batteries show a decreasing trend with the capacity throughput in the long-term.

The operational averaged SOC and SOC swing do have significant impacts on the capacity fading rate. The rough trend is: batteries cycled with higher averaged SOC show a superior performance than those cycled with lower averaged SOC. For battery cycled with lower averaged SOC, it is preferable to have a smaller SOC swing. It is the opposite for battery cycled with higher averaged SOC that larger SOC swing is better for the battery. This result is understandable that higher averaged SOC with larger SOC swing means the battery can always get recovery by sufficient recharge. It is considered that battery cycled under 50% SOC suffers from increased sulfation on positive mass [174], and regularly recharges to the full state can eliminate part of the adverse impact. This conclusion is in accordance with the ageing mechanism review in Section 4.2.2.

Moreover, in the latter half of the capacity fading curves, the fading trend of most batteries became gradual and eventually turned to constant. Some of them even showed a slightly increasing trend. It is because the sharp decrease of battery capacity drifted the real operational averaged SOC and SOC deviation from their original value into a much higher value. That means some of the batteries were regularly fully charged in the final stage of the ageing test due to the SOC drift, which might lead to the mitigation of the capacity declining trend. Similar results were also obtained in partial cycling tests in [175] as shown in Figure 4-21(a). The capacity declining trend was also explained with sulfation mechanism, and the slight recovery of capacity may relate with the preserving of charge acceptance. An extreme exploration reported in [175] that a VRLA battery which stored open circuit for five years did recover from 0% rated capacity to 75% rated capacity after a prolonged sufficient recharge. This experiment demonstrated that a battery strongly sulphated could still possibly recovered with proper charge strategy.

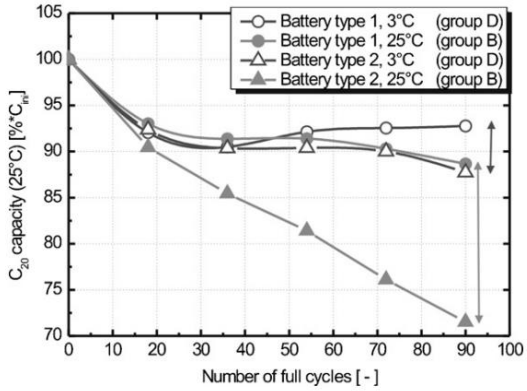

(a) VRLA battery capacity fading due to partial cycling in EV (Fig. 12 in[175]**)**

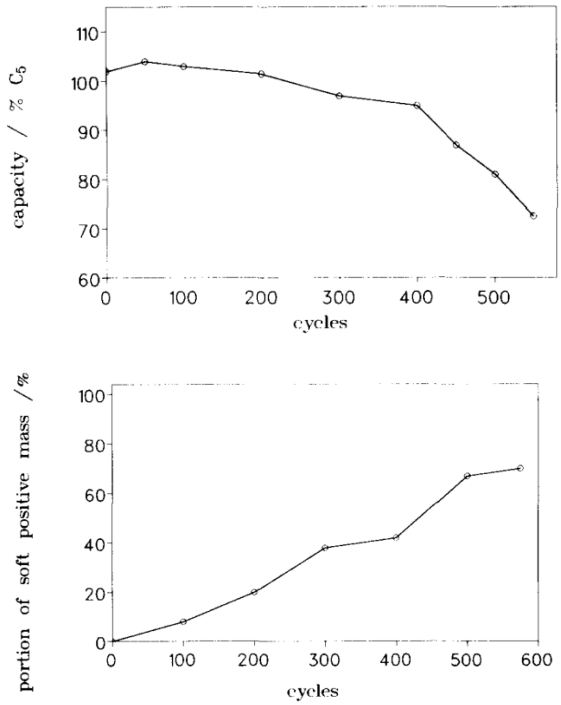

(b) VRLA Battery capacity fading trend (upper figure) and the softening trend (lower figure)correlated with the upper fading curve (Fig.4 and 5 in [155]**)**

Figure 4-21 VRLA battery fading with different rate

As an exception, the result of battery avg70-swi20 has a distinct fading trend among all the other batteries, and a similar result was reported in [155]. The parabolic shaped fading trend line compared with the positive mass softening trend line in Figure 4-21(b), and it revealed that this ageing trend was a result of softening dominant ageing mechanism.

Therefore, a hypothesis can be summarized that the different dominant ageing mechanisms could lead to a variable ageing trend in VRLA batteries as well. This deserves further studies in the future works.

Similar to the modelling method of LFP, the r_{nF} is employed to model the SOH of VRLA batteries since they also have nonlinear ageing trends during the experiments. The r_{nF} value of VRLA batteries was calculated and plotted versus three stress factors: capacity throughput, averaged SOC and the SOC deviation in Figure 4-22. In the calculation, the SOC swing has been converted to SOC deviation. For VRLA batteries, the r_{nF} was calculated in the interval of 3 battery state measurement data points.

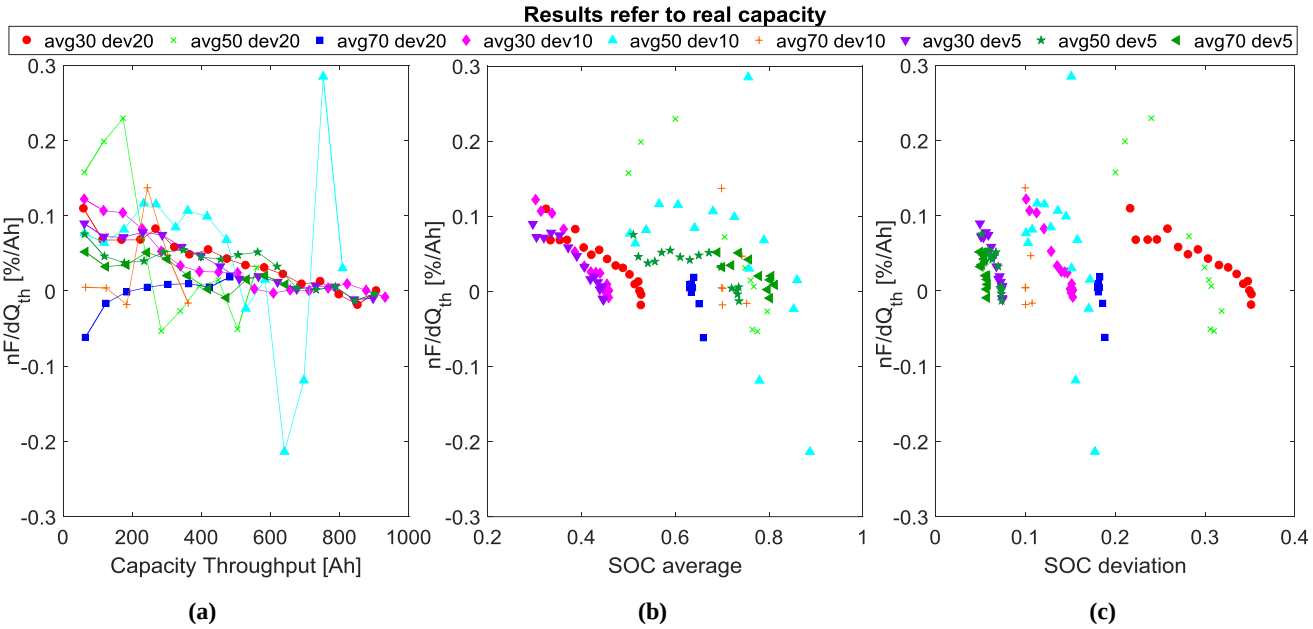

Figure 4-22 Rate of normalised capacity fading of LFP batteries versus (a) Capacity throughput (b) Real average cycled SOC (c) Real SOC deviation

Figure 4-22 (a) shows that the r_{nF} value can be treated as a linear descending trend with capacity throughput. The data points in Figure 4-22 (b) and (c) are drifted explicitly from lower value to higher value due to the remarkable capacity decrease when the battery ages. The relation with averaged SOC and SOC deviation is not clear with those drift data points, so all those data are replotted versus rated averaged SOC and rated SOC deviation according to rated battery capacity in Figure 4-23.

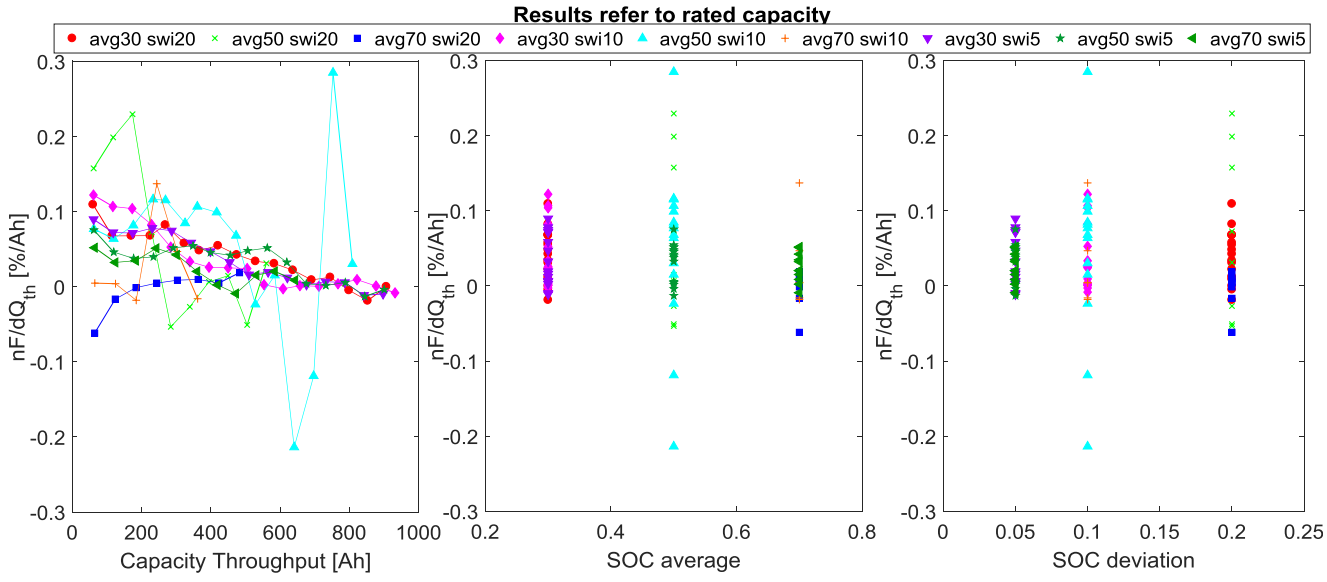

Figure 4-23 Rate of normalised capacity fading of LFP batteries versus (a) Capacity throughput (b) Average cycled SOC according to rated battery capacity (c) SOC deviation according to rated battery capacity

In Figure 4-23(b), the r_{nF} value shows a decreasing trend with the increase in averaged SOC and a relative parabolic tendency with SOC deviation. The variation of r_{nF} under different SOC deviation with same averaged SOC is drawn in Figure 4-24 with the solid line and points.

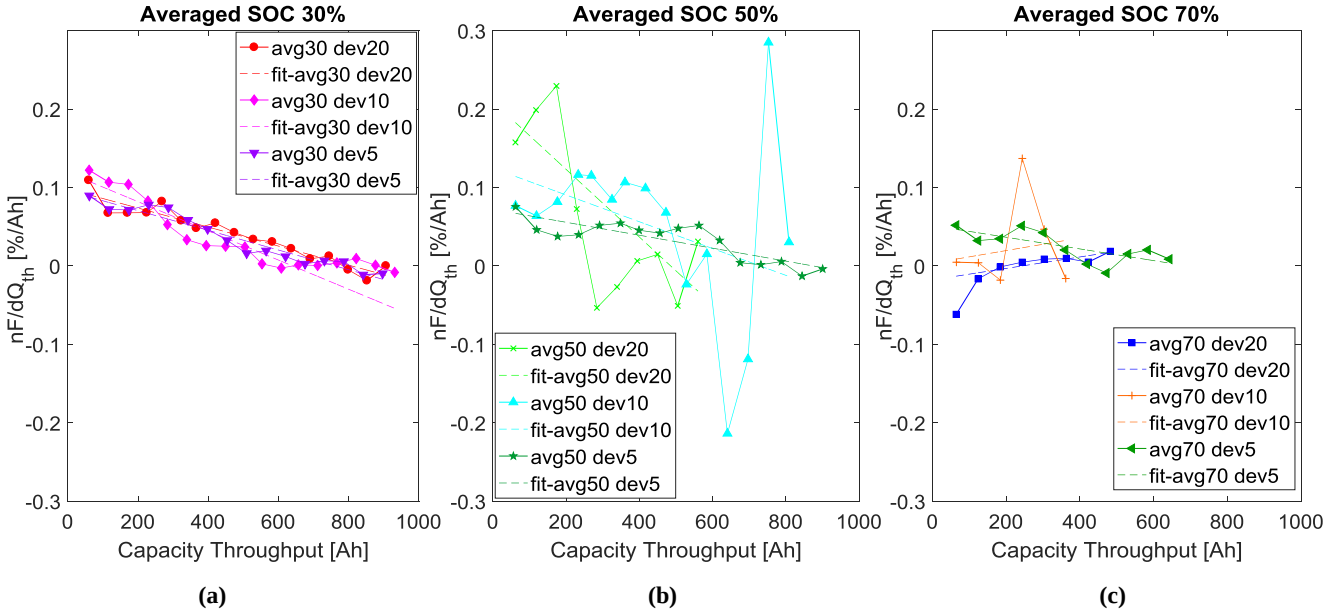

Figure 4-24 Rate of normalised capacity fading and their linear fitted results under different SOC deviation with same averaged SOC of VRLA batteries

All r_{nF} with capacity throughput curves were fitted to a linear equation, and the fitted results are drawn in dash line in Figure 4-24. The parameters, which is the slope of the linear equation (p_1) and y-intercept (p_2) of these linear lines are plotted in Figure 4-25

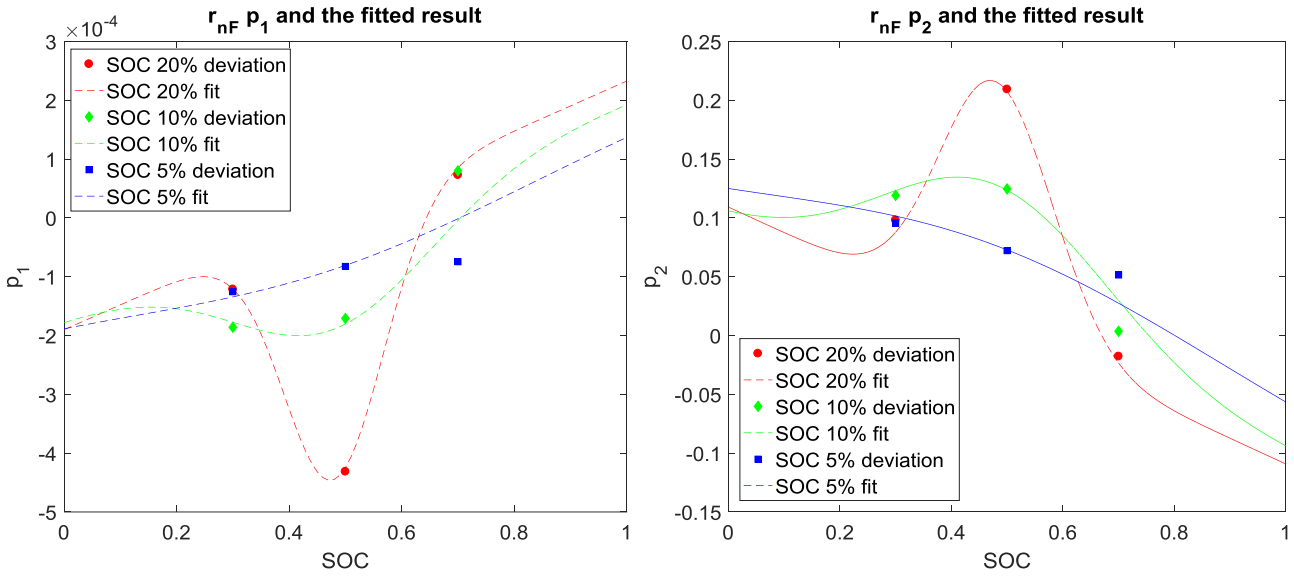

(a) **(b)**

Figure 4-25 Parameters of linear fit equation of r_{nF}, for VRLA batteries
(a) Slope of the linear equation (b) y-intercept

In many papers, the lifetime of lead-acid battery is modelled as the function of DOD, e.g.: [157]

$$L = L_R \times \left(\frac{DOD_R}{DOD} \right)^a \times \exp\left(b \times \left(1 - \frac{DOD}{DOD_R} \right) \right) \tag{4.13}$$

Where L is the lifetime in unit of Ah, DOD is the depth of discharge, subscript R means in rated condition, and a,b are experimental parameters.

Paper [158] summarised the life of lead-acid battery to the function of DOD from datasheets :

$$N = a \times \exp(-b \times DOD) + c \times \exp(-d \times DOD) \tag{4.14}$$

Where N is the number of cycles, and a,b,c,d are experimental parameters.

In [176], a weight throughput model was employed and the influence factor from SOC was modelled into an exponential equation:

$$f_{SOC} = p_1 + p_2 \times \exp(p_3 \times SOC) \tag{4.15}$$

Where p1, p2, p3 are experimental parameters.

Some other authors modelled the VRLA lifetime with weighed throughput model which considered the impact of SOC in time scale. For example, in [177], the impact factor of SOC was modelled into the time since last full charge and the time battery remains at lowest SOC. Paper [174] modelled the VRLA ageing under partial charge in the way of dividing the operational SOC range into five categories, and the influence factor of SOC was then modelled by categories separately.

Even though many existing VRLA SOH models mentioned an exponential dependence of impact factor on SOC, the results found in this study are not suitable for modelling with exponential equations. Consequently, VRLA SOH model is completely empirical based.

From Figure 4-25 it can be seen that p_1 and p_2 have a complex mixed dependency on averaged SOC and SOC deviation. Therefore, the r_{nF} of VRLA battery is fitted into a linear function of three variables, the capacity throughput, the averaged SOC and the SOC deviation according to rated capacity, in Eq. (4.16).

$$r_{nF}\left(SOC_{avg\_rate}, SOC_{dev\_rate}, Q_{th}\right) = p_1 \times Q_{th} + p_2$$
$$p_1 = f_1\left(SOC_{avg\_rate}, SOC_{dev\_rate}\right); p_2 = f_2\left(SOC_{avg\_rate}, SOC_{dev\_rate}\right) \quad \textbf{(4.16)}$$

Both of the parameters p_1 and p_2 are fitted with Gaussian distribution since other extrapolation fitting methods may lead to an anti-intuitive result. The fitting results are listed in Eq. (4.17) and (4.18)

$$p_1 = \left(-0.001561 \cdot exp\left(-\left(y \cdot \frac{x-0.48}{0.025}\right)^2\right)\right) \times (2.328 \cdot y^2 + y)$$
$$+5.833e-4 \cdot (x-0.5) \cdot y^{0.2} + 1.051e-4 \cdot \left((0.15-y)^2 + y\right) \quad \textbf{(4.17)}$$
$$x = SOC_{avg\_rate}; y = SOC_{dev\_rate}$$

$$p_2 = \left(0.7285 \cdot exp\left(-\left(SOC_{dev\_rate} \cdot \frac{SOC_{avg\_rate}-0.48}{0.02875}\right)^2\right)\right) \times SOC_{dev\_rate}^{0.7685} \quad \textbf{(4.18)}$$
$$-0.278 \cdot (SOC_{avg\_rate} - 0.5) \cdot SOC_{dev\_rate}^{0.15}$$

Where SOC_{avg_rate} means the averaged SOC calculated depends on rated capacity, as in (4.7), and the SOC_{dev_rate} means the SOC deviation calculated according to rated capacity.

When applying the equation in models, the real averaged SOC and SOC deviation should be first converted to the rated one by using the following two equations:

$$SOC_{avg\_rate} = SOC_{avg} \times \frac{C_{dsb}}{C_{rated}} \quad \textbf{(4.19)}$$

$$SOC_{dev\_rate} = SOC_{dev} \times \frac{C_{dsb}}{C_{rated}} \quad \textbf{(4.20)}$$

4.5.2 Other critical parameters

All the other parameters calculated for VRLA batteries are using the same method as for LFP battery, so they are not repetitively introduced in this section.

4.5.2.1 Overall efficiencies

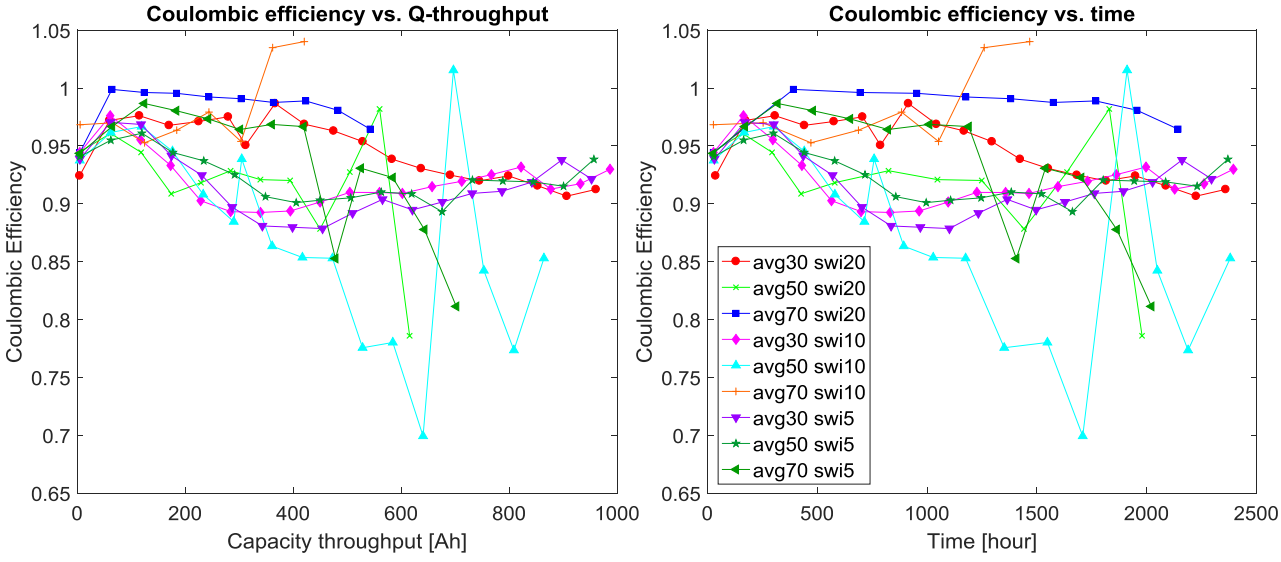

(a) **(b)**

Figure 4-26 Coulombic efficiency of VRLA battery versus (a) capacity throughput (b) time

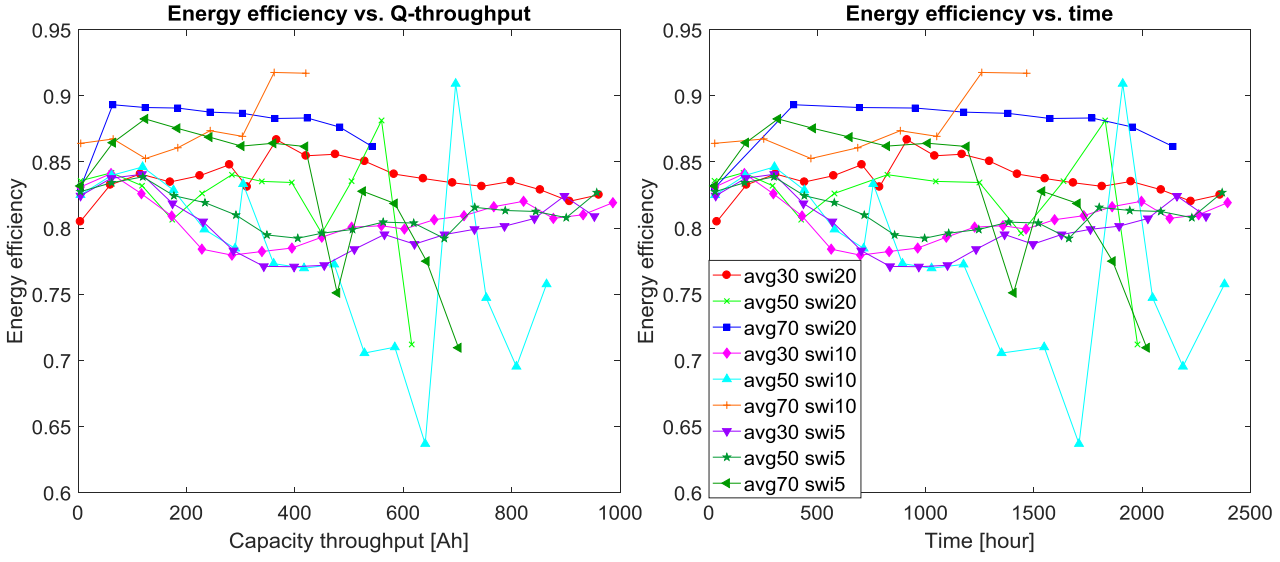

(a) **(b)**

Figure 4-27 Energy efficiency of VRLA battery versus (a) capacity throughput (b) time

Even though VRLA battery has a severe capacity drop during the test, it still able to maintain a relatively steady coulombic and energy efficiency.

Based on the coulombic efficiency equation obtained in chapter 3, the ageing effect was also added into the coulombic efficiency modelling. The coulombic efficiency is calculated into relative coulombic efficiency and then fitted into an empirically based equation. The relative coulombic efficiency is the overall coulombic efficiency at a random point in the ageing progress, divided by the overall coulombic efficiency of a fresh battery. It can be expressed as in Eq. (4.21).

$$cf_r(Q_{th}) = \frac{\eta_c(Q_{th})}{\eta_c(Q_{th}=0)} \tag{4.21}$$

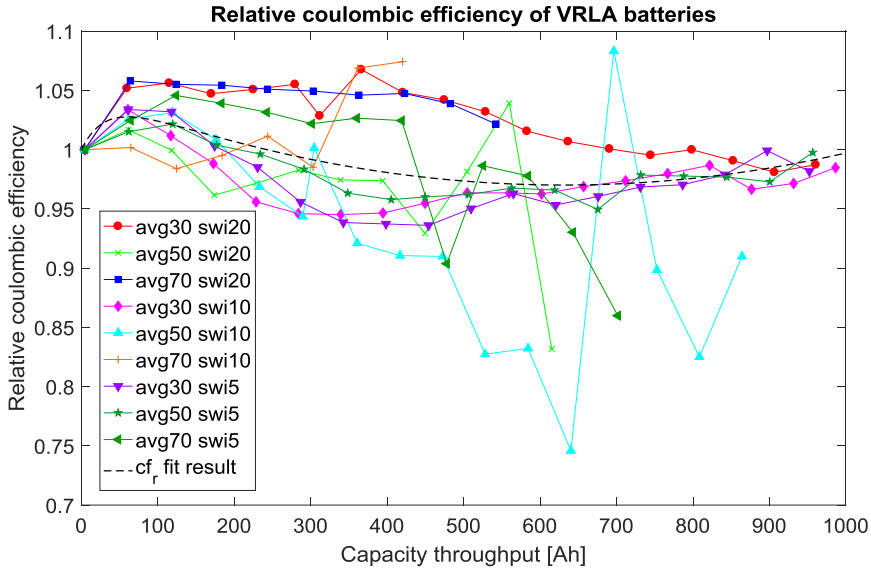

Figure 4-28 Relative coulombic efficiency of VRLA battery and the fitted result

The fitting result of the relative coulombic efficiency is in Eq.(4.22).

$$cf_r(Q_{th}) = 1 + 0.04899 \cdot \left(1 - exp\left(-0.03223 \cdot Q_{th}\right)\right) + 1.983e-7 \cdot Q_{th}^{\ 2} - 2.502e-4 \cdot Q_{th} \tag{4.22}$$

Hence, the coulombic efficiency of VRLA battery including its evolution can be represented by Eq.(4.23).

$$\eta_c(Q_{th}) = \eta_c(Q_{th}=0) \times cf_r(Q_{th}) \tag{4.23}$$

Where $\eta_c(Q_{th}=0)$ is Eq. (3.55).

4.5.2.2 Resistance

The internal resistance evolution of the VRLA battery was also calculated by using Eq. (4.12), and the results are drawn in Figure 4-29.

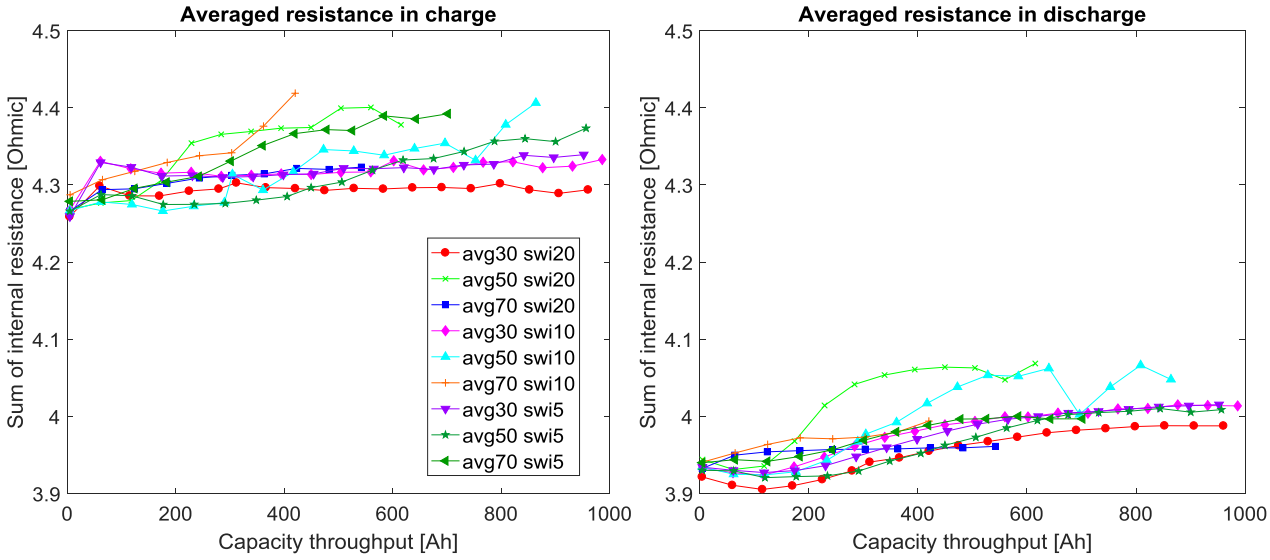

(a) **(b)**

Figure 4-29 Averaged internal resistance of VRLA batteries during (a) charge (b) discharge

From Figure 4-29, it is observed that the charge impedance is higher than the discharge impedance, both of them increased when battery ages but in a mild range which is around 2.5%. It is recommended that for industrial application, the replace time is the battery's resistance increased by 30% [178]. It means that even if the capacity of VRLA battery faded grievously, it is still able to sustain a decent power and energy capability.

4.6 Conclusion

In this chapter, how the battery lifetime experiments are designed, performed and analysed are explained. the lifetime model of both battery technologies are expressed in the form of Rate of normalised capacity fading as the function of capacity throughput, averaged SOC and the SOC deviation for VRLA battery.

From the experimental results, not only the lifetime model and some vital parameters can be extracted, but proper usage guidelines can also be suggested. This is introduced in detail in the next chapter.

5 Battery usage guideline identification and application

In this chapter, the analysis and proposed of the usage guidelines been done for two battery technologies are introduced. Then, one example of the usage guideline implementation in the SHS is simulated. From all the achieved work, one can have a general view of how to design and operate the battery appropriately in order to extend the lifetime in SHSs.

5.1 Usage guidelines concluded from experimental results

Apart from the SOH modelling, what are also valuable to be reached from the lifetime test data are the usage guidelines. First of all, the general conclusions for each battery technology separately are presented, as obtained from the experimental results.

- LFP
  - For LFP batteries, it is preferable to operate it with a lower averaged SOC.
  - Even it is not clearly observed in the experiments; it is still suggested that cycling LFP batteries with a smaller SOC deviation according to literature review in Chapter 4.
- VRLA
  - VRLA batteries are highly recommended to be cycled with a higher averaged SOC. With the high averaged operating SOC, it is even better to approach a larger SOC deviation in the mean while.
  - If the battery has to be operated with a lower averaged SOC to response to the load demand, try to avoid the large SOC deviation at the same time.
  - Inadequate regular fully recharging the battery may lead to a severe capacity drop.Regular fully recharge after each ten equivalent cycles or every five to six days is insufficient when the operational averaged SOC is lower than 70%.
- Comparison of two battery technologies
  - LFP batteries have a much better performance in both capacity and coulombic efficiency than VRLA batteries.
  - Though the LFP battery has a slightly higher energy efficiency than the VRLA battery, both of them have a relatively good energy efficiency and a moderate internal resistance increase during age, which means both power and energy capability are steady enough for long-term applications.
  - LFP battery has a larger degree of freedom on operational SOC range. If continuously cycling an LFP battery with an either high or low averaged SOC and a random SOC deviation, the battery is capable of maintaining a good performance.
  - However, VRLA battery requires a restricted usage constraint in practical applications. The regular fully recharge is necessary and different operational SOC ranges may lead to an enormous difference in the ageing process.

As a summary, the grades of each operational SOC range for two battery technologies are listed in Table 5-1, and the visualised histograms are shown in Figure 5-1. For each averaged SOC there is a maximum SOC deviation value, so the zero score histogram in Figure 5-1 is the non-existent combination of the averaged SOCs and the SOC deviations.

Table 5-1 Overview of recommended operating range for both battery technologies

Battery technology	**LFP**			**VRLA**		
SOC deviation ▼	**Average operational SOC ►►**					
Level	High (≥70%)	Medium (30-70%)	Low (≤30%)	High (≥70%)	Medium (30-70%)	Low (≤30%)
High (≥20%)	★	★★	★★★	★★★★★	★	★★★
Medium (10-20%)	★★★★	★★	★★★★★	★★★★★	★★	★★★
Low (≤10%)	★★★★	★★	★★★★★	★★★★	★★★	★★★

* More stars means higher recommended

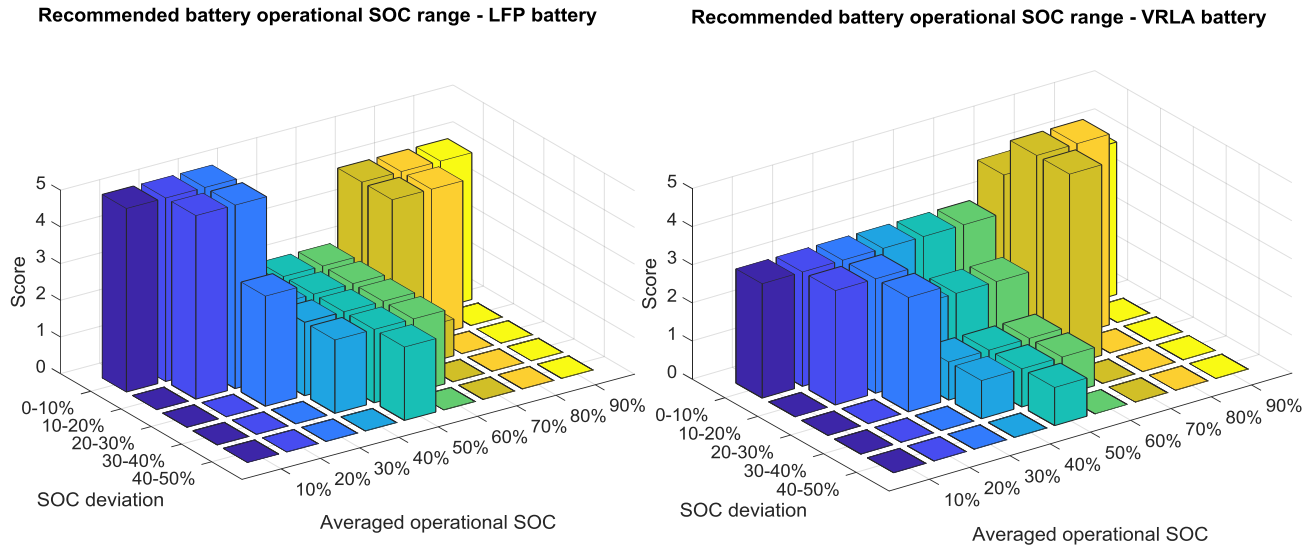

(a) **(b)**

Figure 5-1 Visualization of recommended operational SOC ranges for (a) LFP battery (b) VRLA battery
*** Higher score means more preferable**

In this section, the usage guidelines for both battery technologies have been achieved; then it is a question of how to apply it in a practical SHS.

5.2 One illustrative application of the usage guideline based on practical data

The usage guideline of each battery technology has been given and interpreted in the Section 5.1. In this section, one illustrative application of the usage guideline in a practical SHS is performed. The simulation with an actual system usage case is performed, and the results are analysed and evaluated in this section.

In the simulation, the behaviour of the battery which employed in an SHS in two cases are compared. One is the behaviour of a battery integrated with an illustrative implementation of the guideline, and the other is the battery works without any restriction. How the guideline affects both technologies is also compared and evaluated.

The practical yearly systematic power profile of an SHS for simulation was generated from a field investigation in Cambodia [179], where the SHSs are expected to serve.

The plot of the yearly power requirement is shown in Figure 5-2 (a) and a zoomed-in weekly power profile is presented Figure 5-2 (b). Two types of power compose the figure, one is excessive power, and the other is the deficit power. The excessive power is the surplus power from the PV generation, and the deficit power is the shortage of the load demand. The excessive power is expected to be stored in the battery and then provided from the battery to the load when there is a deficit power required to be replenished.

The power curve in Figure 5-2 (b) shows that for one-day duration, the power continuously flows into the battery then flows out of the battery. It means that the battery usage in one-day duration is approximately one full cycle.

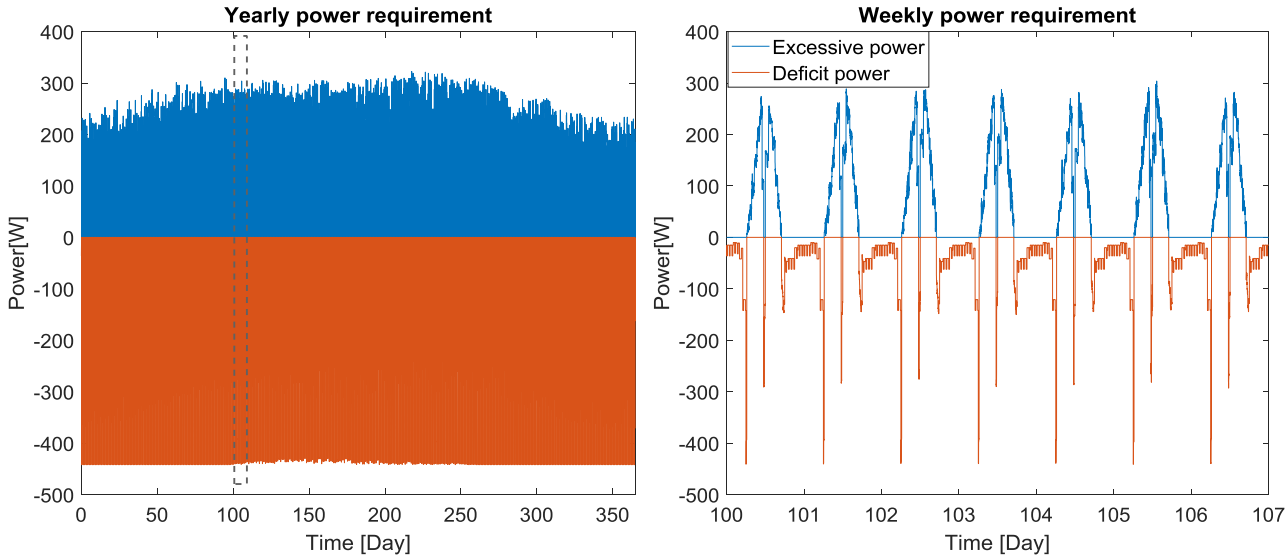

(a) **(b)**

Figure 5-2 Power requirement from a SHS (a) Yearly power pattern (b) Zoom in of the curve in the dashed box in (a)

In this SHS, the energy and power information for battery sizing is summarised in Table 5-2.

Table 5-2 Energy and power information of the practical case

Daily deficit energy	789.83 Wh
Daily excessive energy	1333.34 Wh
Maximum deficit power	442 W
Maximum excessive power	332.38W

According to the energy and power information of this SHS, a normal battery sizing plan is proposed and listed in Table 5-3, column two "Normal sizing strategy". The battery in the SHS sized with "Normal sizing strategy" can just fulfil the load demand of one full-cycle per day sufficiently. This sizing method is the most commonly applied one for SHS battery sizing. For each battery technology, one simulation with the "Normal sizing strategy" has been done.

It is suggested to cycle the LFP battery with a lower averaged SOC according to its usage guideline, so an exorbitant scheme is addressed in this case. That is to double size the battery according to the "Normal sizing strategy". With this extra capacity and a lower initial SOC value (50%), the battery can operate with the SOC range lower than 50%. This scheme is named with "Over sizing strategy", and the battery information is in Table 5-3, column three.

For VRLA batteries, the usage guideline recommends cycling them with a higher averaged SOC, and the SOC deviation can be relatively large in this situation. Hence, a double battery size as the "Normal sizing strategy 1" scheme was also applied in the simulation for VRLA battery. With a higher initial SOC value (80%) and the extra capacity, most of the time the VRLA battery can work with SOC range higher than 50%. Apart from that, a "Over sizing strategy 2" for VRLA was also added in order to make a comparison between the utilities of the usage guideline. The battery sized in over sizing strategy 2 is 1.7 times as the normal sizing strategy. The preliminary calculation shows both over sizing strategies can relatively maintain the battery cycling within 50% of SOC range.

Table 5-3 Battery sizing plan

	Normal sizing strategy		**Over sizing strategy**		
Battery technology	LFP	VRLA	LFP (2x)	VRLA strategy1 (2x)	VRLA strategy2 (1.7x)
Rated capacity of the battery pack [Ah]	240	420	480	840	720
Rated energy of the battery pack [Wh]	792	840	1584	1680	1440
Number of battery cells in series	12	24	12	24	24
Number of battery cells in parallel	8	7	16	14	12
Rated battery pack voltage [V]	39.6	48	39.6	48	48

5.2.1 Simulation result of LFP battery

Since the battery model constructed in this project is with the accuracy in seconds, an entire simulation of the battery life in SHS has a high requirement on the storage and computational ability of the computer. Therefore, a sixty-day simulation of LFP battery was performed mainly to compare the capacity declining trend.

Figure 5-3 shows the ten days zoomed-in power comparison of the system requirement and the battery response. It is shown that all the deficit power, which is the negative part, is fully satisfied by the battery. However, there is some excessive power that has to be dumped in each of the days due to the extra PV generation.

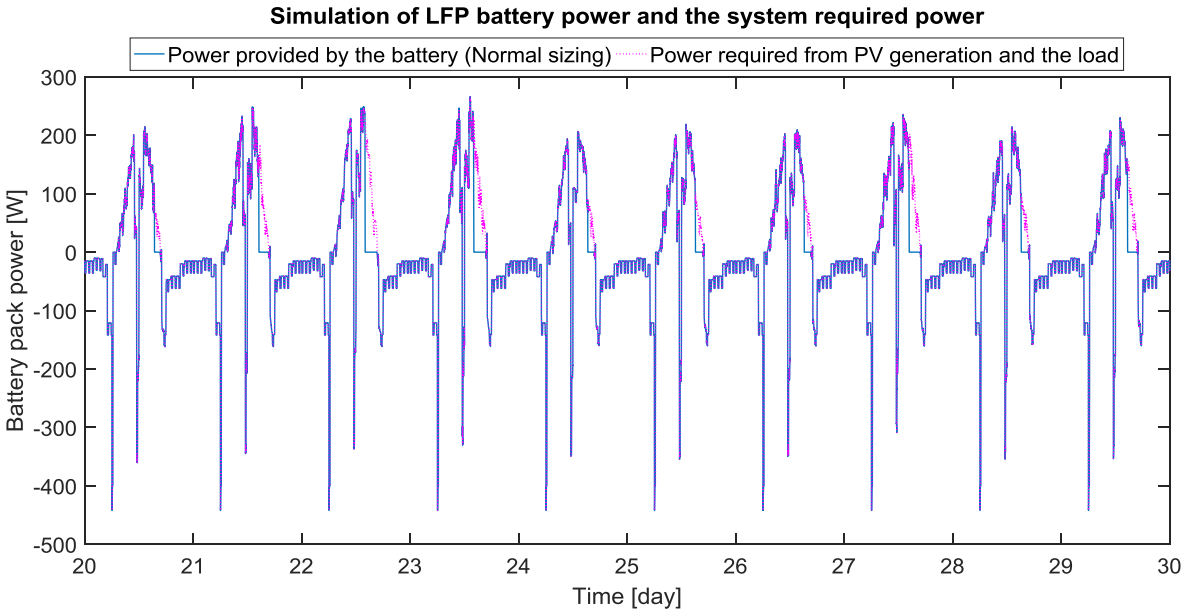

Figure 5-3 Comparison of the required power and the power input-output of the LFP battery pack

The LFP battery pack model with two sizing strategies mentioned in Table 5-3 were simulated.

The input and output power of the battery with different sizing strategies are plotted in Figure 5-4. It is shown in the figure that the battery power with two strategies are the same. Which means there is no extra sacrifice of either load demand or dumped energy in “Over sizing strategy” in comparison with the“Normal sizing strategy”.

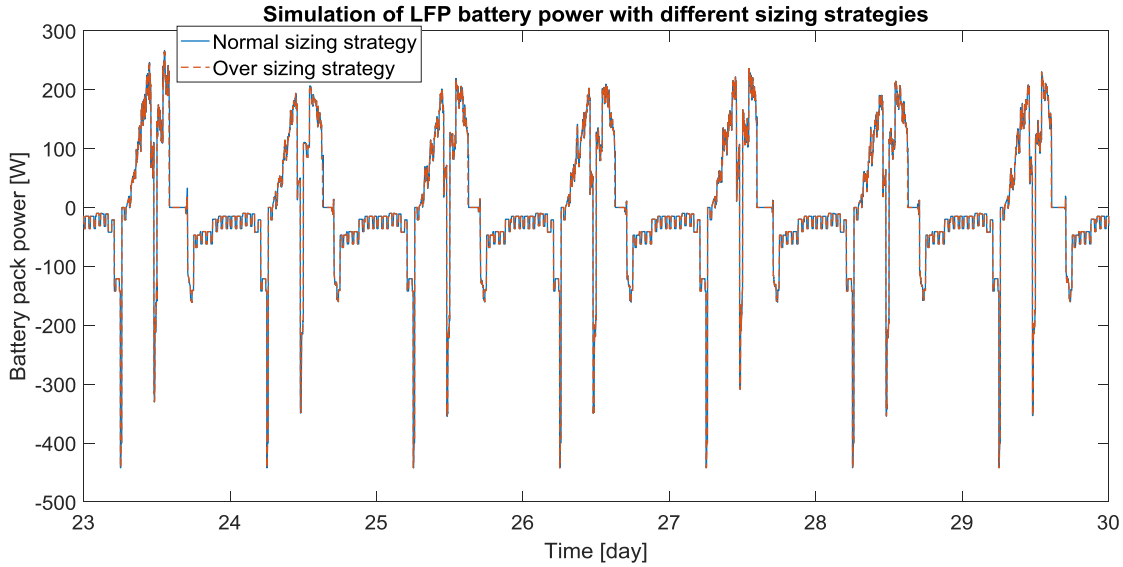

Figure 5-4 Comparison of the power input-output of the LFP battery pack with different sizing strategies

The battery cell current and the SOC during the simulation are plotted in Figure 5-5 and Figure 5-6.

In Figure 5-5, it is observed that the cell current during simulation is no larger than 1.5 A, which is 0.6 C. This value is smaller than the current applied for the lifetime experiments in this study. Hence, the simulated result is valid.

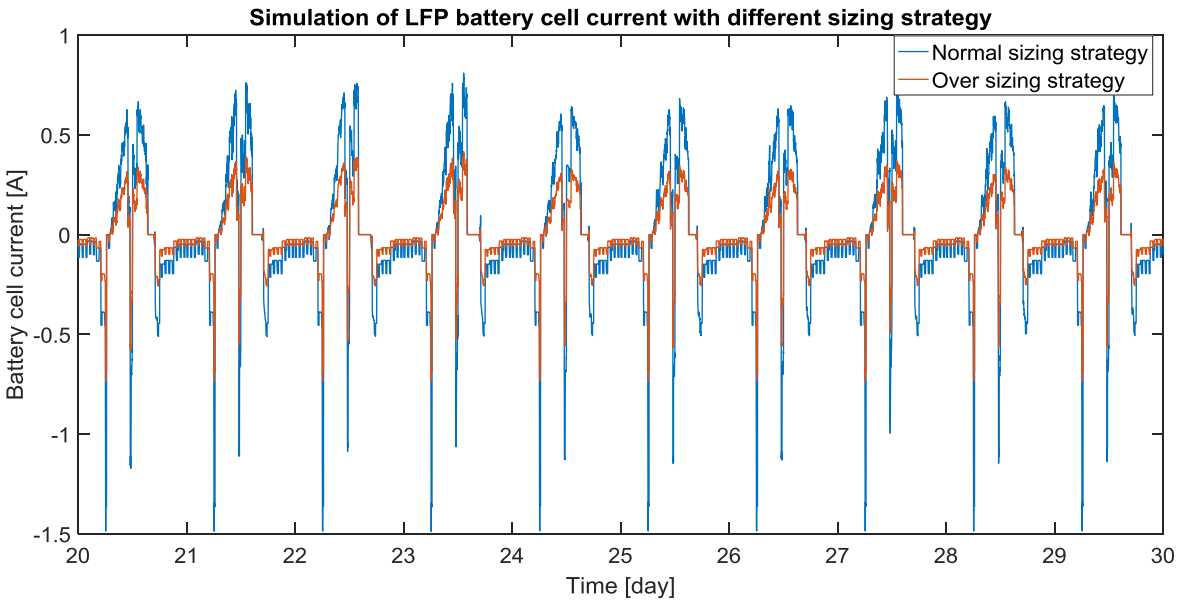

Figure 5-5 Simulation of LFP battery cell current in two strategies

In Figure 5-6, it shows the simulated SOC of normal sizing strategy is fully charged and almost discharged to empty every day, and the simulated SOC of over sizing strategy was cycled between 0% and 50%.

The averaged SOC and SOC deviation calculated referring to the capacity throughput is listed in Table 5-4.

Table 5-4 The averaged SOC and SOC deviation calculated in referring to capacity throughput of LFP battery simulations

Sizing strategy	Averaged SOC	SOC deviation
Normal sizing	55.42%	42.21%
Over sizing	27.67%	21.31%

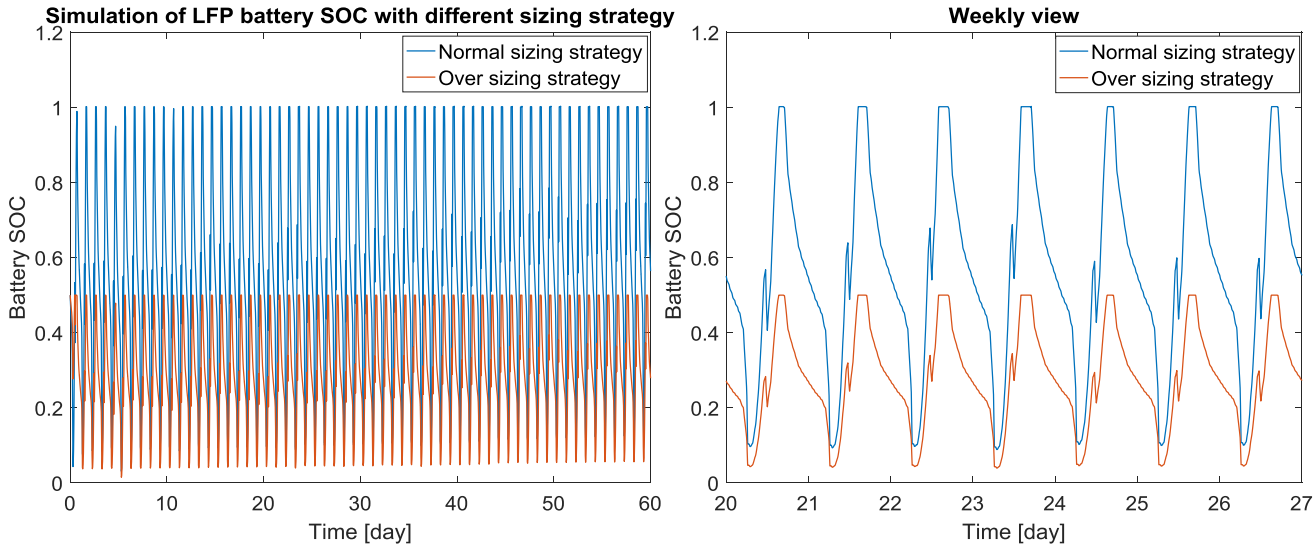

(a) **(b)**

Figure 5-6 Simulation of LFP battery SOC in two strategies; (b) is one-week zoomed-in view of (a)

The simulated battery capacity changing of two sizing strategies are drawn in Figure 5-7.

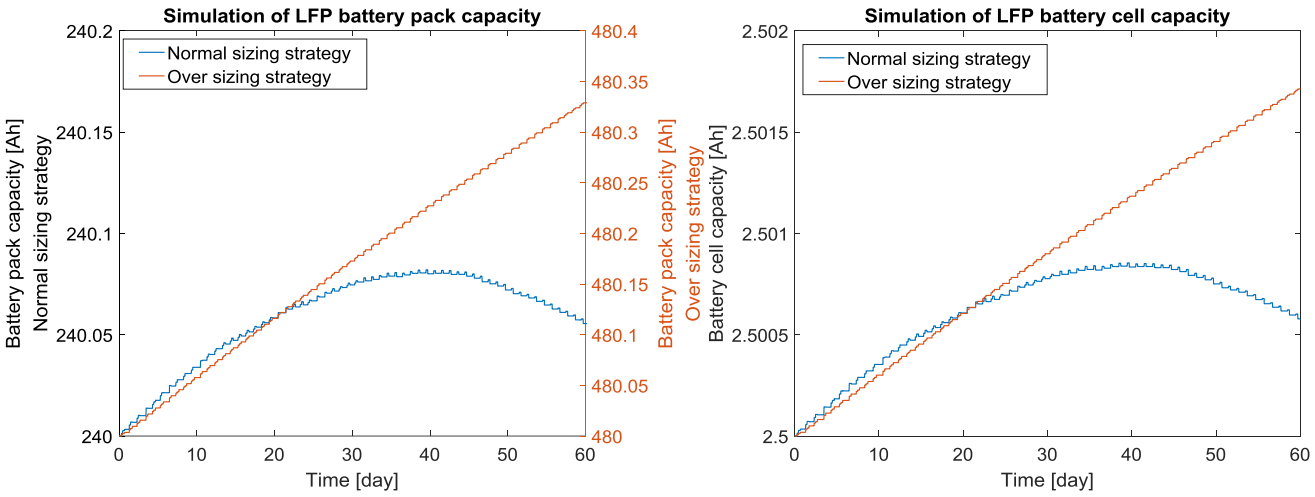

(a) **(b)**

Figure 5-7 LFP battery capacity changing of two sizing strategies in 60 days simulation (a) battery pack capacity (b) battery cell capacity

From Figure 5-7, it can be observed that the over sizing strategy indeed favourable in battery capacity preserving. The improved battery ageing behaviour in cell level is apparent. Nevertheless, it seems wasteful and exaggerative to double size the battery only for gaining a small amount of reserved capacity in battery pack level. However, it also can be comprehended from other two points of view.

The curves in Figure 5-7 are plotted versus time, but the lifetime model was build according to the capacity throughput. In order to make the comparison, the simulated battery cell capacity changes with time and with capacity throughput are drawn in Figure 5-8.

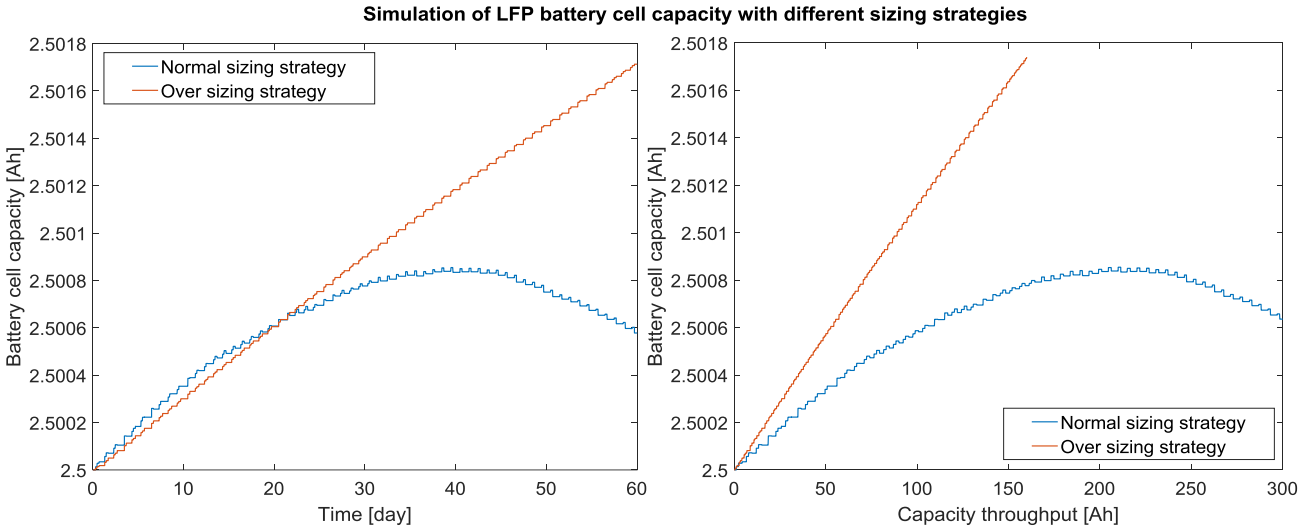

(a) **(b)**

Figure 5-8 LFP battery capacity changing of two sizing strategies (a) in time scale (b) versus capacity throughput

Firstly, in Figure 5-8, the battery cell capacity fading trend shows that the over sizing strategy is superior to the normal sizing strategy in capacity throughput scale. It is because the battery cell in over sized situation only experienced half of the capacity throughput compared to the normal sizing strategy in the same time duration.

Secondly, each battery cell in over sized situation was performed with a lower current, as presented in Figure 5-5. The experimental results introduced in Chapter 4 shows that LFP battery cycling with a lower current has its advantages in cycle time scale.

For LFP batteries, the application of the usage guideline in the form of different sizing strategy is advantageous. However, how to design a proper over sizing plan sufficiently as well as economically deserves further studying in the future.

5.2.2 Simulation result of VRLA battery

For the simulation of VRLA battery, a thirty days duration was chosen since the VRLA battery has a more noticeable trend than the LFP battery and this duration is sufficient for the VRLA battery to show the ageing process.

The simulated power of VRLA battery pack and the power required from the SHS are plotted in Figure 5-9. It indicates that the deficit power can be supplied perfectly by the battery, which is the same with the simulation result of the LFP battery pack. However, only a small portion of excessive power was dumped. That is because the coulombic efficiency of VRLA battery drops drastically when its SOC is higher than 90%. Therefore, an adequate amount of input current is required to charge the battery until it reaches 100% SOC.

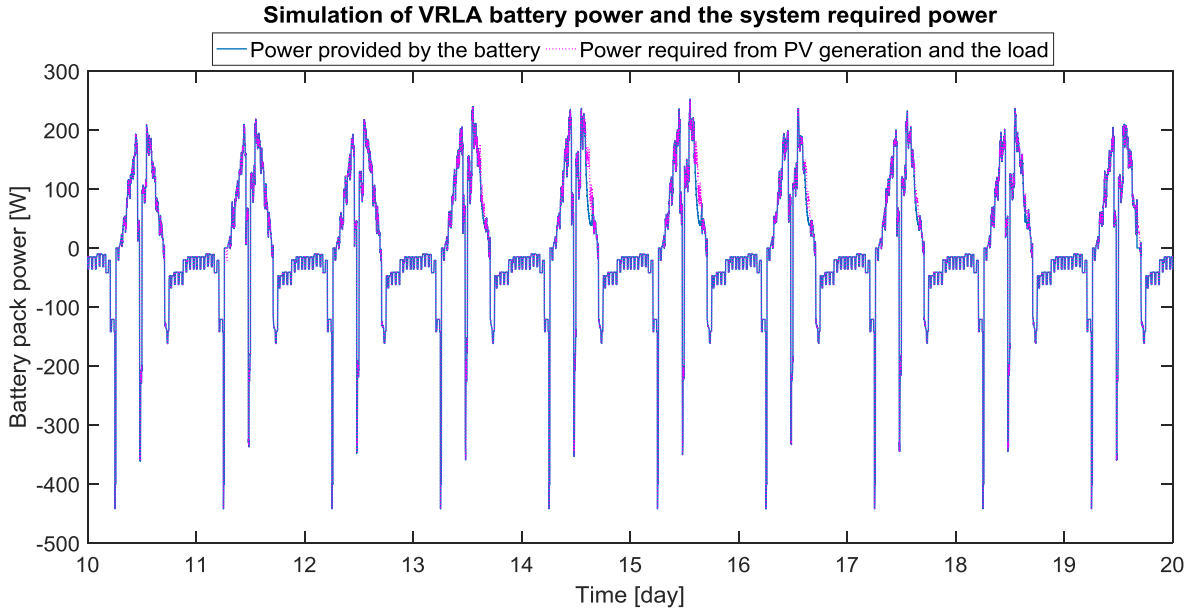

Figure 5-9 Comparison of the required power and the power input-output of the VRLA battery pack

The simulated input and output power of the VRLA battery with different sizing strategies are plotted in Figure 5-10. It can be observed that these three strategies have almost complete overlapped power curves. There is slight difference in between these strategies when it is in charge state. It might because of the capacity decline of the "Normal sizing strategy" made it no longer able to store as much energy as when it was new.

This means the adjustment of the sizing strategy would have no influence on the load demand supplement but only a trivial impact on the energy that dumped, so far as simulated.

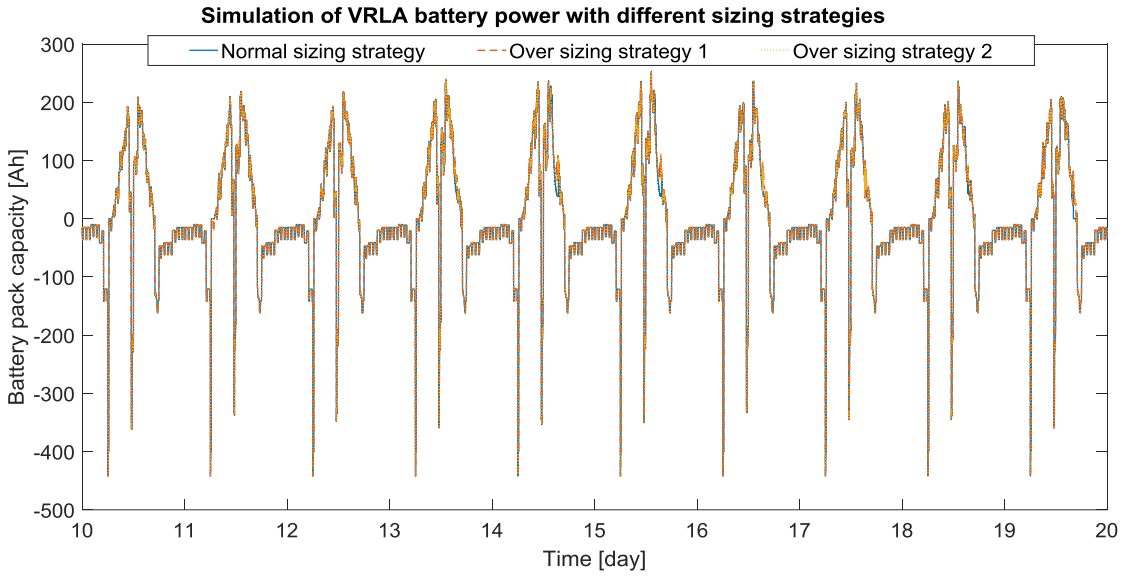

Figure 5-10 Comparison of the power input-output of the VRLA battery pack with different sizing strategies

In Figure 5-11, the simulated cell current of the VRLA battery is present. The curves in Figure 5-11 shows that for all three simulation schemes, most of the operating current is within the window of value -0.5 to +0.5 A, which is marked with the dashed line. It means the current is smaller than 0.2 C in most of the time. The lifetime experiments for VRLA battery were performed with current 0.2 C, as introduced in Chapter 4. In the simulation, there were some short time periods each day that the battery was working with a much higher current than 0.2 C. However, the current peak did not hold for too long so the simulation results can still be considered as conforming with the experiments.

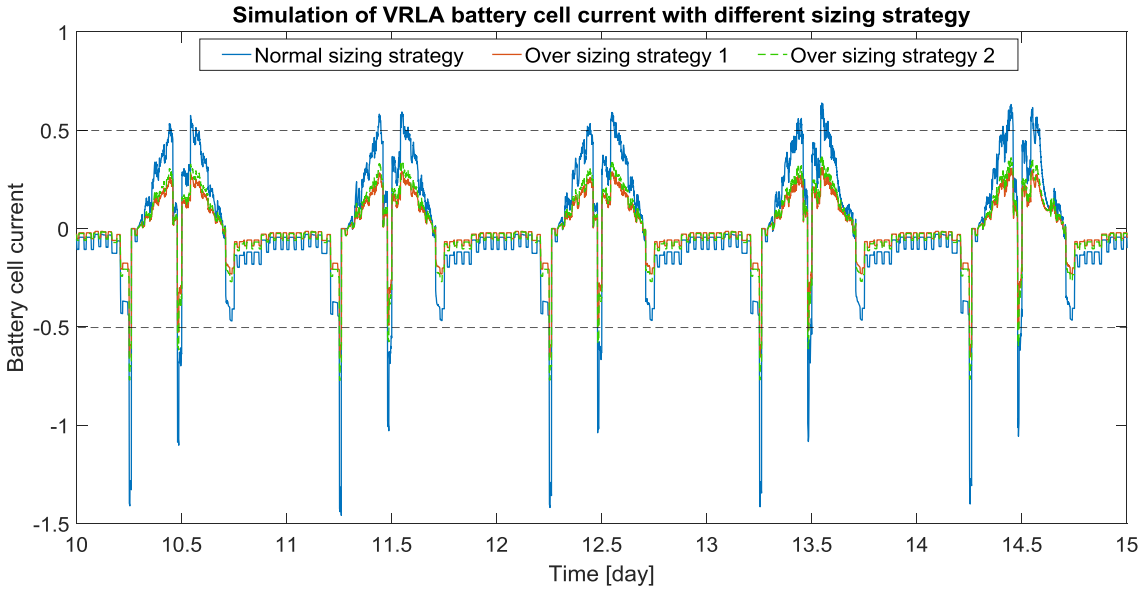

Figure 5-11 Simulation of VRLA battery cell current in three strategies

The SOC values obtained from the simulation is drawn in Figure 5-12.

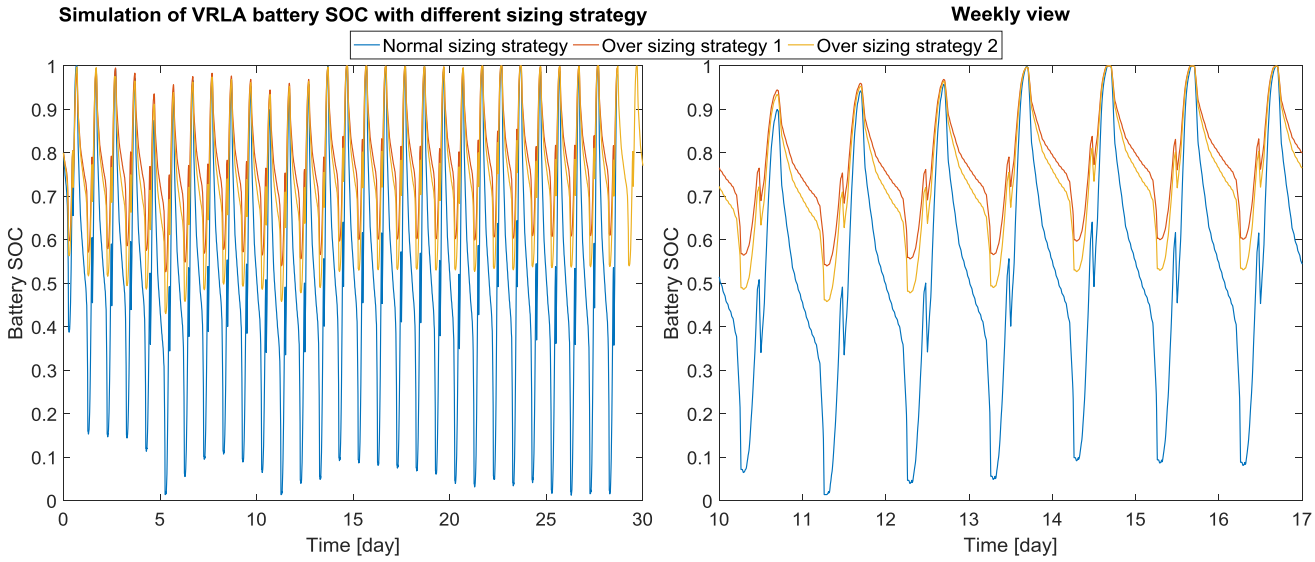

Figure 5-12 Simulation of VRLA battery SOC in two strategies (b) is one week zoomed in view of (a)

As can be observed in Figure 5-12, the battery in the normal sizing strategy scheme experienced nearly full cycles every day, which is similar to the simulation results of the LFP battery. The results of both over sizing strategy demonstrated that the lowest SOCs were higher than 40%.

In addition, the simulated averaged SOC and SOC deviation according to the capacity throughput is calculated and summarised in Table 5-5.

Table 5-5 The averaged SOC and SOC deviation calculated in referring to capacity throughput of VRLA battery simulations

Sizing strategy	Averaged SOC	SOC deviation
Normal sizing	62.93%	48.60%
Over sizing 1	78.54%	19.31%
Over sizing 2	74.70%	22.77%

The simulated capacity results are plotted in Figure 5-13 and Figure 5-14.

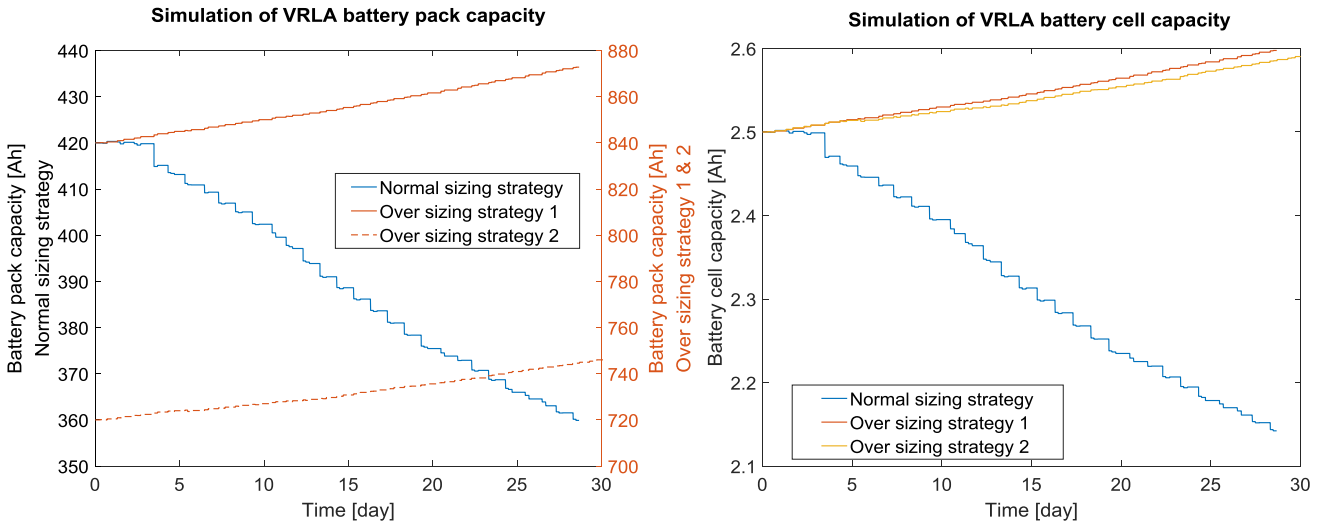

(a) **(b)**

Figure 5-13 VRLA battery capacity changing of three sizing strategies in 30 days simulation (a) battery pack capacity (b) battery cell capacity

Curves plotted in Figure 5-13 shows that the implementation of the usage guideline on VRLA battery improved its performance prominently in terms of ageing. The improvement is considerable even at the battery pack level. However, there is not much difference between two over sizing strategies in the promotion of battery lifetime.

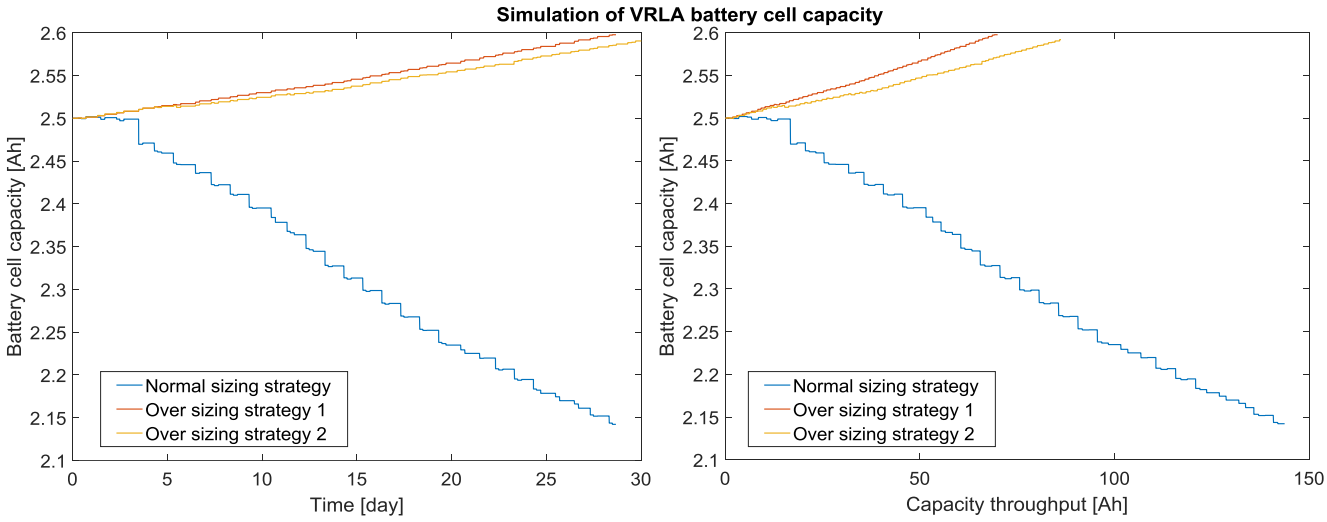

(a) **(b)**

Figure 5-14 VRLA battery capacity changing of two sizing strategies (a) in time scale (b) versus capacity throughput

In Figure 5-14 is the comparison of the capacity changing with the time and with the capacity throughput. It demonstrates that the application of the usage guideline in the form of over sizing always has preponderance on capacity throughput which each cell was experienced. The over sizing strategy 1 does not have many extra advantages in comparison with over sizing strategy 2.

As a conclusion, the application of the usage guideline is necessary for VRLA batteries, and the manner of over sizing is profitable. However, the battery did not get much extra benefit from an excessive over sizing (2x) compare with a tolerable over sizing (1.7x). It is worthy of looking for an optimal over sizing strategy in the future studies.

5.3 Conclusion

As a conclusion, the implementation of the battery usage guideline in the form of over sizing strategy has advantages in preserving capacity for both battery technologies. However, only one example implementation of the usage guideline is explored in this study, which is over sizing the system. The results show that applying the usage guidelines is a complex. It involves not only operational SOC range but also other variables like the operational current and the capacity throughput.

Apart from adjusting the battery size, other approaches can also be further looked into. For example intelligent load profile management, battery charge plan management. It could also be applying two battery technologies having disparate recommended SOC ranges in one SHS, in order to compensate each other. For example, the hybrid battery system which composed by more than one type of battery to optimise the storage system,would be a suitable candidate.

6 Conclusions and recommendations

6.1 Retrospection of the thesis

In this project, two battery technologies (LFP and VRLA) were picked for the research of batteries' performance. The study involved an experimental part, a modelling part and the simulation section which considered the dynamic behaviour and a long term lifetime prediction function for the batteries.

6.1.1 Answers to the research questions

The main objective of this study is to develop a tool and a method that includes the usage guideline of different battery technologies in low power off-grid SHSs. Some sub-objectives construct the bridge to the main objective and all of the studies were achieved. This has been done by answering the following research questions:

- **How should the battery cell dynamic behaviour be modelled?**

In this project, EECM was the chosen approach to model the battery behaviour. This is because this type of models is compatible with other electrical models, and it is quite practical for electrical engineers. For both battery technologies, the model was constructed with a 2nd order RC-pair electrical circuit as a compromise between complexity and accuracy. The main variables which of interest in dynamic modelling are the SOC and the operational current. All the parameters used for battery modelling, i.e. the capacity, the internal impedances and the efficiencies, were tested and extracted from experiments. The model works well with the SOC range of 0-100% and the current range of 0.05C-0.5C, with an error lower than 2%. That is to say, this model provides an excellent accuracy in representing the dynamic behaviour of a battery in SHSs for simulation.

- **How to predict the battery cell's lifetime?**

A performance based lifetime prediction model has been chosen, and the capacity was picked as the anchor performance parameter. It is because, for long-term operation in SHSs, the storage ability is the most attractive feature.

Moreover, the impact on the battery's lifetime of the SOC's utilisation range (i.e. SOC average range and its deviation), and the operational current were explored.

A series of experiments focused on battery capacity fading was performed, with a focus on the battery capacity's fading under different stress factors. Finally, and the battery lifetime model was extracted from the experimental results. The battery lifetime was modelled in the form of rate of normalised capacity fading.

- **How should the usage guidelines be obtained and how to apply it in SHSs?**

The battery usage guidelines were obtained through analysing the experimental data. After the acquisition of the guidelines, a feasible method to apply them in SHS was proposed. This method is to adjust the battery sizing strategy so the battery operational SOC can be controlled within a desired range.

- **How to compare the results and evaluate the achievements?**

The evaluation and comparison is not a separate task, and all of them were distributed arranged through the whole study.

The evaluation of the battery dynamic behaviour model was accomplished by calculating the error between the experimental data and the simulation results.

The comparison of the battery behaviour between two technologies was done in terms of comparing their efficiencies, internal impedances and the battery capacity in both short and long term time scale.

The evaluation of the usage guideline and its implementation was obtained by simulating the model and comparing the simulation results.

In this study, all the questions were perfectly answered and interesting conclusions were drawn through it. Besides, there are highlights and contributions have been harvested.

6.1.2 Highlights and contributions

- In this thesis, two battery models especially suitable working for SHSs were built. The model proposed in this study is more appropriate for SHSs applications or other systems with lower operational C rates, which require higher accuracy than those previously presented.
- Normally the battery modelled for SHSs simulation is built from a battery pack level. Although there was some work done on battery cell level modelling, these studies were for EV applications with a high C rate (usually higher than 1 C). In this study, an accurate cell level battery model was built. That is to say, out of this study, the achieved battery model is modular that with high flexibility in scale-up in the future work.
- In this study, a lifetime modelling contains the ageing evolution iwas proposed and the battery lifetime was modelled in the form of rate of normalised capacity fading (r_{nF}). In this study, the variation of the battery capacity due to fading was also taken into account when predicting the battery lifetime.
- Furthermore, a first step has been taken towards finding a more practical method for determining an optimal design, size and usage guide (i.e. mean and operational range of the SOC) for battery storage in SHSs. This has been done by means of analysing the empirical data and the simulations. In the results of this study, a relation between the stress factors and lifetime has been observed. This provides a significant starting point for future studies in the field of designing, sizing and guiding the battery usage to extend its lifetime.

6.2 Final conclusions

In this project, many experiments on both dynamic and lifetime behaviour exploration were performed.

- The dynamic results show that LFP batteries have a perfect coulombic efficiency that is equal to one, as far as measured. However, because of the gassing related side reactions, VRLA batteries can only ensure an average 95% overall coulombic efficiency. LFP batteries also have higher energy efficiency (around 90%) in comparison with VRLA batteries (around 85%). This is because VRLA batteries have a much higher internal impedance than LFP batteries, which indicates that more energy charged into a VRLA is converted into heat because of these internal impedances.
- From lifetime experimental results, the conclusions can be drawn as follows.

  For LFP batteries, the lifetime tests were accomplished with 1 C rate, and a change in average SOC operation range seemed to have an impact on battery lifetime. Battery cycled under lower averaged SOC has a lower fading rate value, and the rate has a gradual trend of increasing. However, the SOC deviation did not show a clear impact on battery lifetime, and this is partly because of the interruptions and environmental interferences during experiments. This could be investigated further in future works. The experiments also added a test performed with a lower C rate (0.5C) in order to explore the impact of the operating current. From a capacity throughput scale, lower C rate did not show clear advantages.

Nonetheless, the battery does have a mitigating fading trend in cycle-time scale with the lower cycling C rate. This is also worth more studies in the future.
For VRLA batteries, the lifetime tests were operated with a 0.2 C rate. Both averaged SOC and SOC deviation influence the battery ageing. It is has been observed that VRLA batteries may have a longer lifetime with a higher averaged operational SOC. That is, to prolong the lifetime of a VRLA battery, it is preferable to fully charge it regularly in operation. The influence of the SOC deviation showed a mixed effect with the averaged SOC, but a general trend can be summarised. With a higher averaged SOC, it is better to have a larger SOC deviation. When the averaged SOC is lower, e.g. than 50%, it is then suggested that to cycle the battery with a smaller SOC deviation. No other C rate than 0.2C was explored with VRLA batteries. Thus it is suggested that future research on different C rates for this technology to be studied.

- When comparing the experimental results of these two battery technologies, some interesting conclusions have been drawn.

  Under long-term cycling with different stress factors, the LFP batteries have shown a better performance than VRLA batteries. The coulombic efficiency of LFP was constantly equal to one until the experiment finished. On the contrary, the coulombic efficiency of VRLA kept decreasing with the ageing of the battery. The energy efficiency of VRLA batteries slightly diminished while the energy efficiency of LFP even showed a rising trend. The overall internal impedance of the batteries from both technologies increased with ageing.

- For SHSs applications, both battery technologies can be employed, but different precautions should be considered with their usage.
  Although the LFP batteries have a recommended SOC usage range that lower than 50%, they are still able to retain a quite steady and superior performance in other SOC ranges. Contrarily, a discrepancy of ageing speed in VRLA batteries appeared with different operational SOC ranges. This result suggests that a restriction on sizing and usage management is required in VRLA battery applications.

- From the usage guideline identification and simulation, it is concluded that the application of the proposed usage guideline can improve the battery long term performance regarding to capacity preservation. It is indispensable to apply the usage guideline for VRLA batteries. The application of the usage guideline on LFP battery can make a noticeable improvement in its long term behaviour.
  The implementation of the usage guidelines in the form of adjusting the battery sizing strategy is efficacious**.** Moreover, this manner is correlated with other factors like capacity throughput and current as well.

6.3 Recommendations on future work

Due to practical reasons and time constraints, limited points of interest have been thoroughly investigated in this study. Some simplifications have been made through this work, which allows some recommendations for the future work.

6.3.1 Battery modelling

- For both dynamic and lifetime modelling, the battery temperature would be a quite crucial factor which may have a significant influence on both battery dynamic performance and lifetime.
  It contains two aspects. First, to build the thermal model of the battery cell. For example by using other software like COMSOL to build an accurate battery thermal model. An analytical thermal model based on thermal transport theory could also be an attempt.
  The second aspect is to explore how the battery temperature influences the battery's performance. In a dynamic battery model, OCV and internal impedance were reported significantly influenced by the battery's temperature. In the battery lifetime prediction, both excessive higher and lower battery temperatures e considered as a vital stress factor. In order to achieve this, more experiments should be performed.
  Moreover, how the ageing process influences the battery thermal behaviour and how its thermal behaviour varies while ageing, in turn, changing the battery lifetime is also an attractive topic for the future work.

- In this study, the battery's dynamic behaviour was modelled only when the battery was in the fresh stage. The dynamic performance evolution through ageing was ignored. For example, the VOC and the values of electrical elements were reported as the function of battery's state of health. The data needed for modelling the battery's internal impedance evolution during ageing has been recorded in the lifetime experiments, so this work could be continued by using the existed data directly in the future. Additionally, how the battery coulombic efficiency and its energy efficiency change and how is the battery power capability influenced by battery ageing deserve further explorations in the future.

6.3.2 Experimental design

- In the dynamic modelling of the VRLA battery, the coulombic efficiency was extracted with an approximate test method. Even though the accurate test methods which are commonly applied for measuring coulombic efficiency are mostly chemical-based, it is still worth to searching for a simple method with sufficient accuracy, especially for electrical engineers.
- In lifetime experiments, the averaged SOC, SOC deviation and the operational current were chosen for exploration. However, the test setting branches, the test operating time and the number of samples could all be extended. In order to obtain the results with a higher authentic level, there are some recommendations on future lifetime experiments. First to add more combinations of averaged SOC and SOC deviation, with which all the possible battery SOC operation range could be covered. Secondly, triple the number of samples in each test, so the errors between each cell due to uneven manufacturing can be eliminated. Lastly, prolong the whole ageing test time and try to avoid interruptions in between. In this case, it is possible to obtain more and complete lifespan experimental results, with which a more accurate lifetime model could be built. In addition to the stress factors which have been considered in this thesis, some other stress factors could also be added for example battery temperature and operational current. Then the battery behaviour could be mapped in a model which is suitable for extensively applicational conditions.

6.3.3 A systematic solution to the optimisation problem

- All of the models built in this study are at the battery cell level. This provides a possibility for future research on creating a scalable battery pack model with cell models. Although the current cell model could be simply scaled up by linear multiplying the current and voltage, transferring this model to a real battery pack model would need more effort. For example, balancing the current and voltage of each cell when they are connected in parallel or series, predicting the SOC of the whole battery pack and managing the thermal behaviour of each cell. Nonetheless, creating a scalable battery pack model which consisted of the accurate battery cell models would be valuable for future studies and simulations of SHSs.
- In this study, some suggestions on battery usage in SHSs were provided in order to improve the battery lifetime. Those suggestions are not only related with how the users employ the battery, but also provide a direction to follow for considering the battery lifetime while designing and sizing the battery. Future work could keep focusing on finding a systematic method which involves a battery lifetime optimisation algorithm, for designing, sizing and guiding the usage of SHSs batteries. That is to say, a method for a practical battery storage system design in SHSs is the future goal. The previously mentioned scalable battery cell model with high flexibility in battery capacity affords a suitable simulation module for the future studies.
- In this project, only one possible method was tried to apply the proposed battery usage guideline in SHS, which is to change the battery sizing strategy. However, there are many other feasible methods, for example managing the system power flow intelligently in order to control the battery usage range. Further more, the usage guideline can even be applied in battery storage design in the way of giving instructions on composing the storage system with different battery technologies.
  How to apply the usage guidelines in SHSs effectively as well as economically can be further studied in the future research.
- There are more things worth of investigating after a systematic approach for designing and sizing of SHSs batteries is found, a further and important step is to search the relation between these optimisation

variables and a financial cost-benefit analysis considering the gained lifetime. That is, to compare the financial costs of different battery design and usage patterns with the benefits obtained in lifetime.

References

[1] T. Muneer and Y. Kotak, *Solar Photovoltaic System Applications: A Guidebook for Off-Grid Electrification*. Springer International Publishing, 2016.

[2] D. Linden and T. B. Reddy, *Handbook Of Batteries*. McGraw-Hill, 2002.

[3] D. U. Sauer, G. Bopp, A. Jossen, J. Garche, M. Rothert, and M. Wollny, "State of charge - What do we really speak about?," *21st Int. Telecommun. Energy Conf.*, no. February 2016, 1999.

[4] D. Doerffel and S. A. Sharkh, "A critical review of using the Peukert equation for determining the remaining capacity of lead-acid and lithium-ion batteries," *J. Power Sources*, vol. 155, no. 2, pp. 395–400, 2006.

[5] M. Root, *The TAB Battery Book An In-Depth Guide to Construction, Design, and Use*. McGraw-Hill Companies, 2010.

[6] V. Pop, H. J. Bergveld, D. Danilov, P. P. L. Regtien, and P. H. L. Notten, *Battery Management Systems : Accurate State-of-Charge Indication for Battery-Powered Applications*. Springer Science & Business Media, 2008.

[7] T. R. Crompton, *Battery Reference Book*. Reed Educational and Professional Publishing Ltd, 1990.

[8] C. A. Vincent and B. Scrosati, *Modern batteries: An introduction to electrochemical power sources*. Butterworth-Heinemann publications, 1984.

[9] M. Dubarry, V. Svoboda, R. Hwu, and B. Yann Liaw, "Incremental Capacity Analysis and Close-to-Equilibrium OCV Measurements to Quantify Capacity Fade in Commercial Rechargeable Lithium Batteries," *Electrochem. Solid-State Lett.*, vol. 9, no. 10, pp. A454–A457, 2006.

[10] M. Dubarry and B. Y. Liaw, "Identify capacity fading mechanism in a commercial LiFePO4 cell," *J. Power Sources*, vol. 194, no. 1, pp. 541–549, 2009.

[11] H. J. Bergveld, W. S. Kruijt, and P. H. L. Notten, *Battery Management Systems*, vol. 9. Dordrecht: Springer Netherlands, 2002.

[12] T. Levin and V. M. Thomas, "Can developing countries leapfrog the centralized electri fi cation paradigm ?," *Energy Sustain. Dev.*, vol. 31, pp. 97–107, 2016.

[13] P. Sandwell, N. Lam, A. Chan, S. Foster, D. Nagpal, C. J. M. Emmott, C. Candelise, S. J. Buckle, N. Ekins-daukes, A. Gambhir, and J. Nelson, "Solar Energy Materials & Solar Cells Off-grid solar photovoltaic systems for rural electri fi cation and emissions mitigation in India," *Sol. Energy Mater. Sol. Cells*, vol. 156, pp. 147–156, 2016.

[14] Deutsche Gesellshaft fur Sonnenenergie, *Planning and Installing Photovoltaic Systems: A Guide for Installers, Architects and Engineers*. 2008.

[15] J. Hoppmann, J. Volland, T. S. Schmidt, and V. H. Hoffmann, "The economic viability of battery storage for residential solar photovoltaic systems – A review and a simulation model," *Renew. Sustain. Energy Rev.*, vol. 39, pp. 1101–1118, 2014.

[16] V. Marioleas, "Cycle life analysis and cost evaluation of the main battery technologies for off-grid PV

systems," Delft, 2016.

[17] P. Van den Bossche, F. Vergels, J. Van Mierlo, J. Matheys, and W. Van Autenboer, "SUBAT: An assessment of sustainable battery technology," *J. Power Sources*, vol. 162, no. 2, pp. 913–919, 2006.

[18] V. Srinivasan and J. Newman, "Discharge Model for the Lithium Iron-Phosphate Electrode," *J. Electrochem. Soc.*, vol. 151, no. 10, p. A1517, 2004.

[19] J. Wang, Z. Sun, and X. Wei, "Performance and characteristic research in LiFePO4 battery for electric vehicle applications," *5th IEEE Veh. Power Propuls. Conf. VPPC '09*, vol. 4, no. 1, pp. 1657–1661, 2009.

[20] G. Pistoia, *Lithium-Ion Batteries: Advances and Applications*. 2013.

[21] K. C. Divya and J. Østergaard, "Battery energy storage technology for power systems-An overview," *Electr. Power Syst. Res.*, vol. 79, no. 4, pp. 511–520, 2009.

[22] J. Leadbetter and L. G. Swan, "Selection of battery technology to support grid-integrated renewable electricity," *J. Power Sources*, vol. 216, pp. 376–386, 2012.

[23] A. K. Padhi, K. S. Nanjundaswamy, J. B. Goodenough, A.K.Padhi, K.S.Nanjundaswamy, and J.B.Goodenough, "Phospho-olivines as Positive-Electrode Materials for rechargeable Lithium Batteries," *Electrochem. Soc.*, vol. 144, no. 4, pp. 1188–1194, 1997.

[24] E. M. Bauer, C. Bellitto, M. Pasquali, P. P. Prosini, and G. Righini, "Versatile Synthesis of Carbon-Rich LiFePO4 Enhancing Its Electrochemical Properties," *Electrochem. Solid-State Lett.*, vol. 7, no. 4, p. A85, 2004.

[25] P. P. Prosini, *Iron Phosphate Materials as Cathodes for Lithium Batteries*. London: Springer London, 2011.

[26] J. Jung, L. Zhang, and J. Zhang, *Lead-acid Battery TechnoLogies*. CRC Press, 2015.

[27] D. Pavlov, *Lead-acid Battery： Science and Technology*. Elsevier, 2011.

[28] D. A. J. Rand, P. T. Moseley, J. Garche, and C. D. Parker, "Valve-regulated Lead–Acid Batteries," in *Climate Change 2013 - The Physical Science Basis*, Cambridge: Elsevier, 2004.

[29] Gates-Energy-Products, *Rechargeable Batteries Applications Handbook*. Elsevier, 1998.

[30] Y. Wu, *LITHIUM-ION BATTERIES： Fundamentals and Applications*. CRC Press Taylor & Francis Group, 2015.

[31] W. A. van Schalkwijk and B. Scrosati, *Advances in Lithium-Ion Batteries*. Kluwer Academic Publishers, 2002.

[32] A123 Systems, "Nanophosphate High Power Lithium Ion Cell ANR26650M1-B," pp. 2–3, 2012.

[33] EnerSys®, "CYCLON® batteries application manual," no. December, 2008.

[34] C. Zhang, K. Li, S. McLoone, and Z. Yang, "Battery modelling methods for electric vehicles - A review," *2014 Eur. Control Conf. ECC 2014*, pp. 2673–2678, 2014.

[35] H. Wenzl, I. Baring-Gould, R. Kaiser, B. Y. Liaw, P. Lundsager, J. Manwell, A. Ruddell, and V. Svoboda, "Life prediction of batteries for selecting the technically most suitable and cost effective battery," *J. Power Sources*, vol. 144, no. 2, pp. 373–384, 2005.

[36] R. Rao, V. Sarma, and D. N. Rakhmatov, "Battery Modeling for Energy-Aware System Design," *Computer (Long. Beach. Calif).*, vol. 36, no. December, pp. 77–87, 2003.

[37] M. Jongerden and B. Haverkort, "Battery modeling," *Thecnical Rep. Fac. Electr. Eng. Math. Comput. Sci.*, p. 18, 2008.

[38] M. R. Jongerden and B. R. Haverkort, "Which battery model to use?," *IET Softw.*, vol. 3, no. 6, p. 445, 2009.

[39] M. Chen, S. Member, and G. A. Rinc, "Accurate Electrical Battery Model Capable of Predicting Runtime and I – V Performance," vol. 21, no. 2, pp. 504–511, 2006.

[40] J. Wehbe and N. Karami, "Battery Equivalent Circuits and Brief Summary of Components Value Determination of Lithium Ion A Review," pp. 45–49, 2015.

[41] A. A. H. Hussein and I. Batarseh, "An overview of generic battery models," *IEEE Power Energy Soc. Gen. Meet.*, no. 4, pp. 4–9, 2011.

[42] A. Seaman, T. S. Dao, and J. McPhee, "A survey of mathematics-based equivalent-circuit and electrochemical battery models for hybrid and electric vehicle simulation," *J. Power Sources*, vol. 256, pp. 410–423, 2014.

[43] T. K. Dong, A. Kirchev, F. Mattera, J. Kowal, and Y. Bultel, "Dynamic Modeling of Li-Ion Batteries Using an Equivalent," pp. 326–336, 2011.

[44] J. Groot, "State-of-health estimation of li-ion batteries: Cycle life test methods," *Chalmers Univ. Technol. Göteborg*, 2012.

[45] E. Wood, M. Alexander, and T. H. Bradley, "Investigation of battery end-of-life conditions for plug-in hybrid electric vehicles," *J. Power Sources*, vol. 196, no. 11, pp. 5147–5154, Jun. 2011.

[46] K. Asakura, M. Shimomura, and T. Shodai, "Study of life evaluation methods for Li-ion batteries for backup applications," *J. Power Sources*, vol. 119, pp. 902–905, 2003.

[47] V. Marano, S. Onori, Y. Guezennec, G. Rizzoni, and N. Madella, "Lithium-ion batteries life estimation for plug-in hybrid electric vehicles," *Veh. Power Propuls. Conf. 2009. VPPC '09. IEEE*, pp. 536–543, 2009.

[48] D. U. Sauer and H. Wenzl, "Comparison of different approaches for lifetime prediction of electrochemical systems-Using lead-acid batteries as example," *J. Power Sources*, vol. 176, no. 2, pp. 534–546, 2008.

[49] E. Barsoukov and J. R. Macdonald, *Impedance Spectroscopy: Theory, Experiment, and Applications*, vol. 177, no. 3. Hoboken, NJ, USA: John Wiley & Sons, Inc., 2005.

[50] A. Bard, G. Inzelt, and F. Scholz, *Electrochemical Dictionary*, vol. 54, no. 3. Berlin, Heidelberg: Springer Berlin Heidelberg, 2012.

[51] V. F. Lvovich, *Impedance Spectroscopy: Applications to Electrochemical and Dielectric Phenomena*. Hoboken, NJ, USA: John Wiley & Sons, Inc., 2012.

[52] F. Huet, "A review of impedance measurements for determination of the state-of-charge or state-of-health of secondary batteries," *J. Power Sources*, vol. 70, no. 1, pp. 59–69, 1998.

[53] W. H. Zhu, Y. Zhu, and B. J. Tatarchuk, "A simplified equivalent circuit model for simulation of Pb-acid batteries at load for energy storage application," *Energy Convers. Manag.*, vol. 52, no. 8–9, pp. 2794–2799, 2011.

[54] H. Blanke, O. Bohlen, S. Buller, R. W. De Doncker, B. Fricke, A. Hammouche, D. Linzen, M. Thele, and D. U. Sauer, "Impedance measurements on lead-acid batteries for state-of-charge, state-of-health and cranking capability prognosis in electric and hybrid electric vehicles," *J. Power Sources*, vol. 144, no. 2, pp. 418–425, 2005.

[55] A. J. Salkind, P. Singh, A. Cannone, T. Atwater, X. Wang, and D. Reisner, "Impedance modeling of intermediate size lead-acid batteries," *J. Power Sources*, vol. 116, no. 1–2, pp. 174–184, 2003.

[56] M. Hughes, R. T. Barton, S. A. G. R. Karunathilaka, and N. A. Hampson, "The estimation of the residual capacity of sealed lead-acid cells using the impedance technique," *J. Appl. Electrochem.*, vol. 16, no. 4, pp. 555–564, 1986.

[57] E. Karden, S. Buller, and R. W. De Doncker, "A method for measurement and interpretation of impedance spectra for industrial batteries," *J. Power Sources*, vol. 85, no. 1, pp. 72–78, 2000.

[58] J. Melorose, R. Perroy, and S. Careas, *Modern Aspects of Electrochemistry, Number 43*, vol. 43, no. Part II. 2009.

[59] S. Buller, M. Thele, R. W. De Doncker, and E. Karden, "Impedance-Based Simulation Models of Supercapacitors and Lithium-ion Batteries for Power Electronic Applications," *IEEE Ind. Appl. Mag.*, vol. 11, no. 2, pp. 742–747, 2005.

[60] M. Greenleaf, H. Li, and J. P. Zheng, "Modeling of Li_xFePO_4 Cathode Li-Ion Batteries Using Linear Electrical Circuit Model," *IEEE Trans. Sustain. Energy*, vol. 4, no. 4, pp. 1065–1070, 2013.

[61] T. K. Dong, A. Kirchev, F. Mattera, and Y. Bultel, "Modeling of Lithium Iron Phosphate Batteries by an Equivalent Electrical Circuit: Method of Model Parameterization and Simulation," *ECS Trans.*, vol. 25, no. 35, pp. 131–138, 2010.

[62] S.A.ILANGOVAN and S.SATHYANARAYANA, "Impedance parameters of individual electrodes and internal resistance of sealed batteries by a new nondestructive technique," *J. Appl. Electrochem.*, vol. 22, pp. 456–463, 1992.

[63] B.-Y. Chang and S.-M. Park, "Electrochemical Impedance Spectroscopy," *Annu. Rev. Anal. Chem.*, no. 3, pp. 207–229, 2010.

[64] A. K. Shukla, V. Ganesh Kumar, N. Munichandraiah, and T. S. Srinath, "A method to monitor valve-regulated lead-acid cells," *J. Power Sources*, vol. 74, no. 2, pp. 234–239, 1998.

[65] S. Sathyanrayana and M. L. Gopikanth, "Impedance parameters and the state-of charge.II.Lead-acid battery," *J. Appl. Electrochem.*, vol. 9, pp. 125–139, 1979.

[66] S. Buller, "Impedance-based simulation models for energy storage devices in advanced automotive power systems," RWTH Aachen University, 2003.

[67] E. Karden, "Using low-frequency impedance spectroscopy for characterization, monitoring, and modeling of industrial batteries," no. October, 2002.

[68] P. Mauracher and E. Karden, "Dynamic modelling of lead/acid batteries using impedance spectroscopy for parameter identification," *J. Power Sources*, vol. 67, pp. 69–84, 1997.

[69] IEEE-SA-Standards-Board, *IEEE Guide for Selecting, Charging, Testing, and Evaluating Lead-Acid Batteries Used in Stand-Alone Photovoltaic (PV) Systems*, vol. 2014. 2014.

[70] N. Jantharamin and L. Zhang, "A new dynamic model for Lead-acid batteries," *4th IET Int. Conf. Power Electron. Mach. Drives (PEMD 2008)*, pp. 86–90, 2008.

[71] C.-J. Zhan, X. G. Wu, S. Kromlidis, V. K. Ramachandaramurthy, M. Barnes, N. Jenkins, and A. J. Ruddell, "Two electrical models of the lead–acid battery used in a dynamic voltage restorer," *IEE Proc. - Gener. Transm. Distrib.*, vol. 150, no. 2, p. 175, 2003.

[72] J. B. Copetti and F. Chenlo, "Lead/acid batteries for photovoltaic applications. Test results and modeling," *J. Power Sources*, vol. 47, no. 1–2, pp. 109–118, 1994.

[73] M. Ceraolo, "New Dynamical Models of Lead – Acid Batteries," *IEEE Trans. Power Syst.*, vol. 15, no. 4, pp. 1184–1190, 2000.

[74] R. a. Jackey, "A Simple, Effective Lead-Acid Battery Modeling Process for Electrical System Component Selection," *SAE Pap.*, pp. 1–778, 2007.

[75] J. H. Aylor, A. Thieme, and B. W. Johnson, "A Battery State-of-Charge Indicator for Electric Wheelchairs," *IEEE Trans. Ind. Electron.*, vol. 39, no. 5, pp. 398–409, 1992.

[76] S. P. S. Pang, J. Farrell, J. D. J. Du, and M. Barth, "Battery state-of-charge estimation," *Proc. 2001 Am. Control Conf. (Cat. No.01CH37148)*, vol. 2, pp. 1644–1649, 2001.

[77] M.Coleman, C. B. Zhu, C. K. Leel, and W. G. Hurley, "A Combined SOC Estimation Method Under Varied Ambient Temperature for a Lead-Acid Battery."

[78] R. T. Barton and P. J. Mitchell, “Estimation of the residual capacity of maintenance-free lead acid batteries Part 1. Identification of a parameter for the prediction of state-of-charge,” *J. Power Sources*, vol. 27, no. 4, pp. 287–295, 1989.

[79] V. V. VISWANATHAN, A. J. SALKIND, J. J. KELLEY, and J. B. OCKERMAN, “Effect of state of charge on impedance spectrum of sealed cells Part II: Lead-acid batteries,” *J. Appl. Electrochem.*, vol. 25, pp. 729–739, 1995.

[80] M. Greenleaf, O. Dalchand, H. Li, S. Member, J. P. Zheng, and S. Member, “A Temperature-Dependent Study of Sealed Lead-Acid Batteries Using Physical Equivalent Circuit Modeling With Impedance Spectra Derived High Current / Power Correction,” vol. 6, no. 2, pp. 380–387, 2015.

[81] S. Tian, M. Hong, and M. Ouyang, “An experimental study and nonlinear modeling of discharge I-V behavior of valve-regulated lead-acid batteries,” *IEEE Trans. Energy Convers.*, vol. 24, no. 2, pp. 452–458, 2009.

[82] R. Kaushik and I. G. Mawston, “Coulombic efficiency of lead/acid batteries, particularly in remote-area power-supply (RAPS) systems,” *J. Power Sources*, vol. 35, no. 4, pp. 377–383, 1991.

[83] A. S. Andersson, J. O. Thomas, B. Kalska, and L. Häggström, “Thermal Stability of LiFePO4-Based Cathodes,” *Electrochem. Solid-State Lett.*, vol. 3, no. 2, pp. 66–68, 2000.

[84] R. Ravishankar, V. Sarma, and D. N. Rakhmatov, “Battery Modeling for energy- aware system design,” *IEEE Comput. Soc.*, no. December, 2003.

[85] N. Omar, P. Van den Bossche, T. Coosemans, and J. Van Mierlo, “Peukert revisited-critical appraisal and need for modification for lithium-ion batteries,” *Energies*, vol. 6, no. 11, pp. 5625–5641, 2013.

[86] R. C. Kroeze and P. T. Krein, “Electrical Battery Model for Use in Dynamic Electric Vehicle Simulations,” pp. 1336–1342, 2008.

[87] Y. Xing, W. He, M. Pecht, and K. L. Tsui, “State of charge estimation of lithium-ion batteries using the open-circuit voltage at various ambient temperatures,” *Appl. Energy*, vol. 113, pp. 106–115, 2014.

[88] Y. Hu, S. Yurkovich, Y. Guezennec, and B. J. Yurkovich, “Electro-thermal battery model identification for automotive applications,” *J. Power Sources*, vol. 196, no. 1, pp. 449–457, 2011.

[89] J. Lindgren and I. A. and P. D. L. Department, “A hybrid lithium-ion battery model for system-level analyses,” *Arch. Thermodyn.*, vol. 33, no. 4, pp. 23–40, 2012.

[90] W. Waag, S. Käbitz, and D. U. Sauer, “Experimental investigation of the lithium-ion battery impedance characteristic at various conditions and aging states and its influence on the application,” *Appl. Energy*, vol. 102, pp. 885–897, 2013.

[91] W. Waag, C. Fleischer, and D. U. Sauer, “On-line estimation of lithium-ion battery impedance parameters using a novel varied-parameters approach,” *J. Power Sources*, vol. 237, pp. 260–269, 2013.

[92] D. Andre, M. Meiler, K. Steiner, C. Wimmer, T. Soczka-Guth, and D. U. Sauer, “Characterization of high-power lithium-ion batteries by electrochemical impedance spectroscopy. I. Experimental investigation,” *J. Power Sources*, vol. 196, no. 12, pp. 5334–5341, 2011.

[93] J. Gomez, R. Nelson, E. E. Kalu, M. H. Weatherspoon, and J. P. Zheng, “Equivalent circuit model parameters of a high-power Li-ion battery: Thermal and state of charge effects,” *J. Power Sources*, vol. 196, no. 10, pp. 4826–4831, 2011.

[94] B. Y. Liaw, R. G. Jungst, G. Nagasubramanian, H. L. Case, and D. H. Doughty, “Modeling capacity fade in lithium-ion cells,” *J. Power Sources*, vol. 140, no. 1, pp. 157–161, 2005.

[95] Enersys, “Application Manual of CYCLON AGM single cell,” no. December, 2008.

[96] L. Lam, “A Practical Circuit-based Model for Li-ion Battery Cells in Electric Vehicle Applications,” *Master Sci. Thesis*, p. 174, 2011.

[97] J. H. Yan, H. Y. Chen, W. S. Li, C. I. Wang, and Q. Y. Zhan, “A study on quick charging method for

small VRLA batteries," *J. Power Sources*, vol. 158, no. 2 SPEC. ISS., pp. 1047–1053, 2006.

[98] MACCOR, "Series 4000 Automated Test System," pp. 1–4.

[99] Y. Hu, S. Yurkovich, Y. Guezennec, and B. J. Yurkovich, "A technique for dynamic battery model identification in automotive applications using linear parameter varying structures," *Control Eng. Pract.*, vol. 17, no. 10, pp. 1190–1201, 2009.

[100] INL, "Battery Technology Life Verification Test Manual," no. February, 2005.

[101] D. Doerffel, "Testing and Characterisation of Large High-Energy Lithium-Ion Batteries for Electric and Hybrid Electric Vehicles," 2007.

[102] M. A. Roscher and D. U. Sauer, "Dynamic electric behavior and open-circuit-voltage modeling of LiFePO 4-based lithium ion secondary batteries," *J. Power Sources*, vol. 196, no. 1, pp. 331–336, 2011.

[103] V. Coroban, I. Boldea, and F. Blaabjerg, "A novel on-line state-of-charge estimation algorithm for valve regulated lead-acid batteries used in hybrid electric vehicles," *Int. Aegean Conf. Electr. Mach. Power Electron. Electromotion ACEMP'07 Electromotion'07 Jt. Conf.*, pp. 39–46, 2007.

[104] A. Mariani, T. Stockley, and K. Thanapalan, "Simple and Effective OCV Prediction Mechanism for VRLA Battery Systems," *Avestia.Com*, no. 140, pp. 1–10, 2014.

[105] A. Mariani, K. Thanapalan, P. Stevenson, T. Stockley, and J. Williams, "Techniques for monitoring and predicting the OCV for VRLA battery systems," *2015 21st Int. Conf. Autom. Comput. Autom. Comput. Manuf. New Econ. Growth, ICAC 2015*, no. September, pp. 11–12, 2015.

[106] L. Lam, "A practical circuit-based model for state of health estimation of li-ion battery cells in electric vehicles," TU Delft, Delft University of Technology, 2011.

[107] 陈洪亮, 田社平, 吴雪, and 徐雄, 电路分析基础. 清华大学出版社, 2009.

[108] S. Abu-Sharkh and D. Doerffel, "Rapid test and non-linear model characterisation of solid-state lithium-ion batteries," *J. Power Sources*, vol. 130, no. 1–2, pp. 266–274, 2004.

[109] B. Schweighofer, K. M. Raab, and G. Brasseur, "Modeling of high power automotive batteries by the use of an automated test system," *IEEE Trans. Instrum. Meas.*, vol. 52, no. 4, pp. 1087–1091, 2003.

[110] H. G. Schweiger, O. Obeidi, O. Komesker, A. Raschke, M. Schiemann, C. Zehner, M. Gehnen, M. Keller, and P. Birke, "Comparison of several methods for determining the internal resistance of lithium ion cells," *Sensors*, vol. 10, no. 6, pp. 5604–5625, 2010.

[111] INL, "Battery Test Manual For Low-Energy Energy Storage System for Power-Assist Hybrid Electric Vehicles," 2013.

[112] IEEE-Standards-Coordinating-Committee, "IEEE Std 1661™-2007, IEEE Guide for Test and Evaluation of Lead-Acid Batteries Used in Photovoltaic (PV) Hybrid Power Systems," *Ieeexplore.Ieee.Org*, no. February, 2008.

[113] Deutsche-Gesellschaft-fur-Sonnenenergie, *Planning and Installing Photovoltaic Systems: A guide for installers, architects and engineers*. 2007.

[114] W. E. M. Jones and P. Scientific, "Behavior of vrla cells on long term float: part 2," pp. 358–366, 1996.

[115] Y. Yamaguchi, M. Shiota, M. Hosokawa, Y. Nakayama, N. Hirai, and S. Hara, "Study of charge acceptance for the lead-acid battery through in situ EC-AFM observation - Influence of the open-circuit standing time on the negative electrode," *J. Power Sources*, vol. 102, no. 1–2, pp. 155–161, 2001.

[116] M. Thele, J. Schiffer, E. Karden, E. Surewaard, and D. U. Sauer, "Modeling of the charge acceptance of lead-acid batteries," *J. Power Sources*, vol. 168, no. 1 SPEC. ISS., pp. 31–39, 2007.

[117] L. Lam, P. Bauer, and E. Kelder, "A practical circuit-based model for Li-ion battery cells in electric vehicle applications," in *Telecommunications Energy Conference (INTELEC), 2011 IEEE 33rd International*, 2011, pp. 1–9.

[118] C. Mikolajczak, M. Kahn, Kevin White, and R. T. Long, *Lithium-Ion Batteries Hazard and Use Assessment*, no. July. 2011.

[119] B. Scrosati and J. Garche, "Lithium batteries: Status, prospects and future," *J. Power Sources*, vol. 195, no. 9, pp. 2419–2430, 2010.

[120] X. Han, M. Ouyang, L. Lu, J. Li, Y. Zheng, and Z. Li, "A comparative study of commercial lithium ion battery cycle life in electrical vehicle: Aging mechanism identification," *J. Power Sources*, vol. 251, pp. 38–54, 2014.

[121] P. Verma, P. Maire, and P. Novák, "A review of the features and analyses of the solid electrolyte interphase in Li-ion batteries," *Electrochim. Acta*, vol. 55, no. 22, pp. 6332–6341, 2010.

[122] E. Peled, "The Electrochemical Behavior of Alkali and Alkaline Earth Metals in Nonaqueous Battery Systems-- The Solid Electrolyte Interphase Model," *J. Electrochem. Soc.*, vol. 126, no. 12, pp. 2047–2051, 1979.

[123] J. Vetter, P. Novâk, M. R. R. Wagner, C. Veit, K.-C. C. Möller, J. O. O. Besenhard, M. Winter, M. Wohlfahrt-Mehrens, C. Vogler, A. Hammouche, P. Nov??k, M. R. R. Wagner, C. Veit, K. C. M??ller, J. O. O. Besenhard, M. Winter, M. Wohlfahrt-Mehrens, C. Vogler, A. Hammouche, P. Novâk, M. R. R. Wagner, C. Veit, K.-C. C. Möller, J. O. O. Besenhard, M. Winter, M. Wohlfahrt-Mehrens, C. Vogler, and A. Hammouche, "Ageing mechanisms in lithium-ion batteries," *J. Power Sources*, vol. 147, no. 1–2, pp. 269–281, Sep. 2005.

[124] M. Broussely, P. Biensan, F. Bonhomme, P. Blanchard, S. Herreyre, K. Nechev, and R. J. Staniewicz, "Main aging mechanisms in Li ion batteries," *J. Power Sources*, vol. 146, no. 1–2, pp. 90–96, 2005.

[125] V. Agubra and J. Fergus, "Lithium ion battery anode aging mechanisms," *Materials (Basel).*, vol. 6, no. 4, pp. 1310–1325, 2013.

[126] M. Wohlfahrt-Mehrens, C. Vogler, and J. Garche, "Aging mechanisms of lithium cathode materials," *J. Power Sources*, vol. 127, no. 1–2, pp. 58–64, 2004.

[127] D. Li, D. Danilov, L. Gao, Y. Yang, and P. H. L. Notten, "Degradation Mechanisms of C6/LiFePO4 Batteries: Experimental Analyses of Cycling-induced Aging," *Electrochim. Acta*, vol. 210, pp. 445–455, 2016.

[128] M. Koltypin, D. Aurbach, L. Nazar, and B. Ellis, "More on the performance of LiFePO4 electrodes-The effect of synthesis route, solution composition, aging, and temperature," *J. Power Sources*, vol. 174, no. 2, pp. 1241–1250, 2007.

[129] M. Koltypin, D. Aurbach, L. Nazar, and B. Ellis, "On the Stability of LiFePO[sub 4] Olivine Cathodes under Various Conditions (Electrolyte Solutions, Temperatures)," *Electrochem. Solid-State Lett.*, vol. 10, no. 2, p. A40, 2007.

[130] P. Liu, J. Wang, J. Hicks-Garner, E. Sherman, S. Soukiazian, M. Verbrugge, H. Tataria, J. Musser, and P. Finamore, "Aging Mechanisms of LiFePO[sub 4] Batteries Deduced by Electrochemical and Structural Analyses," *J. Electrochem. Soc.*, vol. 157, no. 4, p. A499, 2010.

[131] L. Castro, R. Dedryvère, J.-B. Ledeuil, J. Bréger, C. Tessier, and D. Gonbeau, "Aging Mechanisms of LiFePO4 // Graphite Cells Studied by XPS: Redox Reaction and Electrode/Electrolyte Interfaces," *J. Electrochem. Soc.*, vol. 159, no. 4, p. A357, 2012.

[132] J. H. Kim, S. C. Woo, M. S. Park, K. J. Kim, T. Yim, J. S. Kim, and Y. J. Kim, "Capacity fading mechanism of LiFePO4-based lithium secondary batteries for stationary energy storage," *J. Power Sources*, vol. 229, pp. 190–197, 2013.

[133] J. Shim and K. A. Striebel, "Cycling performance of low-cost lithium ion batteries with natural graphite and LiFePO4," *J. Power Sources*, vol. 119–121, pp. 955–958, 2003.

[134] R. Deshpande, M. Verbrugge, Y.-T. Cheng, J. Wang, and P. Liu, "Battery Cycle Life Prediction with Coupled Chemical Degradation and Fatigue Mechanics," *J. Electrochem. Soc.*, vol. 159, no. 10, pp.

A1730–A1738, 2012.

[135] M. Kassem and C. Delacourt, "Postmortem analysis of calendar-aged graphite/LiFePO4 cells," *J. Power Sources*, vol. 235, pp. 159–171, 2013.

[136] I. Bloom, B. W. Cole, J. J. Sohn, S. A. Jones, E. G. Polzin, V. S. Battaglia, G. L. Henriksen, C. Motloch, R. Richardson, T. Unkelhaeuser, D. Ingersoll, and H. L. Case, "An accelerated calendar and cycle life study of Li-ion cells," *J. Power Sources*, vol. 101, no. 2, pp. 238–247, 2001.

[137] M. Safari and C. Delacourt, "Aging of a commercial graphite/LiFePO4 cell," *J. Electrochem. Soc.*, vol. 158, no. 10, pp. A1123--A1135, 2011.

[138] J. Wang, P. Liu, J. Hicks-Garner, E. Sherman, S. Soukiazian, M. Verbrugge, H. Tataria, J. Musser, and P. Finamore, "Cycle-life model for graphite-LiFePO4 cells," *J. Power Sources*, vol. 196, no. 8, pp. 3942–3948, 2011.

[139] Z. Li, L. Lu, M. Ouyang, and Y. Xiao, "Modeling the capacity degradation of LiFePO4/graphite batteries based on stress coupling analysis," *J. Power Sources*, vol. 196, no. 22, pp. 9757–9766, 2011.

[140] G. Ning, B. Haran, and B. N. Popov, "Capacity fade study of lithium-ion batteries cycled at high discharge rates," *J. Power Sources*, vol. 117, no. 1–2, pp. 160–169, 2003.

[141] P. Keil and A. Jossen, "Charging protocols for lithium-ion batteries and their impact on cycle life-An experimental study with different 18650 high-power cells," *J. Energy Storage*, vol. 6, pp. 125–141, 2016.

[142] S. Grolleau, B. Molina-Concha, A. Delaille, R. Revel, J. Bernard, S. Pelissier, and J. Peter, "The French SIMCAL Research Network For Modelling of Calendar Aging for Energy Storage System in EVs And HEVs - EIS Analysis on LFP/C Cells," *ECS Trans.*, vol. 45, no. 13, pp. 73–81, 2013.

[143] Y. Zhang, C. Y. Wang, and X. Tang, "Cycling degradation of an automotive LiFePO4 lithium-ion battery," *J. Power Sources*, vol. 196, no. 3, pp. 1513–1520, 2011.

[144] L. Tan, L. Zhang, Q. Sun, M. Shen, Q. Qu, and H. Zheng, "Capacity loss induced by lithium deposition at graphite anode for LiFePO4/graphite cell cycling at different temperatures," *Electrochim. Acta*, vol. 111, pp. 802–808, 2013.

[145] S. Sun, T. Guan, B. Shen, K. Leng, Y. Gao, X. Cheng, and G. Yin, "Changes of Degradation Mechanisms of LiFePO4/Graphite Batteries Cycled at Different Ambient Temperatures," *Electrochim. Acta*, vol. 237, pp. 248–258, 2017.

[146] M. Kassem, J. Bernard, R. Revel, S. P??lissier, F. Duclaud, and C. Delacourt, "Calendar aging of a graphite/LiFePO 4 cell," *J. Power Sources*, vol. 208, pp. 296–305, 2012.

[147] S. Bashash, S. J. Moura, J. C. Forman, and H. K. Fathy, "Plug-in hybrid electric vehicle charge pattern optimization for energy cost and battery longevity," *J. Power Sources*, vol. 196, no. 1, pp. 541–549, 2011.

[148] T. Guena and P. Leblanc, "How depth of discharge affects the cycle life of lithium-metal-polymer batteries," *INTELEC, Int. Telecommun. Energy Conf.*, 2006.

[149] Z. Guo and Z. Chen, "Aging property for LiFePO4/graphite cell with different temperature and DODs," *Russ. J. Electrochem.*, vol. 52, no. 6, pp. 546–554, 2016.

[150] A. Millner, "Modeling lithium ion battery degradation in electric vehicles," *2010 IEEE Conf. Innov. Technol. an Effic. Reliab. Electr. Supply, CITRES 2010*, pp. 349–356, 2010.

[151] S. B. Peterson, J. Apt, and J. F. Whitacre, "Lithium-ion battery cell degradation resulting from realistic vehicle and vehicle-to-grid utilization," *J. Power Sources*, vol. 195, no. 8, pp. 2385–2392, 2010.

[152] K.Nakamura, M.Shiomi, K.Takahashi, and M.Tsubota, "Failure modes of valve-regulated lead/acid batteries," *J. Power Sources*, vol. 59, pp. 153–157, 1996.

[153] P. Ruetschi, "Aging mechanisms and service life of lead-acid batteries," *J. Power Sources*, vol. 127, no.

1–2, pp. 33–44, 2004.

[154] B. Culpin and D. A. J. Rand, “Failure modes of lead / acid batteries,” *J. Power Sources*, vol. 36, pp. 415–438, 1991.

[155] R. Wagner, “Failure modes of valve-regulated lead-acid batteries in different applications,” *J. Power Sources*, vol. 53, pp. 153–162, 1995.

[156] W. Merrouche, N. Achaibou, and B. Bouzidi, “Lead-acid Battery Degradation Mechanisms in PV Systems,” *3rd Int. Work. Integr. Sol. Power into Power Syst.*, no. October 2013, pp. 3–7, 2013.

[157] S. Drouilhet and B. Johnson, “A battery life prediction method for hybrid power applications,” *Contract DE-AC36-83CH10093*, no. January, 1997.

[158] T. M. Layadi, G. Champenois, M. Mostefai, and D. Abbes, “Lifetime estimation tool of lead-acid batteries for hybrid power sources design,” *Simul. Model. Pract. Theory*, vol. 54, pp. 36–48, 2015.

[159] D. U. Sauer, M. Bkhler, G. Bopp, W. Hijhe, J. Mittermeier, P. Sprau, B. Willer, and M. Wollny, “Analysis of the performance parameters of lead / acid batteries in photovoltaic systems,” *J. Power Sources*, vol. 64, pp. 197–201, 1997.

[160] V. Svoboda, H. Wenzl, R. Kaiser, A. Jossen, I. Baring-Gould, J. Manwell, P. Lundsager, H. Bindner, T. Cronin, P. Nørgård, A. Ruddell, A. Perujo, K. Douglas, C. Rodrigues, A. Joyce, S. Tselepis, N. van der Borg, F. Nieuwenhout, N. Wilmot, F. Mattera, and D. U. Sauer, “Operating conditions of batteries in off-grid renewable energy systems,” *Sol. Energy*, vol. 81, no. 11, pp. 1409–1425, 2007.

[161] T. Hund, “Test Results from the PV Battery Cycle-Life Test Procedure,” *Sandia Natl. Lab.*, pp. 1–10.

[162] Deutsche Gesellshaft fur Sonnenenergie, *Planning and installing photovoltaic systems A guide for installers, architects and engineers*. 2005.

[163] INL, “Battery Test Manual for Plug-In Hybrid Electric Vehicles,” vol. 158, no. March, pp. 1720–1723, 2010.

[164] A. Eddahech, O. Briat, N. Bertrand, J.-Y. Delétage, and J.-M. Vinassa, “Behavior and state-of-health monitoring of Li-ion batteries using impedance spectroscopy and recurrent neural networks,” *Int. J. Electr. Power Energy Syst.*, vol. 42, no. 1, pp. 487–494, 2012.

[165] A. Eddahech, O. Briat, and J.-M. Vinassa, “Lithium-ion battery performance improvement based on capacity recovery exploitation,” *Electrochim. Acta*, vol. 114, pp. 750–757, 2013.

[166] I. Baghdadi, O. Briat, P. Gyan, and J. M. Vinassa, “State of health assessment for lithium batteries based on voltage???time relaxation measure,” *Electrochim. Acta*, vol. 194, pp. 461–472, 2016.

[167] D. Anseán, M. Dubarry, A. Devie, B. Y. Liaw, V. M. García, J. C. Viera, and M. González, “Fast charging technique for high power LiFePO4 batteries: A mechanistic analysis of aging,” *J. Power Sources*, vol. 321, pp. 201–209, 2016.

[168] M. Dubarry, C. Truchot, and B. Y. Liaw, “Cell degradation in commercial LiFePO4 cells with high-power and high-energy designs,” *J. Power Sources*, vol. 258, pp. 408–419, 2014.

[169] K. Striebel, J. Shim, A. Sierra, H. Yang, X. Song, R. Kostecki, and K. McCarthy, “The development of low cost LiFePO4-based high power lithium-ion batteries,” *J. Power Sources*, vol. 146, no. 1–2, pp. 33–38, 2005.

[170] J. Groot, M. Swierczynski, A. I. Stan, and S. K. K??r, “On the complex ageing characteristics of high-power LiFePO<inf>4</inf>/graphite battery cells cycled with high charge and discharge currents,” *J. Power Sources*, vol. 286, pp. 475–487, 2015.

[171] J. Groot, “State-of-Health Estimation of Li-ion Batteries: Ageing Models,” 2014.

[172] A. Eddahech, O. Briat, and J. M. Vinassa, “Performance comparison of four lithium-ion battery technologies under calendar aging,” *Energy*, vol. 84, pp. 542–550, 2015.

[173] D. Anseán, M. González, J. C. Viera, V. M. García, C. Blanco, and M. Valledor, "Fast charging technique for high power lithium iron phosphate batteries: A cycle life analysis," *J. Power Sources*, vol. 239, pp. 9–15, 2013.

[174] J. M. Lujano-Rojas, R. Dufo-López, J. L. Atencio-Guerra, E. M. G. Rodrigues, J. L. Bernal-Agustín, and J. P. S. Catalão, "Operating conditions of lead-acid batteries in the optimization of hybrid energy systems and microgrids," *Appl. Energy*, vol. 179, pp. 590–600, 2016.

[175] S. Schaeck, A. O. Stoermer, and E. Hockgeiger, "Micro-hybrid electric vehicle application of valve-regulated lead-acid batteries in absorbent glass mat technology: Testing a partial-state-of-charge operation strategy," *J. Power Sources*, vol. 190, no. 1, pp. 173–183, 2009.

[176] G. Pilatowicz, H. Budde-Meiwes, D. Schulte, J. Kowal, Y. Zhang, X. Du, M. Salman, D. Gonzales, J. Alden, and D. U. Sauer, "Simulation of SLI Lead-Acid Batteries for SoC, Aging and Cranking Capability Prediction in Automotive Applications," *J. Electrochem. Soc.*, vol. 159, no. 9, pp. A1410–A1419, 2012.

[177] J. Schiffer, D. U. Sauer, H. Bindner, T. Cronin, P. Lundsager, and R. Kaiser, "Model prediction for ranking lead-acid batteries according to expected lifetime in renewable energy systems and autonomous power-supply systems," *J. Power Sources*, vol. 168, no. 1 SPEC. ISS., pp. 66–78, 2007.

[178] E. Kona, "Stationary VRLA battery health estimation by resistance measurement - comparison of dc and ac test methods," in *2016 IEEE International Conference on Power Electronics, Drives and Energy Systems (PEDES)*, 2016, pp. 1–5.

[179] T. Den Heeten, N. Narayan, J.-C. Diehl, J. Verschelling, S. Silvester, J. Popovic-Gerber, P. Bauer, and M. Zeman, "Understanding the present and the future electricity needs: Consequences for design of future Solar Home Systems for off-grid rural electrification," *2017 Int. Conf. Domest. Use Energy*, pp. 8–15, 2017.